# RESPONSE OF CONCRETE STRUCTURES TO SEISMIC MOTIONS

A thesis
submitted in partial fulfilment of the requirements
for the Degree of
Doctor of Philosophy in Civil Engineering
at the University of Canterbury
by

Grant Keith Wilby

University of Canterbury,
Christchurch, New Zealand
1975

ABSTRACT

In this report the strength and behaviour of model reinforced concrete structures subjected to simulated seismic disturbances are examined.

The performance of a closed loop electrohydraulic testing system used in conjunction with a small shaking table is described. This testing system could accurately reproduce seismic disturbances and was used in the testing of a single storey structure and two six storey structures. All structures had a single bay in each direction and they were approximately one fifth of full size. The problems associated with modelling work are discussed and techniques suitable for constructing small scale three-dimensional model reinforced concrete structures are reported.

Loading tests were conducted on typical beam and column structural members and the moment-curvature curves obtained are compared with those determined using theoretical methods. Both static and dynamic cyclic lateral loading tests were conducted on the structures and the apparent strengths of the structures under each type of loading are compared. The accuracy of an existing frame analysis program in predicting the displacement response of the model structures to simulated seismic disturbances is discussed and the more important parameters affecting the response are investigated.

The experiments revealed that under lateral loading considerable torsion is induced into the lateral beams and that this may be sufficient to cause failure of those beams. A method is presented for calculating the distribution of torsion induced in the lateral beams and for calculating the magnitude of the torsional contribution to the flexural strength of the longitudinal beams. A discussion on collapse mechanisms is included and a design recommendation is made to reduce the likelihood of the structure collapsing by a column sidesway mechanism.

to

Linda

# ACKNOWLEDGEMENTS

The research for this report was carried out in the Department of Civil Engineering, University of Canterbury, under the overall guidance of its Head, Professor H.J. Hopkins.

The author wishes to record his appreciation of the support and guidance provided by Professor Robert Park during his supervision of the author's studies and the preparation of this report. I am also grateful to Dr. Athol J. Carr for his assistance in this respect.

I wish to thank the technical staff of the Civil Engineering Department for their assistance in the experimental programme, particularly Messrs. Harold Watson, Geoff Hill, Aardt Schouten, Peter Robinson and Henry Patterson. My special thanks go to Mr. Ken Marrion to whom the credit for the successful completion of the experimental programme largely belongs.

I am indebted to Dr. Richard D. Sharpe, former graduate student, for his help with computing work and for making available his dynamic frame analysis program.

I wish to record my appreciation of the assistance given by Mr. W.K. Kennedy of the University's Electrical Engineering Department in programming the simulated earthquakes and in tracing the electrical fault in the MTS structures testing system. The assistance of Mr. P.L. Squires in this latter respect is also appreciated.

I gratefully acknowledge the financial aid given by the University Grants Committee in the form of a Postgraduate Scholarship. The generosity of GKN (NZ) Ltd in donating the reinforcing wire is acknowledged.

I thank Mrs. Alice Watt for typing this report.

Finally, I am deeply grateful to my wife, Linda, to whom this report is dedicated, not only for her typing of the draft copy of this report but also for her support and encouragement during the studies which led up to it.

CONTENTS

# LIST OF FIGURES

# LIST OF TABLES

# CHAPTER ONE

# INTRODUCTION AND SCOPE OF RESEARCH

## 1.1 INTRODUCTION

Earthquakes are one of the most frightening natural phenomena known to man, not only because of the devastation to life and property that they inflict but also because they cannot, as yet, be predicted with any reasonable degree of accuracy. With the rapid advancement of research into earthquake prediction in recent years, it is possible that accurate prediction of major earthquakes in well instrumented areas may be possible within a few decades. However, while warning of an imminent major earthquake will reduce loss of life, it can only be prevented completely, and the damage to property minimised, by careful design procedures based on a clear understanding of the response of structures to seismic excitations.

Engineers have traditionally relied upon the performance of existing structures to use as a yardstick in evaluating the adequacy of existing design procedures. In the case of earthquake resistant design this evaluation has been hampered by the fact that major earthquakes often occur far from the centres of population or in regions where structures have been poorly designed and detailed as a result of inadequate building codes. The infrequent occurrence of major earthquakes necessitates the introduction of some form of simulated earthquake which can be used to test complete structures or parts of structures.

Current design philosophy is to design a structure to resist only small or medium earthquakes elastically; the extra energy of a major earthquake is assumed to be absorbed by plastic deformation and the building, although badly damaged, should not collapse. With the advent of limit state design, the importance of providing adequate ductility and of preventing the formation of catastrophic collapse mechanisms is now recognised.

In recent years the advent of large digital computers and the development of numerical integration techniques have enabled major advances in the dynamic analysis of structures to be made. In turn, the mathematical model used to represent the structure has markedly increased in complexity as the effect of further parameters which

affect the response of the structure have been included. Given the complexity of the mathematical model and the unique transient nature of the earthquake to which it is subjected, it is difficult for the designer to develop a feel as to whether the response predicted by an inelastic frame analysis is reasonable. Ultimately, the only means the designer has to verify this predicted response is to carry out tests on the completed structure. Existing structures can be used for this purpose if it is desired to test the structure using small amplitude sine waves in the elastic range but unfortunately structures subjected to major earthquakes rarely behave in a linearly elastic manner. The designer is then left with the choice of either testing small scale models of a prototype structure or testing full scale models of selected critical parts of the structure and then deducing the behaviour of the complete structure from the behaviour of the parts of the structure.

The latter method has generally been restricted to static tests and suffers in that the testing of only a part of the structure is necessarily a gross approximation of the real situation and important features of the behaviour of the structure may not be recognised because their effects were not apparent in that portion of the structure selected for testing. The testing of small scale models introduces the problem of accurately modelling the prototype structure and the small size of the models often means that measurement of their response is difficult.

## 1.2 THE MODELLING PROBLEM

The most acute problem in small scale model work is associated with the fact that if a prototype structure is faithfully reproduced at some smaller scale, then the dead load forces and moments induced in the small model are reduced substantially more than are the strengths of the various members of which the model is composed. This is a consequence of the fact that the laws of similitude relating prototype quantities to model quantities require that the density of the modelling material must be substantially increased. Usually this requirement must be satisfied artificially in some way, generally by placing additional dead loads on the structure. An alternative approach is not to construct a model of a specific structure at all and so the responses obtained are then analysed strictly in terms of the behaviour

of the small structure actually tested.

Construction of small scale models necessitates close quality control since errors are magnified in the extrapolation of model results to the prototype. Tolerances which are adequate for large scale experimental work are totally unacceptable for small scale models. Measurement of experimental results is often difficult due to the small size of the model. Electric resistance strain gauges are usually difficult to bond onto the small diameter reinforcing wire and the use of mechanical strain gauges is impractical due to the small dimensions of the model structure.

The behaviour of both concrete and steel have been found to vary as the size of the test specimen is decreased. Numerous investigators [1, 2, 3, 4] have found that the apparent strength of concrete increases as the specimen size decreases. This is commonly thought to occur because failure is probably initiated at a small stress raising cavity or flaw which causes a local fracture in the most highly stressed zone and the fracture is propagated until the specimen fails. The presence of a weakness in the most highly stressed zone is likely to be proportional to the volume of the specimen so that large specimens, on the average, are weaker.

The effect of scaling the concrete mix as well as the size of the test specimen is to often increase the ratio of tensile to compressive strengths of the concrete. This results in fewer cracks in the model structure and cracking similitude between prototype and model is often poor. Because deformed bars are not easily obtainable in the small diameters used for typical model reinforcement, plain wire is often used instead and this is usually left to rust to improve the bonding characteristics of its surface. In spite of using wires slightly pitted as a result of rusting, the bond between the steel and the concrete may still be inadequate and this could result in fewer cracks in the model than in the prototype. However, extensive modelling studies conducted by White and Chowdhury [5] showed that fewer cracks in the model does not produce any measurable differences in the moment-rotation and the load-deflection characteristics of the model structure.

Hansen and Mattock [6] have found that both the rate and final values of shrinkage and creep increase as the member becomes smaller. Both shrinkage and creep increase with an increase in the rate of moisture transfer and small members dry rapidly due to their large

surface area to volume ratio.

Both the strengths and modulii of elasticity of steel and concrete increase with an increase in the rate of application of the load [2, 7]. Thus the strength and stiffness of a structure tested dynamically will be greater than when it is tested statically. If, as is often the case, the time scale for the model is decreased, then the model can be expected to show a further small strength gain over the prototype structure.

The strength of small scale reinforced concrete members have often appeared to be significantly higher than predicted by theory. This aspect of modelling is further discussed in Section 1.3. However most investigators agree that model results can be used to closely predict the behaviour of the prototype, if due care is exercised.

## 1.3 REVIEW OF PREVIOUS RESEARCH

It is only in recent years with the introduction of ultimate strength design that the importance of examining the response of a structure beyond the linearly elastic range has been realised. Most previous work on the dynamic response of structures has been carried out on existing buildings which were excited into small amplitude vibrations in the elastic range by a vibration apparatus clamped to the structure [11, 12]. Few attempts have been made to model entire structures or frames and subject them to simulated seismic disturbances.

Shaking tables have been used in research for many years and an account of their use is given by Dawson [13]. These tables have generally been limited to sinusoidal motion although some attempts were made to simulate a random earthquake motion using a cam follower principle. However, with the advent in the last decade of sophisticated closed loop electrohydraulic rams it has become possible for the first time to accurately simulate complex seismic disturbances over a wide range of frequencies and displacements. A number of shaking tables driven by these electrohydraulic rams have been constructed and some results of research have been reported in the literature, for example [13, 16]. Some of the results of this work is discussed later in this Section.

A large amount of work has been carried out on investigations into the properties of concretes suitable for small scale model work. Neville [3] noted that both the mean strength and the standard deviation

increased with decreasing specimen size. Price [2] found that the 28 day concrete strength indicated by 2 in. dia. x 4 in. (50.8 mm dia. x 101.6 mm) cylinders was 8.7% greater than that indicated by 6 in. dia. x 12 in. (152.4 mm dia. x 304.8 mm) cylinders and attributed this to the possible faster strength gain of the smaller diameter cylinders, although Gyengo [1] had earlier reported that the ratio of strengths of small to large specimens was invariant with age. Litle and Paparoni [4] found that the apparent concrete compressive and tensile strengths increased from 6 in. dia. x 12 in. (152.4 mm dia. x 304.8 mm) cylinders to 2 in. dia. x 4 in. (50.8 mm dia. x 101.6 mm) cylinders but were unable to find any further significant strength increases in smaller cylinders, although nearly 700 specimens were tested.

The effect of scaling the mix as well as scaling the specimen size was investigated by Johnson [14] who found that the strengths of $\frac{1}{4}$ and $\frac{1}{8}$ scale mixes were comparable. Johnson reported that the variability increased with the ratio of the maximum aggregate size to the minimum dimension of the test specimen and he concluded that $1\frac{1}{2}$ in. dia. x 3 in. (38.1 mm dia. x 76.2 mm) cylinders gave results sufficiently consistent for laboratory tests.

Many, though not all, investigators have found that the strengths of small scale reinforced concrete members have often appeared to be significantly higher than predicted by theory. Litle and Paparoni [4] conducted a series of tests on small scale beams with scaling factors varying from 1 to 22.1 and found increases in flexural strength for the smaller beams ranging up to 43% above those predicted by theory. They concluded that the reinforcing steel, as it existed in a reinforced concrete beam, developed a hyperstrength which was not apparent from tests on the bare wire in a tension testing machine. Mirza et al [8] suggested that the increased flexural strength of small scale beams was due to the increased strain gradient. Magura [15] found an increase of up to 10% over theory in the flexural strength of beams with a cross section of 1 x 2 in. (25.4 x 50.8 mm) which he attributed to an increase in strength of the reinforcing steel. Alami and Fergusson [9] conducted a series of tests on beams designed to fail in diagonal tension, flexural compression and bond. They concluded that models as small as a quarter scale predicted the behaviour of the prototype sufficiently accurately when shear or flexural compression were the causes of failure but not when bond caused failure.

More complex reinforced concrete models have also been tested. The behaviour of small scale reinforced concrete portal frames under cyclic loads has been investigated by Sabnis and White [10]. They used a geometric scaling factor of 4.75 and a model cross section of 1 x $1\frac{1}{2}$ in. (25.4 x 38.1 mm). Good agreement was obtained between model and prototype results for ultimate loads, deflections, moment-rotation characteristics, and overall structural behaviour.

White and Chowdhury [5] studied the response of a series of 2 bay, 3 storey reinforced concrete frames subjected to a fixed level of gravity load and reversing static lateral loads. They initially constructed and tested $\frac{1}{10}$ scale exterior beam column joint connections and compared the results of these tests with full scale prototype test results. The agreement between model and prototype for cracking, beam end deflections and reinforcing steel stresses ranged from good to excellent, and they attributed this to the care with which the model materials were chosen. They concluded that properly designed frames do not deteriorate significantly under severe lateral cyclic loads.

An important contribution was made by Otani and Sozen [16] who subjected a number of small scale 1 bay, 3 storey frames to base motions simulating one horizontal component of representative earthquake motion records. They found that the frames resisted severe base motions without collapse and that the strain hardening characteristics of the steel greatly influenced the test results. A theoretical analysis based on an inelastic model utilizing the hysteresis rule developed by Takeda et al [42] reproduced the large amplitude response of the test frames satisfactorily.

Shiga et al [17] have carried out dynamic loading tests on small scale reinforced concrete structures. The tests were of two types:

(i) small amplitude dynamic loading tests on one and two storey single bay structures excited by a mechanical vibrator clamped to the floor slab. They measured resonance curves by continuously varying the vibrator frequency through the desired frequency range and concluded that the damping was independent of the vibrating frequency and was therefore hysteretic, not viscous;

(ii) large amplitude dynamic loading tests on single storey portal frames mounted on a shaking table which had a large mechanical vibrator clamped to it. They found that the static and dynamic load-deflection hysteresis loops closely resembled each other and could be closely

modelled using a cubic curve. They also found that an envelope curve connecting the peaks of the dynamic hysteresis loops agreed with the static virgin load-deflection curve.

Higashi and Ohkubo [20] subjected a number of small scale reinforced concrete frames with thin spandrel walls to static and dynamic loading tests. The structure was able to carry the repeated reversed static lateral load for over 5 cycles as long as the failure was a flexural one but the strength of the frames decreased drastically when the columns failed in shear. They found that the static and dynamic hysteresis loops were very similar although the maximum strength as determined from the dynamic tests was appreciably lower than that determined from the static tests.

## 1.4 SCOPE OF THE RESEARCH

The aim of this research project was to carry out a fundamental investigation into the response of a reinforced concrete structure to simulated seismic excitation. This could be subdivided into two broad areas:

(i) to study the behaviour of the structure, and

(ii) to give physical verification to the accuracy and applicability of some of the available analytical methods.

It was decided to construct a complete three dimensional structure rather than a two dimensional frame in order that the influence of the connecting floor slabs and lateral beams on the response of the structure could be evaluated. Reinforced concrete was chosen as the modelling material, both because it presents a relatively greater earthquake risk than does structural steel and because it is by far the most commonly used building material in New Zealand. It was appreciated that before the complete structure could be analysed, the behaviour of the critical parts of the structure would have to be evaluated experimentally in order to check the validity of the theoretical predictions.

A real building contains many features which cannot be adequately modelled, such as the influence of the mechanical services and the stiffening effect of partition walls which also will tend to absorb energy and help dampen the response of the building. With so little known about the response of the bare structural members themselves it would be premature to attempt to model these kind of effects but it may

be possible in the future to make some sort of empirical evaluation, the results of which could be used to modify the response of the building. Although these secondary elements will often be badly damaged in a medium or severe earthquake, they are of minor importance compared to the necessity of ensuring that the building does not collapse.

The New Zealand design loading code [18] utilizes an equivalent static load in the design of buildings, the magnitude of which is based on some statistical expectation of the accelerations which the building might experience during its lifetime. The validity of using this equivalent static load is based partly on the performance of existing structures and partly on destructive cyclic loading tests on model buildings and parts of buildings, almost all of which have been static tests. There is, however, a considerable difference between static and dynamic tests, since the transient nature of the dynamic motion permits collapse mechanisms to form within the building but without collapse actually occurring. It was hoped to investigate the strength of the structure under both static and dynamic loading.

The author was fortunate in having access to a comprehensive and flexible inelastic frame analysis program which was recently developed by Sharpe [19] and it was decided to employ this for the main dynamic and structural analysis of the building. This obviated the necessity of the author expending considerable effort in writing a suitable program and although constrained to a limited extent to keep within the options offered by the program, this was considered a very minor drawback to having a reliable and comprehensive means of analysis.

The initial task was the development of the shaking table and the associated testing facilities and a complete description of this work is given in Chapter Two. Chapter Three discusses the laws of similitude governing modelling work as well as the design of the structure and describes the development of the techniques used in its construction. The testing of beams and columns identical to those in the structure is detailed in Chapter Four and the test results are compared with a theoretical moment-curvature analysis.

Some dynamic testing theory is covered in Chapter Five and the tests carried out on the single storey structure are described and analysed. Chapters Six and Seven describe the testing of the two six storey structures and the results obtained. Chapter Six includes a comprehensive section on the torsion induced in lateral members during

sidesway of the building and also a discussion on collapse mechanisms. Chapter Seven describes the main dynamic tests and the accuracy of current analytical methods in predicting the motion of the structure. A summary and discussion of important results is given in Chapter Eight and areas requiring further research are indicated.

# CHAPTER TWO

## MTS TESTING SYSTEM AND ASSOCIATED FACILITIES

### 2.1 INTRODUCTION

In 1968 the University of Canterbury purchased from the Minneapolis Testing Systems Corporation (MTS) a single channel closed loop electro-hydraulic dynamic structural testing system. The model was MTS 903.79 and the testing system was bought primarily to drive a small shaking table, upon which various model structures could be mounted and tested. The testing system was modelled on a similar one which had been purchased by the University of Calgary in Alberta, Canada and information was available on the development of their testing facilities [13].

The MTS 903.79 testing system is comprised primarily of five components which are shown in figure 2-1:

(i) a hydraulic actuator

(ii) a hydraulic pump which supplies oil under pressure to the actuator

(iii) a hydraulic service manifold which controls the oil flow in the hydraulic lines

(iv) a control console which is the electronic command centre controlling the actuator

(v) external programming devices which supply input signals to the control console.

The maximum capabilities of the MTS 903.79 system are:

| | |
|---|---|
| double amplitude displacement | = 4 in. (102 mm) |
| velocity | = 15.7 in/sec (399 mm/sec) |
| acceleration | = 10 g |
| static force rating | = 14,700 lb (65,400 N) |

The basic philosophy of the MTS closed loop control system is the comparison of the desired condition of a controlled parameter with the actual condition of the parameter and resultant generation of correction signals that cause the actual condition to equal the desired condition.

The controlled parameter of the MTS 903.79 system is displacement. The servac is the electronic control centre of the system and it compares the command signal to the feedback signal as detected by a linear variable differential transformer (LVDT) mounted in the hydraulic actuator. If the command signal is changed, this

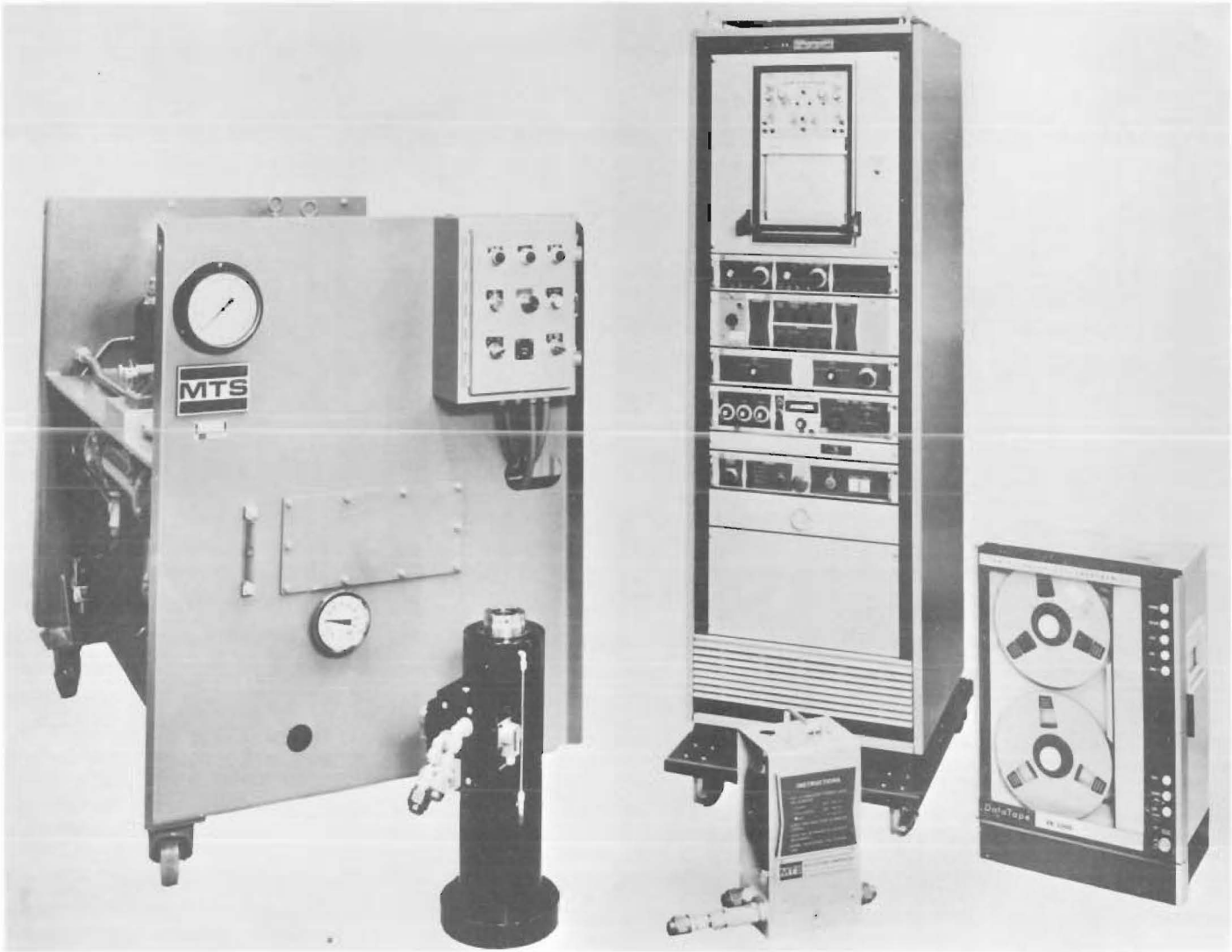


FIGURE 2-1 : MTS MODEL 903.79 STRUCTURES TESTING SYSTEM

will cause a discrepancy between command and feedback and the servac will send out a correction signal, which is amplified by the servoamplifier, to the servovalves which control the flow of hydraulic fluid to the actuator.

As the actual position of the actuator nears the desired position, the difference between command and feedback signals is reduced and proportionally smaller signals are sent to the servovalves. This operation is performed 10,000 times per second and it continues until the command and feedback signals are equal.

## 2.2 MTS COMPONENT DESCRIPTION

### 2.2.1 Model 501.02 hydraulic power supply

Hydraulic pressure is supplied by an electric motor which drives a fixed volume positive displacement pump of the axial piston type. The average output flow is 13.8 UKgal/min (16.6 USgal/min or 62.8 litres/min) although peak flows of 21.7 UKgal/min (26.1 USgal/min or 98.8 litres/min) can be supplied with the help of accumulators mounted in the hydraulic lines. The pump supplies a low output pressure of 100 $lb/in^2$ (0.69 $N/mm^2$) when the hydraulic power is first switched on and the high output pressure is adjustable up to a maximum of 3000 $lb/in^2$ (20.7 $N/mm^2$).

The pump may be operated either locally or by remote control from the control console. A circulating pump ensures that any accidental impurities are filtered out and a running time meter automatically logs the total number of hours of operation of the main pump. A fluid-to-water heat exchange maintains the fluid temperature at a safe level and failsafe devices automatically switch off the pump if the fluid temperature exceeds 60°C or if the volume of hydraulic fluid falls below a certain level.

### 2.2.2 Model 205.32 hydraulic actuator

The hydraulic actuator has a stroke of 4 in. (102 mm) and it is a robust type designed to withstand large side thrusts. The speed of response of the actuator is largely governed by two servovalves which are attached to it. These are Moog model 73-233 series 53 industrial servovalves with a maximum flow rating of 8.33 UKgal/min (10 USgal/min or 37.8 litres/min). The servovalves have a two-stage mechanical feed-

back with a flapper-nozzle pilot stage. An LVDT is mounted in the base of the actuator to sense the displacement of the piston rod.

The force output of the actuator depends on the dynamic conditions prevailing. The piston area is 4.9 $in^2$ (3160 $mm^2$) and a maximum system pressure of 3000 $lb/in^2$ (20.7 $N/mm^2$) gives a static force rating of 14,700 lb (65,400 N). Maximum power transfer across the servovalves occurs at a pressure drop of 1000 $lb/in^2$ (6.9 $N/mm^2$) which establishes the nominal dynamic rating as 9800 lb (43,600 N). This is over-conservative however, and the actual pressure across the piston will generally be midway between these two extremes, giving a force of 12,250 lb (54,500 N).

### 2.2.3 Model 284.11 line tamer service manifold

The hydraulic service manifold is connected into the hydraulic lines between the hydraulic power supply and the actuator and it performs two main functions:

(i) accumulators connected into both the pressure and return legs of the manifold supply the surges of hydraulic fluid demanded by the servovalves and reduce fluctuations and snapping in the hydraulic lines during dynamic programs

(ii) a filter mounted in the pressure leg of the manifold collects contaminants in the fluid to help prevent wear of the servovalves.

### 2.2.4 Model 485.01 control console

The control console is the electronic command centre of the testing system and it is comprised of the following plug-in components.

### 2.2.4(a) Model 413.05 control panel

The control panel houses the failsafe devices which activate if an abnormal condition develops and it provides centralized control of the following functions:

(i) console power on/off

(ii) hydraulic pressure on/off

(iii) simultaneous starting and stopping of programmers and recorders.

### 2.2.4(b) Model 401.03 servac

The servac is the electronic command centre and it provides the summing circuit for the command and feedback signals. The servac controls can be adjusted to obtain optimum performance from the servo loop.

2.2.4(c) Model 401.32 input module

The input module is an auxiliary electronic component which plugs directly into the servac. The input module uses a 10 KHz system to excite the LVDT mounted in the actuator and it amplifies the output of the LVDT and supplies the feedback signal, as well as the command signal, to the servac. The feedback amplifier can be adjusted to give four stroke operating ranges and a set point control can be used to add a static or mean component to the composite command formed at the summing circuit.

2.2.4(d) Conditioner - jack panel

This contains the servoamplifier and the test jacks for monitoring the servoamplifier output, the tape transport output, and the output of the input module.

2.2.4(e) Model 428.02 command mode selector

The command mode selector allows the operator to:

(i) select the programming device (usually the function generator or magnetic tape recorder)

(ii) select the form of the input signal, i.e. either displacement, velocity or acceleration. If velocity or acceleration waveforms are used as input, integrator circuits in the command mode selector will carry out a single or double integration respectively to produce an equivalent displacement command signal

(iii) attenuate the command signal to any desired magnitude using the span control.

2.2.4(f) Model 414.02 recorder input selector

This selects the signals to be recorded on the pen recorder. Any of the following four signals may be independently recorded on either channel:

(i) input signal from the magnetic tape recorder

(ii) command displacement signal

(iii) feedback displacement signal from the LVDT mounted in the actuator

(iv) accelerometer feedback.

2.2.4(g) Brush Mark 280 pen recorder

This chart recorder has 2 channels each of 80 mm width. The pens are fed by pressurized ink and give a trace which dries instantly. Pen response is flat to 35 c.p.s. and essentially flat to 100 c.p.s. The pen sensitivity can be varied continuously from 25 mV to 500 V full channel width and twelve chart speeds are available ranging from 0.05 mm/sec to 200 mm/sec.

2.2.5 Programming

The testing system has no programming device built into it with the exception of the static set point control. The two external programming devices available are briefly described in the following subsections.

2.2.5(a) Hewlett Packard 3310A function generator

This function generator has a frequency range of 0.0005 Hz to 5 MHz and it can be used to generate any of the following regular waveforms: sine, triangular, ramp, square or pulse. The maximum output amplitude is 30 V p-p and all functions may be internally offset by up to 10 V d-c.

2.2.5(b) CEC Datatape VR-3300

The Datatape is a 6-speed 7-channel magnetic tape recorder using all solid-state electronics. It can record signals ranging in frequency from d-c to 20 KHz when used in conjunction with the frequency modulated recording technique. The speed ranges from $1\frac{7}{8}$ in/sec to 60 in/sec (47.6 mm/sec to 1524 mm/sec) and the input voltage can vary up to 10 V d-c although the output voltage is restricted to 1 V rms. The Datatape may be operated either locally or by remote control from the MTS control console. At the time of use, sufficient amplifier cards were available to equip only two of the seven channels.

2.3 TESTING FACILITIES

Prior to the commencement of this thesis work, construction had begun on a welded aluminium shaking table suitable for operation with the MTS 903.79 structures testing system. In addition, a suitable support system for the table had already been purchased. A general view

of the shaking table and the foundation support system is shown in figure 2-2.

### 2.3.1 Shaking table

The shaking table was modelled on one designed by Dawson [13] for use at the University of Calgary. It is 4'-6¾" x 4'-6¾" (1391 mm x 1391 mm) plan dimensions, 11 in. (279 mm) deep and weighs 520 lb (2310 N). The table is supported on either side by a pair of dual Thomson Roundway bearings, which run on 1½ in. dia. (38.1 mm dia.) case hardened roundways. The bearings have a travel life of two million inches (five million centimetres) and they can withstand a maximum vertical load of 4300 lb (19,100 N) when mounted as used on the table.

It is difficult to prevent warping when welding with aluminium and it was found that the surface of the table had a dished appearance, with the centre $\frac{5}{16}$ in. (7.9 mm) below the edges. Consequently, the surface of the table was milled to a depth of $\frac{3}{16}$ in. (4.8 mm) and the small dish remaining at the centre of the table was filled in with araldite. A $\frac{1}{4}$ in. (6.4 mm) thick sheet of aluminium was then glued to the surface of the table using araldite, which increased the minimum thickness of the table surface to $\frac{7}{16}$ in. (11.1 mm). At the same time that the table surface was being milled, a section of the front of the table was also milled to ensure that it was perfectly vertical and square in relation to the table surface. A grid pattern of $\frac{1}{2}$ in. dia. (12.7 mm dia.) bolt holes at 8 in. (203 mm) centres was drilled into the table surface. These holes were drilled into 1 in. dia. (25.4 mm dia.) steel inserts to eliminate wearing.

### 2.3.2 Foundation support system

The foundation support system basically consists of an open box, the sides of which are comprised of channel sections and the front and back of which are formed by steel plates. The case hardened roundways span between the steel plates, parallel to and supported by the channel sections. The actuator is rear-mounted on a supporting structure beyond the front plate and the piston is joined to the table by a connecting rod passing through a hole in the plate. A hole giving access to the underside of the table is provided in the rear plate. The working drawings from which the foundation support system was constructed are presented in Appendix A.

The sides of the box are mounted on steel plates which are bolted to the floor. The foundation sits on a reinforced concrete strongfloor which is 43 $\frac{1}{6}$ ft x 27 ft (13.18 m x 8.23 m) plan dimensions and 2 ft (0.61 m) thick and which is isolated from the rest of the building. Steel inserts of 3$\frac{1}{2}$ in. dia. (88.9 mm dia.) and 6 in. (152.4 mm) long have been placed in the concrete at 15 in. (381 mm) centres with one end flush with the surface of the floor. Each steel insert has a hole drilled into it to accommodate a 1$\frac{1}{2}$ in. dia. (38.1 mm dia.) bolt. Any slight irregularities in the surface of the floor were accounted for by placing packing beneath the shaking table foundations.

It was essential that the table foundations were perfectly rigid but they also had to be sufficiently flexible to enable precise alignment of the actuator and the roundways. The roundways were gripped by steel chucks at their ends and at approximately their third points. The roundway bearings would be operating along only a short length of each roundway, at about the centre of the end thirds of each roundway, and so the roundways were further supported at these locations by two sets of steel wedges, which were designed to allow a large vertical and horizontal adjustment. The roundway supports were adjusted until they were perfectly parallel and horizontal.

The Thomson Roundway bearings were bolted into steel inserts fitted to the sides of the shaking table and the bearings were adjusted until the table ran freely along the roundways. The success of the table support system largely depended on how precisely the actuator could be aligned with the roundways and so considerable time was spent adjusting the actuator base mounting. A length of 2 in. dia. (50.8 mm dia.) steel rod connected the actuator piston to the shaking table.

The connecting rod screwed into an internal thread in the piston whilst the other end fitted through a slightly oversize hole in the front of the shaking table and was secured on either side by special nuts. These nuts had a concave surface on the side nearest the table and the special washers which went with them had a convex surface of the same radius which fitted neatly into them. If the front surface of the table was not perfectly perpendicular to the connecting link, then slip would occur along the curved surface between the nuts and washers as the nuts were tightened, thus preventing any undesirable sidethrusts in the actuator.

Electric resistance strain gauges were placed on the connecting rod and these were routinely checked to determine the magnitude of sidethrust present in the actuator. Practically all strains present in the connecting rod were induced when the nuts were tightened and virtually no change in strain was observed as the table was moved back and forth along the roundways, indicating that the alignment between the actuator and the roundways was almost perfect. The maximum sidethrust that was observed to occur in the connecting link amounted to only 0.7% of the rated static load of the actuator and this was considered insignificant since the actuator was a robust type designed to withstand large sidethrusts.

### 2.3.3 Pump soundproofing

The laboratory in which the shaking table was mounted was located in the midst of graduate student studies and so it was necessary to construct a small soundproof room in which to house the hydraulic pump. Two rooms were actually constructed, one placed inside the other, with a 6 in. (152 mm) airgap separating them. Both rooms were constructed from Plycopyne particle board with Dexion structural framing. A large fan in the ceiling of the inner room drew sufficient air to keep the room cool through an air vent to the laboratory. This air vent was well clad with fibreglass as were the ceiling and walls of the inner room. A hole in one of the inner walls allowed the air to circulate in the gap between the two rooms, which had been partially insulated with fibreglass, before escaping to the laboratory through an insulated vent in one of the outer walls.

All walls were insulated from the floor by rubber pads. A large panel in one wall of each room could be removed to enable the pump to be removed if necessary. A window panel in one wall of each room allowed the control panel of the pump to be observed without having to enter the room. The soundproofing was found to be successful and the occupants of nearby rooms were not disturbed even when the pump was operating for extended periods.

### 2.3.4 Data acquisition

Data acquisition was a problem due mainly to the fact that the recorded displacements and accelerations could not be permanently stored on magnetic tape since only two channels were available for use

on the Datatape and one of these was used to input the command earthquake record to the MTS testing system. This meant that the signals had to be recorded directly onto chart recorders and the number of channels required was sufficiently large that use had to be made of some chart recorders that were unsuitable for the task.

The dynamic displacements were all measured using Hewlett Packard Model 24DCDT-3000 linear variable differential transformers (LVDTs). These operate on a 24 V d-c power supply and have a built-in carrier oscillator and phase sensitive demodulator providing d-c output proportional to linear displacement. They have a stroke range of 6 in. (152 mm) double amplitude with a linearity of ± 0.5% and a sensitivity of 4.4 V d-c/inch.

A Kistler Model 305A servo accelerometer together with matching Model 515 servo amplifier was supplied with the MTS testing system. The accelerometer generates direct current signals proportional to the acceleration forces and the amplifier boosts the signal to up to ± 20 ma and also supplies the accelerometer with regulated ± 15 V d-c. The full scale range is adjustable from 0.1 g to 50 g/volt with an accuracy of 1% and an output of ± 1 V. The nominal accelerometer size is 1 in. dia. x 2 in. long (25.4 mm dia. x 50.8 mm long) and the weight is approximately 3.3 oz (0.92 N).

Three Kyowa AS-10B accelerometers were purchased. These basically consisted of a fluid-damped seismic mass supported by a spring on which foil strain gauges were bonded in a full bridge circuit configuration. The accelerations are then a measure of the strains due to the inertia force of the small mass. The accelerometers could measure accelerations of up to 10 g in frequencies ranging from d-c to 240 Hz. The accelerometer size is a cube of side 16 mm and weight of 0.13 N. They are powered by a 4.5 V d-c battery supply.

The strains from all electric resistance strain gauges were determined using a Budd Model P-350 digital strain indicator. The strain indicator could be used in either a full, half or quarter (internal dummy) bridge configuration. The strain indicators were also used as an amplifier to boost the output from the Kyowa accelerometers.

Apart from the Brush Mark 280 pen recorder supplied as part of the MTS testing system, the only other suitable chart recorder that was available was a Hewlett Packard Model 7402A oscillographic recorder, which is a two-channel, rectilinear ink chart recorder. This recorder

employs all solid-state circuitry and a pressurized ink writing system which dries on contact. Each channel width is 50 mm and the frequency response is d-c to 40 Hz for the full channel width. The maximum chart speed is 125 mm/sec and the sensitivity can vary from 50 mV to 250 V for full channel width.

Two Rapet series RMS-11CPT six channel light-beam galvanometer chart recorders were also used. These produced visible records on direct writing photo-recording paper without chemical dark-room processing. The light sources were tungsten incandescent lamps with a flat frequency response from d-c to 300 Hz. The recorders were very light and compact and chart speeds of up to 200 mm/sec were available. Unfortunately the Rapets recorded current, not voltage, and their very low input impedance drastically reduced the signal available for recording. In addition, the chart width was inadequate, the position of the tungsten lamps could not be altered without removing the chart paper, the trace could not be viewed until several minutes after it was recorded, the recorder sensitivity could not be altered and preservation of the recordings was unsatisfactory.

Some use was also made of two Model PT 2108 Phillips Oscilloscripts. These each had four wide-script channels of width 42 mm. The method of writing was styli on carbon paper up to a maximum frequency of 300 Hz. The chart speed was adjustable up to a maximum of 200 mm/sec using cog wheels. However, these recorders were heavy and clumsy, the clarity of image was poor, the linearity and sensitivity on some of the channels were unstable and their reliability was not such as to inspire confidence.

### 2.3.5 Loading reaction frame

A structural framework was required around the shaking table to act as a reaction frame from which the lateral loads could be applied to the model structure during the static loading tests. These static loading tests, in which the table was stationary, were conducted in order to obtain a comparison between the static and dynamic behaviour of the model structures. Also, a scaffolding was required during construction of the model structure and to provide access for examination of the damage caused to the model structure during testing. The framework that was eventually decided upon was suitable for all of these purposes.

Two lengths of universal column (both 8 x 8 in. (203 x 203 mm) UC and 6 x 6 in. (152 x 152 mm) UC were used) were bolted to the laboratory floor at either end of the shaking table directly in line with the columns of the model structure. A series of bolt holes was drilled up the UC

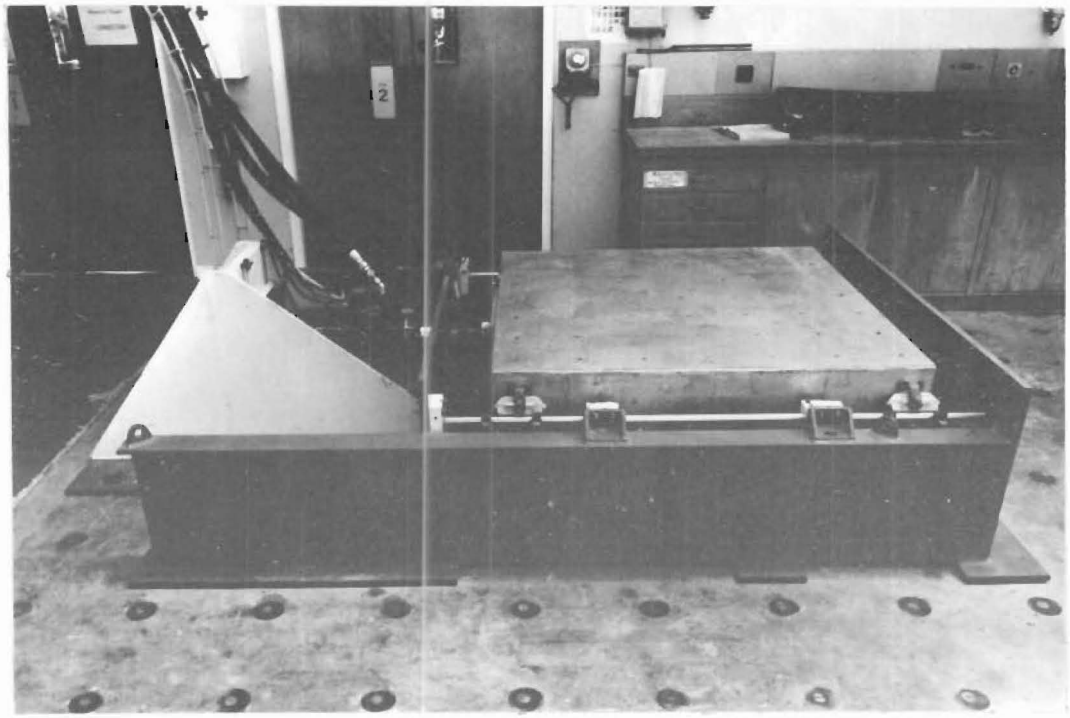

FIGURE 2-2 : GENERAL VIEW OF SHAKING TABLE AND FOUNDATION SUPPORT SYSTEM

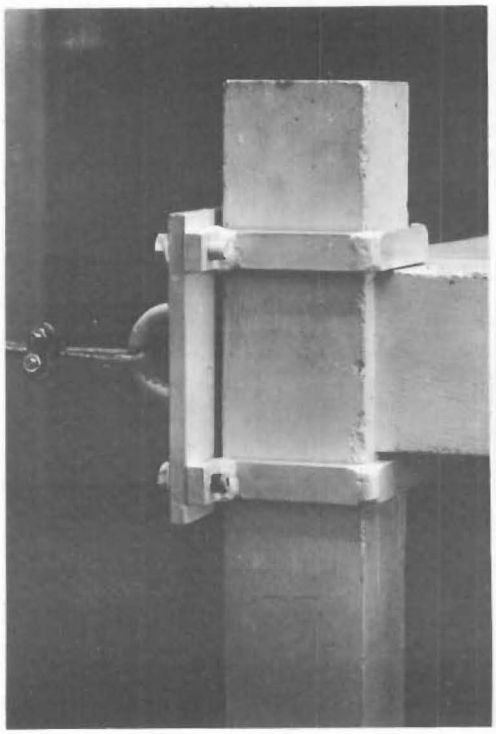

FIGURE 2-3 : COLUMN LOADING YOKES

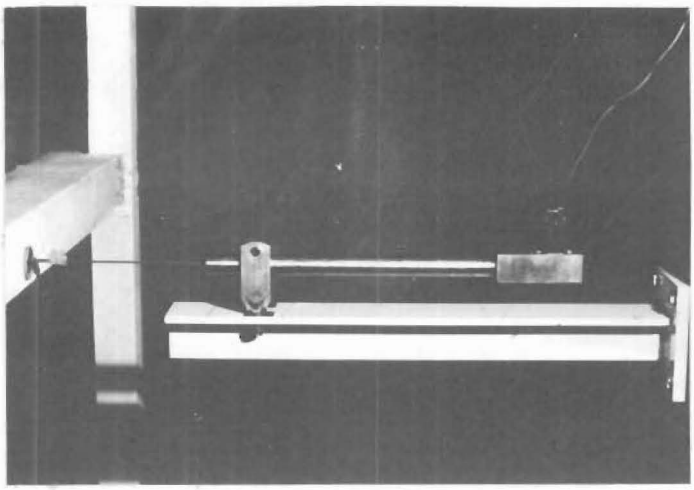

FIGURE 2-4 : DEFLECTION MEASUREMENT

sections and short steel arms were bolted on at levels corresponding to each floor of the model structure. Each loading arm supported a steel pulley mounted at its end. Yokes were placed around the two nearside columns at each floor level as shown in figure 2-3 and to these were attached wire ropes which ran over the pulleys and which were connected to buckets at the other end. Lateral loading of the model structure was achieved by placing steel weights in each bucket.

The basis of the scaffolding consisted of 7 ft (2.13 m) lengths of rectangular hollow section (RHS) of dimensions 2.5 x 1.5 x 0.160 in. (63.5 x 38.1 x 4.06 mm) which were bolted to the UC sections, spanning laterally across each end of the shaking table. Wooden planks were placed upon these making it possible to move completely around the model structure. The RHS members could easily be moved up or down the UC sections, making the platform height readily adjustable and sufficient material was available for two platforms. Additional lengths of RHS were available to span longitudinally between the UC sections and these formed a brace to which were clamped the steel backing frames when the model test structures were initially mounted on the shaking table.

All deflection measurements were made from a braced 6 x 6 in. (152 x 152 mm) UC bolted to the laboratory floor at one end of the model structure. Supporting arms were attached at each floor level and on these were mounted either the Hewlett Packard LVDTs or Mercer dial gauges, depending on whether the tests were static or dynamic. All measurements were taken from the centre of the lateral edge beam. The LVDTs were attached to the structure by standard electrical wire connectors which screwed onto the LVDT rod and onto a short length of wire glued to the structure. Deflection measurement using an LVDT is indicated in figure 2-4.

## 2.4 LIMITATIONS ON THE USE OF THE SHAKING TABLE

### 2.4.1 Actuator force

The maximum acceleration that may be applied to the shaking table is dependent on the force output of the actuator and on the mass of the model and table. Assuming that the accelerations of the table and the model are the same then . . .

$$F = (W_t + W_m)\frac{\ddot{x}}{g}$$

where $W_t$ = weight of shaking table = 520 lb (2310 N)

$W_m$ = weight of model structure = 2860 lb (12,990 N)

$F$ = actuator force = 12,250 lb (54,500 N)

Therefore the maximum acceleration which may be applied to the table is ...

$$\ddot{x} = 3.62\ g = 2\pi^2 X f^2$$

thus $$X = \frac{70.7}{f^2} \qquad (2\text{-}1)$$

where $X$ = double amplitude displacement (inches)

$f$ = frequency

## 2.4.2 Allowable bearing force

The strength of the Thomson roundway bearings limits the maximum acceleration that may be applied to the shaking table given a particular size and weight of model structure. With reference to figure 2-5, the overturning moment due to the shaking table may be neglected, then ...

bearing force due to dead load = $\frac{1}{4}(W_t + W_m)$

= 850 lb

bearing force due to overturning moment = $W\frac{\ddot{x}}{mg} \times 6.5 \times \frac{1}{4} \times \frac{1}{2}$

thus $P = 2320\ddot{x}$ lb

allowable bearing force = 4300 lb

$= 850 + 2320\frac{\ddot{x}}{g}$ lb

therefore $\ddot{x} = 1.48\ g$

which leads to $$X = \frac{29.0}{f^2} \qquad (2\text{-}2)$$

## 2.4.3 Servovalve capacity

The servovalve response is primarily related to the valve's pilot stage response and the flow capacity of the pilot stage in driving the main valve spool. The servovalve flow is proportional to the valve opening and the pressure drop across the valve. Fluid compressibility also affects the frequency obtainable for a certain displacement. Assuming that the rated load occurs at a pressure of 2500 lb/in$^2$ (17.25 N/mm$^2$), then it can be shown [21] that the maximum velocity of the actuator is limited such that ...

$$X = 0.251\frac{Q}{f} - 0.039 \text{ (inches)} \qquad (2\text{-}3)$$

where $Q$ = flow capacity of the servovalves (USgal/min).

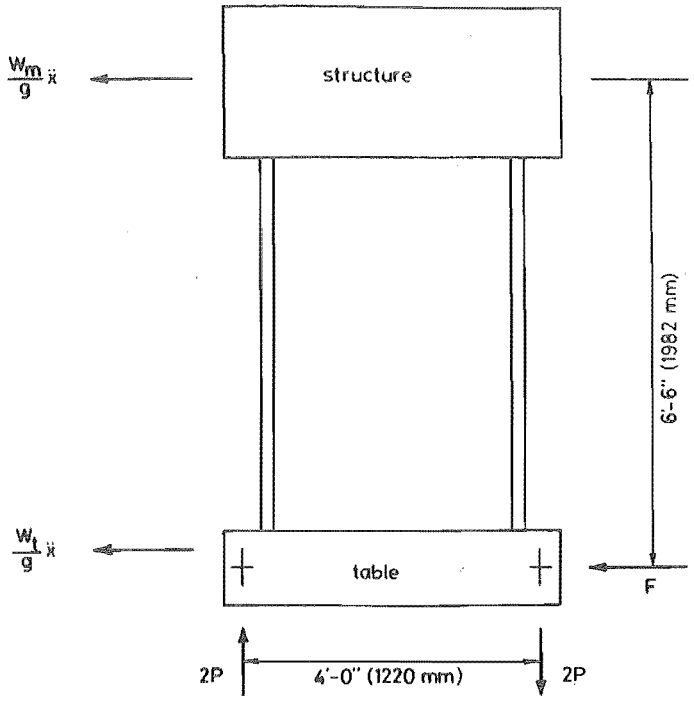


FIGURE 2-5 : IDEALISED MODEL OF THE STRUCTURE AND TABLE USED TO DETERMINE THE BEARING FORCES

The flow capacity of the Moog Series 73 servovalves is constant at 10 USgal/min each up to a frequency of 45 c.p.s., after which it decreases. At a flow rating of 20 USgal/min, equation 2-3 becomes ...

$$X = \frac{5.02}{f} - 0.039 \text{ (inches)} \qquad (2\text{-}4)$$

### 2.4.4 Oil column resonance

The oil which is confined within the actuator exhibits elastic behaviour and can therefore act as a spring. The system may be analysed as a two spring system consisting of the oil column spring and the table mass and of an idealised lumped mass structure and its equivalent spring stiffness. If the actuator piston shakes at a frequency which is close to the natural frequency of the oil column spring and table mass, then resonance will occur, rendering good closed loop control difficult. However, because of the great discrepancy in stiffness between the oil column spring and the structure, little interaction between the two springs occurs. The two natural frequencies of the complete system are

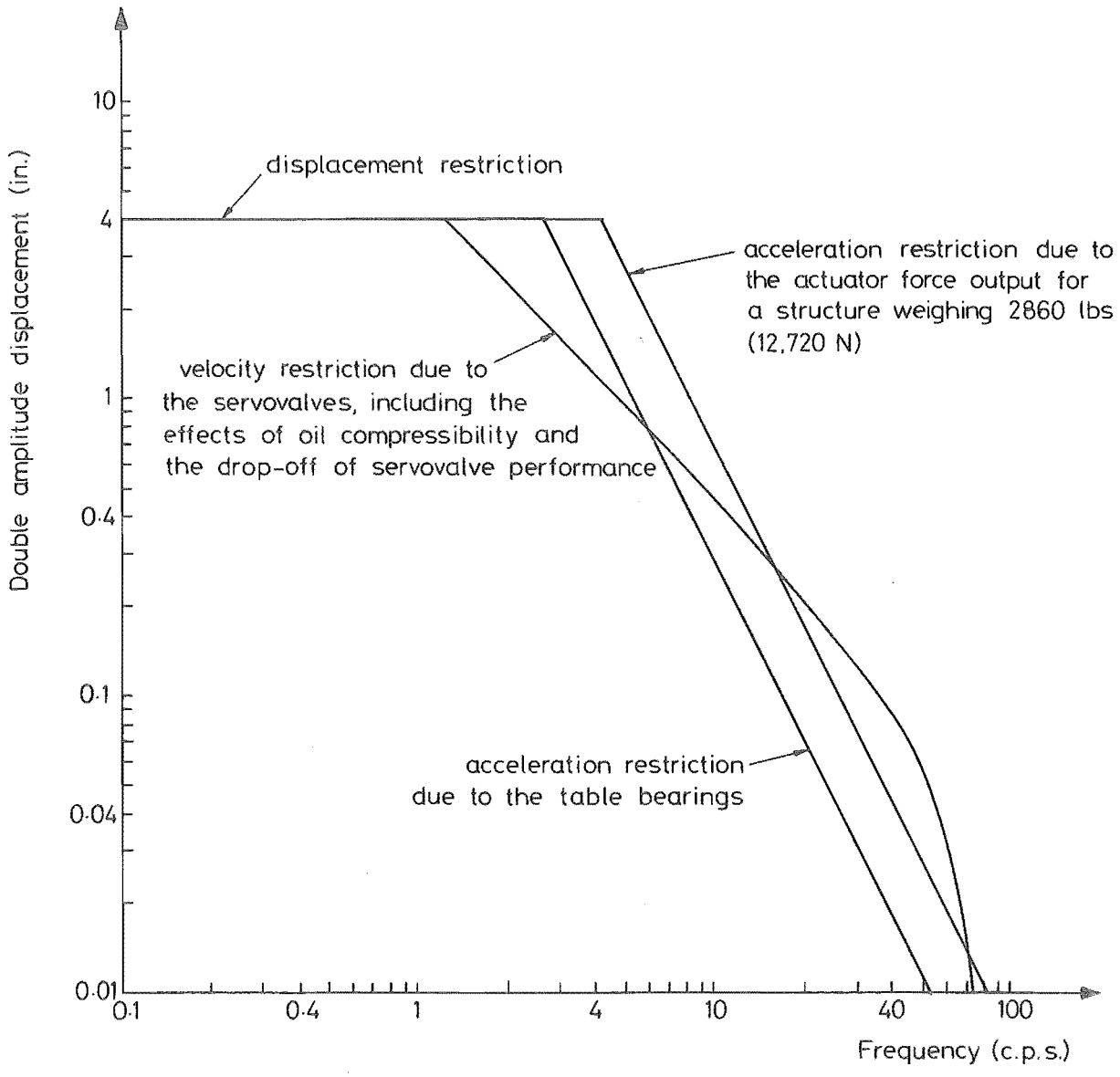


FIGURE 2-6 : THEORETICAL SYSTEM PERFORMANCE

very close to the natural frequency of the structure acting independently as a single degree of freedom system and to the natural frequency of the table mass acting with the oil column spring as an independent single degree of freedom system. This latter natural frequency is over 100 c.p.s which is outside the operating range of the system.

## 2.5 SYSTEM PERFORMANCE

### 2.5.1 Programming

The command waveform from either the function generator or the Datatape may take the form of either displacement, velocity or acceleration The velocity or acceleration programs must have a frequency component greater than about 3 c.p.s.; an amplifier frequency cut-off will not integrate any frequency components of less than 3 c.p.s. The span control attenuates the amplitude of the command signal and operates in terms of percentage of maximum displacement (4 in. = 102 mm), velocity (20 in/sec = 508 mm/sec) or acceleration (10 g). In fact, the peak acceleration is limited according to the mass of the shaking table and model structure and the flow capacity of the servovalves limits the maximum velocity to 15.7 in/sec (399 mm/sec), even though the accumulators can boost the peak hydraulic supply sufficiently to attain the maximum speed of 20 in/sec.

An important feature of the testing system is that it can be programmed to follow irregular waveforms, such as those which might occur as a result of an earthquake. An account of the techniques used to program an earthquake record and the success with which the waveforms were reproduced is included in Chapter 7.

### 2.5.2 Performance

A series of tests were carried out to determine whether the performance of the testing system was accurately described by the equations developed in Section 2.4. Two controls on the servac can be adjusted to obtain optimum performance from the system: the stability control and the gain control. The stability control prevents instability in the loop and the gain control affects the speed with which the system responds to a command signal by controlling the amplitude of the correction signal which the servac sends to the servovalves when a discrepancy exists between the command and feedback signals.

The unloaded shaking table was subjected to a sinusoidal motion at a constant command displacement amplitude and the frequency was gradually increased until the amplitude of the table movement decreased. Theoretically the amplitude of the table response should be constant up to a certain frequency and it should then reduce sharply but it was found that the reduction begins gradually and it is difficult to pinpoint a precise location at which it could reasonably be said that the reduction began.

Figure 2-7 presents graphs of response amplitude versus forcing frequency for double amplitude command displacements of 2 in. (50.8 mm) and 0.2 in. (5.08 mm) respectively. The effect of gain on the system performance was marked. The large amplitude low frequency programs seem to favour a high gain setting of up to 70% whereas the small amplitude high frequency programs become unstable at high gains and the best response for these was obtained with a gain of 50%. The stability control seemed to have no effect on the performance of the system.

Examination of figure 2-7(a) indicates that the response amplitude does not reduce significantly below the command amplitude of 2 in. (50.8 mm) until a forcing frequency of 3.35 c.p.s. is attained. However, according to figure 2-6 for the theoretical system performance, the maximum velocity is restricted by the flow capacity of the servovalves and the maximum frequency which may be attained at an amplitude of 2 in. is only 2.5 c.p.s. The reason for the discrepancy is that if the system performance is limited by the maximum velocity of the actuator, then the table response waveform, instead of remaining sinusoidal, will begin to triangulate, reducing the peak velocity required but allowing an increase in the average velocity. Thus the measured response of the table, such as given in figure 2-7, may be misleading because no account is taken as to whether the quality of the waveshape is maintained.

The system was programmed for a square wave of amplitude 1 in. (25.4 mm) and frequency of 0.5 c.p.s. and the gain was adjusted for optimum performance. The table response was poor at low gains but at high gains the system became unstable and overshoot occurred with a subsequent oscillation about the correct displacement. The optimum gain setting appeared to lie somewhere between 50% and 60%.

An earthquake contains many different amplitudes and frequencies but only one gain setting may be used for each earthquake run. MTS suggest that the earthquake waveform should be run at various gains and the gain giving best response chosen on a trial and error basis, but it is often

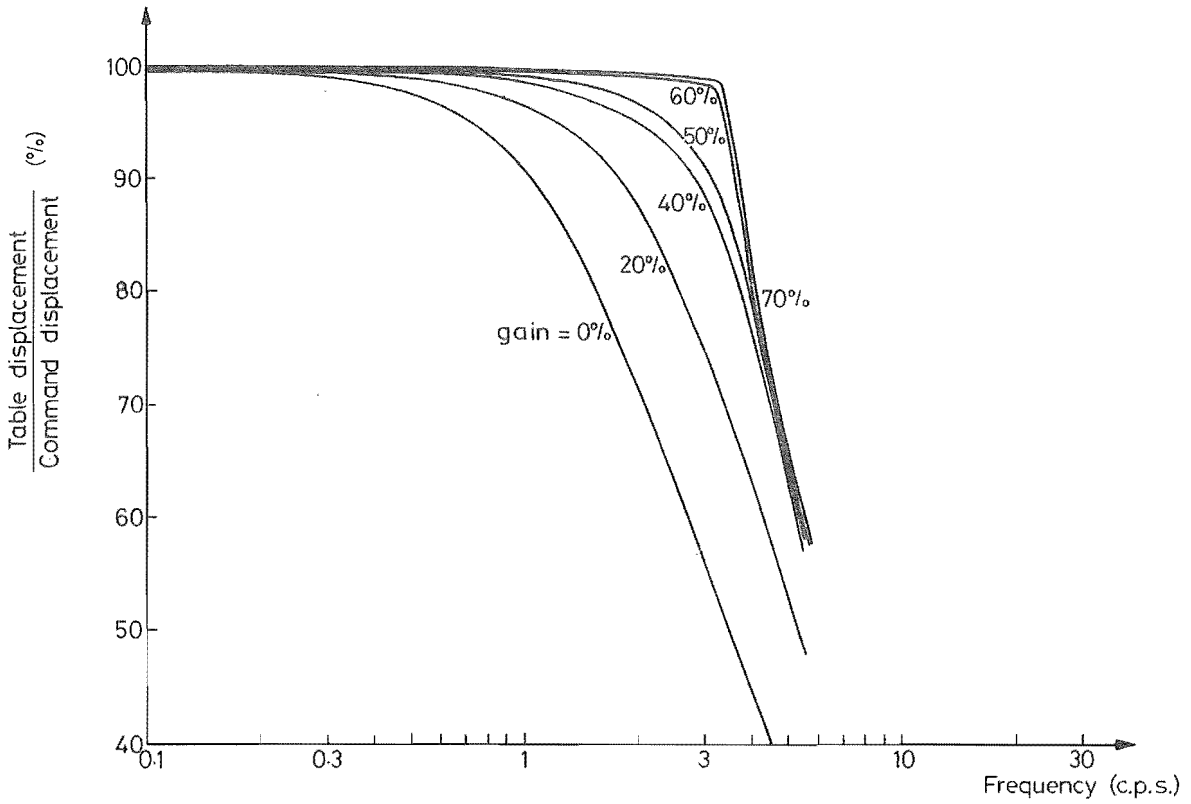


(a) COMMAND DOUBLE AMPLITUDE DISPLACEMENT = 2 in. (50·8 mm)

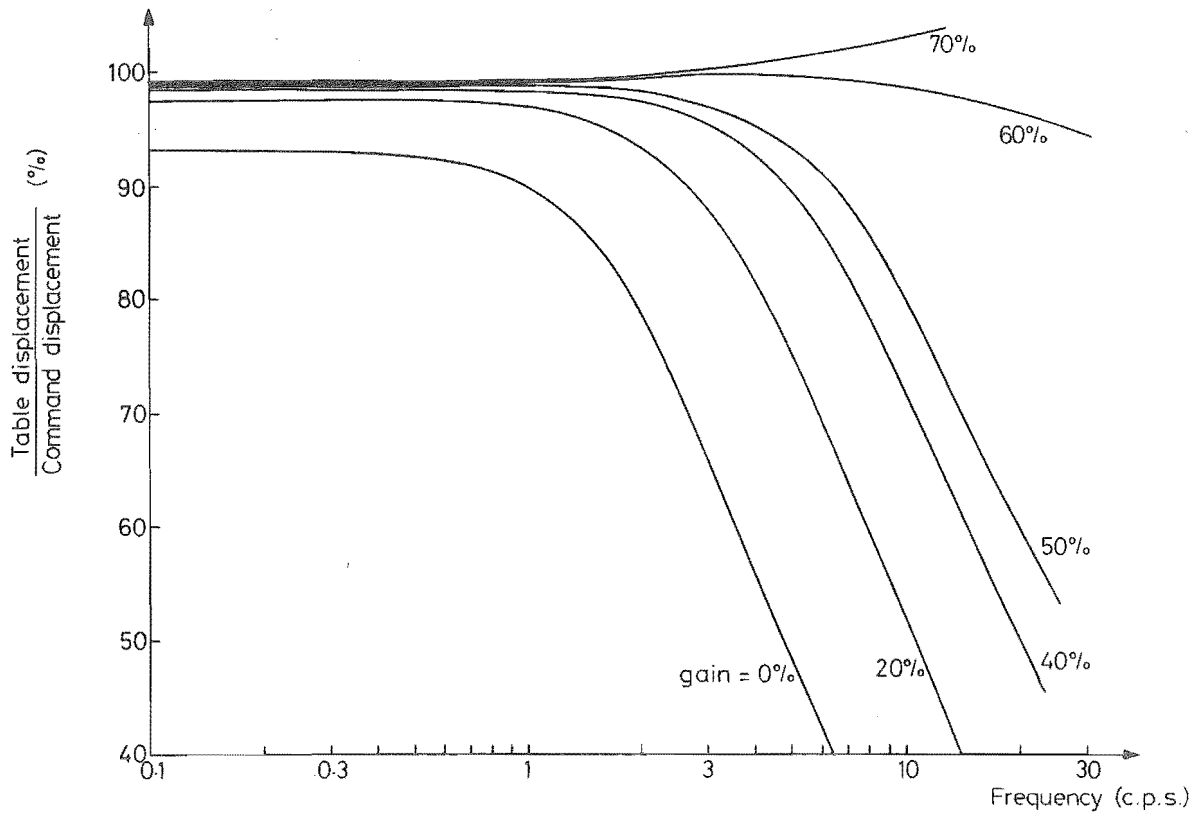


(b) COMMAND DOUBLE AMPLITUDE DISPLACEMENT = 0·2 in. (0·51 mm)

FIGURE 2-7 : MEASURED TABLE RESPONSE

not possible to carry this procedure out. Since a compromise must be reached between speed of response and system instability, a gain of 50% would be a reasonable estimate.

### 2.5.3 Faults

During the course of evaluating the performance of the testing system, it was noticed that occasionally unprogrammed transients were being applied to the actuator piston and that over a period of time these were increasing in frequency and severity. Little assistance was forthcoming from the manufacturers and considerable time was spent trying to trace this fault, spread over a period of about eighteen months. The fault was finally traced to a transistor located in the MTS model 401.32 input module and no further transients occurred after this transistor was replaced.

# CHAPTER 3

# DESIGN OF THE MODEL STRUCTURES

## 3.1 INTRODUCTION

This chapter discusses the factors affecting the design of small scale model structures, details some critical aspects of the design procedure and describes the techniques used to construct the model building structures.

The aim of the research project was to investigate the response of multi-storey reinforced concrete building structures to seismic motions, and the shape of the structure was kept as simple as possible consistent with this aim. The model structure then evolved as a building six storeys high with a single bay in each direction. The columns and longitudinal beams (those beams framing in the direction of the applied forces) were cast monolithically and were joined at each floor by a reinforced concrete slab and lateral beams.

The number of six storey model buildings constructed was two and each took some four to six months to complete. The first model building was tested primarily using static lateral loads whilst the second was tested under dynamic lateral loading. Prior to these tests a single storey model structure of identical horizontal dimensions and reinforcement ratios was built primarily in order to check and evaluate the techniques which were to be used in the construction and testing of the six storey structures.

## 3.2 SIMILITUDE REQUIREMENTS

The scales of size, loading and material properties of the model can be related to those of the prototype by the conditions of similarity. These are generally derived by dimensionless analysis and are summarized in Buckingham's Pi Theorem:

$$\phi_p = \phi_m \left(\pi_1 , \pi_2 , \pi_3 \ldots . \pi_n\right) \qquad (3\text{-}1)$$

where $\phi$ is a particular variable under consideration

and $\pi_1 \ldots \pi_n$ are dimensionless ratios

### 3.2.1 Perfect modelling

A perfect model is obtained when each and all of the dimensionless ratios $\pi_i$ remain unaltered in passing from the prototype to the model. The correspondence between $\phi_p$ and $\phi_m$ is then absolutely general.

To examine the possibility of perfectly modelling a prototype building structure, the independent variables were chosen as mass, length and time and all other variables were defined in terms of these. The independent variables were then combined with each of the dependent variables to form dimensionless ratios and the application of Buckingham's Pi Theorem to these gave the scaling factors shown in table 3-1.

Most of the scaling conditions can be easily satisfied, with the exception of that relating to the specific mass, since it means that the smaller the scale of the model, the denser the model material must be. This requirement can usually only be partially relieved by the use of a very weak modelling material and so it must be satisfied artificially. If gravity forces alone acted on the prototype, then an auxiliary gravitational field could be used in order to increase the effective weight of the structure. If the prototype is to be tested dynamically, however, then the correct simulation of the inertia forces requires that the accelerations applied to the model and prototype should be the same. The most favoured solution to this problem is to attach weights to the model structure; however, apart from altering the distribution of mass, the feasibility of this method drastically reduces, as the scale of the model is decreased, due to the large additional weight necessary.

### 3.2.2 Distorted modelling

In situations such as dynamic testing, where the laws of similitude impose stringent restrictions on the model structure, the concept of a distorted model is often useful. For a distorted model, the effects of a possible alteration of a dimensionless ratio $\pi_l$ are offset by the alteration of another dimensionless ratio $\pi_k$, thus maintaining the correspondence between $\phi_m$ and $\phi_p$. The use of such a model is subject to certain limitations in that it holds true only with respect to the quantity (or quantities) for which the offsetting has been assured.

The dynamic response of a structure depends on the relationship of two types of force which derive from totally different sources:

(i) inertia force $F_i$

(ii) restoring force $F_r$

TABLE 3-1 : SCALING FACTORS FOR PERFECT AND DISTORTED MODELLING

| Quantities \ Similitude | | Ratios of prototype quantity to model quantity | | |
|---|---|---|---|---|
| | | Perfect | Froude | Cauchy |
| length | L | L | L | L |
| modulus of elasticity | E | f | f | f |
| specific mass | ρ | $fL^{-1}$ | ρ | ρ |
| area | A | $L^2$ | $L^2$ | $L^2$ |
| volume | V | $L^3$ | $L^3$ | $L^3$ |
| mass | M | $fL^3$ | $\rho L^3$ | $\rho L^3$ |
| velocity | v | $L^{\frac{1}{2}}$ | $L^{\frac{1}{2}}$ | $f^{\frac{1}{2}}\rho^{-\frac{1}{2}}$ |
| acceleration | a | 1 | 1 | $f\rho^{-1}L^{-1}$ |
| pressure | p | f | ρL | f |
| force | F | $fL^2$ | $\rho L^3$ | $fL^2$ |
| time | T | $L^{\frac{1}{2}}$ | $L^{\frac{1}{2}}$ | $Lf^{-\frac{1}{2}}\rho^{\frac{1}{2}}$ |
| frequency | f | $L^{-\frac{1}{2}}$ | $L^{-\frac{1}{2}}$ | $L^{-1}f^{\frac{1}{2}}\rho^{-\frac{1}{2}}$ |
| strain | ε | 1 | $\rho L f^{-1}$ | 1 |
| stress | σ | f | ρL | f |

Notation: L = length scaling factor

f = stress scaling factor

ρ = specific mass scaling factor

Pereira and Priestley [24] have shown that for dynamic testing, the model should be distorted such that the ratio of these two forces remains unchanged in passing from the prototype to the model.

$$\text{i.e.} \quad \left(\frac{F_i}{F_r}\right)_p = \left(\frac{F_i}{F_r}\right)_m$$

The inertia force, $F_i$, is derived from mass x acceleration and has the dimension $\rho L^4 T^{-2}$.

According to the physical nature of the potential energy generating the restoring force, two idealised extremes can be defined: an elastic restoring force (Cauchy) or a gravitic restoring force (Froude).

(i) Cauchy similitude is applicable when $F_r$ derives from an elastic potential and has the dimensions $EL^2$ and thus corresponds to ...

$$\left(\frac{F_i}{F_r}\right) = \frac{\rho v^2}{E}$$

(ii) Froude similtude is applicable when $F_r$ derives from a gravitic potential and has the dimensions $\rho L^3 g$ and thus corresponds to ...

$$\left(\frac{F_i}{F_r}\right) = \frac{v^2}{Lg}$$

The response of a multi-storey building will derive principally from an elastic potential and so the Cauchy similtude is more applicable. This does approximate the problem however, since in reality both gravitic and elastic forces are always present. The scaling factors resulting from the adoption of either the Cauchy or Froude similitude are presented in table 3-1.

The advantage of adopting the Cauchy similitude criterion is that it allows the choice of any specific mass scaling factor desired. However, the disadvantage is that the criterion also results in a further "speeding up" of the earthquake record, which means that the accelerations applied to the model must be very much greater than those applied to the prototype. This presents little problem insofar as horizontal accelerations are concerned but application of this criterion to vertical accelerations would require the introduction of an auxiliary gravitational field.

In situations where the earthquake effects are very much greater than the gravity load effects, this requirement of an additional gravitational field can be waived without introducing unreasonable errors, but in general this cannot be the case. Correct gravity loading is

particularly important in multi-storeyed buildings, where a reduction in gravity load could lead to tension in the outer columns.

### 3.2.3 Miniature structures

The major difficulties in small scale modelling of prototype structures may be summarized as follows:

(i) perfect modelling.

The problem was to find a modelling material sufficiently dense to satisfy the relation $\rho_p = \frac{f}{L} \rho_m$. If the length scaling factor is of the order of 5, then it is obvious this condition could only be met by a substantial alteration in the stress scaling ratio $f$, which would require the use of unreasonably weak materials.

The most general method of avoiding this situation is to increase the mass by placing additional weights on the structure. If $L = 5$ this means that the weight of the structure would have to be increased fivefold. Attachment of these weights is difficult to achieve without either introducing any additional structural actions or altering the mass distribution of the structure and the weights may interfere with the measurement and/or observation of the response of the structure.

(ii) distorted modelling.

The problem here differs slightly from that for the perfect modelling case in that only the gravitational acceleration needs to be increased, rather than the mass of the structure. The solutions to this problem are difficult and are really only applicable in special circumstances. Magnets could be used to exert a vertical force on the steel contained in the structure but difficulties would be encountered in ensuring an even magnetic field. The axial compression in the columns could be increased by vertical prestressing although this would provide a constant axial load in the columns rather than one which decreases up the height of the structure and problems may also be encountered in fitting the prestressing wires into the column. The value of the gravitational acceleration could be increased by placing the model in a centrifuge but this method is not feasible for dynamic testing; nor is the testing of the model immersed in an inverted position in a dense fluid so that the upthrust experienced by the model more than compensates for the weight of the model itself.

Whilst some researchers [16] have adopted techniques to overcome the modelling problem, others [13] have opted for a different concept and

have constructed and tested miniature buildings, rather than models of some prototype building. The concept of modelling is then not applicable in this case; the small structure is designed in the same manner as are larger buildings and its response is analysed strictly in terms of its own behaviour.

Because the conditions of similitude are not satisfied, care needs to be exercised when extrapolating the results of tests on the small structures to larger buildings. The results will be valid when used as a basis for verifying the accuracy and applicability of various analytical solutions and will give a qualitative understanding of the response of reinforced concrete structures to seismic motions. In a quantitative sense not all the test results can be directly extrapolated but as long as this fact is borne in mind they will still furnish valuable information on the response of larger buildings.

## 3.3 CHOICE OF STRUCTURE SIZE AND SHAPE

The scale of the structure was limited primarily by the size of the shaking table. The shaking table was designed bearing in mind the size of the MTS structural testing system which had been purchased and was intended as a general research tool.

The slenderness ratio of the members of small structures are greater than those of larger structures unless the small structure is a perfect model of the larger structure, in which case they are the same. The reason is that if a geometric scaling factor $L$ relates the size of a large structure to a smaller one of similar design, then in the smaller structure the dead load bending moments reduce by a factor of $L^4$ as compared with the larger structure (unless the specific mass of the smaller structure is increased by a factor of $L$, as for a perfect model) whereas the moment resisting capacity of a section reduces by only $L^3$ if the ratio of steel to concrete area remains the same. If the steel area is reduced by a factor of $L$ this results in undesirably low steel percentages and so the size of the section must be reduced.

There is a point beyond which it is undesirable to further reduce the size of the members. Once this point has been reached in an earthquake governed design, moments in the various members can only be increased to yield by the provision of additional weight, which may take the form of additional storeys.

It was decided that the structure should be multi-storeyed and should be as simple as possible, both for ease of analysis and for ease of construction. The modelling material was chosen as reinforced concrete as this is the most commonly used building material in New Zealand and successful small scale model studies in reinforced concrete have been reported elsewhere [9, 16, 17, 20].

The small structure then evolved as a building six storeys high, with a 24 in. (610 mm) storey height between beam centres. It has a single bay in each direction with a column centre to centre distance of 40 in. (1016 mm). The columns were 2 in. (50.8 mm) square and were connected by edge beams 2.4 in. (61.0 mm) deep and 1.2 in. (30.5 mm) wide. A 1.0 in. (25.4 mm) slab was cast monolithically with the columns and edge beams. The dimensions of the structure are indicated in figure 3-1.

Because of the requirement of as much mass as possible in order to yield the beams under dynamic loading, it was decided to take into account some additional dead loads which would normally occur in a structure, such as plaster finish on floors, suspended ceilings and partition walls which may account for about 35 $lb/ft^2$ (0.241 $N/mm^2$). For the small structure 7 $lb/ft^2$ (0.048 $N/mm^2$) was allowed for these features. In addition to this the New Zealand Code [18] allows a seismic live load of 20 $lb/ft^2$ (0.138 $N/mm^2$) and so a load of 27 $lb/ft^2$ (0.186 $N/mm^2$) was applied at each floor level by means of attached weights.

This applied load was still very much less than that which would have been required for a perfect model. Prior to the decision not to attempt to model a prototype structure, a preliminary analysis was carried out on a structure whose dimensions were five times those of the small structure finally constructed. A one fifth scale model of this large structure would have required a total weight per floor of 2180 lb (9697 N) of which 1744 lb (7758 N) would be provided by the attachment of additional weights whereas the small structure finally constructed had a storey weight of 476 lb (2117 N) of which only 282 lb (1254 N) was made up of extra weights. For a perfect model, the attachment of these weights to each floor level such that the distribution of mass over the structure remained unaltered and no undesirable structural actions were introduced would be difficult to achieve satisfactorily.

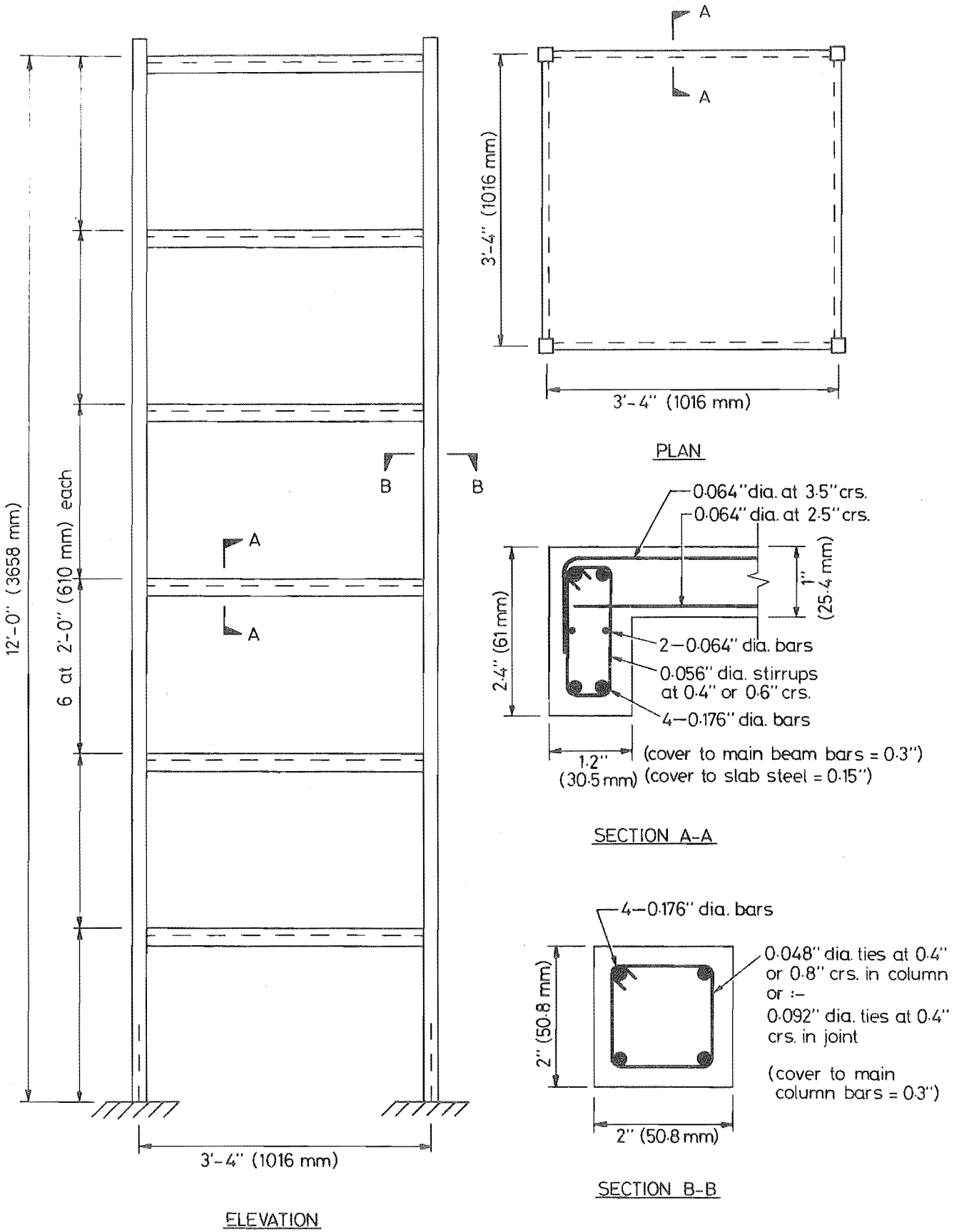


FIGURE 3-1 : THE STRUCTURE

## 3.4 ASPECTS OF THE DESIGN

### 3.4.1 Introduction

The building was designed in 1971 at a time when the New Zealand Building Code was undergoing considerable alteration, ultimately culminating in the 1973 Draft Revision [18]. The design method was by ultimate strength theory and the load factors used were those proposed at that time by the Draft Revision. The structure was assumed to be a non-public building in earthquake zone A with a short natural period and the ultimate static lateral design acceleration was thus 0.15 g.

The floor slabs were designed by yield-line theory utilizing a ratio of hogging to sagging yield moments of 5 to 7. A vertical load analysis of the structural frames was carried out as well as a lateral load analysis based on the methods of Muto [25]. All members were designed for full ductility using the recommendations of Appendix A of ACI Code 318-71 [26].

Some critical aspects of the design procedure are dealt with in the following subsections,and the working drawings giving the reinforcing details may be found in Appendix B.

### 3.4.2 Choice of code loading

At the time the structure was designed the New Zealand loadings code was under revision and so the load factors used in the design were based on the values expected to be recommended in the revised code. When the Draft Revision [18] finally appeared in 1973, it differed somewhat in its treatment of loading, although for the structure under consideration these differences were not expected to be significant.

The load factors actually used in the design of the building were:

dead load + live load $U = 1.4D + 1.7L$

earthquake load $U = 1.05D + 1.3L_e + E$

$U = 0.9D + E$ (reversal case)

where

$D$ = dead load

$L$ = live load

$L_e$ = seismic live load = $\frac{L}{3}$

$U$ = total ultimate load

$E$ = ultimate design earthquake load = $CW_t$

$W_t$ = total seismic load = $D + L_e$

$C$ = ultimate seismic coefficient = 0.15

The value of C depends upon the earthquake risk zone in which the building is located, the fundamental period of vibration of the building, the importance of the building and the energy absorbing characteristics of the building. In the 1973 Draft Revision of the New Zealand Code [18], this latter factor is subdivided into separate considerations of the type of structure and of the building material used and a usage consequence risk factor is also incorporated. For the building under consideration, these additional factors do not alter the value of the ultimate seismic coefficient used in the design however.

The 1973 Draft Revision retains the distribution of the design earthquake lateral loads up the height of the structure which has been long used in New Zealand. Most Codes of Practice require a triangular distribution over the height of the building whereas for any building with a height to depth ratio of the horizontal force resisting system equal to or greater than 3, the New Zealand Code requires that 10% of the total earthquake load be placed at the top of the building and that the remaining 90% be triangularly distributed over the full height of the building.

### 3.4.3 Beam-column joint core design

The primary criterion to be satisfied in an exterior beam-column joint core design is the shear force which must be transferred across the joint. This shear force is equal to the yield force of the tensile steel of the beam framing into the joint minus the shear force in the column above the joint. Ties should be provided to resist the total shear force less the shear force carried by the concrete.

Diagonal tension can be particularly critical in a joint core, especially with exterior columns where the axial load may often be small. Bond conditions are poor because of the cracked concrete and also because of small available bond lengths and inadequate concrete placement in the confined joint region. The bond length for the column steel may be insufficient and often leads to a vertical splitting failure at the outside of the column. Considerable transverse reinforcing is necessary to prevent lateral instability of these column bars and to confine the joint concrete.

The transverse reinforcing required in the joint core was 13g ties at 0.4 in. (10.2 mm) centres, which is considerably more steel than that required for the normal column shear reinforcement outside of the joint core region. The column ties required were 18g ties at 0.4 in. (10.2 mm) centres within 4d i.e. 6.4 in. (163 mm) of the column end and at 0.8 in. (20.3 mm) elsewhere. The closer spacing near the ends of the column was

to ensure that adequate ductility would be available in the column in the event of the formation of a plastic hinge.

The reinforcing forming the beam-column joint region is shown in figure 3-7. The dimensions of each reinforcing wire gauge size used are given in table 3-2.

### 3.4.4 Torsion design

Torsion is induced in the edge beams in proportion to their torsional stiffness when gravity loads act upon the slab. The total torques at the beam ends is equal to the sum of the negative moments acting along the edge of the slab and the maximum negative moments were assumed to occur under full dead load plus live load. The torque induced into the edge beams was assumed to be resisted by both the concrete and stirrups and was proportioned accordingly.

A combined torsion and shear design was carried out for the beam stirrups assuming that the ultimate negative moment of resistance was developed in the slab along the whole length of the edge beam and it was found that torsion accounted for over 80% of the beam stirrup steel required. The stirrup size was 17g and they were at 0.6 in. (15.2 mm) centres except within 4d i.e. 8 in. (203 mm) of the beam ends where ductility requirements necessitated a reduction in spacing to 0.4 in. (10.2 mm).

Longitudinal steel was also required for torsion and this was distributed over the section, requiring the placement of two 16g wires at mid-height and an increase in the size of the top and bottom main reinforcing wires to 7g. As is usual in design, no consideration was given to the torsion introduced in those beams perpendicular to the direction of the lateral loading by way of compatibility when the joints rotate due to a lateral deflection of the structure.

## 3.5 CONSTRUCTION MATERIALS

A major difficulty encountered during model work is that of obtaining suitable construction materials which are similar in behaviour to the building materials normally used. The degree to which the results of tests on the small building are applicable to larger buildings depends on the extent to which similarity is achieved.

### 3.5.1 Concrete

It is unreasonable to use a normal range of aggregate gradation (maximum size = $\frac{3}{4}$ in. = 19.05 mm) in small scale model work and so a quarter scale mix was used, which meant a maximum aggregate size of $\frac{3}{16}$ in. (3.81 mm). By using a quarter scale mix, the aggregate gradation could be standardised at the sieve sizes at which the aggregate was supplied commercially. Obviously this scaling process could only be carried out with the larger aggregates since geometric similarity is meaningless in terms of sand and cement.

A problem with small scale mixes is that the aggregate has a greater surface area to volume ratio than for a full scale mix and so proportionately absorbs a greater quantity of water. Johnson [14] found that the smaller the scale of a mix, the lower the aggregate to cement ratio for a given water to cement ratio and workability. As a consequence of this however, the shrinkage occuring in the concrete is increased.

A series of mixes were designed and tested and after a trial and error process it was decided that the mix detailed in table 3-3 would be suitable. The aggregate/cement ratio was 4.0 and the water/cement ratio was 0.7.

Three 6 in. dia. x 12 in. (152.4 mm dia. x 304.8 mm) cylinders were cast from this mix and tested after 28 days at a rate of 2000 lb/in$^2$/min (13.79 N/mm$^2$/min). The average compressive stress was found to be 4600 lb/in$^2$ (31.03 N/mm$^2$). Many investigators [14] have found that the ratio of tensile to compressive strength of the concrete increases as the scale of the mix decreases and so three 3 x 3 x 12 in. (76.2 x 76.2 x 304.8 mm) prisms were cast from the same mix. The tensile strength of the concrete as given by these modulus of rupture tests was found to be 590 lb/in$^2$ (4.07 N/mm$^2$) and thus $f_r = 8.7\sqrt{f'_c}$, which was considered reasonable.

A limited number of 2 in. dia. x 4 in. (50.8 mm dia. x 101.6 mm) and 6 in. dia. x 12 in. (152.4 mm dia. x 304.8 mm) cylinders were cast to check if there was any difference in the apparent concrete strength indicated by the two sizes of specimen, but no discernible trend could be established, in part because of the extremely variable results given by the 2 in. dia. x 4 in. (50.8 mm dia. x 101.6 mm) cylinders. The most important concrete pours were for the two structural frames and it was decided to determine the strength of this concrete using 6 in. dia. x 12 in. (152.4 mm dia. x 304.8 mm) cylinders but to check the results using 2 in. dia. x 4 in. (50.8 mm dia. x 101.6 mm) cylinders. The concrete strengths of the

TABLE 3-2 : REINFORCING WIRE

| Wire gauge | Diameter in. (mm) | Area $in^2$ ($mm^2$) | Yield strength $lb/in^2$ ($N/mm^2$) |
|---|---|---|---|
| 7 | 0.176 (4.47) | 0.02432 (15.69) | 42,500 (293) |
| 13 | 0.092 (2.34) | 0.00665 ( 4.29) | 45,600 (314) |
| 16 | 0.064 (1.63) | 0.00322 ( 2.08) | 47,000 (324) |
| 17 | 0.056 (1.42) | 0.00246 ( 1.59) | 46,500 (321) |
| 18 | 0.048 (1.22) | 0.00181 ( 1.17) | 48,800 (336) |

TABLE 3-3 : AGGREGATE GRADATION

| B.S. Sieve number | Sieve size in inches (mm) | % passing |
|---|---|---|
| $\frac{3}{16}$ in. | 0.1875 (4.763) | 100 |
| 7 | 0.0949 (2.411) | 70 |
| 14 | 0.0474 (1.204) | 55 |
| 25 | 0.0236 (0.599) | 45 |
| 52 | 0.0116 (0.295) | 20 |
| 100 | 0.0060 (0.152) | 0 |

various floor slabs were indicated by 2 in. dia. x 4 in. (50.8 mm dia. x 101.6 mm) cylinders only.

### 3.5.2 Steel

Almost all steel wire produced in New Zealand is cold-drawn and thus has a high yield strength and lacks a well defined yield plateau. A special batch of mild steel wire with a yield strength of approximately 40,000 lb/in$^2$ (276 N/mm$^2$) was ordered from GKN (NZ) Ltd., an Auckland firm, who supplied the order free of charge. The wire was produced cold-drawn in the normal manner but was then annealed to lower its yield point and coiled into bundles for shipment to Christchurch.

On arrival the 7g wire was straightened and cut into 13 ft (3.96 m) lengths commercially. The other wire sizes were too small for commercial straightening and so special equipment was built in the Civil Engineering Department for this operation. This employed the same technique as that used commercially, consisting of a series of rollers of ever-decreasing offset through which the wire was fed.

Random samples of the wire were taken from the straightened lengths of 7g wire and from coils of each of the other wire sizes and these were tested in an Avery 7109 DCJ testing machine. The yield strength was defined as that stress corresponding to a permanent strain of 0.2% and is listed in table 3-2 for each gauge of wire. All the steel reinforcing wire provided was smooth and consequently would have had poor surface bond characteristics. This was not considered critical for the smaller wire sizes but the main 7g reinforcing was placed in a "fog room" in order to rust and pit the surface. The rusting process was slow due to a black production "slag" on the surface of the wire and consequently the steel had to be left for 4 to 6 months before it was considered adequately pitted.

## 3.6 CONSTRUCTION OF THE MODEL BUILDING

### 3.6.1 Introduction

Ease of construction was one of the prime considerations borne in mind as the design of the structure evolved, especially since no extensive work on small scale reinforced concrete structures had been carried out in the Civil Engineering Department previously.

Tolerances which are reasonable for large scale experimental work are totally unacceptable for small scale structures. Also, it is

desirable to place any construction joints in such a position that they have a minimal effect on the behaviour of the structure. Normal construction methods were ruled out because of the difficulty of accurately placing the steel in the model and the number of construction joints involved, and also because it would be difficult to ensure good compaction of the concrete at the bottom of the columns.

The method of construction finally decided upon involved casting the two longitudinal frames of the structure in a horizontal plane, then standing these vertically while the connecting floor slabs and the lateral beams were cast. This method resulted in only two construction joints per floor, one on each side of the slab, and both ran in a longitudinal direction where their influence on the response of the structure would be negligible.

### 3.6.2 Construction of the reinforcing cages

Over 3000 ties and stirrups of various shapes and sizes were required for each complete model structure and so a special apparatus was constructed for their manufacture (see figure 3-2). The wire was looped around the starting pegs and a stationary peg forced the wire sharply around each stirrup peg in turn as the handle was rotated. The stirrups were checked afterwards for any bowing out and were adjusted by hand if necessary.

Reinforcing cages for the six longitudinal beams and twelve half lateral beams required for each complete frame were constructed initially and were then tied to the main column reinforcing, using templates to ensure accurate spacing of the beams. The column ties and most of the slab reinforcing were then tied into position (all ties and stirrups were secured using florists wire). Once the reinforcing cages for each frame were completed they were lifted and placed into the mould as a unit. The cover to the main reinforcing steel was controlled using spacer wires tied to the cages. The construction of the reinforcing cages is shown in figure 3-4. Figure 3-7 shows the reinforcing in the region of a beam-column joint.

### 3.6.3 Attachment of column reinforcing to base

Sufficient fixity for the base of the columns is obtained by ensuring that the column reinforcing is rigidly anchored to the base plate. However, because of the poor bond between the base plate and concrete, a

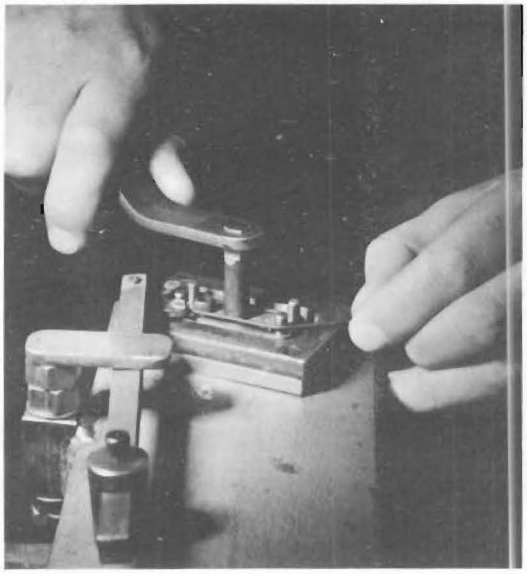

FIGURE 3-2 : APPARATUS FOR BENDING STIRRUPS

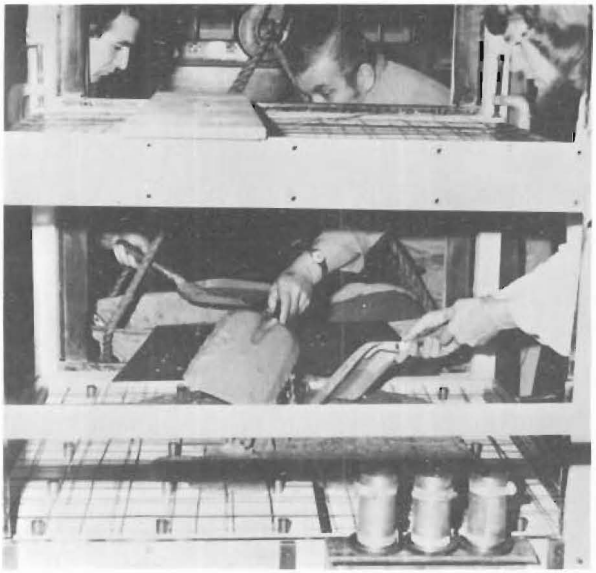

FIGURE 3-3 : CASTING OF A FLOOR SLAB

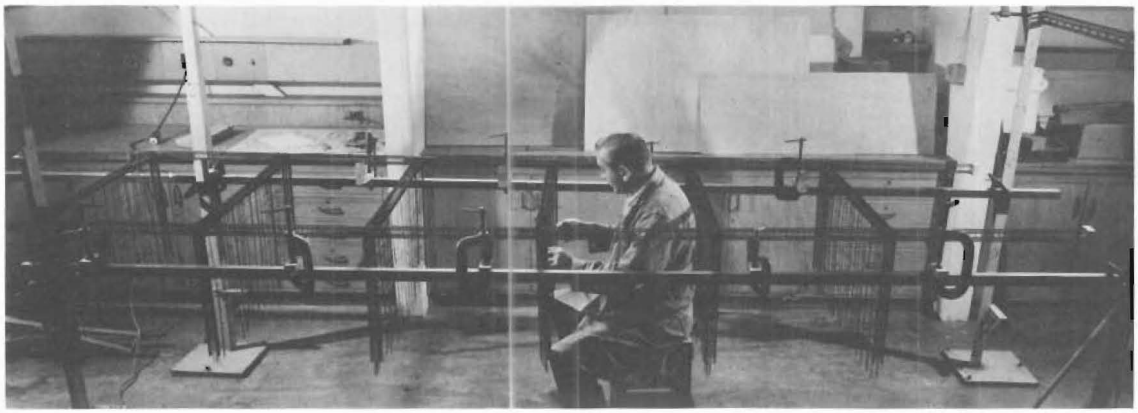

FIGURE 3-4 : CONSTRUCTION OF A REINFORCING CAGE

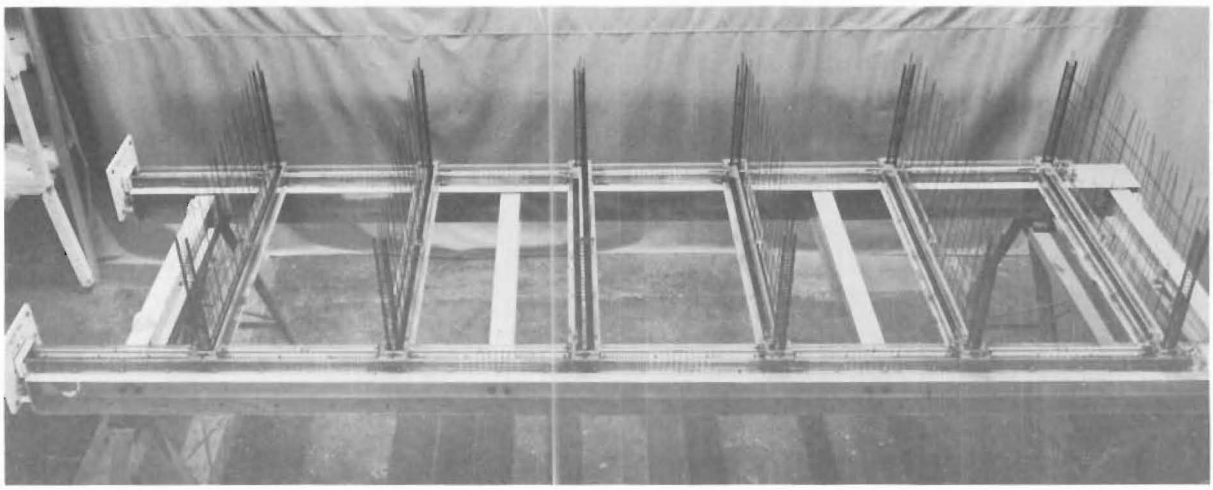

FIGURE 3-5 : FRAME PRIOR TO CASTING

small shear key ½ in. (12.7 mm) high was included in the column footing.

The column reinforcing was originally to be anchored to the base by 4 mm prestressing carrots. It was realised that while these performed adequately when the reinforcing was in tension, they would work loose when it was in compression and so special nuts were made and threaded onto the ends of the reinforcing wire. These nuts were flush with the base plate and would prevent any movement under compression by bearing onto the table.

However, after examination of the anchorages upon completion of the dynamic tests on the single storey structure, it was suspected that some movement may have taken place. Accordingly, it was decided to weld all the reinforcing wires to the footing and a new base plate was provided for this purpose. Performance of this new arrangement was found to be satisfactory.

### 3.6.4 Changes to the original detailing

During construction of the single storey model it became apparent that some changes to the original structural detailing were necessary.

The column reinforcing was comprised of single lengths of wire anchored in the column base footing and near the top of the columns. It was not physically possible to anchor these wires in the beams at the top of the columns and so a 2.5 in. (63.5 mm) high stub was cast at the top of each column specifically for this purpose.

As is often the case in multi-storey buildings, it was difficult to fit all the reinforcing steel of the column, and of the lateral and longitudinal beam anchorages, into the beam-column joint region. The problem was solved by decreasing the spacing between the top and bottom main reinforcing in the lateral beam by two bar diameters. Consequently the ultimate moment capacity of the lateral beams was less than that of the longitudinal beams but this was not considered significant in view of the small loads that the lateral beams were expected to carry.

### 3.6.5 Moulds

A backing frame of similar dimensions to the structure was constructed from two 13 ft (3960 mm) lengths of 6 x 6 in. UC (152 x 152 mm UC) connected at intervals by short lengths of channel and I sections bolted to the web. This framework was milled after assembly to ensure that it was perfectly flat and true. Lengths of 4 x ½ in. (102 x 12.7 mm) bright flat

steel spanning between the Universal Column sections were then bolted on at positions corresponding to the longitudinal beams of the structure.

Perspex was chosen as the main moulding material. The moulding was bolted together and also bolted to the steel backing frame and it was designed for ease of assembly and disassembly. The advantages of using perspex were that it was light, easily worked, bolts screwed into it did not work loose with repeated removal and replacement, concrete did not adhere to it and it was sufficiently transparent to determine if any air voids were present in the concrete. The disadvantages of using perspex were that it was expensive and that its thickness was not constant. The magnitude of the latter problem was not realised until too late or else the perspex would have been milled to a constant thickness. The perspex had a nominal thickness of 0.5 in. (12.7 mm) but in fact varied from 0.495 in. (12.57 mm) to 0.580 in. (14.73 mm).

The reinforcing cages and moulding prior to the casting of the concrete are shown in figures 3-5 and 3-8.

### 3.6.6 Attachment of additional weights to floor slabs

It was important to ensure that the steel weights placed at each floor level to simulate the seismic live load plus some dead load should introduce no undesirable structural actions and that the effect of the blocks on the mass distribution of the structure should be minimal. It was decided to place the steel blocks immediately above each floor level since this is where the live load is positioned in normal buildings and the connection between the blocks and floor slab was required to be rigid to prevent movement of the blocks under dynamic conditions.

Twentyfive steel blocks of dimensions 4.4 x 4.4 x 2.0 in. (112 x 112 x 50.8 mm) were placed on each floor slab. Each of these blocks, together with the connecting bolt, insert, nuts and washers, weighed 11.3 lb (50.3 N) making a total weight of 282 lb (1258 N) per floor. Each block was connected to the floor slab by a single bolt.

To ensure that the bolts did not work loose in the concrete, steel inserts of $\frac{3}{4}$ in. (19.05 mm) diameter and with a $\frac{3}{8}$ in. (9.52 mm) diameter threaded hole were cast into the floor slab. A length of threaded stock was screwed through the insert and fastened above and below by a nut and washer. These washers were specially made to ensure a large bearing area on the concrete and were 1 in. (38.1 mm) in diameter and $\frac{1}{8}$ in. (3.17 mm) thick. The steel blocks were then placed on the threaded stock and secured by a nut. The clearance between the blocks and the floor slab was about $\frac{1}{2}$ in. (12.7 mm).

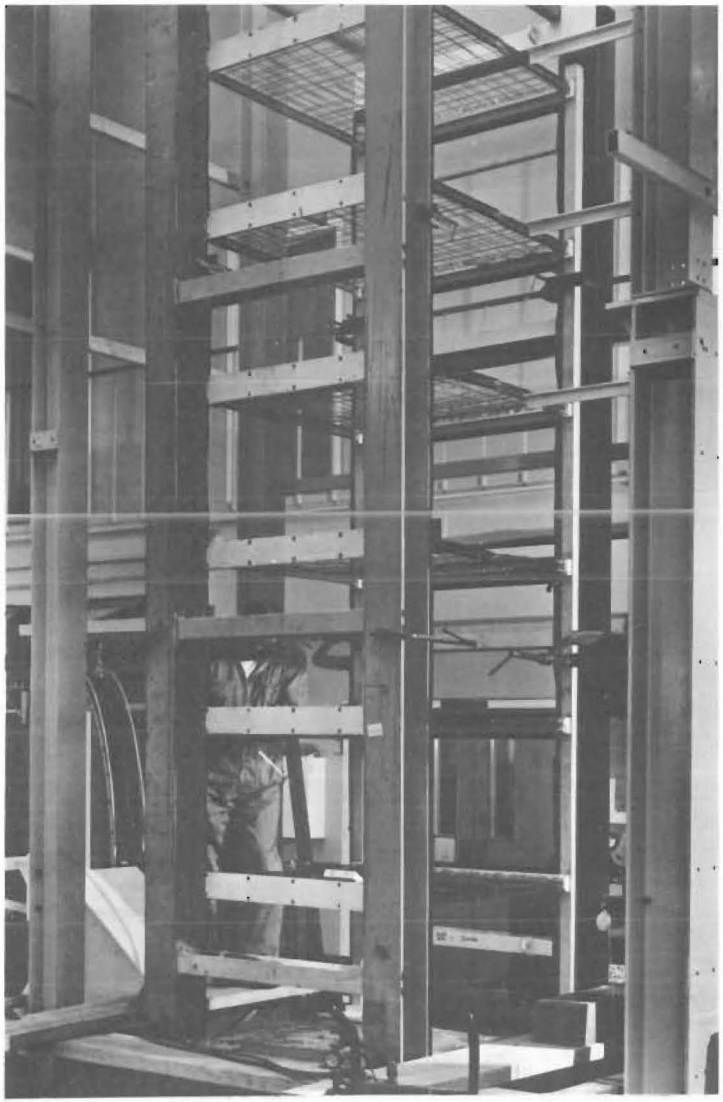

FIGURE 3-6 : BUTT WELDING OF THE LATERAL BEAM REINFORCING

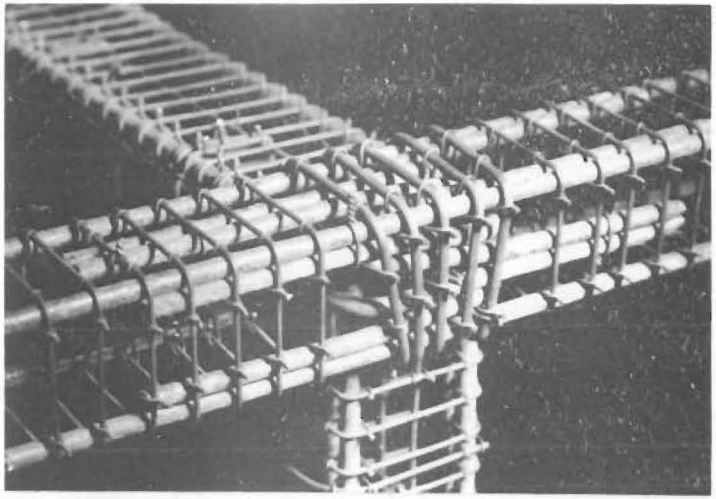

FIGURE 3-7 : BEAM-COLUMN JOINT

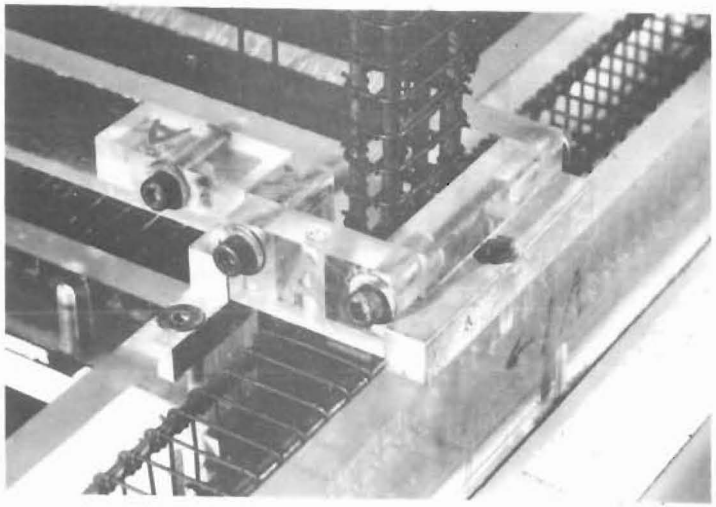

FIGURE 3-8 : JOINT ENCLOSED BY MOULD

### 3.6.7 Construction of the frames

A single storey structure was constructed initially in order to evaluate the construction techniques employed. The mould and the steel backing were lightly coated with oil before the structure was cast but adhesion still occurred between the concrete and steel however and difficulty was experienced in separating the structure from the mould.

In an attempt to overcome this problem when the first six storey model was poured, a thin polythene sheet was stretched over the steel backing and secured beneath the perspex moulding, a technique which had been reported as being successfully used elsewhere [27]. However, it was found that air bubbles formed beneath the polythene as it expanded and contracted with the change in room temperature, and the weight of the concrete was insufficient to expel the air. Although not significant structurally, these air bubbles did result in unsightly wrinkles which marred the surface of the concrete. When the second six storey model was cast the steel was coated with a plastic sealant, Durapon, and this was successful in preventing adhesion between the concrete and the steel.

The steel backing frames were laid horizontally and were separated from their supports by thick rubber pads. Before casting the model frames, oil was lightly rubbed onto the moulding to facilitate removal of the structure, although this was not strictly necessary, and the positioning of the reinforcing cages was checked. The following moulds for control specimens were bolted onto each of the backing frames:

(i) six 2 in. dia. x 4 in. (50.8 mm dia. x 101.6 mm) cylinders

(ii) three 4 in. dia. x 8 in. (101.6 mm dia. x 203.2 mm) cylinders

(iii) three 3 x 3 x 12 in. (76.2 x 76.2 x 304.8 mm) prisms.

The two frames were poured on consecutive days. A vibrator bolted beneath the frame was run for 30 seconds and was found to give satisfactory vibration to both the main structural frame and the control specimens. The concrete surface was trowelled smooth except for the slab joint which was kept in a roughened condition to ensure a good construction joint with the connecting slab and lateral beams which were to be cast later. The concrete was covered with strips of sacking and black polythene and was kept damp for 7 days after casting.

After 7 days the perspex moulding was stripped and cleaned. The concrete frames were clamped to the backing frames and lifted by an overhead crane into a vertical position on to the shaking table, where they were bolted down. The frames were temporarily secured by clamping them to braces attached to the framework which had been constructed around the shaking table.

### 3.6.8 Construction of the floor slabs and lateral beams

The main reinforcing for the lateral beams, which protruded from each of the concrete frames, was butt welded together, as shown in figure 3-6. Since the welds occurred at midspan and the lateral beams were expected to carry little load, this was not considered to affect the response of the structure at all. This welding had a beneficial effect, since shrinkage which occurred in the welds as they cooled drew the two concrete frames together, thus breaking the bond between the concrete and the steel backing frame. The slab reinforcing spanning in the lateral direction was lapped and the remaining longitudinal slab reinforcing wires needed to complete the grid were provided. Special spacer wires were devised to maintain the correct cover to the reinforcing and also the correct spacing between the top and bottom slab reinforcing.

The mould for the slab was comprised basically of a piece of seven-ply wood which was mounted on a steel backing frame and which had been milled so that its surface was flat and smooth and then sealed with Durapon. The edges of this mould were bevelled where they formed the interior boxing for the lateral beams in order to facilitate their removal after the slab had cured. However, during construction of the single storey model, the mould was jammed so tightly due to shrinkage of the concrete that it had to be cut out.

As a consequence of this difficulty the piece of plywood forming the mould was cut into two pieces, which were screwed onto the steel backing frame with a $\frac{1}{8}$ in. (3.175 mm) gap between them. Tape was placed over this gap when casting the concrete. After the concrete had cured, the steel backing frame was unscrewed from one of the mould halves and each mould half was then easily removed.

The moulding for the lateral beams was comprised of several lengths of perspex, which were bolted to the slab mould once it was in position. The edges of the mould were plugged with grey plasticine to prevent leaks and special clamps were constructed to ensure that the lateral beam moulding remained flush with the existing beam stubs while another series of special clamps attached to the steel backing frame held the slab mould in position.

A vibrator was bolted underneath the mould and was separated from it by rubber absorption pads. This gave good vibration to the floor being poured without distressing other parts of the structure. Three moulds for 2 in. dia. x 4 in. (50.8 mm dia. x 101.6 mm) control cylinders were clamped to the steel backing frame and were cast with the floors. The concrete was prepared in a concrete mixer and then poured into a wheelbarrow which

was hoisted by an overhead crane to the level of the floor slab under construction, from where it was transferred to the mould by hand shovel, as shown in figure 3-3. After levelling, the concrete was left for 3 hours and the surface was then finished by trowel.

Wet sacking was placed over the concrete to prevent it from drying too quickly and the moisture loss through evaporation was reduced by spreading sheets of black polythene over the sacking. Special drainage trays were constructed to catch the overflow when the water was being poured onto the sacking. The concrete was kept wet for 7 days after pouring, at which time the moulds were stripped from the slab and lateral beams. Two floor moulds were available so it was possible to cast 2 floors per week.

### 3.6.9 Completion of the structure

The steel backing frames were removed by jacking against opposite sides of the structure. Patches of cover concrete were chipped off at several beam-column joints by moulding which had not been bevelled. This concrete has a negligible effect on the behaviour of the structure. A sand-cement mortar was used to fill these patches and they appeared to behave no differently from either the joint concrete or the cover concrete on other beam-column joints.

The structure was then painted white to facilitate crack detection and the steel blocks representing the seismic live load plus some dead load were placed in position.

# CHAPTER FOUR

# DETERMINATION OF BEAM AND COLUMN PROPERTIES

## 4.1 INTRODUCTION

Although favourable results using small scale reinforced concrete structural elements have been reported elsewhere, for example [9, 10], it was considered advisable to check on the accuracy with which deformation characteristics and failure loads of the elements could be predicted by theory, since this would govern the accuracy of any analyses carried out on the complete structure.

Beam and column members typical of those present in the complete structure were selected for testing, and these were subjected to loads of differing types and magnitudes. The most important information to be obtained from these tests were the moment-curvature response curves for the beam and column members, although additional information on the load-deflection characteristics, the cracking patterns and the crack widths was also recorded.

## 4.2 METHOD OF TESTING

Because the magnitude of the forces induced in the structure by earthquakes were very much greater than those induced by the gravity loads, both the maximum positive and negative beam moments occurred at the faces of the columns, in a region of rapidly changing moments. Thus the portion of beam selected for testing was cast with a column stub in the centre and was tested under mid-point loading; the maximum bending moment then occurred at the faces of the column. Similarly, a beam-slab stub was cast in the centre of the column members. In addition to the lateral mid-point loading, an axial load was applied to the ends of the column and its magnitude was varied for each test.

It was decided to test six column members and four beam members, and the details of these tests are given in table 4-1. Five of the six columns were monotonically loaded to failure under varying axial loads whereas the sixth was cyclically loaded. All the cyclic loading tests carried out involved an elastic cycle in each direction followed by four cycles into the yield range in each direction.

The beams were tested in conjunction with a width of slab which was considered to be effective in acting with the beam. This meant that the

TABLE 4-1 : DETAILS OF ELEMENT TESTS

| Member | Method of Testing |
|---|---|
| Beam 1 | Monotonic positive moment |
| Beam 2 | Monotonic negative moment |
| Beam 3 | Cyclic with positive moment first cycle |
| Beam 4 | Cyclic with negative moment first cycle |
| Column 1 | Montotonic with no axial load |
| Column 2 | Monotonic with 1000 lb (4450 N) axial load |
| Column 3 | Monotonic with 2000 lb (8900 N) axial load |
| Column 4 | Monotonic with 3000 lb (13340 N) axial load |
| Column 5 | Monotonic with 4000 lb (17790 N) axial load |
| Column 6 | Cyclic with 1000 lb (4450 N) axial load |

beam members were of L cross-section and the resulting biaxial bending greatly complicated the analysis of the beam and obscured those parameters it was hoped to investigate. This biaxial bending does not occur in the structure since the beams, although of L cross-section, are prevented by the slab from bending in the horizontal plane. Thus a further series of four beams was cast and this time the section was T shaped, with the slab flange split equally either side of the beam web. Two of the beams were tested with monotonically increasing loads, one producing positive moment and one producing negative moment, and the other two were tested under cyclic loading, with an initial positive moment cycle in one and an initial negative moment cycle in the other.

The test setup is shown in figures 4-1 and 4-6. All the beams and columns were tested simply supported and the supports were designed to prevent the occurrence of any restraint against end rotation. The length of the beams was 42 in. (1067 mm) and they were simply supported over a span of 40 in. (1016 mm), which is the centre to centre distance between the columns. The length of the columns was 24 in. (610 mm), which is the

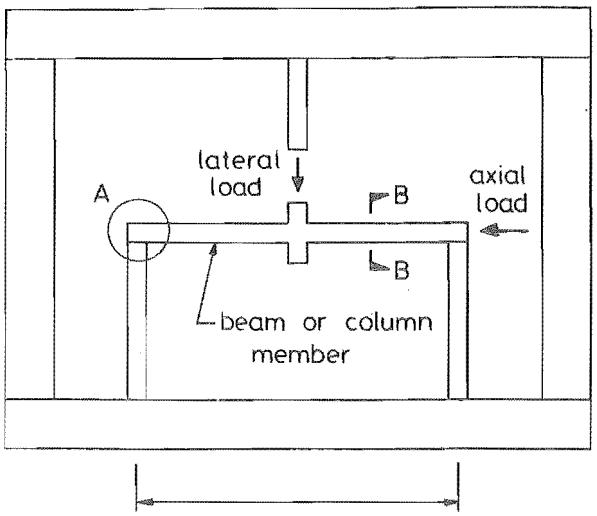


40" (1016 mm) for beams
24" (610 mm) for columns

ELEVATION

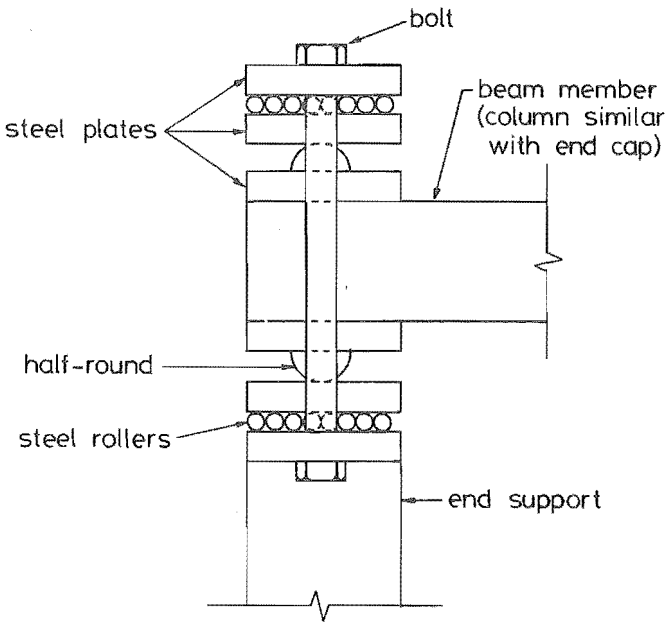


DETAIL A

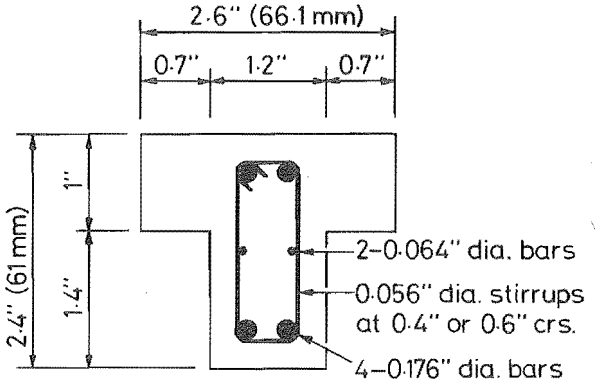


(a) BEAM

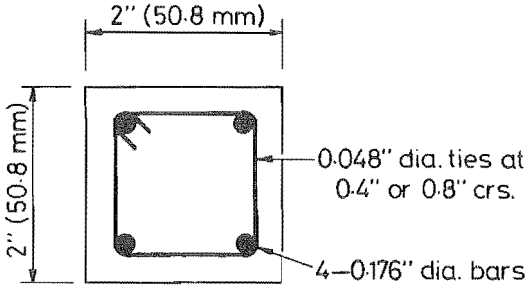


(b) COLUMN

SECTION B-B

FIGURE 4-1 : GENERAL TEST SET-UP

inter-storey height. The columns were simply supported over this length. This was achieved by placing steel caps over the ends of the column members; these had a negligible stiffening effect and also enabled the axial load to be transferred to the columns.

The load was applied (both laterally and axially) by means of two small screw jacks, each of which had a travel of about 1.25 in. (31.8 mm). The screw jacks controlled the displacement of the test specimen accurately but no precise control of the load was possible, since relaxation in the test specimen caused a reduction in the applied load. The loads were measured using load cells which were connected to Budd Model P-350 strain indicators. The load cells had a range of 2 tons (19.93 KN) and the strain readings were measured utilizing a half Wheatstone bridge circuit for the lateral loads and a full Wheatstone bridge circuit for the axial loads.

The critical region where the plastic deformations occur which govern the inelastic behaviour of the member is adjacent to the centre stub, and so it was decided to place electric resistance strain gauges at these locations. Each main reinforcing wire on both sides of the stub was strain gauged and the elastic curvature was also measured at one quarter point by placing strain gauges on a top and a bottom wire. This made a total of ten strain gauges per member and provided a safeguard against the premature failure of a particular strain gauge. The two readings obtained for both the two top and the two bottom wires were averaged and moment-curvature curves were constructed for each side of the stub. Often the plastic deformation would predominantly occur on one side of the stub and so the moment-curvature curve for that side most accurately represented the characteristic moment-curvature curve of the section.

Measurements were also taken of the vertical deflection, the horizontal deflection and the rotation of the centre stub. The latter measurement was carried out by cementing a strip of metal vertically to the stub and recording the horizontal movement of the metal strip at two separate locations; the difference between these two readings was then a measure of the rotation occurring. All deflection measurements were made with $\frac{1}{2}$ in. (12.7 mm) Mercer dial gauges excepting the vertical deflection, which required a 2 in. (50.8 mm) dial gauge. The development of the cracking patterns was monitored and checks on the crack widths at the level of the tensile reinforcing steel were carried out.

## 4.3 PREPARATION OF THE TEST MEMBERS

The electric resistance strain gauges were placed on the outside of the 7g reinforcing wire after the reinforcing cages had been constructed and they were separated from the strain gauge terminals by a stirrup. The area between the stirrups was barely large enough to accommodate the strain gauges as can be seen from figure 4-2, and the small size of the reinforcing cages made the whole strain gauging operation difficult.

Kyowa series KFC-5-C1-11 foil strain gauges were selected to measure the strains in the 7g reinforcing steel. This gauge was chosen because it was one of the few gauges available that was small enough to fit into the confined area required (the gauge length is 5 mm) and because it was temperature compensated for steel. The gauge backing was phenol/epoxy resin which was soft and flexible with good creep characteristics and heat and moisture resistance.

The steel wire was cleaned with emery paper and then degreased using methyl-ethyl-ketone (MEK). The strain gauges were cemented using Eastman Adhesive 910 which is a quick setting room temperature adhesive. The strain gauge terminals were the Kyowa T-F7 type and they were cemented adjacent to the strain gauges. The backing was a glass epoxy backed foil which was much stiffer than the backing used on the strain gauges and consequently they were much more difficult to mould around and cement onto the steel wire. A Budd GW-1 waterproofing compound was used to protect the gauges and terminals from moisture and then they were sealed with a micro-crystalline wax, as shown in figure 4-3.

Virtually all of the strain gauges performed adequately except that most appeared to fail at a relatively low strain level in the yield range (about 7000 microstrains). It was thought that the most likely cause for this was inadequate waterproofing and so a different waterproofing process was used when the second series of beams was cast. These beams were waterproofed again using Budd GW-1 and sealed with a rubber sealant, Silastic 728. However, when the reinforcing cages were placed under water, the resistance between many of the gauges and the reinforcing wire was found to be undesirably low and so the gauges were further sealed using a Bostik rubber compound. Unfortunately, the performance of the strain gauges on this second series of beams was inferior to those on the first.

The members were cast in perspex moulds which had been lightly brushed with oil. The cover to the main reinforcing was accurately controlled using spacer wires tied to the reinforcing cages. Three 2 in. dia. x 4 in. (50.8 mm dia. x 101.6 mm) control cylinders were cast

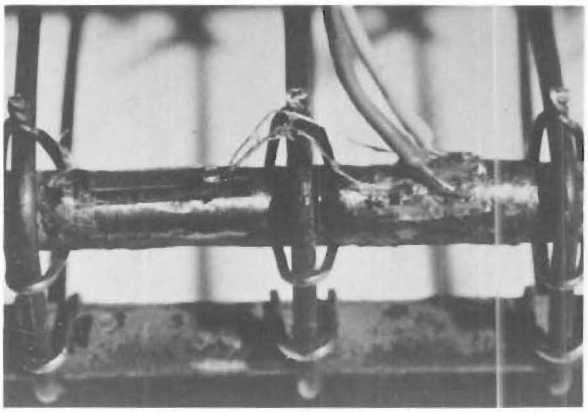

FIGURE 4-2 : STRAIN GAUGE AND TERMINAL BONDED TO REINFORCING

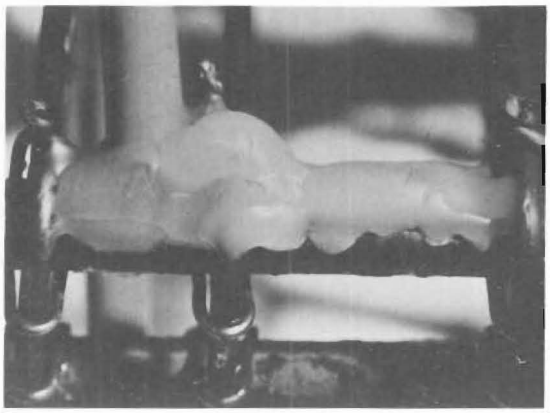

FIGURE 4-3 : WATERPROOFING OF STRAIN GAUGE

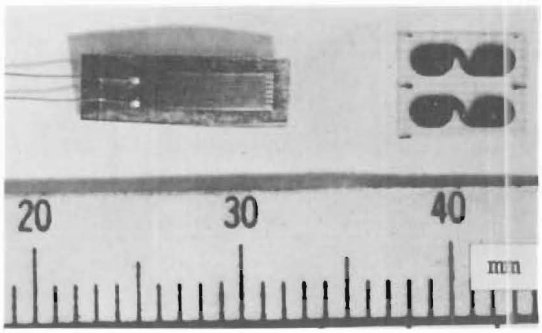


FIGURE 4-4 : STRAIN GAUGE AND TERMINAL

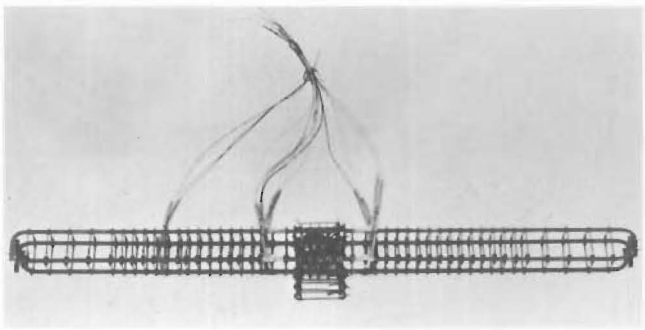

FIGURE 4-5 : COLUMN REINFORCING CAGE

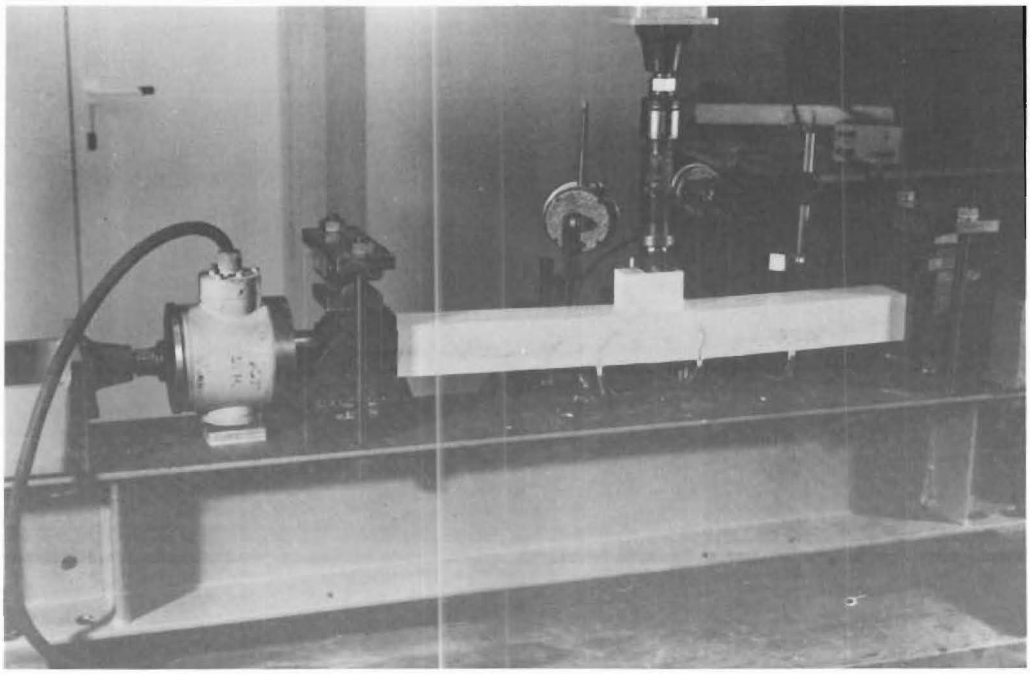

FIGURE 4-6 : GENERAL VIEW OF STRUCTURAL MEMBER TESTS

with each member. The concrete was mixed by hand and the moulds were vibrated at 2500 revs/min. for 20 seconds. The surface was finished after 3 hours and the specimens placed in a "fog room" until required. The moulds were stripped after 4 days.

## 4.4 BEHAVIOUR OF THE TEST MEMBERS

The first cracks in the columns and in several beams appeared at the positions of the electric resistance strain gauge leads which protruded from the members. The strain gauge leads acted as crack initiators and the cracks formed at these points at a somewhat lower load than would otherwise have been the case. In several beams it was suspected that the initial crack formed at the junction of the beam and the column stub but this was impossible to confirm since crack detection microscopes would not fit into the corner.

The behaviour of the members was largely governed by the formation of two very large cracks, one on either side of the centre stub. These formed at the position of the strain gauge leads in the case of the columns, and either at the position of the strain gauge leads or at the beam-column stub interface in the case of the beams. Since there was naturally some variation in member strength on either side of the centre stub, these two crack widths were not generally the same and one would often gain predominance.

The cracks in all beams and columns were flexural cracks, although some of the column cracks became very inclined when approaching ultimate load. The crack widths increased linearly with increasing load until the onset of yielding of the tension reinforcement, as shown in figure 4-7. The extrapolated graph for Column 3 does not pass through the origin because the column was subjected to a 2000 lb (8900 N) axial load.

The number of cracks in the columns stayed constant or increased slightly with increasing axial load but the average crack spacing reduced from $b$ for Column 2 to $0.65b$ for Column 5, where $b$ is the total width of the section (measurements were incomplete for Column 1). For Beam 1 (tested under positive moment) 25 cracks were evident at an average spacing of 1.08 times the web width while for Beam 2 (tested under negative moment) only 8 cracks were evident at 0.89 times the flange width. The stirrup and tie spacing in the middle half of each beam and column respectively was 0.4 in. (10.2 mm) and the measured crack spacings correspond approximately with integer multiples of this distance.

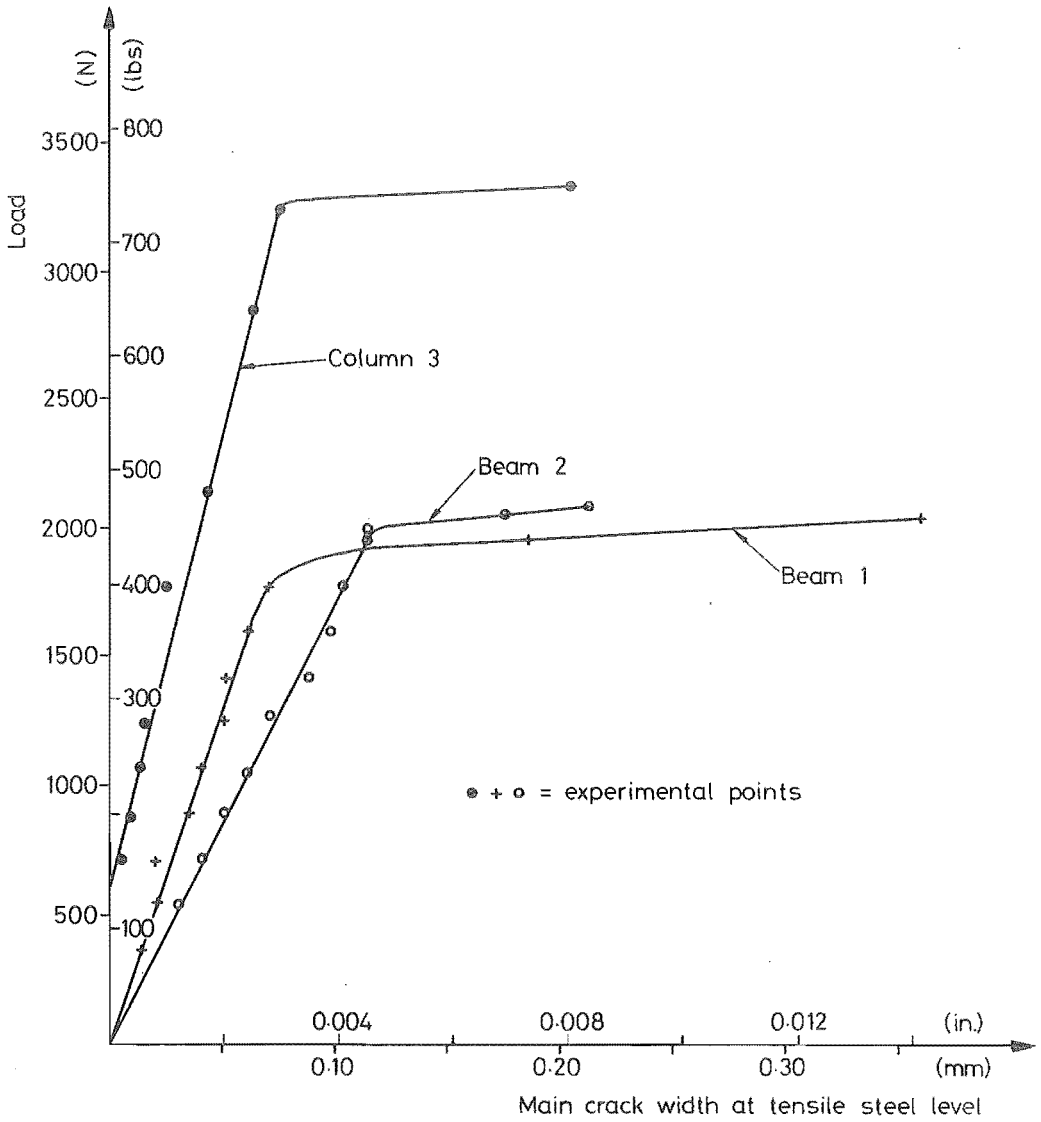


FIGURE 4-7 : INCREASE IN MAIN CRACK WIDTH WITH LOAD

## 4.5 THEORETICAL MOMENT-CURVATURE RELATIONSHIP OF A SECTION

The moment-curvature relationship of a section is the most important parameter influencing the load-deflection behaviour of the member and the structure. The theoretical moment-curvature relationships for the sections may be derived assuming plane sections remain plane and using mathematical functions which represent the stress-strain relationships of the concrete and the reinforcing steel.

### 4.5.1 Stress-strain relationship for concrete

A large amount of research has been carried out to determine the stress-strain curve for concrete. The shape of the stress-strain curve has been discussed by Hognestad et al [28]. A parabolic curve has been verified by many independent investigators and this was adopted without further testing.

Hognestad, et al, found that the maximum stress attained in flexure appeared to be less than the cylinder strength and suggested a maximum value of $0.92f'_c$ as well as suggesting limiting values for the other parameters of the curve.

The equation for the ascending portion of the concrete stress-strain curve then becomes ...

$$f_c = f''_c \left[ 2 \frac{\varepsilon_c}{\varepsilon_o} - \left(\frac{\varepsilon_c}{\varepsilon_c}\right)^2 \right] \qquad (4\text{-}1)$$

where $\varepsilon_c$ = strain at which the maximum concrete stress occurs
$f_c$ = concrete stress corresponding to a strain $\varepsilon_c$
$f''_c$ = maximum concrete flexural strength = $k_3 f'_c$
$f'_c$ = concrete cylinder strength
$k_3$ = 0.92

The strain $\varepsilon_o$ at which the maximum stress occurs varies a little according to the concrete but it does not have a significant effect on the section moment-curvature relationship. In this study $\varepsilon_o$ was assumed to be 0.002 .

The equation of the falling branch is more indefinite and it is difficult to measure in a compression test; however, many investigators agree on a linear relationship between stress and strain of the form ...

$$f_c = f''_c \left[1 - Z(\varepsilon_c - \varepsilon_o)\right] \qquad (4\text{-}2)$$

Hognestad proposed that $Z = \frac{250}{3} = 83$. Kent and Park [29] proposed a relationship based on the strain at 50% maximum stress on the falling branch. Their relationship indicates that the slope of the falling branch decreases as the amount of confining reinforcement provided increased, and when a stress level of $0.2f''_c$ is reached the stress remains constant with further increase in strain. From calculations based on the formulae suggested by Kent and Park, a much lower value for Z was determined. However, the value assumed for Z has a negligible effect on the section moment-curvature curves for underreinforced beams and lightly loaded columns, and the structural members used in this study fell into these categories. This was confirmed by an investigation conducted by Otani and Sozen [16], who found negligible difference in the section moment-curvature curves using Z = 50 and Z = 100. Accordingly, it was decided to choose Z = 80 and thus equation 4-2 becomes

$$f_c = k_3 f'_c \left[1 - 80(\varepsilon_c - 0.002)\right] \qquad (4\text{-}3)$$

Substitution into equation 4-3 indicates that the concrete stress will reduce to $0.2f''_c$ at a strain of $0.012 = \varepsilon_{20c}$.

Up to tensile failure, the tensile part of the concrete stress-strain curve is normally assumed to have the same shape as the initial part of the compressive stress-strain curve. Because of the low strains involved however, this was idealised to a straight line with a modulus of elasticity = $4 \times 10^6$ lb/in$^2$ ($2.76 \times 10^3$ N/mm$^2$) for the concrete used in the members tested, and thus the maximum tensile strain becomes $\varepsilon_t = 0.00015$.

The assumed concrete stress-strain relationship may be summarised as follows:

when $\varepsilon_t \leq \varepsilon_c < 0$ $\qquad f_c = 4 \times 10^6 \, \varepsilon_c$ (lb/in$^2$) $\qquad (4\text{-}4)$

when $0 \leq \varepsilon_c < \varepsilon_o$ $\qquad f_c = k_3 f'_c \left[2 \frac{\varepsilon_c}{\varepsilon_o} - \left(\frac{\varepsilon_c}{\varepsilon_o}\right)^2\right]$ $\qquad (4\text{-}5)$

when $\varepsilon_o \leq \varepsilon_c < \varepsilon_{20c}$ $\qquad f_c = k_3 f'_c \left[1 - 80(\varepsilon_c - \varepsilon_o)\right]$ $\qquad (4\text{-}6)$

when $\varepsilon_{20c} \leq \varepsilon_c$ $\qquad f_c = 0.2 k_3 f'_c$ $\qquad (4\text{-}7)$

where $\varepsilon_t = -0.00015$

$\varepsilon_o = 0.002$

$\varepsilon_{20c} = 0.012$

$k_3 = 0.92$

The assumed concrete stress-strain relationship is shown graphically in figure 4-8.

### 4.5.2 Stress-strain relationship for steel

The moment-curvature relationship for a reinforced concrete section is strongly influenced by the shape of the steel stress-strain curve and thus it is essential to determine this accurately. The steel was tested in an Avery 7109 DCJ testing machine. A 2 in. (50.8 mm) Baty extensometer was used to measure the strain. This extensometer had a range of $\frac{1}{8}$ in. (3.18 mm) and could be read to $5 \times 10^{-6}$ in. ($1.27 \times 10^{-3}$ mm). Accurate stress-strain curves could only be obtained in this manner for the 7g wire since the other wire diameters were too small for attachment of the extensometer.

The samples of 7g wire tested gave consistent results and the stress-strain relationship is plotted in figure 4-9. Because of the method of production of this type of wire, the virgin stress-strain curve does not exhibit a sharply defined yield point. The virgin stress-strain curve was assumed to be symmetric with respect to the origin in tension and compression.

A series of piece-wise functions were fitted to the steel stress-strain curve and these are listed below (all stress values are in $lb/in^2$). The steel stress-strain curve was modelled up to the ultimate stress of 67,500 $lb/in^2$ (465 $N/mm^2$). The function chosen to represent the strain hardening region was only a crude approximation since it is only the maximum value of moment corresponding to strain hardening which is of importance. The assumed steel stress-strain relationship may be summarized as follows:

when $0.0 \leqslant \varepsilon_s < 0.0068$ $f_s = 30 \times 10^6 \varepsilon_s$ ($lb/in^2$) (4-8)

when $0.00077 \leqslant \varepsilon_s < 0.0068$ $f_s = 47{,}000 - \frac{18.4}{\varepsilon_s}$ ($lb/in^2$) (4-9)

when $0.0068 \leqslant \varepsilon_s < 0.0189$ $f_s = 182{,}000\, \varepsilon_s + 43{,}060$ ($lb/in^2$) (4-10)

when $0.0189 \leqslant \varepsilon_s \quad 0.07102$ $f_s = 403{,}000\, \varepsilon_s + 38{,}800$ ($lb/in^2$) (4-11)

when $0.07102 \leqslant \varepsilon_s$ $f_s = 67{,}500$ ($lb/in^2$) (4-12)

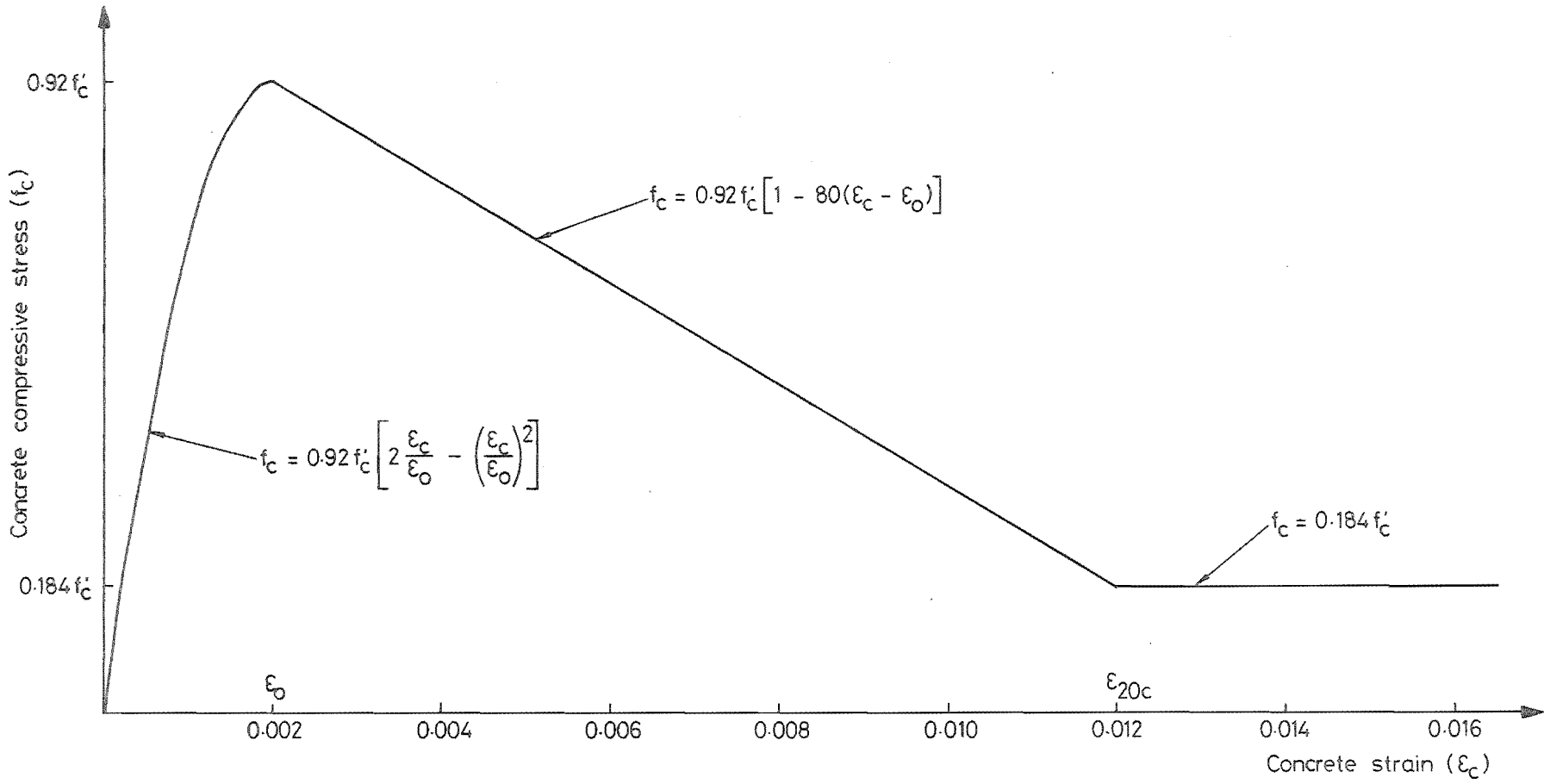


FIGURE 4-8 : ASSUMED COMPRESSIVE STRESS-STRAIN CURVE FOR CONCRETE

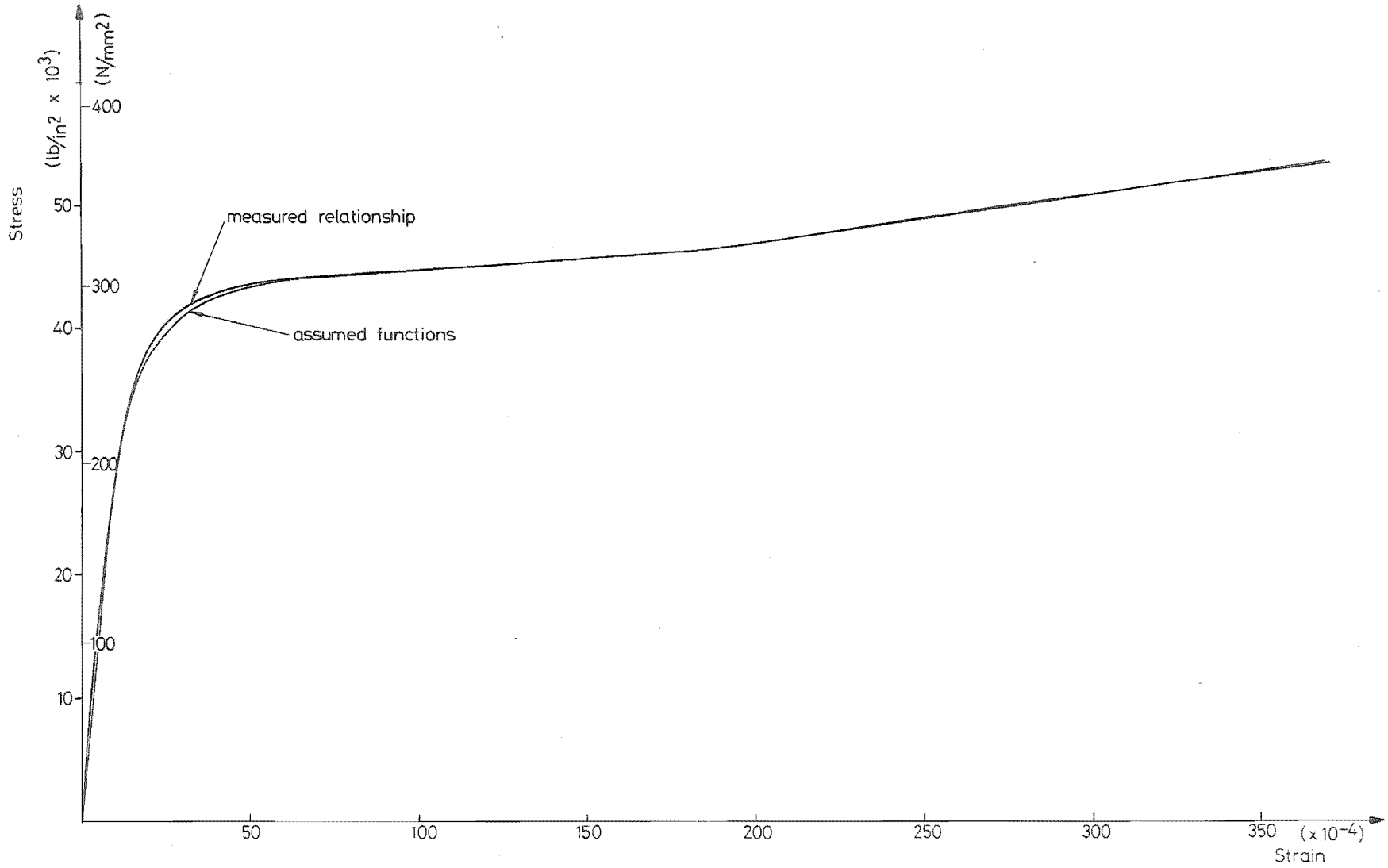


FIGURE 4-9 : COMPARISON BETWEEN MEASURED STRESS-STRAIN RELATIONSHIP OF 7G REINFORCING WIRE AND ASSUMED PIECEWISE FUNCTIONS

4.5.3 Concrete compressive stress block parameters

Since the concrete stress-strain curve is non-linear, those parameters which define the magnitude and location of the resultant concrete compressive force must be calculated for each new value of strain.

(i) $0 \leq \varepsilon_c < \varepsilon_o$ (with reference to figure 4-10(a))

Strain at $x$ from the neutral axis $\varepsilon = \frac{x}{c} . \varepsilon_c$ (4-13)

$\therefore \quad x = \frac{c}{\varepsilon_c} . \varepsilon$ and $dx = \frac{c}{\varepsilon_c} . d\varepsilon$ (4-14)

Total force taken by concrete $= \int_o^c f_c \, b dx$

$$= \frac{bc}{\varepsilon_c} \int_o^{\varepsilon_c} k_3 f'_c \left(2 \frac{\varepsilon}{\varepsilon_o} - \frac{\varepsilon^2}{\varepsilon_o^2}\right) d\varepsilon$$

$$= \frac{bc}{\varepsilon_c} k_3 f'_c \left[\frac{\varepsilon_c^2}{\varepsilon_o} - \frac{1}{3} \frac{\varepsilon_c^3}{\varepsilon_o^2}\right] \quad (4\text{-}15)$$

$\therefore$ average stress over neutral axis depth $= k_3 f'_c \left[\frac{\varepsilon_c}{\varepsilon_o} - \frac{1}{3} \left(\frac{\varepsilon_c}{\varepsilon_o}\right)^2\right]$

$$= k_3 f'_c r \left(1 - \frac{r}{3}\right)$$

(4-16)

where $r = \frac{\varepsilon_c}{\varepsilon_o}$

Moment of concrete force about top of section $= \int_o^c f_c b (c - x) dx$

$$= \frac{bc^2}{\varepsilon_c} \int_o^{\varepsilon_c} k_3 f'_c \left(2 \frac{\varepsilon}{\varepsilon_o} - \frac{\varepsilon^2}{\varepsilon_o^2}\right) d\varepsilon - \frac{bc^2}{\varepsilon_c^2} \int_o^{\varepsilon_c} k_3 f'_c \left(2 \frac{\varepsilon^2}{\varepsilon_o} - \frac{\varepsilon^3}{\varepsilon_o^2}\right) d\varepsilon$$

$$= \frac{bc^2 k_3 f'_c}{\varepsilon_c} \left[\frac{\varepsilon_c^2}{\varepsilon_o} - \frac{1}{3} \frac{\varepsilon_c^3}{\varepsilon_c^2}\right] - \frac{bc^2 f'_c k_3}{\varepsilon_c^2} \left[\frac{2}{3} \frac{\varepsilon_c^3}{\varepsilon_o} - \frac{1}{4} \frac{\varepsilon_c^4}{\varepsilon_o^2}\right]$$

$$= \frac{1}{12} bc^2 k_3 f'_c \, r(4 - r) \quad (4\text{-}17)$$

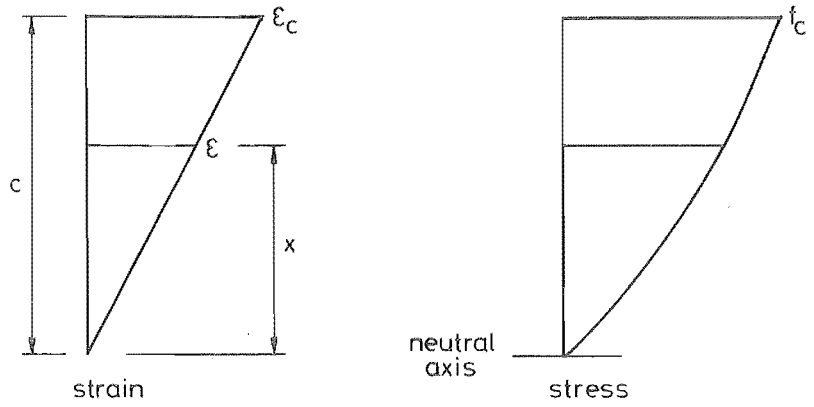


(a) $0 \leq \varepsilon_c < \varepsilon_o$

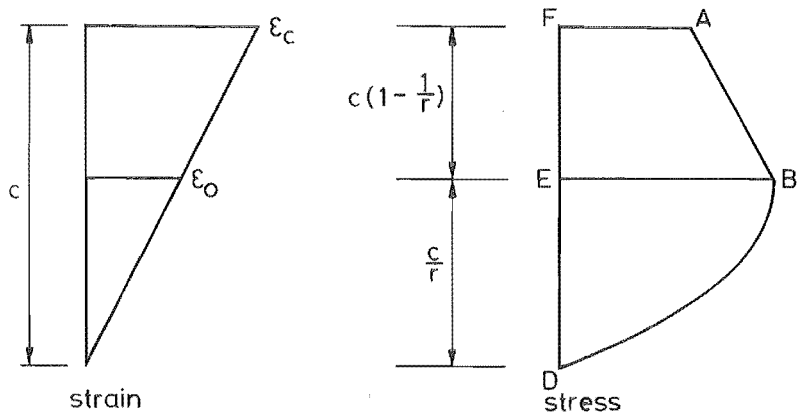


(b) $\varepsilon_o \leq \varepsilon_c < \varepsilon_{20c}$

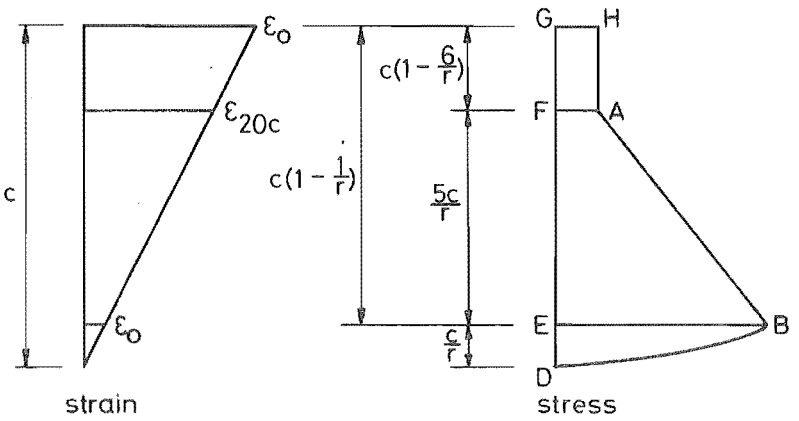


(c) $\varepsilon_{20c} \leq \varepsilon_c$

FIGURE 4-10 : DISTRIBUTION OF COMPRESSIVE STRAIN AND STRESS IN THE CONCRETE AT ULTIMATE

Then ratio $\dfrac{\text{depth to line of action of concrete force}}{\text{depth to neutral axis}}$

$$= \frac{\frac{1}{12}\, bc^2 k_3 f'_c r(4 - r)}{cbck_3 f'_c r(1 - \frac{r}{3})}$$

$$= \frac{1 - \frac{r}{4}}{3 - r} \qquad (4\text{-}18)$$

(ii) $\varepsilon_o \leqslant \varepsilon_c < \varepsilon_{20c}$ (with reference to figure 4-10(b))

Using a similar approach as previously ...

Average stress over BDE $= \frac{2}{3} k_3 f'_c$ (4-19)

Force from BDE $= \frac{2}{3} k_3 f'_c b \frac{c}{r}$ (4-20)

Average stress over ABEF $= k_3 f'_c[1 - 40(\varepsilon_c - \varepsilon_o)]$ (4-21)

Force from ABEF $= k_3 f'_c(1.08 - 0.08r)bc(1 - \frac{1}{r})$ (4-22)

$\therefore$ average stress over ABDEF $= k_3 f'_c\left[\frac{2}{3r} + (1 - \frac{1}{r})(1 - 40(\varepsilon_c - \varepsilon_o))\right]$

$$= k_3 f'_c(1.16 - \frac{0.4133}{r} - 0.08r) \qquad (4\text{-}23)$$

and total force over ABDEF $= k_3 f'_c bc(1.16 - \frac{0.4133}{r} - 0.08r)$ (4-24)

Moment of ABEF about FA $= k_3 f'_c(1.16 - 0.16r)bc(1 - \frac{1}{r})\frac{c}{2}(1 - \frac{1}{r})$

$$+ 0.16(r - 1)\frac{bc}{2}(1 - \frac{1}{r})\, k_3 f'_c \frac{2}{3}c\,(1 - \frac{1}{r})$$

$$= k_3 f'_c bc^2 (1 - \tfrac{1}{r})^2 (0.5267 - 0.0267r) \qquad (4\text{-}25)$$

Moment of BDE about FA $= \frac{2}{3} k_3 f'_c b \frac{c}{r}[c(1 - \frac{1}{r}) + \frac{3}{8}\frac{c}{r}]$

$$= k_3 f'_c bc^2 \left(\frac{0.6667}{r} - \frac{0.4167}{r^2}\right) \qquad (4\text{-}26)$$

Then ratio $\dfrac{\text{depth to line of action of concrete force}}{\text{depth to neutral axis}}$

$$= \frac{k_3 f'_c bc^2 \left[(1 - \frac{1}{r})^2 (0.5267 - 0.0267r) + \frac{0.6667}{r} - \frac{0.4167}{r^2}\right]}{k_3 f'_c bc^2 (1.16 - \frac{0.4133}{r} - 0.08r)}$$

$$= \frac{0.08r^2 - 1.74r + 1.24 - \frac{0.33}{r}}{0.24r^2 - 3.48r + 1.24} \qquad (4\text{-}27)$$

(iii) $\varepsilon_{20c} \leqslant \varepsilon_c$ (with reference to figure 4-10(c))

Using a similar approach as previously ...

Average stress over BDE $= \frac{2}{3} k_3 f'_c$ (4-19)

Force from BDE $= \frac{2}{3} k_3 f'_c b \frac{c}{r}$ (4-20)

Average stress over ABEF $= 0.6\, k_3 f'_c$ (4-28)

Force from ABEF $= 3\, k_3 f'_c b \frac{c}{r}$ (4-29)

Average stress over GHAF $= 0.2\, k_3 f'_c$ (4-30)

Force from GHAF $= 0.2\, k_3 f'_c bc\,(1 - \frac{6}{r})$ (4-31)

$\therefore$ average stress over ABDEFGH $= k_3 f'_c [0.2(1 - \frac{6}{r}) + \frac{3}{r} + \frac{2}{3r}]$

$= k_3 f'_c (\frac{2.467}{r} + 0.2)$ (4-32)

and total force over ABDEFGH $= k_3 f'_c bc (\frac{2.467}{r} + 0.2)$ (4-33)

Moment of BDE about GH $= \frac{2}{3} k_3 f'_c \frac{bc}{r} [c(1 - \frac{1}{r}) + \frac{3}{8} \frac{c}{r}]$

$= k_3 f'_c bc^2 (\frac{0.6667}{r} - \frac{0.4167}{r^2})$ (4-34)

Moment of ABEF about GH $= k_3 f'_c \frac{5bc}{r} [c(1 - \frac{6}{r}) + \frac{5c}{2r}]$

$- 0.8\, k_3 f'_c \frac{5bc}{2r} [c(1 - \frac{6}{r}) + \frac{1}{3} \frac{5c}{r}]$

$= k_3 f'_c bc^2 (\frac{3}{r} - \frac{9.5}{r^2})$ (4-35)

Moment of AFGH about GH $= 0.2\, k_3 f'_c bc (1 - \frac{6}{r}) \frac{c}{2} (1 - \frac{6}{r})$

$= k_3 f'_c bc^2 (0.1 + \frac{3.6}{r^2} - \frac{1.2}{r})$ (4-36)

Then ratio $\dfrac{\text{depth to line of action of concrete force}}{\text{depth to neutral axis}}$

$$= \frac{k_3 f'_c bc^2 (0.1 + \frac{2.467}{r} - \frac{6.317}{r^2})}{k_3 f'_c bc^2 (\frac{2.467}{r} + 0.2)}$$

$$= \frac{6r^2 + 148r - 379}{148r + 12r^2} \qquad (4\text{-}37)$$

(iv) Summary:

If $\varepsilon_o = 0.002$ and if $r = \frac{\varepsilon_c}{\varepsilon_o}$, and denoting

AS = average stress

and RD = $\frac{\text{depth to line of action of concrete force}}{\text{depth to neutral axis}}$, then

(a) $0 \leqslant \varepsilon_c < \varepsilon_o$

$$AS = k_3 f'_c r(1 - \frac{r}{3}) \qquad (4\text{-}16)$$

$$RD = \frac{1 - \frac{r}{4}}{3 - r} \qquad (4\text{-}18)$$

(b) $\varepsilon_o \leqslant \varepsilon_c < \varepsilon_{20c}$

$$AS = k_3 f'_c(1.16 - \frac{0.4133}{r} - 0.08r) \qquad (4\text{-}23)$$

$$RD = \frac{0.08r^2 - 1.74r + 1.24 - \frac{0.33}{r}}{0.24r^2 - 3.48r + 1.24} \qquad (4\text{-}27)$$

(c) $\varepsilon_{20c} \leqslant \varepsilon_c$

$$AS = k_3 f'_c(\frac{2.467}{r} + 0.2) \qquad (4\text{-}32)$$

$$RD = \frac{6r^2 + 148r - 379}{148r + 12r^2} \qquad (4\text{-}37)$$

### 4.5.5 Method of analysis

The method of analysis is an iterative procedure which firstly involves choosing a strain in the extreme concrete compressive fibre, which in the case of the columns must be greater than the strain due to the axial load to be meaningful, and calculating the stress block parameters corresponding to this strain. The assumption of a depth to the neutral axis immediately gives the strain distribution for the chosen extreme fibre strain and allows calculation of the stresses and forces in all of the reinforcing steel and in the concrete. These forces are summed to determine whether internal equilibrium of the section is satisfied within certain limits and the depth to the neutral axis is adjusted if this is not the case. The iterative procedure thus involves continually

adjusting the depth to the neutral axis until internal force equilibrium of the section is obtained. Once equilibrium is obtained the moment and curvature corresponding to that particular extreme fibre concrete strain are calculated. The strain in the extreme concrete compressive fibre is then increased and the iterative process continued allowing determination of the moment-curvature curve. A computer program MOCU was written which utilizes this method of analysis and a listing of the program may be found in Appendix C.

## 4.6 THEORETICAL AND EXPERIMENTAL MOMENT-CURVATURE CURVES

### 4.6.1 Monotonic loading

The accuracy with which the response of the structure can be predicted by mathematical idealisations for the behaviour of the structural elements depends on how closely those idealisations describe the response of the beams and the columns. By far the most important parameter influencing the response of these elements is their characteristic moment-curvature curves.

The theoretical moment-curvature curves determined using MOCU are compared with the experimental points in figures 4-11 to 4-17. Two sets of results are presented for each beam or column tested; each set corresponds to a particular side of the centre stub. Obviously it is unreasonable to expect the member on either side of the centre stub to have exactly the same strength and therefore the two sides will yield at slightly different levels. If one side yields slightly before the other then the ratio of curvature of one to the other will greatly increase, even though both are carrying the same bending moment. This effect is best illustrated by the graphs for Column 5 in figure 4-15.

The theoretical moment-curvature curves generally agree well with the experimental results. The experimental moments vary by no more than 6% from the theoretical moments and they err by being both too high and too low, indicating that there is no consistent error involved. This was fortunate since the conclusions of some previous investigators [4, 8] indicated that size effects might cause the experimental member strengths to be consistently greater than the member strengths determined theoretically.

It was possible to determine a definite point at which the concrete first cracked on both the experimental and theoretical curves - this point was less pronounced in columns with increased axial load. In many of the graphs it is apparent from the experimental points plotted that the curvature increased more than expected immediately the section cracked.

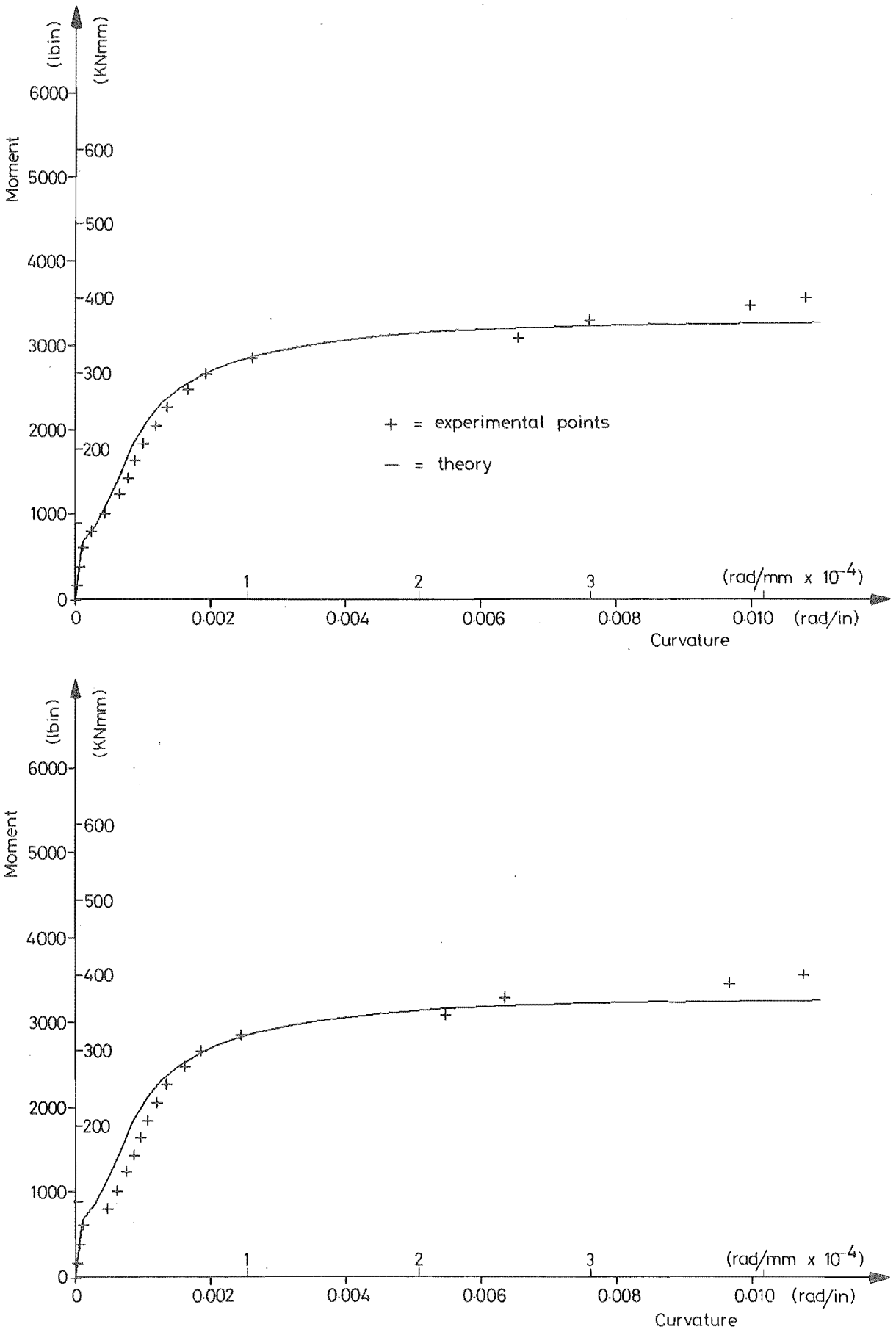


FIGURE 4-11 : EXPERIMENTAL AND THEORETICAL MOMENT-CURVATURE CURVES FOR COLUMN 1 (NO AXIAL LOAD)

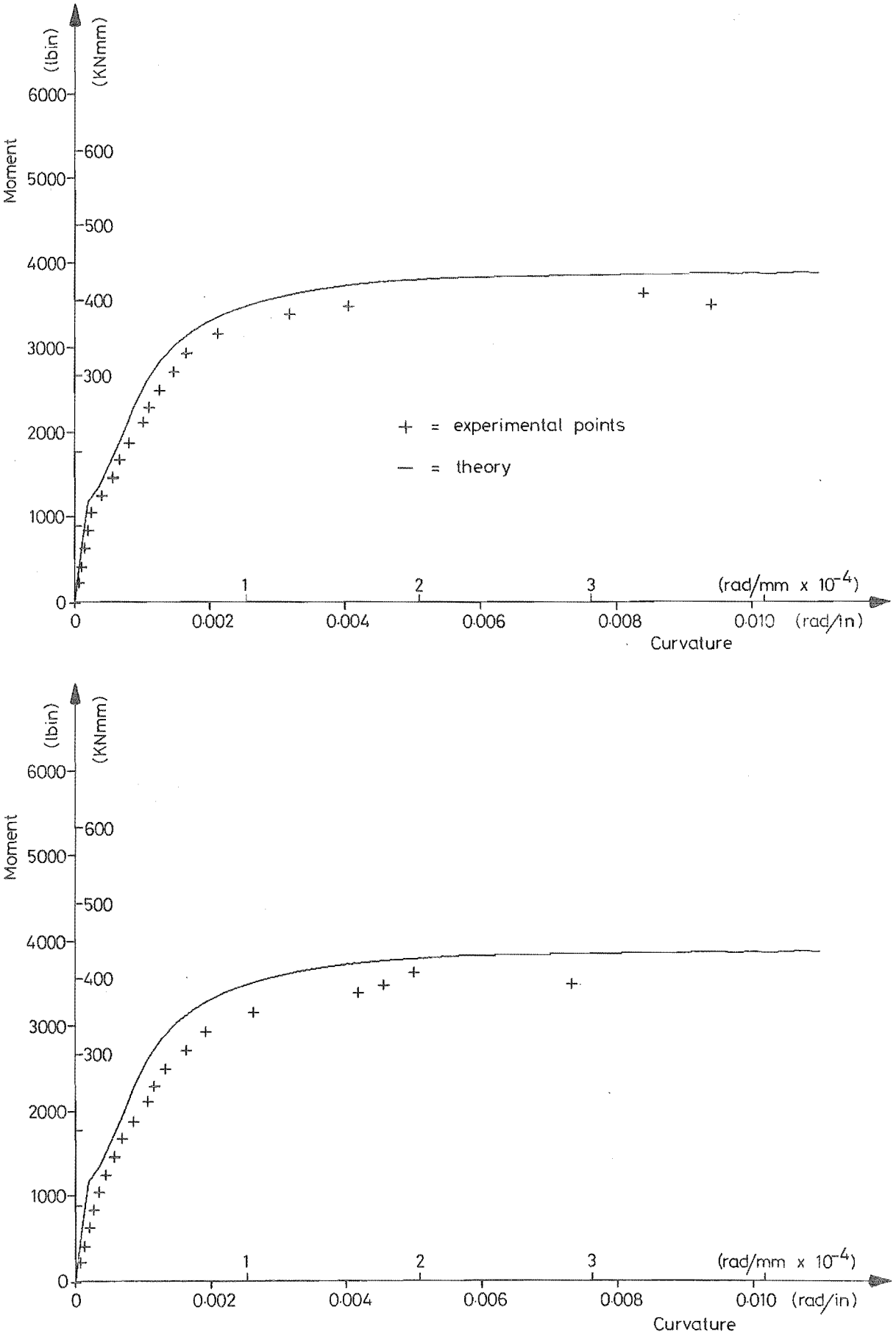


FIGURE 4-12 : EXPERIMENTAL AND THEORETICAL MOMENT-CURVATURE CURVES FOR COLUMN 2 (1000 LBS AXIAL LOAD)

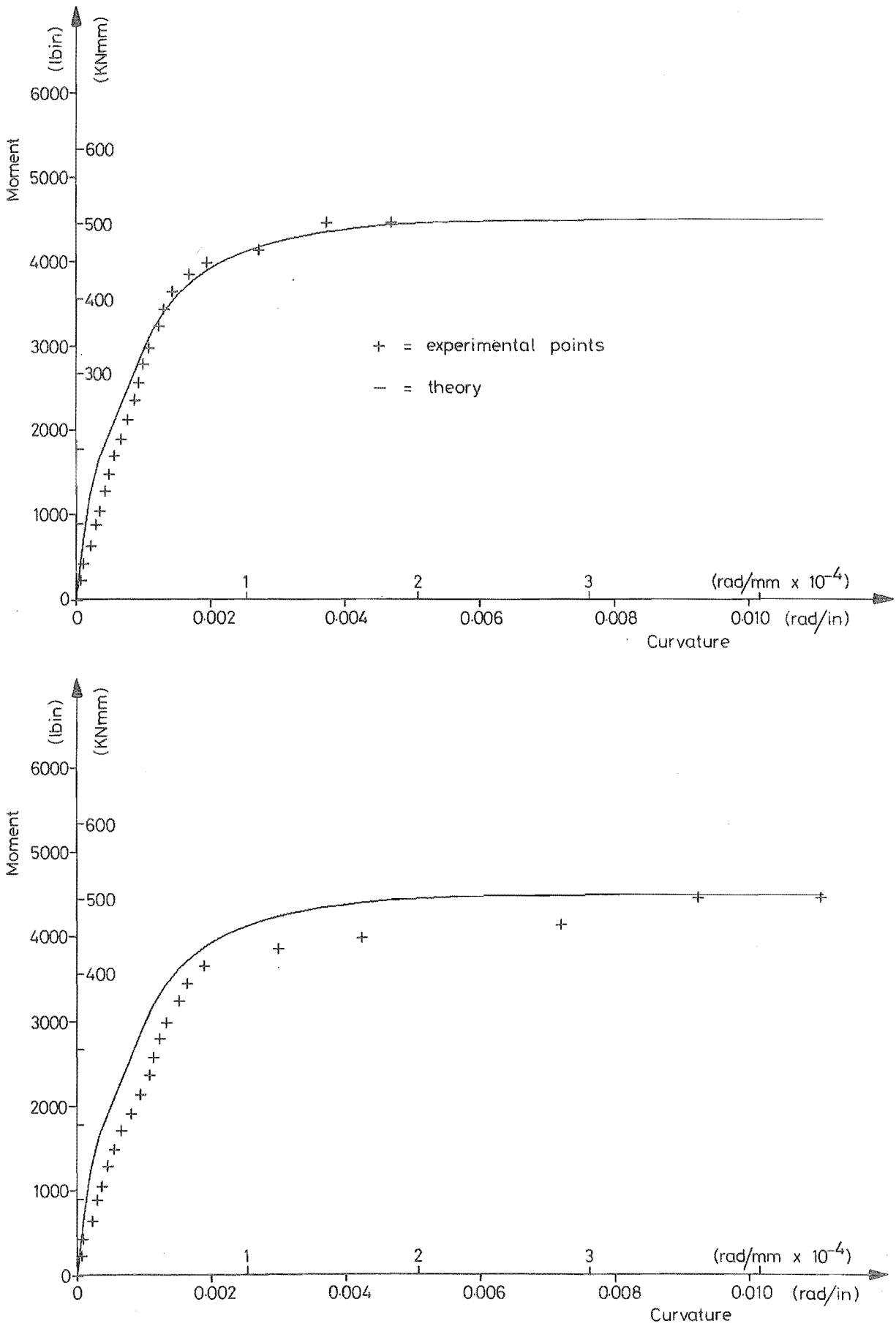


FIGURE 4-13 : EXPERIMENTAL AND THEORETICAL MOMENT-CURVATURE CURVES FOR COLUMN 3 (2000 LBS AXIAL LOAD)

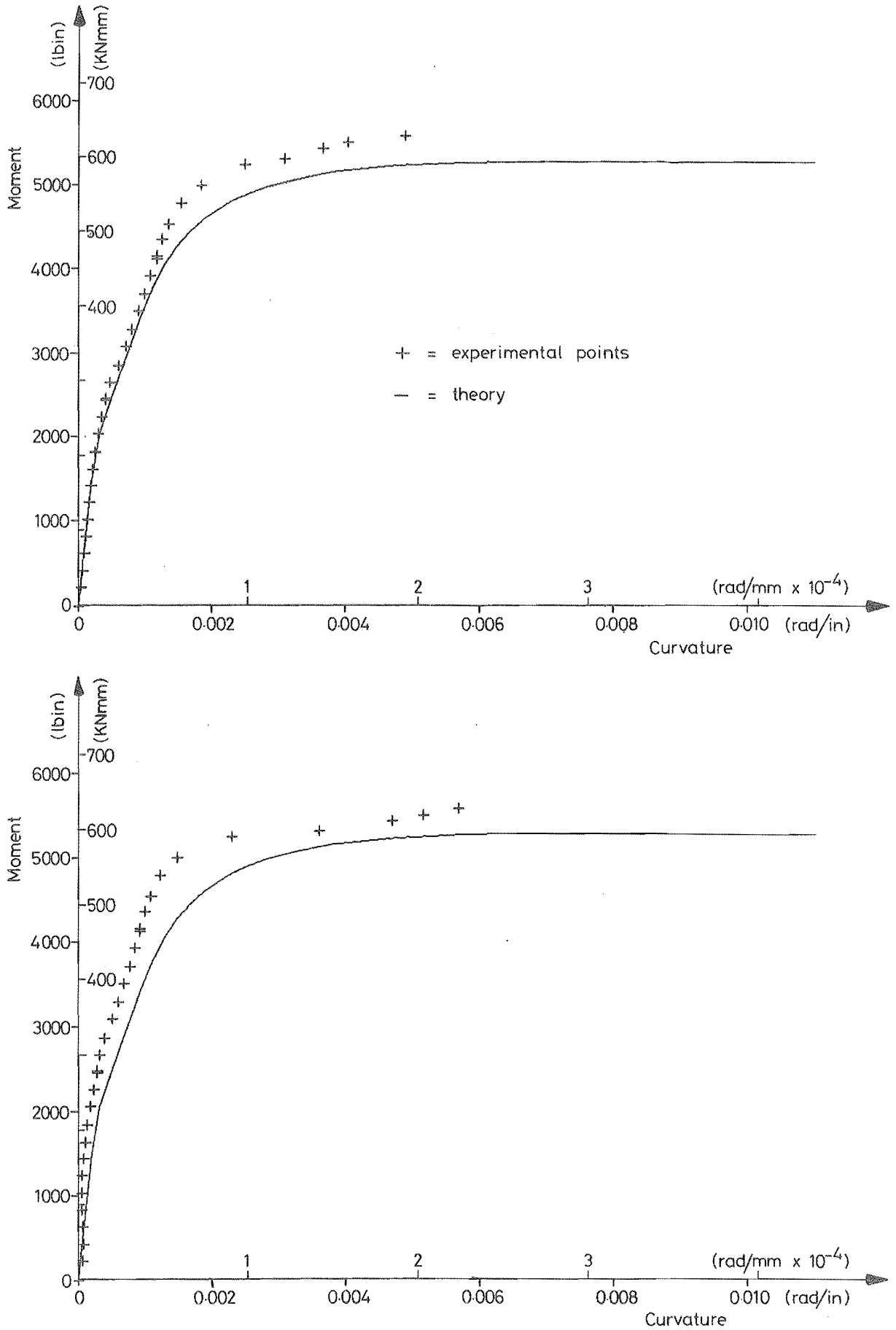


FIGURE 4-14 : EXPERIMENTAL AND THEORETICAL MOMENT-CURVATURE CURVES FOR COLUMN 4 (3000 LBS AXIAL LOAD)

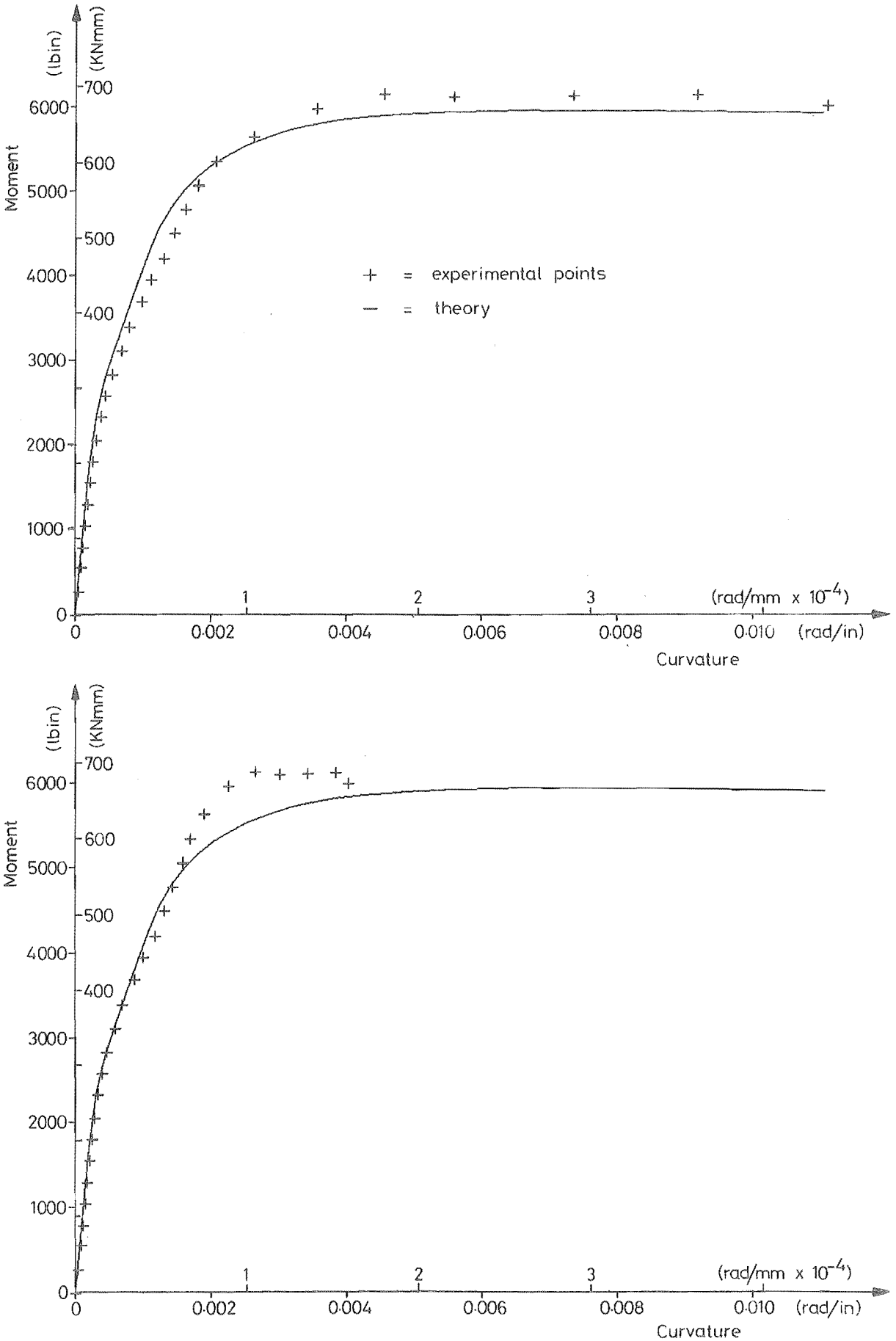


FIGURE 4-15 : EXPERIMENTAL AND THEORETICAL MOMENT-CURVATURE CURVES FOR COLUMN 5 (4000 LBS AXIAL LOAD)

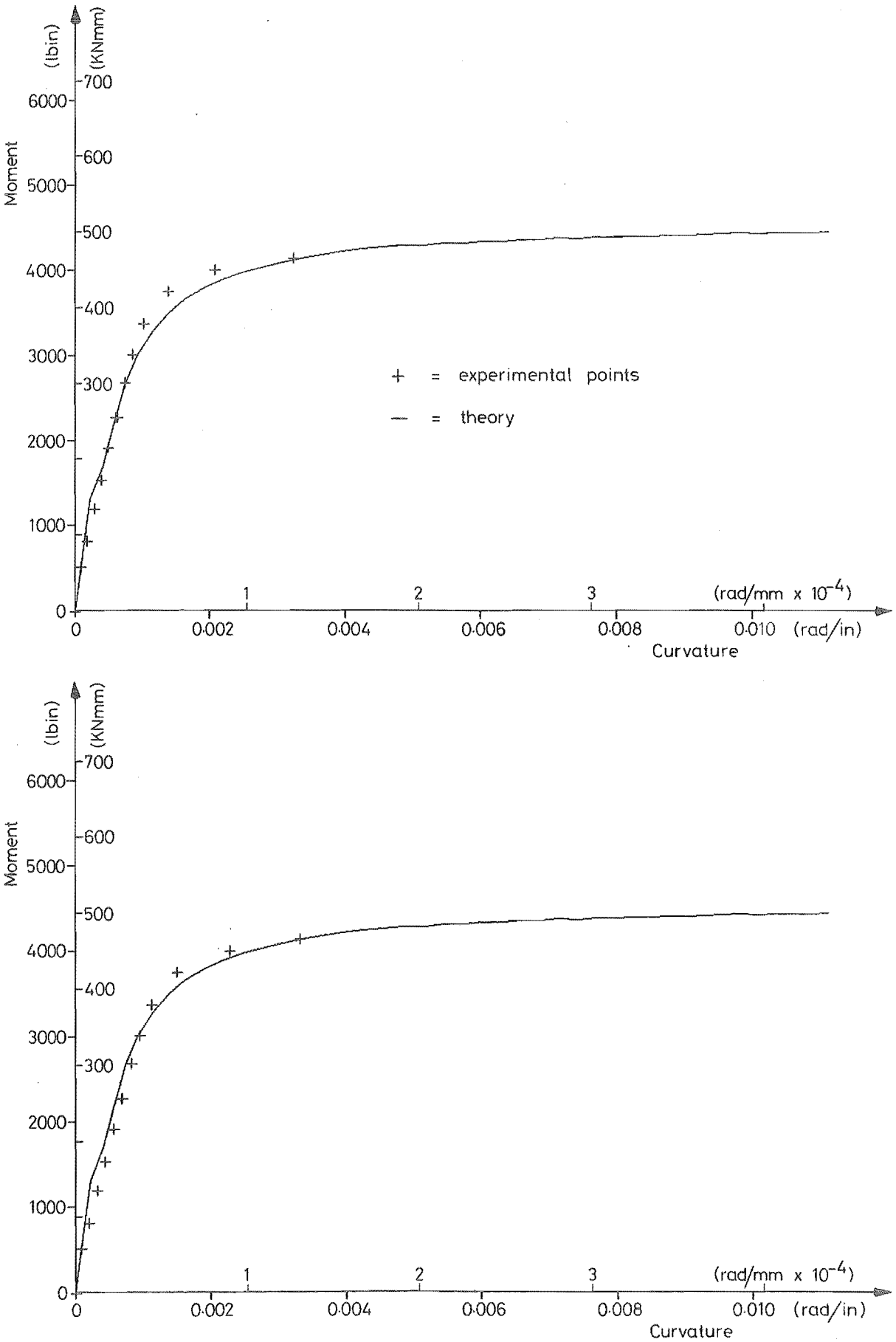


FIGURE 4-16 : EXPERIMENTAL AND THEORETICAL MOMENT-CURVATURE CURVES FOR BEAM 1 (POSITIVE MOMENT)

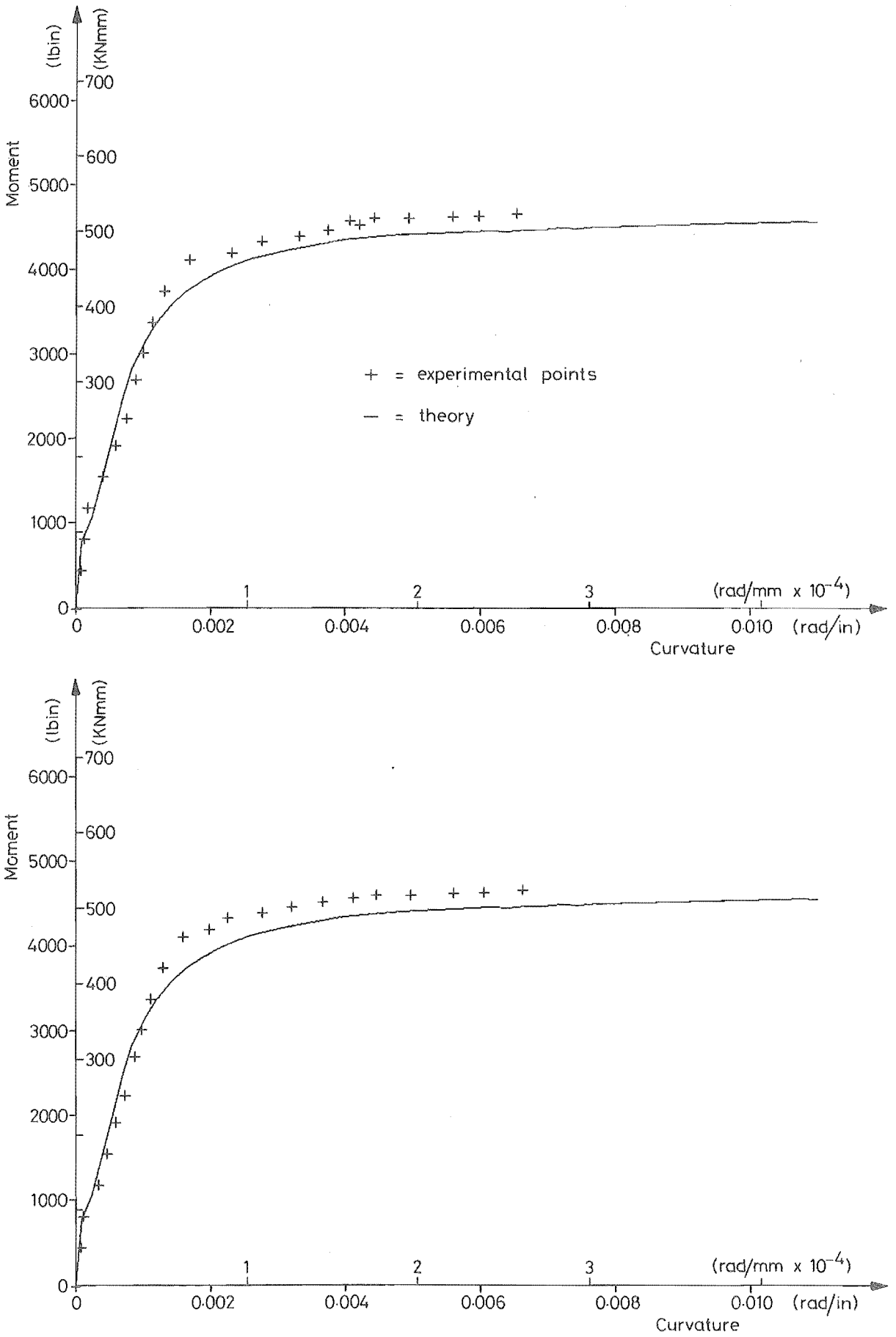


FIGURE 4-17 : EXPERIMENTAL AND THEORETICAL MOMENT-CURVATURE CURVES FOR BEAM 2 (NEGATIVE MOMENT)

This is probably due to the vertical plane of weakness caused by the electric resistance strain gauge leads permitting the main crack to penetrate higher than normally expected. On the other hand the gauge recording the curvature for the top graph for Column 4 was probably between two cracks, where the concrete was carrying some tension, thus lowering the neutral axis and reducing the curvature.

### 4.6.2 Reversed loading

Beam 3, Beam 4 and Column 6 were tested under reversed cyclic lateral loading. In all cases the members were given an initial elastic cycle followed by four cycles into the yield range. Beam 3 was given an initial positive moment half cycle while Beam 4 was given an initial negative moment half cycle. Column 6 was tested under an axial load of 1000 lb (4450 N).

The purpose of these reversed loading tests was to examine the shape of the moment-curvature loop under reversed cyclic loading and to determine if there was any decrease in member strength with each excursion into the yield range. At no stage was it envisaged matching these moment-curvature loops with theoretical moment-curvature loops; in any case, the method of analysis used in MOCU rendered it unsuitable for this purpose.

The extent to which the beam and column members were cycled in each direction depended upon the condition of the strain gauges. The strain gauges had a tendency to fail in the yield range because it was difficult to bond them to the small diameter wire and to waterproof them sufficiently. Since it was desired that the members should be cycled at least several times in each direction, the initial cycles were conducted cautiously to avoid any premature failure of the strain gauges. The condition of the strain gauges thus governed the extent to which the members were cycled, which is why some members were cycled further in one direction than in the other.

From examination of figures 4-18 to 4-20, it is apparent that the moment-curvature loops are strongly influenced by the stress-strain curve for the steel, which in turn is strongly influenced by the Bauschinger effect. This is a characteristic of members with equal steel in the top and bottom of the section. Very little damage was incurred by the members and their behaviour was largely determined by the opening and closing of two large cracks, one on either side of the centre stub.

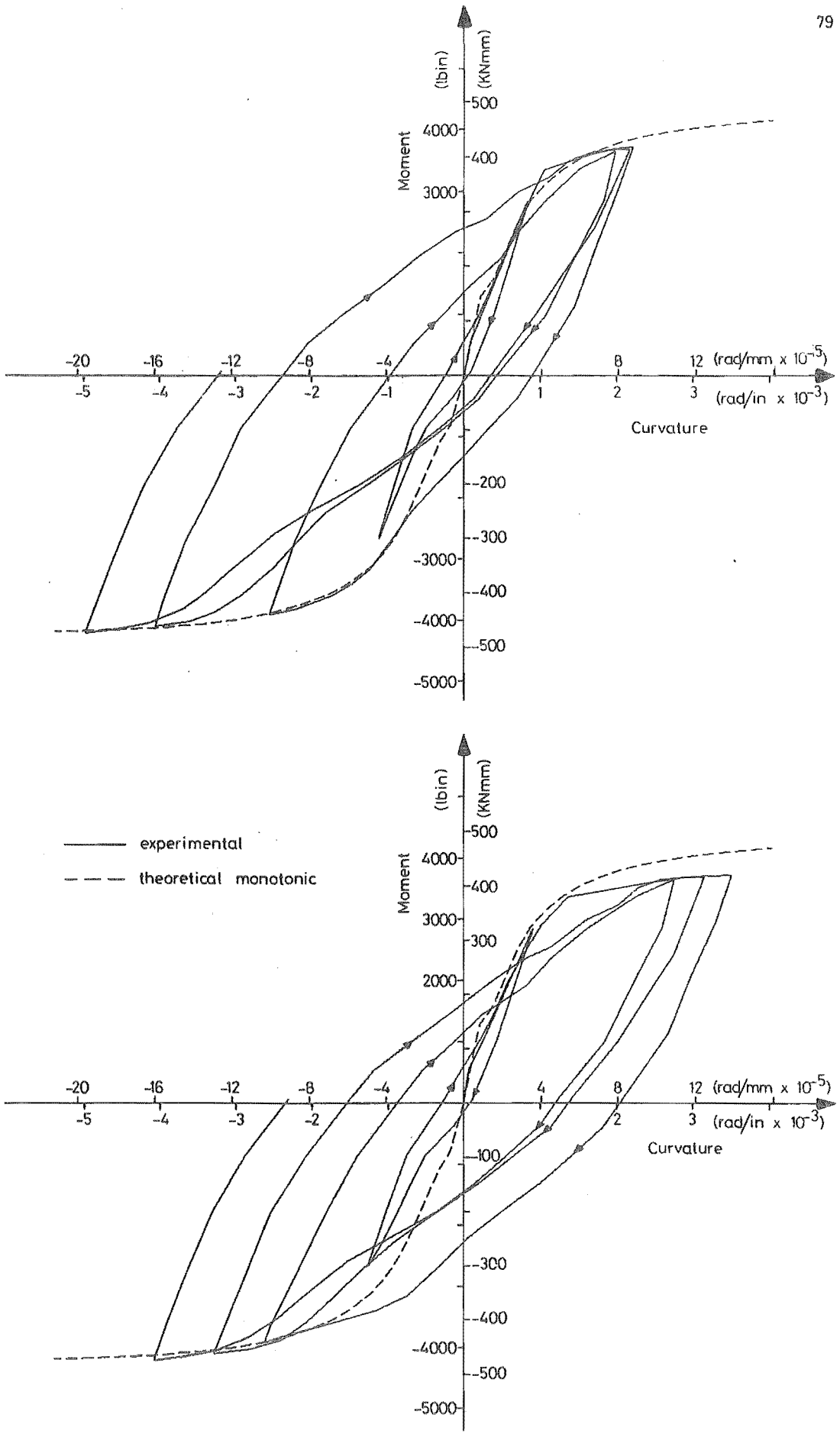


FIGURE 4-18 : EXPERIMENTAL AND THEORETICAL MOMENT-CURVATURE CURVES FOR BEAM 3 (CYCLIC LOADING)

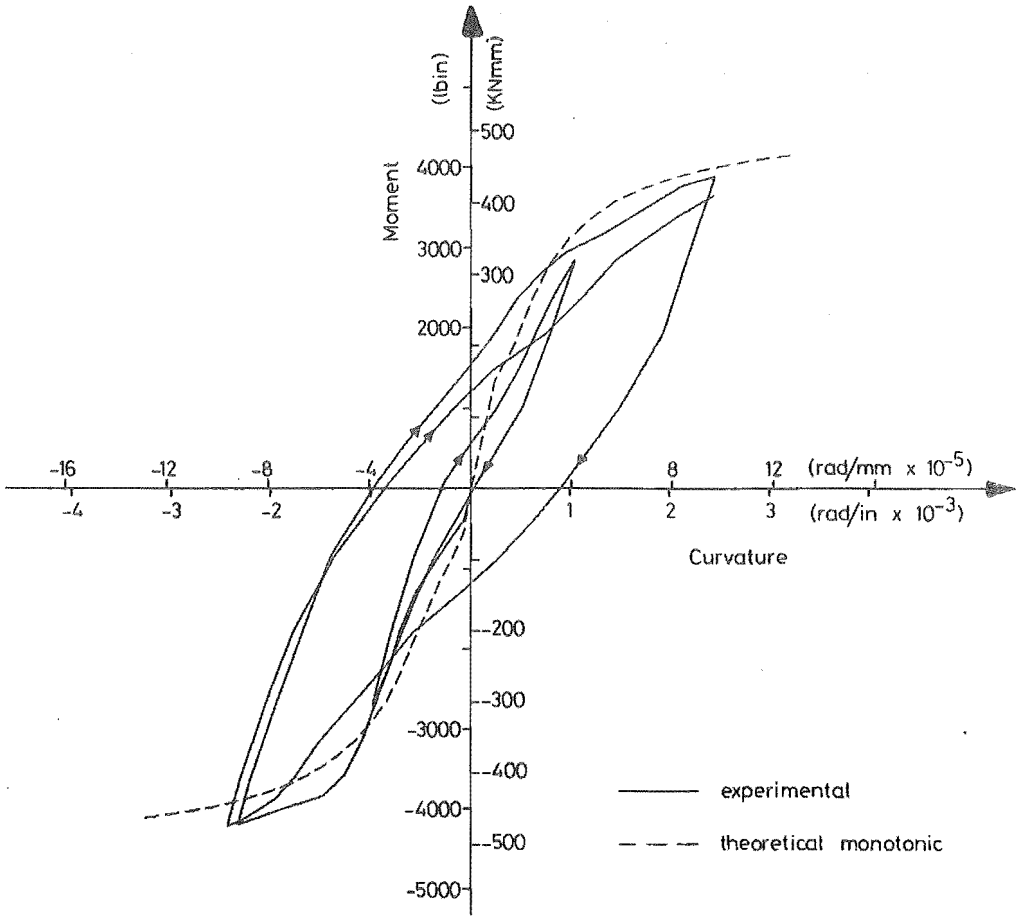


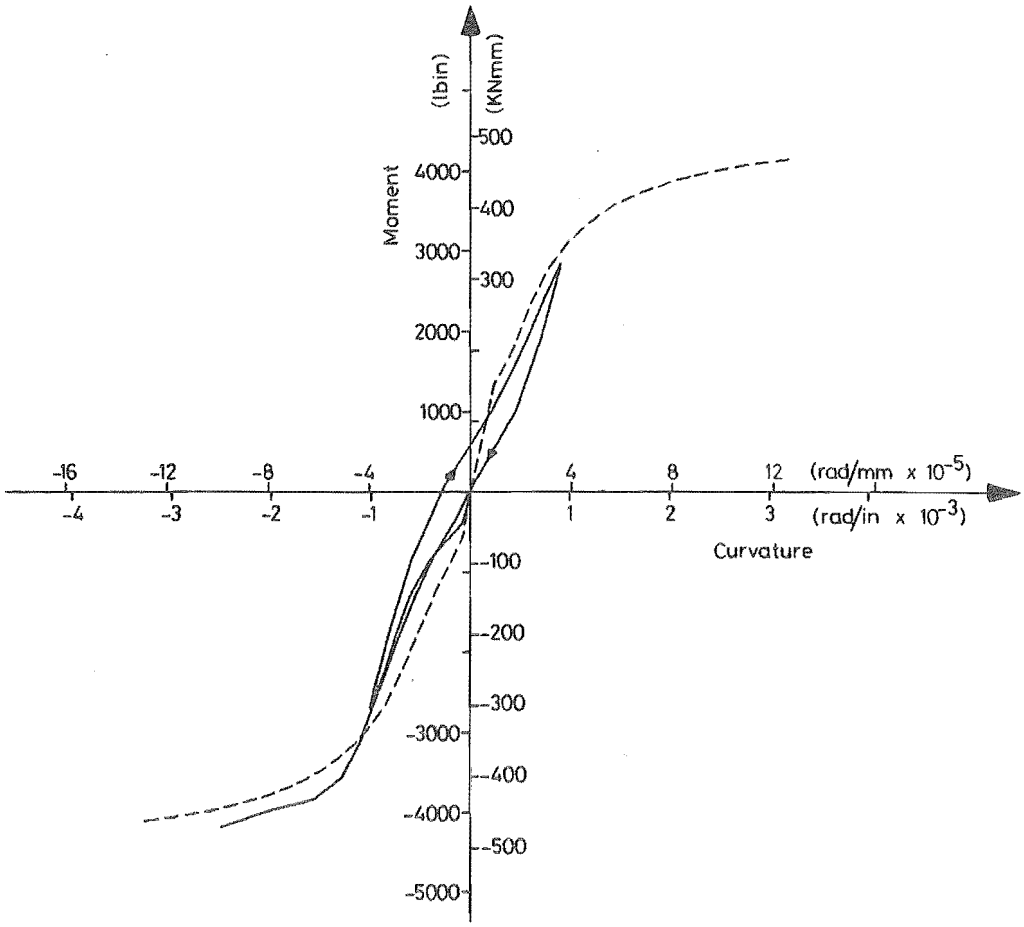


FIGURE 4-19 : EXPERIMENTAL AND THEORETICAL MOMENT-CURVATURE CURVES FOR BEAM 4 (CYCLIC LOADING)

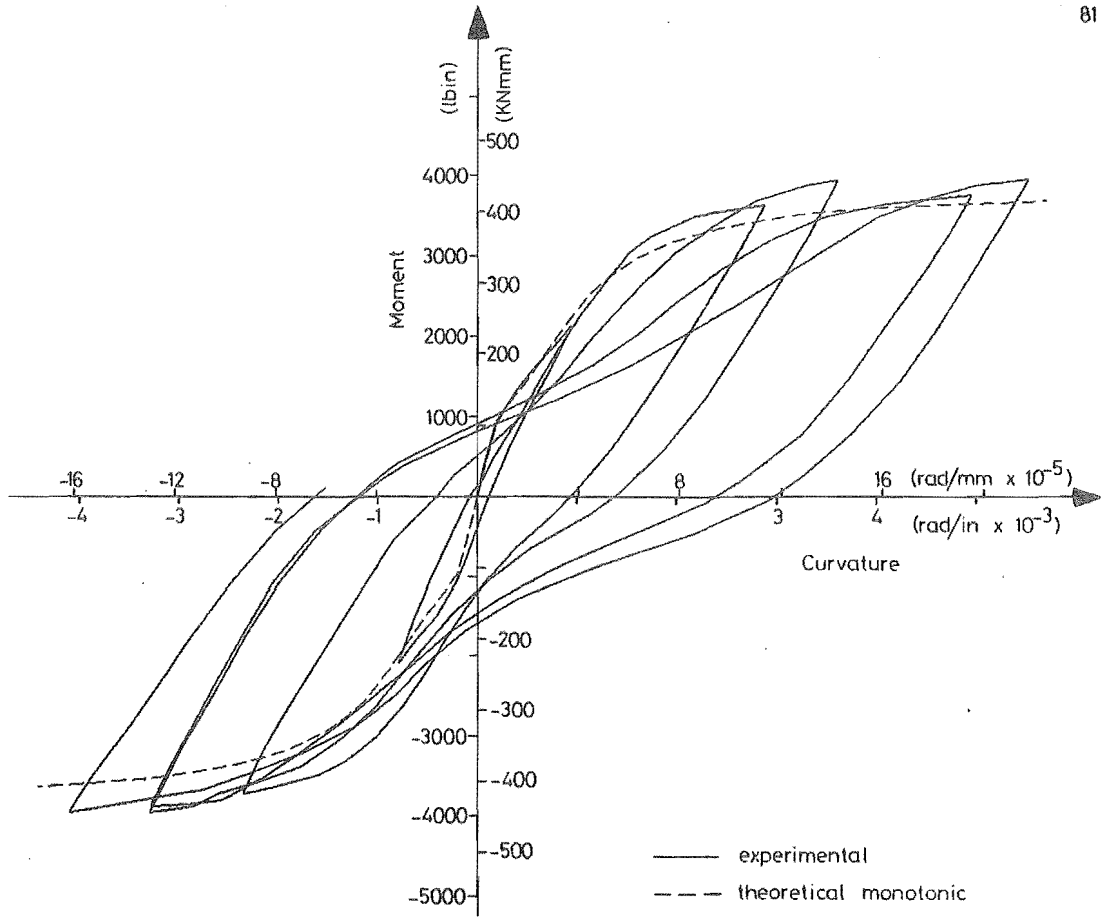


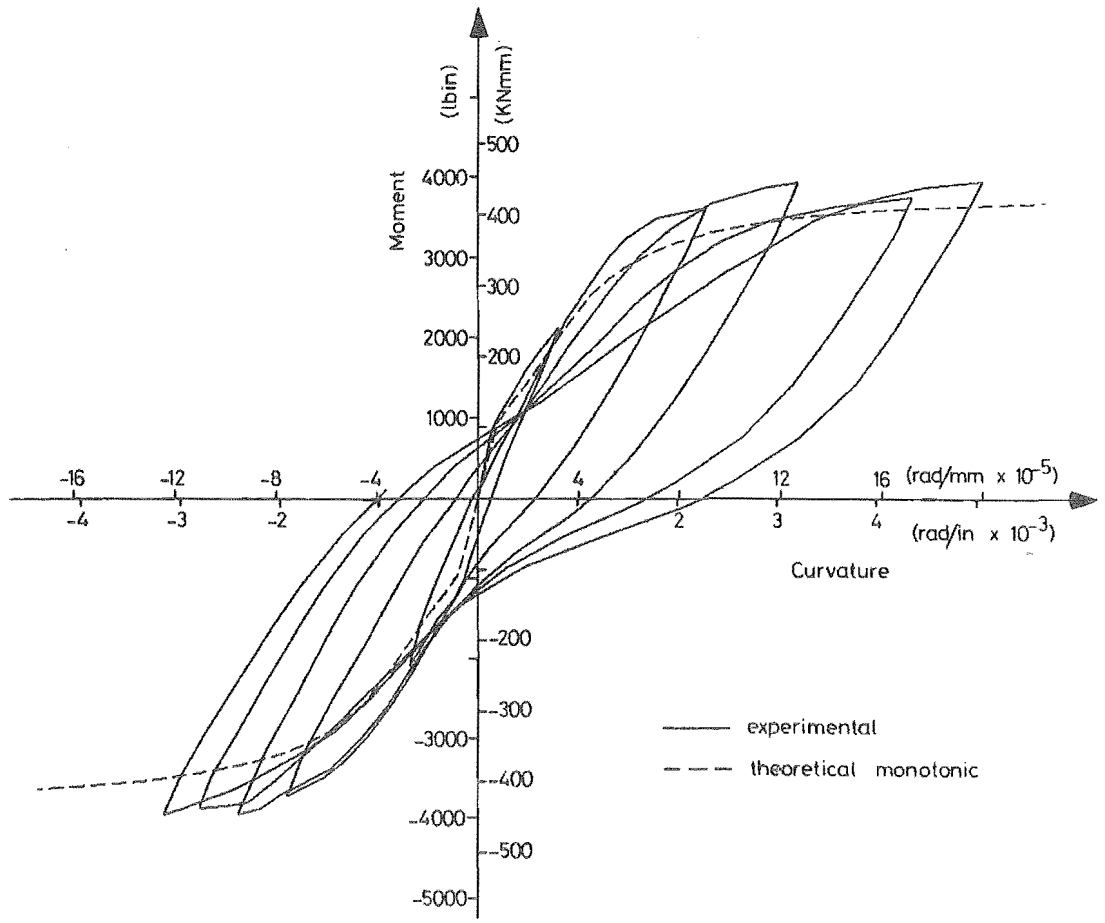


FIGURE 4-20 : EXPERIMENTAL AND THEORETICAL MOMENT-CURVATURE CURVES FOR COLUMN 6 (1000 LB AXIAL LOAD - CYCLIC LOADING)

A greater variation between experimental and theoretical ultimate strengths was found in these cyclic tests than had been the case in the monotonic tests. The theoretical monotonic moment-curvature curve is represented by the dotted lines in figures 4-18 to 4-20 and it could be expected that these represent an envelope of the peaks of the moment-curvature loops. While the negative moment for Beam 3 is predicted accurately, the positive moment estimation is too high. Beam 4 suffered a premature failure of the strain gauges but it is apparent that the theoretical negative moment is too low and that the theoretical positive moment is too high. For Column 6, in which the strain gauges performed the most satisfactorily, the theoretical moments can be seen to underestimate the actual moments recorded. The strains were insufficient to involve the onset of steel strain hardening according to the monotonic stress-strain curves. However with cyclic loading several cycles of loading can cause strain hardening and a resulting increase in steel stress at relatively low strain levels. Also these tests do give some credence to the claim that size effects may cause the results of experimental strength tests on small scale models to be larger than theory would predict.

### 4.6.3 Theoretical beam and column moments

The actual moment-curvature curve of a member can be approximated by an elasto-plastic curve, with the flexural strength of the member put equal to a suitably defined yield moment. The yield moment in this study is defined as either the moment corresponding to a curvature of 0.010 rad/in. (0.004 rad/mm) or as the maximum moment reached, if that maximum moment occurred at a curvature of less than 0.010 rad/in.

Assuming that the modulus of elasticity for concrete is $4 \times 10^6$ lb/in$^2$ (27.6 GN/mm$^2$), the flexural rigidity and yield moments of the beams and columns are found to be ...

(i) Beam. (assuming a width of slab equal to that used in the beam member tests)

uncracked section flexural rigidity = 2.54 in$^4$ ($10.57 \times 10^4$ mm$^4$)

cracked section flexural rigidity = 0.95 in$^4$ ($3.95 \times 10^4$ mm$^4$)

positive yield moment = 4620 lbin (522 KNmm)

negative yield moment = 4440 lbin (502 KNmm)

(ii) Column.

uncracked section flexural rigidity = 1.60 in$^4$ ($6.66 \times 10^4$ mm$^4$) (no axial load)

cracked section flexural rigidity = 0.55 in$^4$ ($2.29 \times 10^4$ mm$^4$) (no axial load)

cracked section flexural rigidity = 0.56 $in^4$ (2.33 x $10^4$ $mm^4$)
at an axial load of 119 lb (530 N)
(single storey structure)
cracked section flexural rigidity = 0.61 $in^4$ (2.54 x $10^4$ $mm^4$)
at an axial load of 715 lb (3180 N)
(six storey structure)

4.6.4 Column axial load - moment interaction

The flexural strength of the columns varies according to the axial load level. The structural analysis program of Sharpe [19], used in this study and discussed in Section 5.4.3, includes a subroutine which uses three straight lines to approximate the interaction curve. These lines connect four points: the point of axial compressive strength, the point of balanced flexural failure, the point of ultimate moment corresponding to zero axial load, and the point of axial tensile strength.

A concrete strength of 4700 lb/$in^2$ (32.4 N/$mm^2$) was used in the theoretical moment-curvature calculations when determining the interaction curve. The interaction curve could not be established for axial loads greater than 15,000 lb (66,700 N) without some adjustments to the moment-curvature computer program MOCU, but this was felt to be unwarranted since it was well beyond the range of interest.

The following points were determined:

(i) axial compressive strength (at a strain of 0.002) = 22,000 lb (97,900 N)

(ii) balanced flexural failure

moment = 6206 lbin (701 KNmm)
axial load = 7200 lb (32,000 N)

(iii) flexural strength corresponding to zero axial load
= 3270 lbin (255 KNmm)

(iv) axial tensile strength (assuming steel strength = 46,500 lb/$in^2$ = 321 N/$mm^2$)
= 4520 lb (20,100 N).

However, as can be seen from figure 4-21, the region of the interaction curve of interest for this series of tests is small since the axial load levels expected during the tests are small and do not fluctuate greatly. Therefore a better approximation for the interaction curve in the region of interest would be obtained by introducing ficticious points for the point of balanced flexural failure and the point of axial tensile strength. These become ...

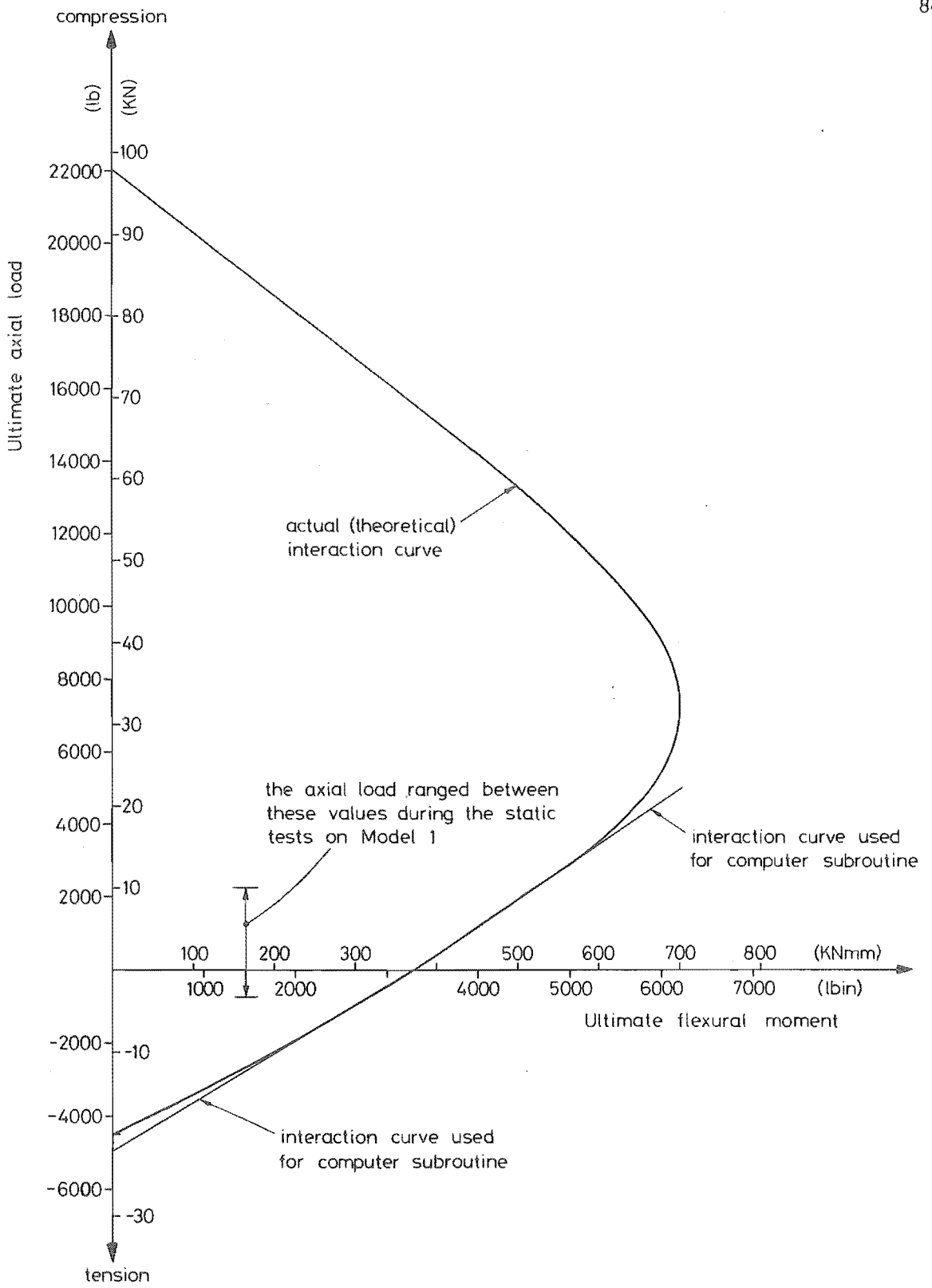


FIGURE 4-21 : COLUMN AXIAL LOAD - MOMENT INTERACTION CURVE

(i) balanced flexural failure

moment = 6220 lbin (703 KNmm)

axial load = 5000 lb (22,200 N)

(ii) axial tensile strength = 4880 lb (21,700 N).

# CHAPTER FIVE

# DYNAMIC THEORY AND TESTING OF SINGLE STOREY STRUCTURE

## 5.1 INTRODUCTION

In view of the fact that no work involving small scale structures of this type had previously been carried out at the University of Canterbury, it was considered advisable to initially construct and test a single storey structure prior to attempting a full six storey structure.

The advantages of this were:

(i) it presented a good opportunity for checking methods of casting the frames and erecting the structure, and it enabled these techniques to be refined where necessary for later work.

(ii) it enabled an evaluation of the methods of testing the structure and the performance of the testing equipment.

(iii) it gave a preliminary indication of any modifications which might have been required to the structural detailing, such as joint detailing, anchorages, etc.

In addition to acting as a trial run for the methods of constructing and testing a full six storey model, much information of value in its own right could be obtained from the tests. Interpretation of the results would be straightforward because the structure has only one lateral degree of freedom. Some points about which it was hoped information could be obtained were:

(i) stiffness degradation

(ii) damping

(iii) displacement response curve

(iv) load-deflection hysteresis curves

The plan dimensions, member sizes and reinforcement ratios of the single storey structure are identical with those of the six storey structure, the details of which are given in Chapter Three.

## 5.2 VIBRATION TESTING THEORY

The following treatment is based on that given by Newmark and Rosenblueth [30]. Although derived for the particular case of a single degree of freedom structure, the general equation of motion can be applied to a particular mode of multi-degree of freedom structure, since each mode is governed by its own equation independent of the other modes.

### 5.2.1 General equation of motion

Consider the single degree of freedom structure shown in figure 5-1 which is assumed to have viscous damping. Denoting ...

$x_o$ = ground displacement

$x$ = total displacement of the mass

$y$ = $x - x_o$ = displacement of the mass relative to the ground

$P$ = external force applied to the mass

$y_o = \frac{P}{K}$

$w_n^2 = \frac{K}{M}$

$\lambda w_n = \frac{C}{2M}$

$w_n$ = undamped natural frequency

$\lambda$ = fraction of critical damping,

then the general equation of motion of the above system may be written ...

$$M\ddot{x} + C\dot{y} + Ky = P \qquad (5\text{-}1)$$

which upon rearranging becomes ...

$$M\ddot{y} + C\dot{y} + Ky = Ky_o - M\ddot{x}_o$$

and which reduces to ...

$$\ddot{y} + 2\lambda w_n \dot{y} + w_n^2 y = w_n^2 y_o - \ddot{x}_o \qquad (5\text{-}2)$$

### 5.2.2 Free vibration

A structure undergoes free vibration when its base remains motionless and there are no external forces.

thus $y_o = 0$ and $x = y$

The general solution of equation 5-2 then becomes ...

$$y(t) = ae^{-\lambda w_n (t-t_1)} \sin [w_d (t-t_1)] \qquad (5\text{-}3)$$

where $w_d$ = damped natural frequency = $w_n(1-\lambda^2)^{\frac{1}{2}}$

$C_{cr}$ = coefficient of critical damping, i.e. $\lambda = 1.0$

$= 2(KM)^{\frac{1}{2}}$

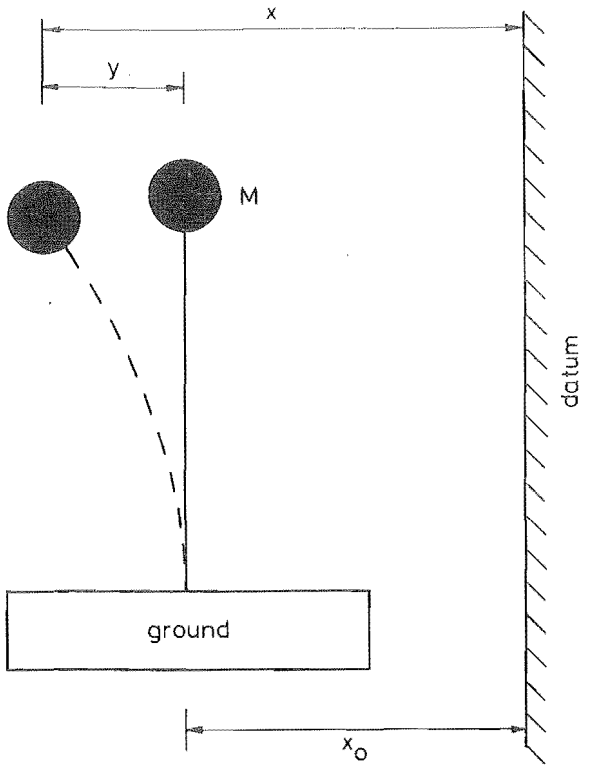


FIGURE 5-1 : IDEALISED LINEAR SINGLE DEGREE OF FREEDOM STRUCTURE

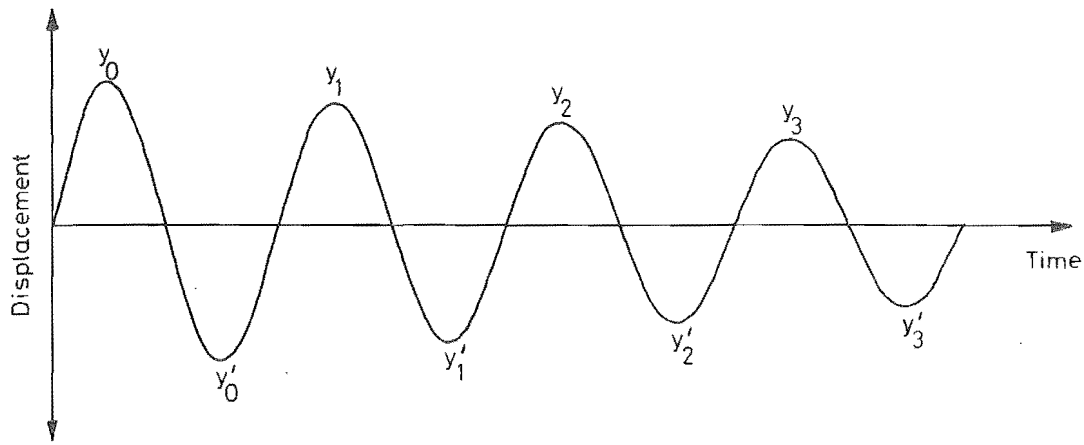


FIGURE 5-2 : LOGARITHMIC DECREMENT DURING FREE VIBRATION

Equation 5-3 may be written ...

$$y(t) = Ae^{-\lambda w_n t} \sin (w_d t + \theta) \qquad (5\text{-}4)$$

If the damping is less than critical, oscillatory motion will occur which will gradually tend to zero, as shown in figure 5-2. The rates of any two maxima separated by n cycles of oscillation may be written ...

$$\frac{y_n}{y_o} = e^{-2\pi n\lambda (1-\lambda^2)^{-\frac{1}{2}}} = e^{-2\pi n\lambda} \qquad (5\text{-}5)$$

to good accuracy if $\lambda < 0.2$

For successive peaks $n = 1$ , and equation 5-5 reduces to ...

$$\lambda = -\frac{1}{2\pi} \log_e \frac{x_1}{x_o} \qquad (5\text{-}6)$$

An approximate relation to this equation is often found by expressing equation 5-6 in terms of the logarithmic decrement $\Delta$ .

$$\lambda = \frac{1}{2\pi} \Delta \qquad (5\text{-}7)$$

$$\text{where } \Delta = \log_e \frac{x_1}{x_2} \text{ or } \frac{x_2}{x_1} = e^{-\Delta} \qquad (5\text{-}8)$$

Expanding equation 5-8 as a series and considering only the first two terms ...

$$\frac{x_2}{x_1} = 1 - \Delta$$

$$\text{and thus } \lambda = \frac{1}{2\pi} \left( \frac{x_1 - x_2}{x_1} \right) \qquad (5\text{-}9)$$

Equation 5-9 is often considered in the literature, e.g. Blake [31] to give a good approximation to $\lambda$ where $\lambda < 0.1$ . In fact the approximation is reasonable only if $\Delta < 0.1$ i.e. $\lambda < 1.68\%$ as indicated by the comparison between equations 5-6 and 5-9 shown in figure 5-3.

### 5.2.3 Forced vibration

If the system shown in figure 5-1 is subjected to a constant forced vibration, the motion of the mass will gradually settle into a steady state vibration. If no external force is present and the ground moves with a sinusoidal motion, then ...

$$y_o = 0 \quad \text{and} \quad x_o = a \sin wt \quad \text{i.e.} \quad \ddot{x}_o = -aw^2 \sin wt$$

where $a$ = amplitude of the ground motion

$w$ = angular frequency of the ground motion

$t$ = time

The general solution is still given by equation 5-4 and represents the vibration of the structure as its fundamental natural frequency due to the initial impulse when the forced vibration began.

$$y(t) = Ae^{-\lambda w_n t} \sin (w_d t + \theta) \tag{5-4}$$

The particular solution describes the steady state vibration of the structure at the frequency of the forcing function and is ...

$$\frac{y}{a} = B_d \sin (wt - \phi) \tag{5-10}$$

$$\text{where } B_d = \left[\left\{1 - \left(\frac{w_n}{w}\right)^2\right\}^2 + \left[2\lambda\frac{w_n}{w}\right]^2\right]^{-\frac{1}{2}} \tag{5-11}$$

$$\text{and } \phi = \tan^{-1}\left[\frac{2\lambda\frac{w_n}{w}}{1 - \frac{w_n^2}{w^2}}\right]$$

$\phi$ is an angular phase shift and $B_d$ is a dimensionless response factor, equal to the ratio of the dynamic to the static displacement response amplitudes.

When a structure is excited by a ground motion it initially responds at both its natural frequency, as given by equation 5-4, and at the forcing frequency of the ground motion, as given by equation 5-10. If the ground motion consists of a series of random impulses such as might occur in an earthquake, then the motion of the structure will consist principally of vibrations at or near the natural frequency of the structure. However, if the ground motion consists of vibrations of constant frequency and amplitude, then the vibrations of the structure at its own natural frequency will tend to zero over a sufficiently long time no matter how small the damping ratio. Thus the steady state vibration is described completely by equation 5-10 and it is this vibration which is of interest when carrying out forced vibration tests.

From consideration of equations 5-10 and 5-11, the nature of the governing force corresponding to various ranges of input frequency can be identified.

(i) if $\frac{w}{w_n} \to 0$, then $y$ assymptotically $\to (\frac{w}{w_n})^2 a \to 0$ and the system is essentially mass controlled, i.e. dynamic effects are negligible.

(ii) if $w = w_n$, then $y = \frac{a}{2\lambda}$ and the vibrating system is essentially damping controlled.

(iii) if $\frac{w}{w_n} \to \infty$, then $y \to a$ and the vibrating system is essentially spring controlled.

Thus the influence of damping is important in the region of the natural frequency of the structure.

Differentiation of equation 5-10 yields the ratios of dynamic to static amplitude of velocity and acceleration.

$$B_v = (\frac{w_n}{w}) B_d \quad \text{and} \quad B_a = (\frac{w_n}{w})^2 B_d$$

The forcing function is in resonance with the system when the response factor is a maximum. Each quantity has a separate resonance frequency which is different from the natural frequency, although for usual amounts of structural damping ($0.01 < \lambda < 0.2$) these differences are very small. The resonance frequencies and response amplitudes are given in table 5-1.

### 5.2.4 Experimental determination of damping

The energy dissipated by a simple dash-pot damper is known as hysteresis loss and is proportional to the forcing frequency. However, the hysteresis loss of most materials and structures has been found to be independent of frequency and so structural damping is defined as the damping force equal to the viscous damping force at some frequency ($w_n$) but being invariant with frequency. Structural damping is thus dependent on the velocity of the body, and it results from internal friction within the material or at connections between elements of a structural system.

It was once common practice to construct a nearly continuous curve of response as a function of frequency of excitation by running a vibrator to a high frequency and letting it coast to rest, under the erroneous assumption that the amplitude attained at each instant equalled the steady-state amplitude for the frequency of excitation considered. The percentages of damping derived from these curves grossly overestimated the actual damping ratios. Hudson (quoted by reference [30]) suggests that tolerances considerably better than 1 in 1,000 in the frequency of the disturbing force are necessary or else the damping ratios derived from forced vibration tests will be systematically too high.

TABLE 5-1 : RESONANCE FREQUENCIES AND RESPONSE AMPLITUDES

| Quantity | Resonant frequency | Response amplitude |
|---|---|---|
| undamped natural frequency | $w_n$ | - |
| damped natural frequency | $w_n(1-\lambda^2)^{\frac{1}{2}}$ | - |
| displacement | $w_n(1-2\lambda^2)^{\frac{1}{2}}$ | $(2\lambda)^{-1}\ (1-\lambda^2)^{-\frac{1}{2}}$ |
| velocity | $w_n$ | $(2\lambda)^{-1}$ |
| acceleration | $w_n(1-2\lambda^2)^{-\frac{1}{2}}$ | $(2\lambda)^{-1}\ (1-\lambda^2)^{-\frac{1}{2}}$ |

TABLE 5-2 : VARIATION OF DAMPING AND NATURAL FREQUENCY WITH LATERAL LOAD

| Test number | Lateral load lbs (N) | % of critical damping | Natural frequency $f_n$ c.p.s. | Stiffness K lb/in (N/mm) |
|---|---|---|---|---|
| 1 | 87 (387) | 2.0 | 14.7 | 9980 (1750) |
| 2 | 414 (1840) | 2.8 | 13.1 | 7930 (1390) |
| 3 | 327 (1450) | 2.7 | 13.0 | 7810 (1370) |
| 4 | 632 (2810) | 3.2 | 11.75 | 6380 (1120) |
| 5 | 1091 (4850) | 4.3 | 9.2 | 3910 (685) |
| 6 | 414 (1840) | 4.1 | 9.2 | 3910 (685) |
| 7 | 1312 (5840) | 5.0 | 8.5 | 3340 (585) |
| 8 | 414 (1840) | 4.6 | 8.45 | 3300 (578) |
| 9 | 414 (1840) | 4.6 | 12.75 | 2820 (494) |

## 5.3 TESTING PROCEDURE

### 5.3.1 Testing technique

Both static and dynamic lateral loading tests were to be carried out on the structure. Reversed loading was to be a feature of the static tests and the loading system chosen had to be flexible enough to enable the relatively stiff structure to be readily excited into free vibration.

When considering any system for use in structural testing, a basic decision must be made as to whether the test is to be force controlled or deflection controlled. Both methods suffer because of creep in the test specimen, especially when using flexible test specimens such as in this case. In a force controlled test, the specimen will deflect under constant load due to creep. If the test is deflection controlled, the force as measured by a load cell will reduce as the specimen relaxes.

It was decided to test the structures under a constant gravitational loading system. This greatly simplified the design of the reaction frame but it did mean that control over the test specimen was reduced to some extent although this reduction was minimal if due care was exercised.

A full description of the reaction frame is given in Section 2.3.5. Briefly, yokes were placed around the two nearside columns at each floor level to which were attached wire ropes. The wire ropes ran over a series of pulleys attached to the reaction frame and were connected to the loading pan by a short length of thin wire. To set the structure into free vibration the load was suddenly released by cutting the short length of wire.

Packing was placed at both ends of the shaking table to ensure that it did not deflect due to the static loading. Dial gauges (2 in. (50.8 mm) Mercer) were mounted on the reference frame to measure the deflection of the structure at the level of the floor slab and also any possible table deflection.

During dynamic testing, both dial gauges were removed and the deflection of the shaking table and of the structure at the level of the floor slab were measured using Hewlett Packard Model 24DCDT - 3000 LVDTs. These deflection readings were subtracted using a differential amplifier and the difference, which was the deflection of the structure relative to the table, was recorded on the Brush Mark 280 pen recorder, together with the deflection of the table. The ratio of these two recordings, which was

the displacement response factor, could then be seen at a glance.

The acceleration of the floor slab during dynamic testing was measured using a Kistler 305A accelerometer. This acceleration, together with the deflection of the floor slab relative to the table, were recorded simultaneously on the Brush pen recorder and this enabled dynamic load-deflection hysteresis curves to be readily determined.

### 5.3.2 Testing program

The structure was loaded with a monotonically increasing lateral load until its ultimate capacity was attained. At various points the load was suddenly released, which excited the structure into free vibration and enabled its damping ratio and natural frequency to be measured. From this, the variation in damping and stiffness with variations in deflections could be determined.

After completion of the static tests, the MTS testing system was switched on in preparation for the dynamic tests. Intermittent breakdowns had been occurring in a faulty transistor which was located in the MTS input module, a full description of which is given in Section 2.5.3. On this occasion the transistor emitted a transient which caused a violent shock wave to be applied to the table, badly cracking the structure. Fortunately the testing program was sufficiently advanced that this unplanned shock wave was not critical, since the structure would have cracked badly in the course of the dynamic testing anyway. No further breakdowns occurred in the transistor during the testing of the single storey structures.

The dynamic testing program commenced with a series of forced vibration tests. All of these tests were conducted at different frequencies and the amplitude of the forcing function was always of such a magnitude that the resultant deflection of the structure relative to the table never exceeded $\frac{1}{2}$ in. (12.7 mm). As indicated in Section 5.2.3, the response of a structure to a steady forced vibration is composed of two parts; steady state motion at the frequency of the forcing function, and free vibrations at the natural frequency of the structure which are rapidly damped out. For a structure with damping of 5% of critical and a natural frequency of 5 c.p.s., only 3 seconds is required to dampen the free vibrations to less than 1% of their initial amplitude and so the forced vibration was allowed to continue for 10 seconds before the motion was recorded on the pen recorders.

Several free vibration tests were then carried out and the damping and natural frequency thus obtained were checked with those obtained from forced vibration theory.

A dynamic load-deflection hysteresis curve was obtained by

simultaneously measuring the acceleration and deflection of the structure during steady state vibration testing. A static load-deflection hysteresis curve was also determined from several static cyclic loading tests. Care was taken to try to ensure that the maximum deflections of the two loops were approximately the same, in order that a valid comparison could be made.

All recording instruments were then removed from the structure to avoid possible damage and a series of square wave and sine wave functions of increasing severity were applied to the table until the structure was in danger of imminent collapse.

## 5.4 ANALYSIS OF TEST RESULTS

### 5.4.1 Weight of the structure

The mass of the supporting columns is often disregarded when calculating the natural frequency of a single degree of freedom structure such as that shown in figure 5-1. If the total mass of the columns is $mL$, where $L$ is the length of the columns, then using Rayleigh's Method wherein the assumption is made that the deflected curve of the column during vibration has the same shape as the static deflection curve, it can be shown with good accuracy that the period of vibration of the structure is the same as that of a massless cantilever carrying at its end a mass $M'$ ;

where $M' = M + \frac{33}{140} mL$

mass of columns $= mL = 0.08$ slugs (1.17 Kg)

mass of remaining structure plus steel blocks

$= M = 1.09$ slugs (15.92 Kg)

therefore $M' = 1.17$ slugs (17.1 Kg)

if the steel blocks are removed then

$M' = 0.44$ slugs ( 6.4 Kg)

the stiffness of the structure $K = M' \times (2\pi f_n)^2$

### 5.4.2 Degradation of stiffness

There are several different ways that the stiffness of a non-linear structure may be defined:

(i) the local secant stiffness, which is the value of the next load increment divided by the deflection due to that increment

(ii) the tangential stiffness, which is the slope of the tangent to the point on the load-deflection curve

(iii) the secant stiffness, which is the slope of the line joining the peak value to the origin of the load-deflection curve

(iv) the slope of the line joining the peak to peak values of the load-deflection curve (this is not necessarily the same as (iii)).

Methods (i) and (ii) define the "instantaneous" stiffness of the structure at a particular point on the load-deflection curve whereas methods (iii) and (iv) represent attempts to evaluate the overall stiffness of the structure. The stiffness as defined by method (iv) may be found from forced or free vibration tests and is the definition of stiffness to be used in conjunction with dynamic testing.

As described in Section 5.3.2 the structure was loaded monotonically until its ultimate load was attained. At various points along the static load-deflection curve the load was suddenly released, which set the structure into free vibration and enabled its damping ratio, natural frequency and stiffness to be determined. The results obtained from these tests are tabulated in table 5-2, in the order in which they were conducted.

The uncracked structure had a damping ratio of 2% of critical damping which is in general agreement with the results of many other investigators. From comparison of test run 3 with 2, 6 with 5 and 8 and 9 with 7, it can be seen that both the stiffness and the natural frequency stay constant or reduce only slightly when the structure is vibrated at less than the maximum deflection it has already experienced. Test run 9 was conducted with the steel weights removed from the slab floor. By the completion of this series of tests the stiffness of the structure had reduced to 30% of the original stiffness and its damping ratio had more than doubled.

After the structural frames were cast it was found that minute shrinkage cracks had formed in the concrete, grouped mainly near the tops and bottoms of the columns, and these tended to open up as load was applied. Thus the columns were never in a completely uncracked state at any stage of the testing and so the initial condition of the structure could best be described as having cracked columns and uncracked beams. This is borne out by the results of analyses tabulated in table 5-3, where the measured initial natural frequency of the structure is closely predicted by the model analysis conducted on a structure with cracked columns and uncracked beams.

This shrinkage cracking is difficult to prevent in small scale reinforced concrete models since the large ratio of surface area to volume causes the concrete to dry out rapidly.

### 5.4.3 Frame analysis program

The author was fortunate in having access to a two-dimensional dynamic inelastic frame analysis program which had been recently developed by Sharpe [19] . This was a digital computer program and was run on a Burroughs B6718 computer belonging to the University Computer Centre. The program was intended for use by both researchers and practicing engineers and so was kept flexible and readily comprehensible. The importance of ensuring that the printout of results of the response of the frame was easy to follow was fully appreciated and a valuable feature of the program was a pictorial display of the frame being analysed with the plastic hinge locations indicated whenever the plasticity of the frame changed.

Giberson's one-component non-linear beam model was used for the frame members; this is simply a one-dimensional prismatic beam with sprung hinges of variable stiffness incorporated at infinitesimal distances from either end. This permitted the modelling of a full range of moment-curvature loops; the options offered to the user included elasto-plastic, bi-linear and Ramberg-Osgood hysteresis loops. The problem of moment overshoot in the moment-curvature loops was satisfactorily overcome by reinvesting the overshoot onto the incremental dynamic load vectors in the next time step. A subroutine incorporating an axial load - moment interaction curve for the columns was offered as an option and it proved to be very useful. A limitation of this subroutine was that it could only be used in conjunction with the elasto-plastic moment-curvature loop.

The program included all of those features which by now should be regarded as standard; namely, allowance for shear deformations, axial deformations and rigid end blocks. The frame being analysed could be simultaneously subjected to the vertical component of an earthquake as well as a horizontal component and provision was made to scale the earthquake or to vary the value of gravitational acceleration. A variety of numerical integration schemes were offered as options - the constant average acceleration method was used throughout this study.

The program printout consists firstly of a basic description of the analysis and the options chosen, followed by a data echo check. A static analysis of the dead loads and a determination of the natural modes would then be carried out, if these options had been chosen. The time-history response of the frame is printed next, with details of selected node displacements and member forces and also the amount by which the selected member curvatures exceed the curvature at first yield. At the

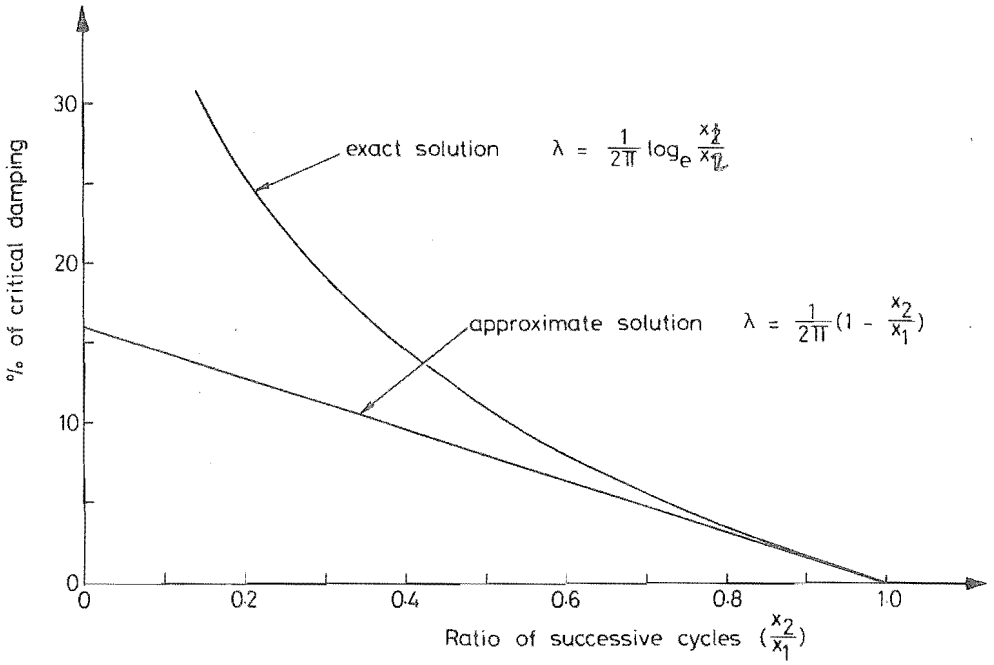


FIGURE 5-3 : COMPARISON BETWEEN EXACT AND APPROXIMATE SOLUTIONS FOR DETERMINING DAMPING FROM SUCCESSIVE CYCLES OF A FREE VIBRATION TEST

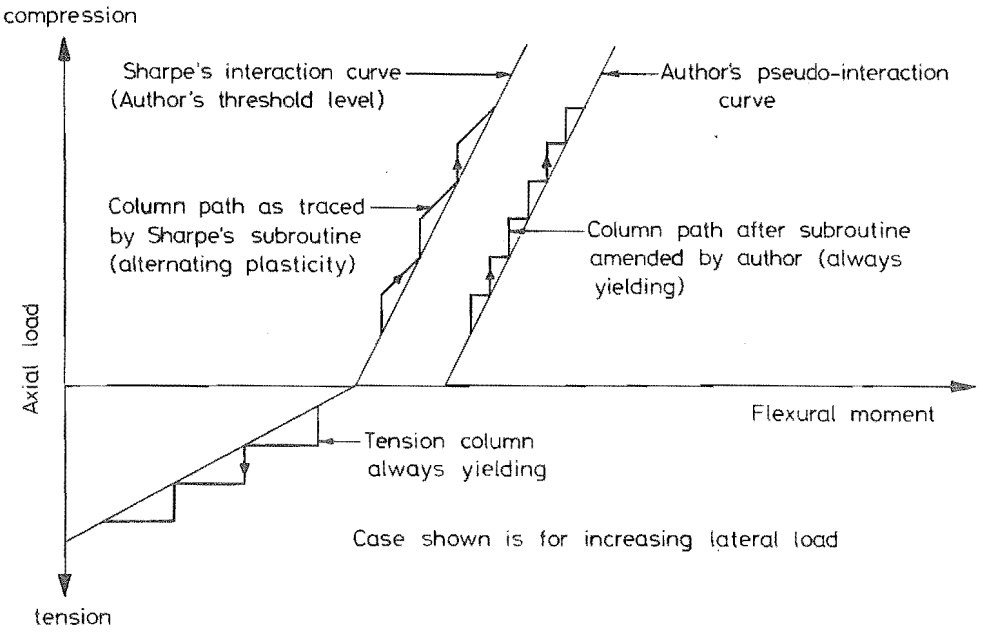


FIGURE 5-4 : AMENDMENT MADE TO COLUMN AXIAL LOAD - MOMENT INTERACTION SUBROUTINE OF SHARPE (19)

conclusion of the time-history, a summary of maximum displacements, moments and plastic displacements is produced.

A special version of the dynamic program was adapted for the author by Sharpe [19]. This consisted of a static analysis program which would analyse a step-by-step incremental static loading applied to the structure. During the operation of this version it was noticed that after a plastic hinge formed in a column carrying a compressive load, on subsequent load increments the hinge alternately disappeared and then reappeared. The reason for this, and the method used to overcome the problem, are explained with reference to figure 5-4.

Once yield had occurred, the column axial load - moment interaction subroutine assumed a constant moment at that plastic hinge over the next load increment. However, at the end of the increment the yield moment corresponding to the increased level of axial load was greater than the actual moment and so the hinge was removed for the next load increment. The solution used was to treat the interaction curve only as a threshold level to determine whether yield had occurred; if it had, then the hinge was given a slightly increased moment (0.5% was found to be adequate) for the next time increment. As long as the load increment was not too large, the increase in axial load was insufficient to remove the plastic hinge. This modification was also required for a column with a decreasing tensile load.

### 5.4.4 Structural analysis

The mode of failure was a column sidesway mechanism as expected, since the beams were stronger than the columns. Analysis using the step-by-step static structural analysis program developed by Sharpe [19], indicated that the point of contraflexure in the columns was initially at a height of 0.60h and thus hinges initially formed at the column bases.

The structure was analysed assuming that only the beams had cracked and including the torsional strength of the lateral beams in with the flexural strength of the longitudinal beams. However, this increase in beam strength made no difference to the ultimate failure load since failure occurred in the columns. The joint rotations at the floor slab level were sufficiently large to ensure that the lateral beams cracked well before the collapse mechanism formed.

A static analysis using the column axial load - moment interaction subroutine indicated a failure load of 1250 lb (5560 N) which is 92.5% of the actual ultimate failure load of 1352 lb (6014 N). The reason for the

TABLE 5-3 : MEASURED AND PREDICTED NATURAL FREQUENCY

| Initial value obtained from tests | Modal analysis based on a structure with | | |
|---|---|---|---|
| | Uncracked columns Uncracked beams | Cracked columns Uncracked beams | Cracked columns Cracked beams |
| 14.7 | 20.5 | 13.6 | 12.2 |

TABLE 5-4 : DAMPING FOR EACH CYCLE OF FREE VIBRATION TEST

| Cycle | Displacement in inches (mm) ← | → | Damping (% of critical) |
|---|---|---|---|
| $y_0$ | 0.208 (5.28) | | |
| $y'_0$ | | 0.187 (4.75) | 7.2 |
| $y_1$ | 0.132 (3.35) | | 9.5 |
| $y'_1$ | | 0.103 (2.62) | 12.8 |
| $y_2$ | 0.059 (1.50) | | 16.3 |
| $y'_2$ | | 0.037 (0.94) | 18.9 |
| $y_3$ | 0.018 (0.46) | | 24.4 |
| $y'_3$ | | 0.008 (0.20) | |

increase in strength was thought to be probably due to strain hardening occurring in the column reinforcing steel. The probable strain in the column hinges was calculated from the measured deflection of the structure assuming a plastic hinge length of $\frac{d}{2}$ = 0.8 in. (20.3 mm). At this strain the ultimate moment of the column was about 4% greater than the yield moment. Use of this value in a bi-linear analysis led to an ultimate failure load of 1310 lb (5830 N), which is 97% of the measured ultimate failure load.

## 5.5 DISPLACEMENT RESPONSE CURVE

The displacement response curve of a structure is an important parameter in understanding the response of the structure to a dynamic base motion. Most Codes of Practice specify design accelerations which depend on the natural frequency of the structure, the design acceleration increasing with the likelihood that the natural frequency of the structure will lie in the band of most common earthquake frequencies. As was shown in Section 5.2.3 the response of the structure in this region is essentially damping controlled and so determination of the degree of damping is necessary in order to analyse the behaviour of the structure.

By the time the forced vibration tests were carried out the natural frequency of the structure had reduced to 5.7 c.p.s. At this frequency the displacement response ratio was 9.25. Given that $B_d = \frac{1}{2\lambda}$ this corresponded to a damping ratio of 5.4% of critical damping. A second test run was carried out to check the results of the first and a close agreement was obtained and so 5.4% was accepted as the damping ratio.

A free vibration test was carried out to further check the damping ratio and it was found that the damping varied considerably with deflection. Damping ratios were calculated for each cycle of motion and these are tabulated in table 5-4.

It is apparent from table 5-4 that damping increases rapidly with decreasing deflection. The damping ratio is found from forced vibration tests at the point at which the maximum displacement response ratio occurs. Obviously this maximum displacement response ratio can easily be underestimated if the forcing frequency does not exactly coincide with the natural frequency but it cannot be overestimated (barring recording faults etc), and therefore the damping ratio can easily be overestimated but not underestimated. Thus the damping ratio as measured by the forced vibration tests represents an upper limit to the damping ratio as measured from free vibration tests and may be said to be the true

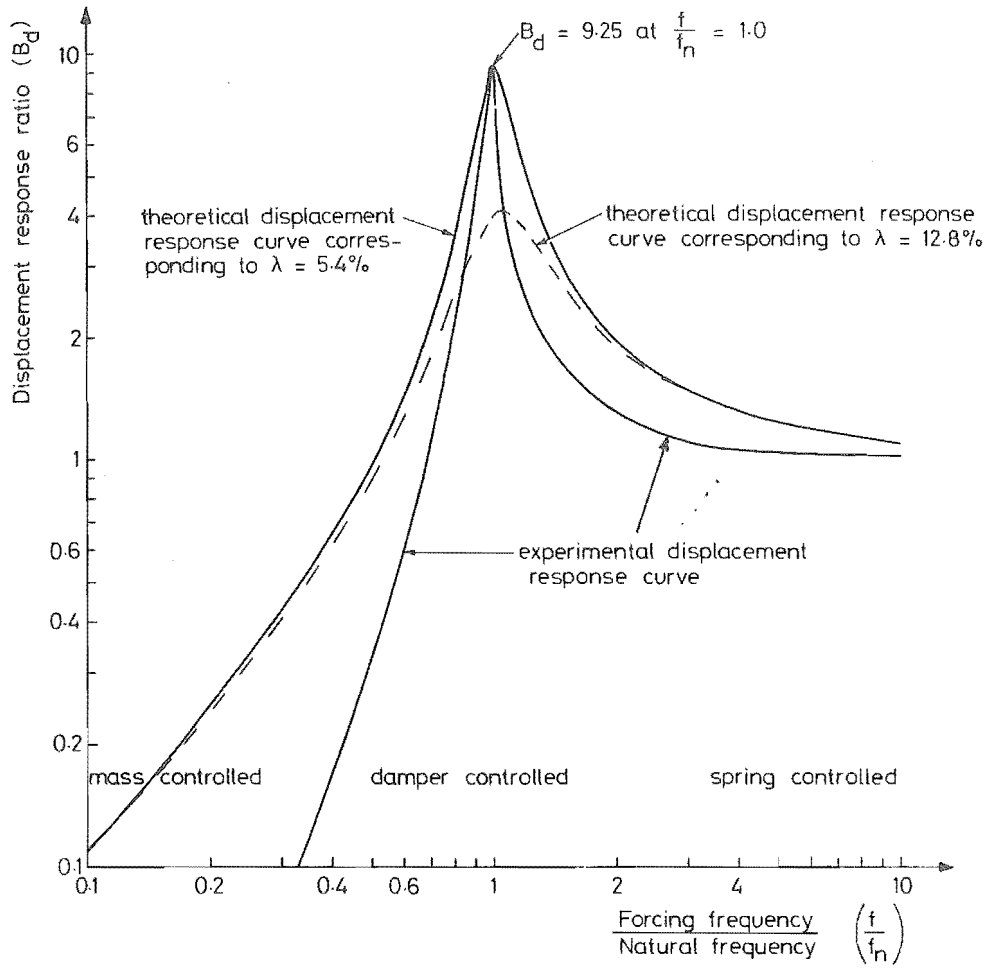


FIGURE 5-5 : COMPARISON OF THEORETICAL AND EXPERIMENTAL DISPLACEMENT RESPONSE CURVES

damping ratio of the structure.

It is often normal practice to measure the damping ratios of structures from free vibration tests and to average the damping over many cycles using equation 5-4 in an attempt to gain greater accuracy. While this may be satisfactory for linear structures, it is apparent that this would lead to an overestimation of the damping ratios of non-linear structures.

An attempt was made to try and determine how much effect the amplitude of the forcing function had on the displacement response ratio but the results were inconclusive. The problem was that the natural frequency of the structure was dependent on the deflection and therefore the ratio of forcing frequency to natural frequency varied with the deflection. Consequently the change in displacement response ratio was due to a lateral shift of the displacement response curve, rather than due to the change in amplitude alone.

The displacement response curve for the structure is shown in figure 5-5. A theoretical displacement response curve, based on $\lambda = 5.4\%$, is shown for comparison. The natural frequency of the structure was taken as that frequency at which the maximum displacement response ratio was obtained. The discrepancy between the experimental and theoretical curves is large. This discrepancy cannot be accounted for by varying the value of $\lambda$ since this merely changes the magnitude of the peak response, as indicated by the theoretical displacement response curve for $\lambda = 12.8\%$ drawn for comparison.

The discrepancy could be accounted for if in fact the structure had a higher natural frequency than that assumed in the region $\frac{f}{f_n} < 1.0$ and if it had a lower natural frequency than that assumed in the region $\frac{f}{f_n} > 1.0$. The deflection of the structure in the region $\frac{f}{f_n} > 1.0$ was very much less than the peak deflection and since a decrease in deflection leads to a decrease in stiffness, then the natural frequency of the structure in this region will be less than that assumed. However, the same reasoning would imply a lower rather than a higher natural frequency in the region $\frac{f}{f_n} < 1.0$ and so the displacement response curve must be primarily influenced by some other factor in this region.

## 5.6 LOAD-DEFLECTION HYSTERESIS CURVES

The load-deflection relationships for the structure for both static and dynamic loading are compared in figure 5-6. The deflection in each case was approximately the same in order that a valid comparison could be

made. The curves are very similar in shape and are of the hysteretic hardening spring loop type. The energy loss in the loop appears to be quite small. The reason for the discrepancy in area of one half of the loops is not known. The static loop was obtained immediately after the dynamic testing was completed and both loops were checked.

The load-deflection curves are at variance with the virgin static load-deflection curve in that as the deflection increases, so does the stiffness, whereas the opposite is commonly assumed to be true. It was felt that this was either due to the effects of large cracks opening and closing at the base of the columns or else the base anchorages for the main column steel were working loose.

The anchorages were examined after testing had been completed but the results were inconclusive. However it was decided to ensure that the reinforcing steel anchorages were not working loose by welding all of the column wires to a steel base plate in subsequent model structures.

If a structure is linearly elastic then it will have a unique natural frequency and stiffness. If a structure is not linearly elastic, possibly due to excursions into the yield range, then the natural frequency of the structure will vary according to the deflection of the structure. It is apparent from figure 5-7 that the natural frequency of the structure, in its damaged condition, will increase with increasing deflection, due to an increase in stiffness. In fact the natural frequency was 5.06 c.p.s. at 0.03 in. deflection rising to 5.72 c.p.s. at 0.15 in. deflection.

Similar results have been reported by Shiga et al [17]. They found that most dynamic hysteresis loops were of the hardening spring loop type with the thin peaks tapering off to a point and almost symmetric with respect to the origin. They found that an envelope curve connecting the peaks of the dynamic hysteresis loops agrees with the static virgin load-deflection curve and that the hysteresis loops could be approximated using a cubic curve. The equation of the cubic curve can be directly related to the area of the dynamic hysteresis loop and the slope of the tangent to the loop on the load axis.

If the $y$ axis is coincidental with the load axis and the $x$ axis is coincidental with the deflection axis, and if the peaks of the dynamic hysteresis curve have coordinates (1,1) and (-1, -1), then the cubic curve is given as ...

$$y = \pm a + bx \mp ax^2 + (1 - b)\, x^3 \qquad (5\text{-}12)$$

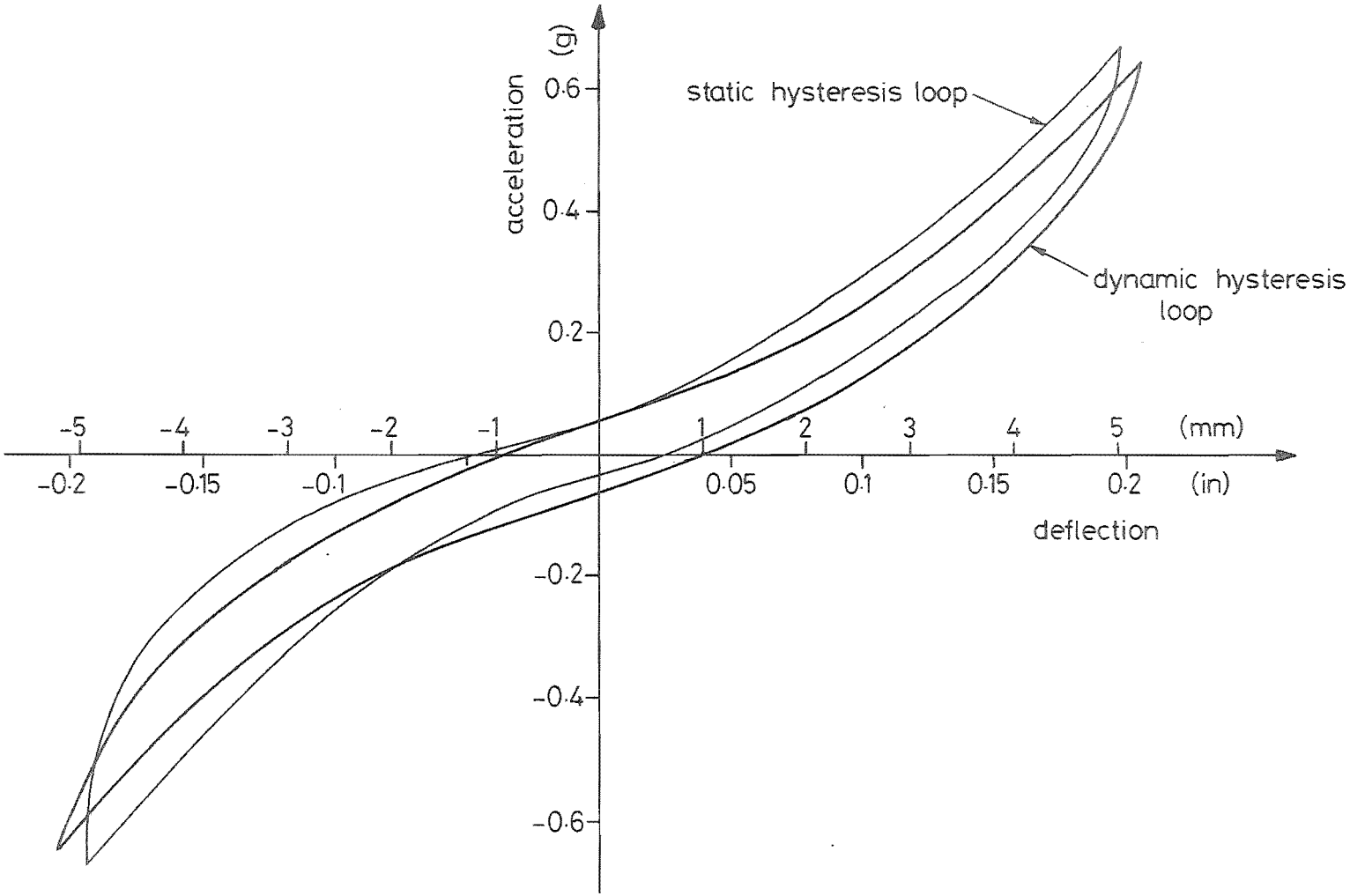


FIGURE 5-6 : STATIC AND DYNAMIC LOAD-DEFLECTION HYSTERESIS LOOPS FOR SINGLE STOREY STRUCTURE

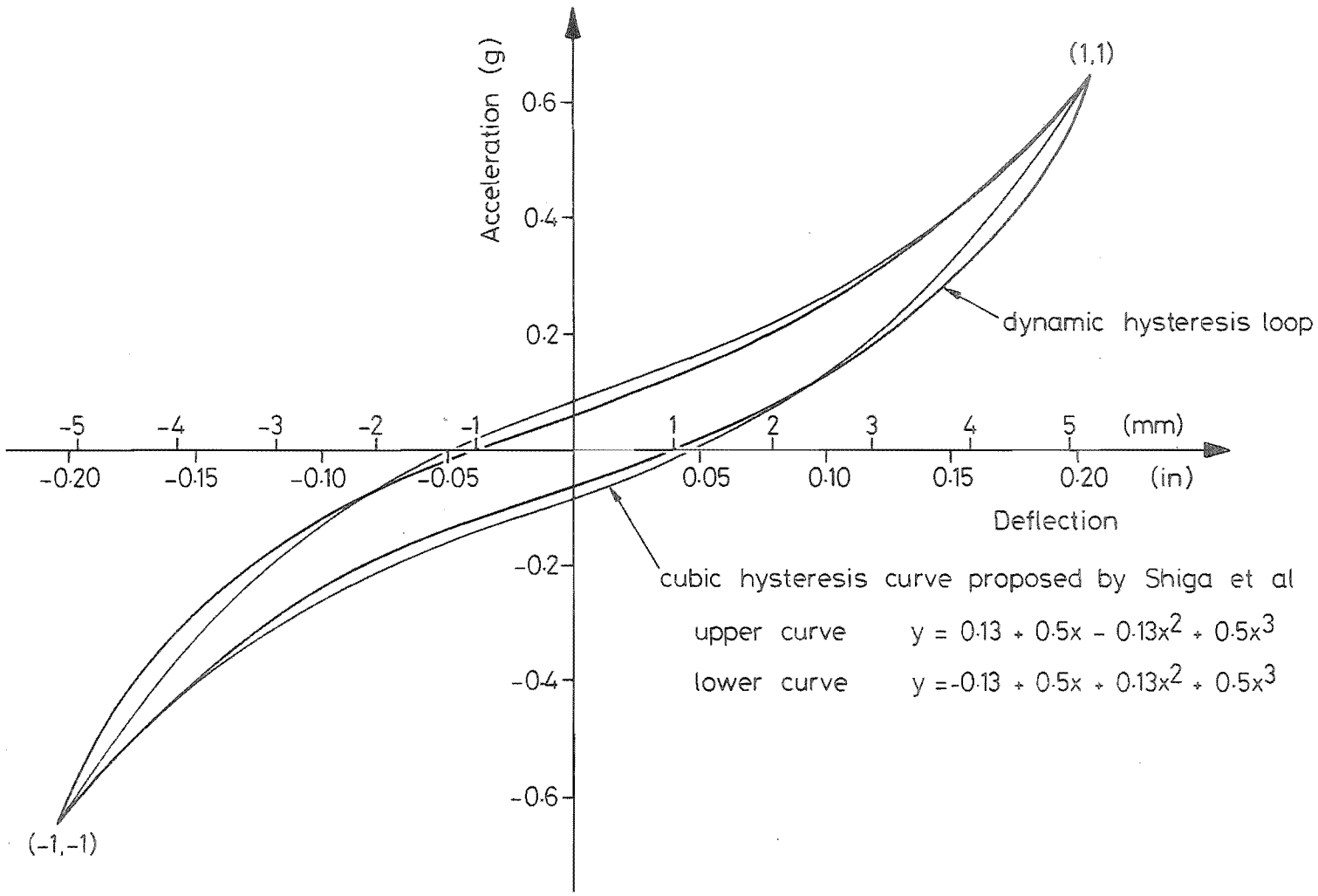


FIGURE 5-7 : MODELLING OF DYNAMIC LOAD-DEFLECTION HYSTERESIS LOOP BY CUBIC HYSTERESIS LOOP PROPOSED BY SHIGA ET AL (17)

where upper signs indicate the upper curve of a half loop and lower signs indicate the lower curve of a half loop, and

a = $\frac{3}{8}$ of the area of the loop

b = slope of tangent to the loop at the intersection of the loop on the load axis.

The equation of the cubic hysteresis loop shown in figure 5-7, which has identical peak values, area and slope as the dynamic hysteresis loop, is

upper curve $y = 0.13 + 0.5x - 0.13x^2 + 0.5x^3$ (5-13a)

lower curve $y = -0.13 + 0.5x + 0.13x^2 + 0.5x^3$ (5-13b)

The area of the hysteresis loop is a measure of the energy absorbed by the system and can be related to damping. The equivalent viscous damping factor $h_e$ is defined as ...

$$h_e = \frac{1}{2\pi} \frac{\Delta W}{W} \qquad (5\text{-}14)$$

where $\Delta W$ = energy loss = area of the hysteresis loop

$W$ = potential energy = $(P_1\Delta_1 + P_2\Delta_2)$

and $(P_1,\Delta_1)$ and $(P_2,\Delta_2)$ are the coordinates of the peaks of the loop.

If the dynamic hysteresis loop is expressed in terms of the cubic hysteresis loop proposed by Shiga et al [17], then ...

$$h_e = \frac{4a}{3\pi}$$

$$= 5.5\% \text{ for the single storey structure.}$$

This is in very good agreement with the 5.4% determined from the displacement response tests. A similar calculation based on the static hysteresis loop indicates an equivalent viscous damping factor 15% greater than that based on the dynamic hysteresis loop, although all of the increase is confined to one half of the loop. Higashi and Ohkubo [20] also found that the equivalent viscous damping factor determined from static loops was larger than when it was determined from dynamic loops.

## 5.7 STRUCTURAL PERFORMANCE

The ratios of reinforcement used in the single storey structure were identical to that designed for the six storey structure. This meant that the columns were designed to be just over half as strong as the beams, in accordance with normal practice. While it is considered that this would probably cause failure to occur in the beams of the six storey structure, it meant that failure occurred in the columns of the single storey structure since both beam and column carry an equal moment.

The mode of failure of the single storey structure was a column sidesway mechanism. Large cracks opened up in the columns about 1 in. (25.4 mm) above the base and about 1 in. (25.4 mm) below the beams and these largely governed the behaviour of the structure. Damage to the beams was very light and for the most part limited to a few cracks.

If a random sample of structural members which are supposedly identical are tested, the strengths will be scattered over a certain range; the smaller the member, the greater the variation. This resulted in the columns of the single storey structure all yielding at different levels and thus having differing stiffnesses at any given instant. The structure was no longer symmetrical and very large torsional rotations occurred about a vertical axis when conducting a small displacement frequency sweep. This caused some concrete to spall off the beams at the column interface and contributed to a small amount of torsional cracking which was apparent in the lateral beams. The slab was undamaged apart from a crack diagonally across each corner.

Confinement of the joints appeared to be excellent and although the concrete outside the ties soon spalled off, there was no sign of damage to the confined concrete. The other noticeable feature about the detailing was the poor anchorage of the column compression steel which punched through the top of the columns, where it had been anchored in a small stub. Although the same method of anchoring the column reinforcement was to be used on the six storey structures, it was not felt that this would be a problem in the six storey structures since the column reinforcement at that level was unlikely to approach yield.

The structure was subjected to a series of square waves of amplitude up to 2 in. (50.8 mm) and with accelerations of over 5g but apart from raising clouds of concrete dust at each major crack, these had surprisingly little effect. It was felt that the only way the structure would fail under this type of loading was a fatigue failure due to the gradual disintegration of the concrete in the joints and adjacent to the reinforcing steel anchorage lengths.

Finally, the structure was subjected to a large amplitude sine wave at or near its natural frequency of 4.5 c.p.s. The input amplitude was 1.5 in. (38.1 mm) which gave an input acceleration of 1.55g. No accelerometer or LVDT was used to measure the response of the structure because of the high risk of damage so that the actual acceleration experienced by the structure is only a matter of conjecture, but it would have been at least 1.55 g and probably several times that. This test

lasted only about 5 seconds as the structure rapidly disintegrated. The stiffness of the structure after completion of all testing was practically zero, since finger pressure was sufficient to move it several inches.

# CHAPTER SIX

# TESTING OF MODEL ONE

## 6.1 INTRODUCTION

Static loading tests are often used instead of dynamic loading tests when testing structures or parts of structures, partly because the complex loading systems required to reproduce dynamic loads are not generally available and partly because data acquisition is vastly more difficult when conducting dynamic tests. It is commonly thought that the determination of the strength of a structure when tested statically is conservative, since the transient nature of a dynamic test will lead to an increase in the strength of the structure and the nature of static tests is such that the structure will collapse immediately a mechanism forms, whereas for dynamic tests this is not necessarily the case.

It was decided to conduct static reversed cyclic loading tests on Model 1. These tests would furnish valuable information in the following areas:

(i) the strength of the structure as determined from the static tests could be compared with the strength predicted theoretically. A close correlation between these results would give further credence to the values used for the member strengths and would permit analysis of the dynamic tests to proceed on a satisfactory basis.

(ii) the load-deflection hysteresis curves for the structure could be obtained. The shape of these curves would indicate which parameters are prominent in influencing the response of the structure.

(iii) the lateral flexibility matrix of the untested structure could be determined. All lateral natural frequencies could be calculated from this and compared with the theoretical predictions, indicating the degree of cracking present in the untested structure.

(iv) the fundamental resonant frequency, mode shape and damping after each loading cycle could be determined. The decrease in natural frequency gives an indication of the degradation of stiffness of the structure and any change in the natural mode shape would indicate a change in the distribution of forces on the structure if it was tested dynamically. The change in damping is important since the degree of damping governs the maximum response of the structure in the region of its natural frequencies.

(v) static tests would allow the formation of plastic hinges to be followed and the degree of damage observed in the structure could be correlated with the mechanism of load transfer within the structure.

Upon completion of the static tests on Model 1, there would be an opportunity to carry out some sinusoidal shaking tests of the structure, primarily in order to evaluate the testing equipment and the proposed methods of testing Model 2.

## 6.2 DESCRIPTION OF THE TESTS

### 6.2.1 Static tests

A constant gravitational loading system was used to test the structure. The reaction frame is described in Chapter Two. Yokes were placed around the two nearside columns at each floor level to which were attached short lengths of chain. The chain was connected to a wire rope which ran over a pulley mounted on the reaction frame and was attached to a loading bucket; this system allowed the total length of the wire rope and chain to be readily altered if necessary. The loading buckets were specially constructed and there were two per floor, making twelve in all. When the direction of loading was to be reversed, the yokes, wires, pulleys and buckets were removed and attached to the other two columns of the structure and to the reaction frame.

Choice of the loading material presented a problem since the loading distribution was triangular and not uniformly distributed up the structure and the load increments were not constant - flexibility in the choice of load size was important. Fortunately about 0.75 tons (7.47 KN) of steel pellets became available and so these were divided up into lots weighing up to 6.6 lb (29.4 N). Each lot was welded inside two plastic bags and the value of the load was written on the outside of the bag. Loading the structure then became a matter of simply placing the plastic bags, which were lifted to the required level by overhead crane, into the buckets. This loading procedure was carried out slowly and evenly to avoid introducing any undesirable effects into the structure.

Mercer dial gauges with a 2 in. (50.8 mm) travel were mounted on the reference frame at each floor level, and at the base, to measure the deflections of the structure. The dial gauges were positioned along the centre line of the structure except at the third and sixth floors where two dial gauges were mounted, one at each column, in order to determine if any twisting of the structure was occurring. A theodolite was

mounted on the laboratory floor perpendicular to the structure and the dial gauges could all be read by swinging the telescope through a vertical arc - this avoided the necessity of climbing up the reaction frame to read all the dial gauges after every load increment. The theodolite was also used to make independent checks on the deflection of the structure.

The total lateral movement at the top of the structure was over 12 in. (305 mm) double amplitude which meant that the dial gauges often had to be either rezeroed or reset and also that sometimes the loading buckets would ground onto the top of the pulley support for the floor below. If this occurred then the bucket was released and the length of chain connecting the wire to the column yoke was shortened by placing a different link from the chain over the hook on the yoke.

Because of the poor control over deflection of the gravitational loading system selected, it was felt necessary to constrain the deflection of the structure to keep within certain variable limits. A piece of rectangular hollow steel section was clamped across the top of the columns at right angles to the direction of loading and a $1\frac{1}{2}$ in. dia. (38.1 mm dia.) hole was drilled in the centre. A length of 1 in. dia. (25.4 mm dia.) round steel was threaded and one end was bolted to the reaction frame whilst the other passed through the hole and was secured by locking nuts on either side. By varying the location of the nuts along the threaded round steel, the deflection of the structure could be constrained to certain limits.

The static tests commenced with an experimental determination of the lateral flexibility matrix of the untested structure. This was obtained by placing a 66 lb (294 N) lateral load on each floor in succession and measuring the deflections induced at all the floors. The 66 lb load was insufficient to cause any cracking.

The main testing program consisted of an elastic loading cycle followed by four cycles into the yield range. The loading pattern is shown in figure 6-1 to an artificial scale. At the peak of each loading cycle, crack patterns on the concrete surface were traced in, measurements of typical crack widths were taken and most of the lower beam-column joints were photographed. After every complete loading cycle the lateral flexibility matrix was determined again. The structure was so flexible that a ten minute wait after applying each load increment was necessary before any measurements could be taken in order that the structure might creep sufficiently that the deflection readings would stabilize.

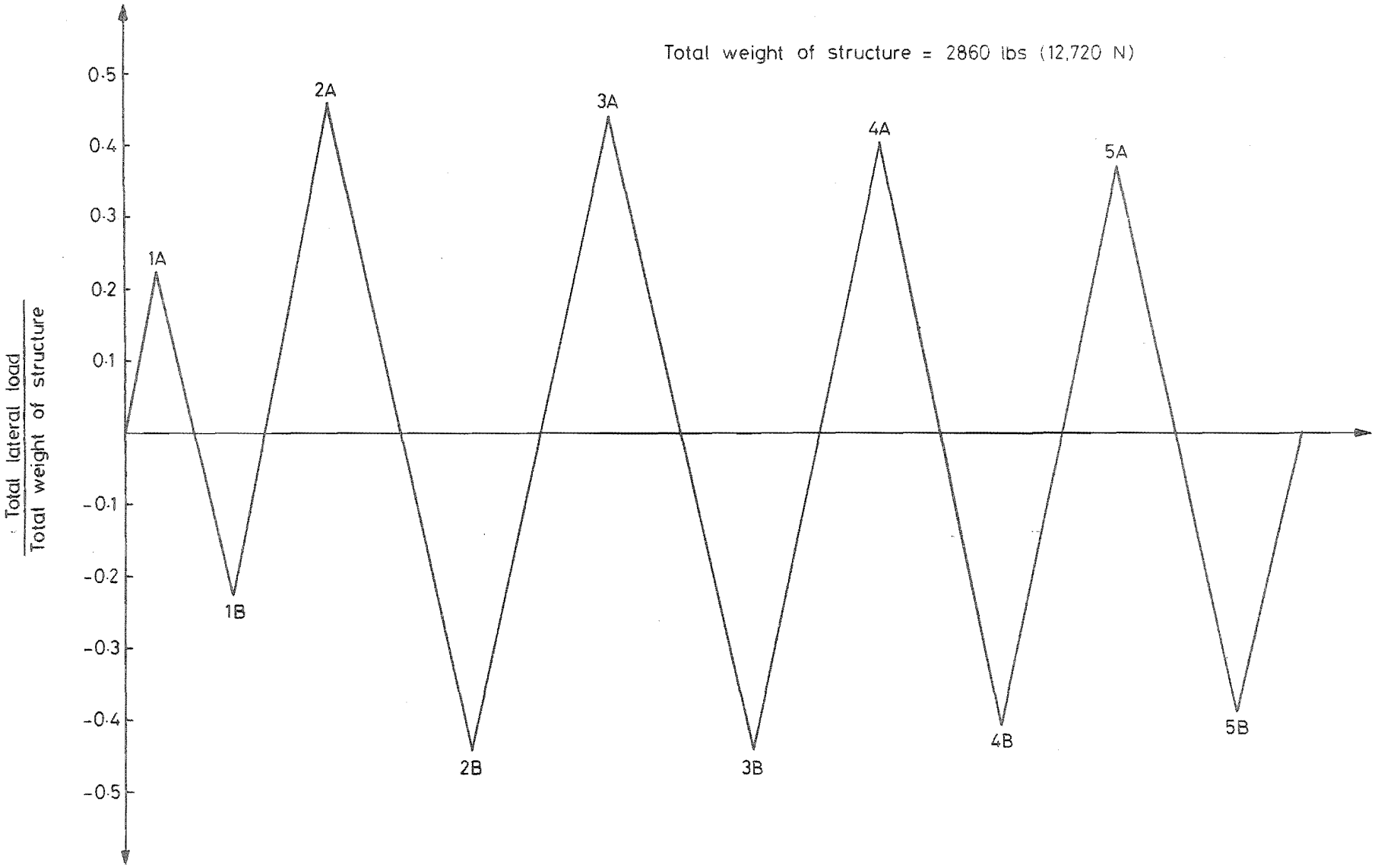


FIGURE 6-1 : STATIC LOADING CYCLES APPLIED TO MODEL 1

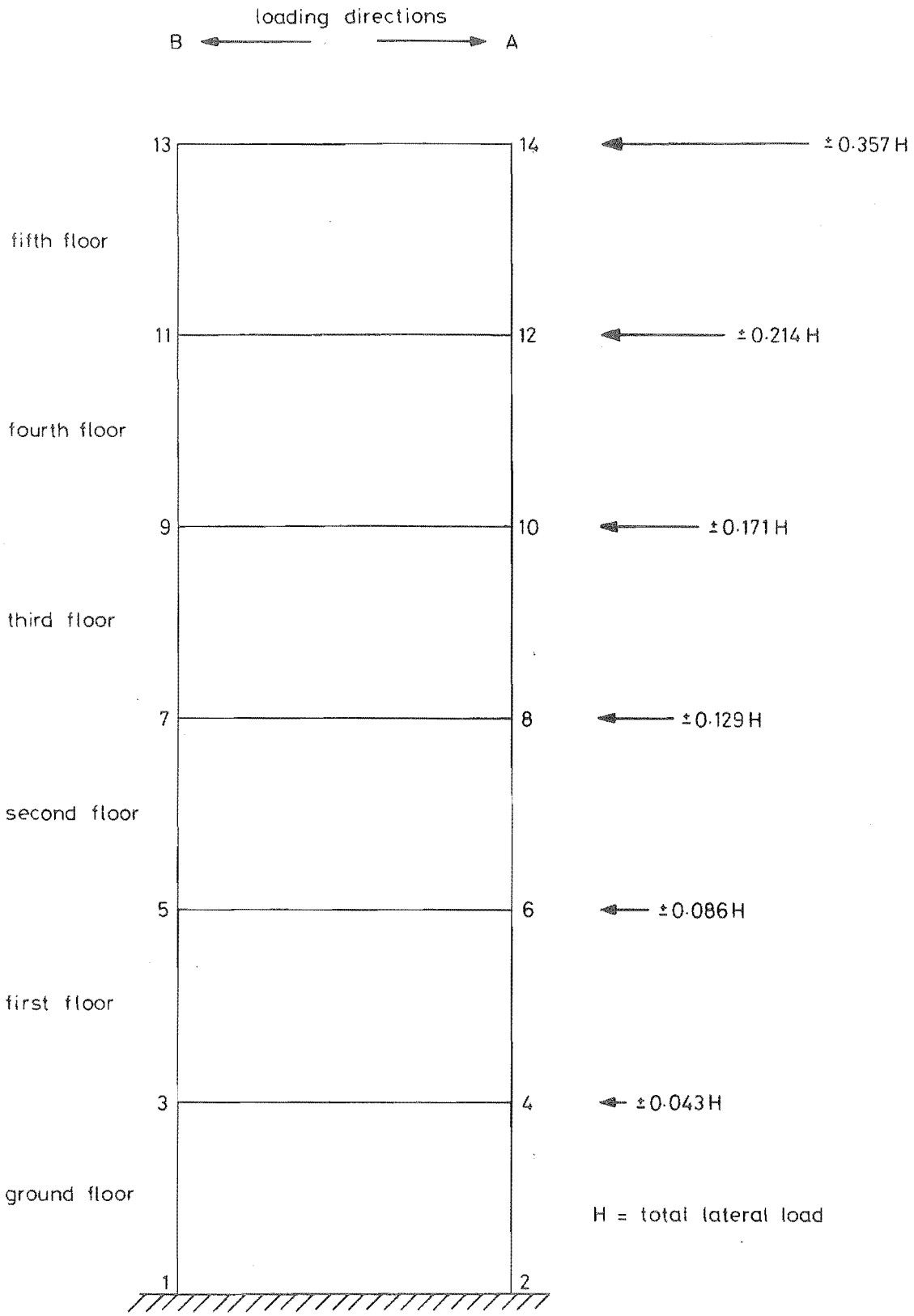


FIGURE 6-2 : FRAME NODES AND LOADING DIRECTIONS

### 6.2.2. Dynamic tests

A free vibration test was carried out on the structure before any testing commenced and also after each static load cycle had been completed. It was found that the structure was sufficiently flexible that a sharp push by a technician at the sixth floor level sent it into free vibration with an amplitude adequate for recording purposes.

A Hewlett Packard LVDT (described in Section 2.3.4) was mounted at each floor level to measure the deflection and the signals were recorded on two Phillips oscilloscripts (see Section 2.3.4) for the purpose of determining the mode shapes. In this situation the sensitivities at which the signals were recorded was unimportant as long as the sensitivities of all the channels were the same. In addition, the deflection of the sixth floor was recorded on the Brush pen recorder mounted in the MTS control console in order that the natural frequency and damping could be determined accurately.

After completion of the static tests some forced vibration tests were carried out. A LVDT was mounted on the reference frame to measure the deflection of the shaking table and this signal was subtracted from the deflection signals measured by the LVDTs mounted at the various floor levels by means of a series of differential amplifiers. An attempt was made to try and determine the natural frequencies of the structure and then it was severely shaken until collapse occurred.

## 6.3 BEHAVIOUR OF THE STRUCTURE

### 6.3.1 Static tests

Some minute shrinkage cracks were present in the structure before testing began, grouped mainly in the columns. The elastic loading cycles 1A and 1B had little effect on the structure other than causing some of these shrinkage cracks to open.

The structure was first loaded to its ultimate load capacity during loading cycle 2A (see figure 6-1) and the structure was examined closely at the peak of this loading cycle. A large crack had formed in the columns about an inch (25.4 mm) above the base at both nodes 1 and 2. Crushing had also occurred at node 2 due to the large axial compression in that column. Some crushing had also occurred in the longitdunal beams at nodes 3, 4 and 6. Some cracking was apparent in the lower floor slabs and severe torsional cracking had spread into the lateral beams. Diagonal tension cracks had appeared in the joints.

Cracking in the column with the even nodes was concentrated at the tops of each column segment extending down almost to midway between the two floors whereas there were only a few cracks at the bottom of each column segment extending little distance up the column. The exception was the ground floor columns where the cracks were almost evenly spread. On the other hand, the column with the odd numbered nodes had a relatively even spread of cracks between the top and bottom of each column segment.

The reason for this was because moment redistribution was occurring in the structure as it tried to adjust itself in order to form a collapse mechanism. Yield had occurred at the base of the columns and the point of contraflexure was dropping in each column segment in order to produce either yield in the beams of the top few floors or yield in the tops of the columns of the lower floors (this point is further explained in Section 6.6). The difference between the two columns arises because the gravity load moments were acting to increase this effect for the even node column and to reduce this effect for the odd node column. In addition, the odd node column had a tensile axial load which tended to increase the incidence of cracking.

With no direct means available of determining whether or not yield has occurred at a particular location, reliance has to be placed on such factors as the extent of the permanent deformations and whether or not crushing has occurred. Using these criteria it was judged that yielding had occurred in the first, second, third and fourth floor beams, as well as at the base of the columns and at the tops of the ground, first and second floor columns. Little crushing occurred, even at the base of the columns, probably because large permanent tensile strains in the reinforcing steel often means that the concrete will not crush when the loading is reversed.

All joints suffered severe diagonal cracking and the cover concrete spalled off at the lower floors, particularly on the side opposite to that from which the longitudinal beams protrude. Perhaps the most startling feature of the tests was the damage caused to the lateral beams by torsion. On each cycle large torsional cracks appeared in the lateral beams and diagonally across the corner of each slab and these cracks did not close on the reverse cycle. Concrete began spalling off the lateral beams after only a few cycles and some of these beams were severely distressed by the completion of the static tests.

Photographs of some of the members at various stages in the test program are shown in figures 6-2 to 6-5. Some typical crack widths obtained during testing (cycle 3B) are given below:

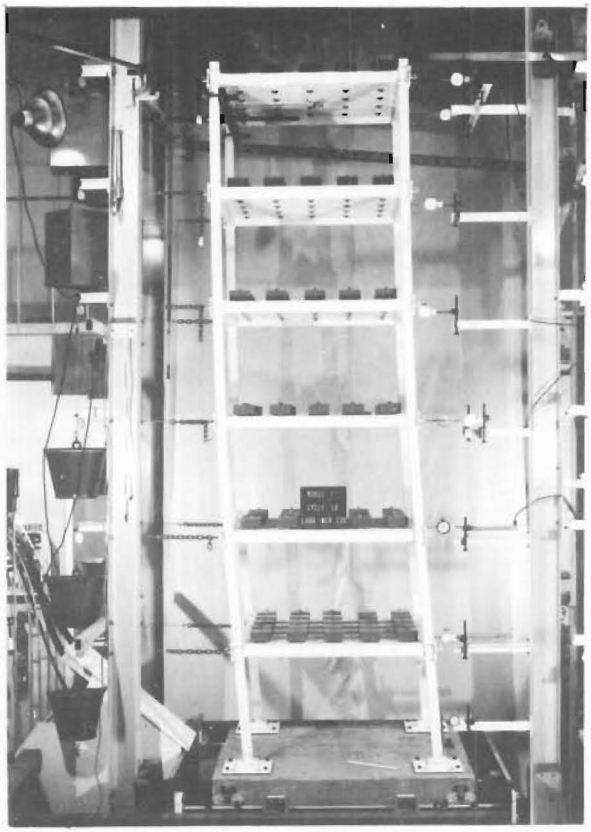

FIGURE 6-3 : STATIC TESTING OF MODEL 1

FIGURE 6-4 : LATERAL BEAM AND COLUMN AT NODE 4

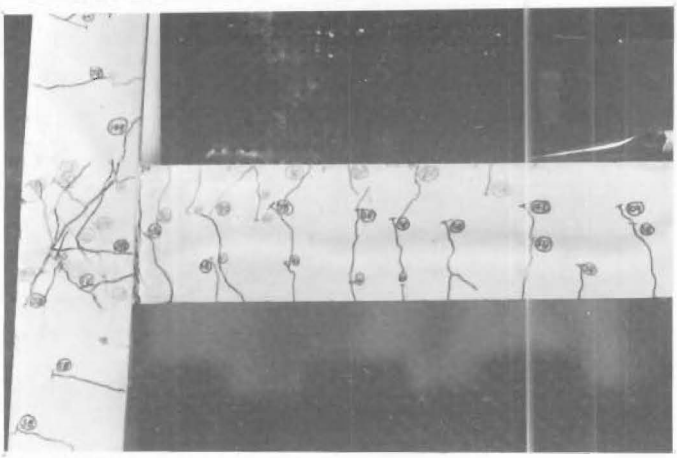

FIGURE 6-5(a) : LONGITUDINAL BEAM AND COLUMN AT NODE 3

FIGURE 6-5(b) : SLAB AT NODE 6

NOTE: All photographs on this page were taken prior to the completion of the static tests of Model 1.

(i) main column crack above base at node 2 = 0.067 in. (1.70 mm)

(ii) typical crack at beam-column interface = 0.080 in. (2.03 mm)

(iii) typical permanent column crack = 0.0002 in. (0.005 mm)

(iv) typical permanent beam crack = 0.00008 in. (0.002 mm)

(v) permanent crack across slab at node 4 = 0.059 in. (1.50 mm)

### 6.3.2 Dynamic tests

By the time the static reversed loading tests had been completed it was obvious that the structure was badly damaged and that a column sidesway mechanism was developing in the ground floor columns. The non-linearity of the structure meant that the stiffness varied with the deflection which meant that the structure did not have unique natural frequencies. If the natural frequency of the structure at a particular deflection coincided with the forcing frequency, then the deflection of the structure would increase, altering its stiffness and thus its natural frequency; the natural frequency of the structure would no longer coincide with the forcing frequency so the deflection would subsequently decrease. When the deflection reduced to close to its original value, the natural frequency of the structure would be close to that of the forcing function and so the deflection would increase again. This cyclic process appeared to repeat itself many times.

Thus it was not possible to identify the natural frequencies of the structure absolutely, but only to define a frequency close to the centre of a band of frequencies within which a natural frequency might commonly lie. The mode shapes of the structure were complex and the motion of the structure was often irregular, as illustrated in figure 6-6, even though the sinusoidal forcing function was of constant amplitude and frequency.

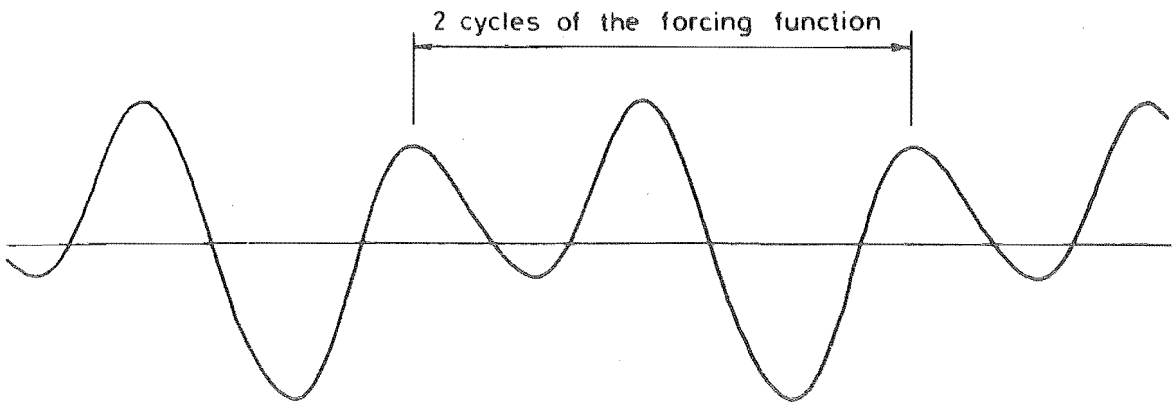


FIGURE 6-6 : IRREGULAR MOTION AT TOP FLOOR DURING FORCED VIBRATION TESTING OF MODEL 1

Examination of the waveform recorded in figure 6-6 leads to the conclusion that it can very nearly be represented by the sum of two separate motions, one with a frequency equal to that of the forcing frequency and the other at a half of that frequency. On the basis of observations made when the waveform was being recorded, one might speculate that the former is the frequency of the column sidesway mechanism and the latter is the frequency of the upper floors vibrating about the first floor level.

As a result of experience obtained when testing the single storey structure to destruction, it was decided to destroy Model 1 by shaking it as closely as possible to its natural frequencies. The base amplitude and the forcing frequency were measured accurately; the base acceleration was not measured directly but was calculated from the frequency and displacement. The amplitudes of motion are indicated in table 6-1.

TABLE 6-1 : DESTRUCTIVE SINUSOIDAL RESONANCE TESTS OF MODEL 1

| Natural mode number | Forcing frequency c.p.s. | Base displacement in. (mm) | Base acceleration 'g' |
|---|---|---|---|
| 1 | 1.0 | 3.92 (99.6) | 0.20 |
| 2 | 3.2 | 1.31 (33.3) | 0.69 |
| 3 | 6.0 | 0.71 (18.0) | 1.31 |
| 4 | 11.0 | 0.295 (6.7) | 1.83 |

The testing program was simply to shake the structure as severely as possible at its first natural frequency; if collapse did not occur then the structure would be shaken at its second natural frequency, and so on until collapse of the structure was achieved. Only when the structure was shaken at its fourth natural frequency did the structure slowly collapse in a ground floor column sidesway mechanism and sink onto several supporting planks placed there specifically for that purpose. The length of time for which the structure was severely shaken appeared to be an important factor in determining whether or not collapse occurred. Once the tests were completed, the planks were removed and the structure was still able to support its own weight, in spite of a lateral deflection of over 4 in. (102 mm) at the first floor level.

Some photographs of the structure after the completion of the dynamic tests are shown in figures 6-7 to 6-10.

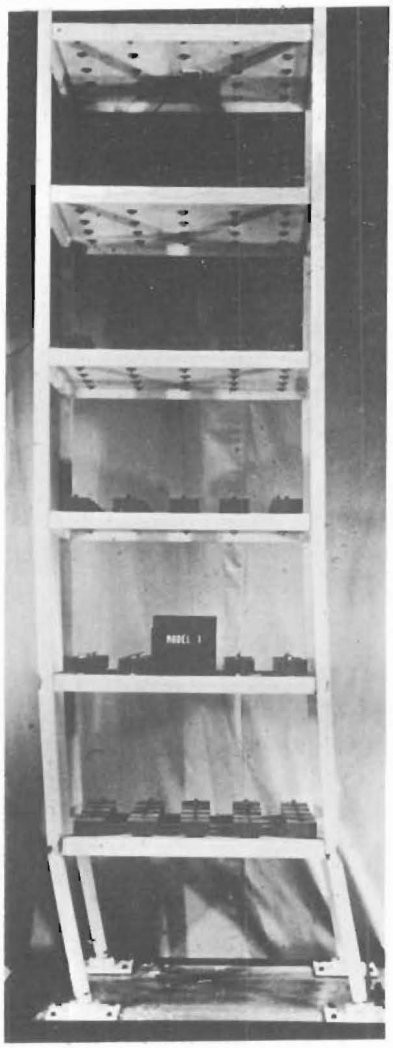

FIGURE 6-7 : MODEL 1 AFTER COLLAPSE

NOTE: All photograpns on this page were taken after Model 1 had collapsed during dynamic testing.

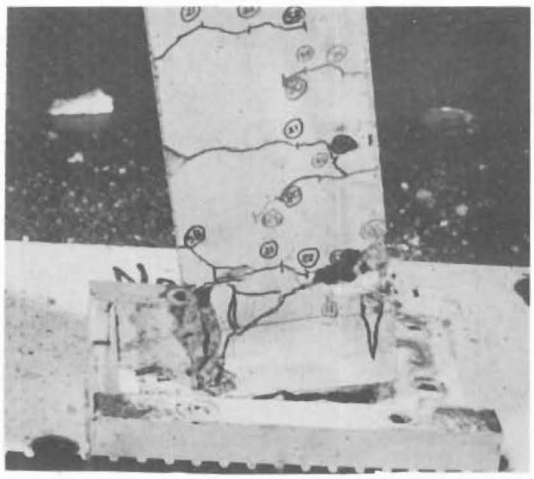

FIGURE 6-8 : NODE 1

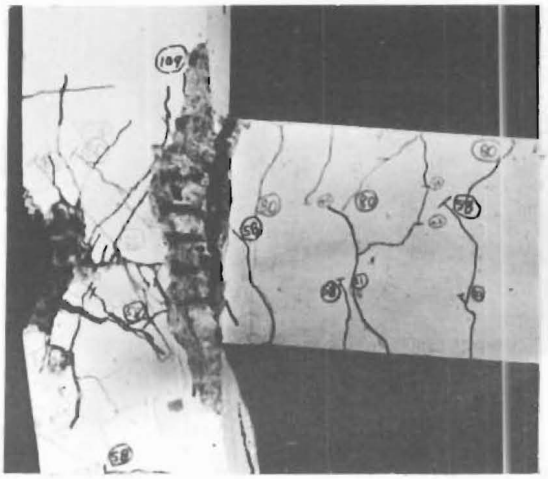

FIGURE 6-9 : LONGITUDINAL VIEW OF NODE 3

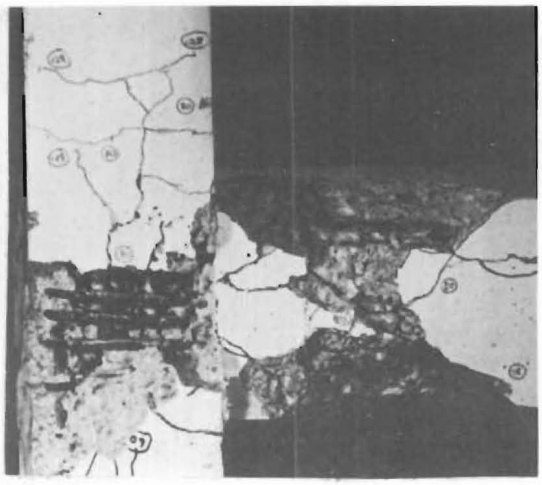

FIGURE 6-10 : LATERAL VIEW OF NODE 4

## 6.4 NATURAL MODES OF VIBRATION

### 6.4.1 Methods of prediction

Comparison of natural frequencies obtained from experimental testing with natural frequencies predicted by theory gives a direct indication as to the accuracy with which the computer based mathematical models describe the stiffness of the structure. The natural frequency of the structure can be obtained or predicted by any one of four different methods:

(i) predicted directly from a mathematical model of the building

(ii) predicted from an experimentally obtained lateral flexibility matrix

(iii) obtained from free vibration tests of the structure

(iv) obtained from forced vibration tests of the structure.

Each of the methods has some drawbacks and limitations. Method (i) is the only true theoretical method but it is limited to predictions based on the elastic state of the structure and can take no account of damage to the structure apart from cracking. Method (ii) will also predict all the natural frequencies and mode shapes but the predictions are based on a particular region of the load deflection curve where the structure will have a particular stiffness which is different from its overall stiffness. Neither method (i) nor method (ii) will predict damping.

The mode shape, damping and natural frequency can all be obtained using method (iii) regardless of the state of the structure, but for the first mode only. Method (iv) can really be subdivided into two separate methods: the first determines the natural frequencies from the displacement response curve while the second determines the first, and possibly the second and third, natural frequencies as being the predominant frequency components in the response of the structure to random transient vibrations. Damping, mode shapes and natural frequencies for all natural modes may be obtained using method (iv) but this often involves severe shaking which will damage the structure, especially at the higher modes, and so this method may often be avoided if it is desired not to alter the properties of the structure.

### 6.4.2 Comparison of results

A comparison of the values obtained for the natural frequencies using methods (i), (ii) and (iii) is given in table 6-2. The values predicted from the experimental lateral flexibility matrix were determined using an assymetric eigenvalue routine; in fact, the results were almost identical to those obtained assuming that the matrix was symmetrical.

TABLE 6-2 : COMPARISON OF NATURAL FREQUENCIES FOR MODEL 1

| After cycle no. | Mode no. | Obtained from free vibration tests | | Predicted from exp. lateral flex. matrix | Predicted from mathematical model | | Obtained from displacement response tests |
|---|---|---|---|---|---|---|---|
| | | damping % | frequency c.p.s. | | theoretical stiffnesses | best fit stiffnesses | |
| - | 1 | 1.81 | 2.67 | 3.00 | 2.85 | 3.00 | |
| | 2 | | | 10.71 | 8.63 | 9.35 | |
| | 3 | | | 15.73 | 14.64 | 16.59 | |
| | 4 | | | 27.36 | 20.51 | 24.59 | |
| | 5 | | | 31.43 | 25.73 | 32.61 | |
| | 6 | | | 38.37 | 29.42 | 38.80 | |
| 1 | 1 | 2.65 | 1.99 | 2.29 | 2.20 | | 2.23 |
| | 2 | | | 8.00 | 6.86 | | 7.55 |
| | 3 | | | 14.39 | 12.19 | | 13.65 |
| | 4 | | | 21.71 | 18.17 | | |
| | 5 | | | 27.67 | 24.24 | | |
| | 6 | | | 33.22 | 28.97 | | |
| 2 | 1 | 13.1 | 1.18 | 1.22 | | | |
| 3 | 1 | 10.2 | 1.14 | 1.16 | | | |
| 4 | 1 | 8.5 | 1.19 | 1.15 | | | |
| 5 | 1 | 8.6 | 1.05 | 1.05 | | | |

The light shrinkage cracking which occurred in the structure made it unrealistic to expect that a mathematical model based on uncracked members would closely predict the natural frequencies of the structure. Since most of the cracking occurred in the columns, a more accurate estimate could be based on a structure with cracked columns and uncracked beams, and this is presented in table 6-2 under the heading "theoretical stiffness". This is rather extreme however, since the columns were not fully cracked and the beams were certainly not devoid of cracks, and so the beam and column stiffness were varied until a reasonable correlation was obtained between predicted natural frequencies and those predicted from the lateral flexibility matrix. These are indicated in table 6-2 under the heading "best fit stiffness".

It was found that the first mode natural frequency was about equally sensitive to a variation in column stiffness or beam stiffness, but the higher the mode, the greater the influence of the column stiffness and the less the influence of the beam stiffness. The sixth mode natural frequency was virtually unaffected by a large change in beam stiffness but was very sensitive to a variation in column stiffness. This fact enabled an estimate of the column stiffness to be made from the sixth mode natural frequency predicted by the lateral flexibility matrix and then the beam stiffness was varied until the first mode natural frequencies were identical. The beam and column stiffness then became the "best fit stiffness" and were $I_b$ = 2.06 $in^4$ (85.7 x $10^4$ $mm^4$) and $I_c$ = 1.10 $in^4$ (45.8 x $10^4$ $mm^4$) for the untested structure. These values are approximately midway between the theoretical cracked and uncracked stiffnesses. The shrinkage cracking was evenly spread over the structure and so the correlation between the natural frequencies predicted using the "best fit stiffnesses" and the experimental lateral flexibility matrix was good.

The natural frequency of the structure as measured from free vibration tests was 11% lower than predicted from the lateral flexibility matrix. The frequency of oscillation would have been insufficient to expect any measurable increase in stiffness during the free vibration tests and the discrepancy is probably due to the fact that the portion of the load-deflection curve from which the experimental lateral flexibility matrix was determined was not necessarily typical of the remainder of the load deflection hysteresis curve. The damping ratio of the untested structure was 1.81% of critical. Pereira and Priestley [24] indicate that a microconcrete typically has an inherent damping ratio of about

0.4% and so most of the damping probably arises from the slippage of joint connections and from the opening and closing of cracks.

The natural frequencies predicted by the experimental lateral flexibility matrix and by a mathematical model based on a fully cracked structure are in close agreement for the first natural frequency but the agreement is not as good for the higher natural frequencies. The reason for this is that the mathematical model assumes that uniform cracking has occurred in every member of the structure whereas in reality the cracking was primarily confined to the lower half of the structure. The higher modes are particularly sensitive to the stiffness of the upper floors and so the discrepancy in natural frequency becomes more pronounced with the higher modes. The first mode natural frequency as measured from a free vibration test was 13% below that estimated from the experimental lateral flexibility matrix. The natural frequencies for the first 3 modes as determined by displacement response tests are also given in table 6-2. The values determined in this manner appear to lie midway between those values predicted from the experimental lateral flexibility matrix and those values predicted by the mathematical model based on a fully cracked structure.

Once the structure had yielded and subsequent deterioration in stiffness had occurred, it was not possible to predict the natural frequencies from a mathematical model. However, the first mode natural frequencies predicted from the experimental lateral flexibility matrix agreed closely with those obtained from free vibration tests.

A problem associated with the free vibration tests was that neither the natural frequency nor the damping ratio stayed constant during a particular test run because of the non-linearity of the structure. The natural frequency tended to increase with decreasing displacement, indicating an increase in stiffness of the structure at low amplitudes. The damping ratio increased with decreasing deflection until the structure began to deteriorate badly, at which stage the damping levelled off at a reduced value as indicated in table 6-2 and merely oscillated randomly about a mean value during subsequent test runs. At this stage the natural frequency also tended to remain constant during a particular test run.

## 6.5 TORSION ANALYSIS

### 6.5.1 Introduction

Torsion caused severe distress to the lateral beams (those beams spanning in a direction perpendicular to the direction of the applied forces) during the static cyclic loading tests and so a detailed analysis of the

structure was carried out to investigate the causes, magnitude and effects of these torsional forces.

Structures are seldom designed to carry loads primarily by torsion; instead, torsion usually arises as a consequence of utilising some other means of carrying the loads. Thus torsion is generally present as a secondary effect and it is not considered critical to the satisfactory performance of the structure. Consequently torsion has been a relatively neglected field of research and the "state of the art" is not as far advanced as is some other aspects of reinforced concrete.

The torsion problem can be subdivided into two separate components:
(i) correctly predicting the ultimate torsional strength of the reinforced concrete section. Although numerous theories have been advanced to explain the mechanism by which a section resists torsion, most of them rely heavily on empirical test results and it is only recently that a satisfactory theory based on the space truss model [33] has been advanced.
(ii) correctly analysing the structure to determine where torsion is present as a result of a particular loading pattern. In an indeterminate structure two types of torsion may be present: equilibrium torsion, where a torsion is required to maintain equilibrium in the structure or compatibility torsion, where a twist is required to maintain compatibility in the structure.

### 6.5.2 Ultimate torsional strength of the lateral beams

The ultimate torsional strength of the lateral beams of the model structure is relatively difficult to determine accurately. The width of slab which acts with the lateral beams is unknown and for the purpose of this analysis has been assumed to be zero. The reason for this is that there is no data available which may be used to calculate the magnitude of the contribution of the slab and anyway, yield lines forming in the slab close to the edge would probably mean that the contribution is minimal. Another assumption made, which has an opposite influence to the previous one, is to consider the flexural stiffness of the slab as the sum of the flexural stiffnesses of a series of one-way strips. This neglects the torsional restraint perpendicular to these strips and so effectively underestimates the stiffness of the slab.

The cross-section of the lateral beam used for the torsion analysis is shown in figure 6-11.

#### 6.5.2(a) plain concrete section

Most early theories on torsion have been based on 45° diagonal tension cracks and take the form ...

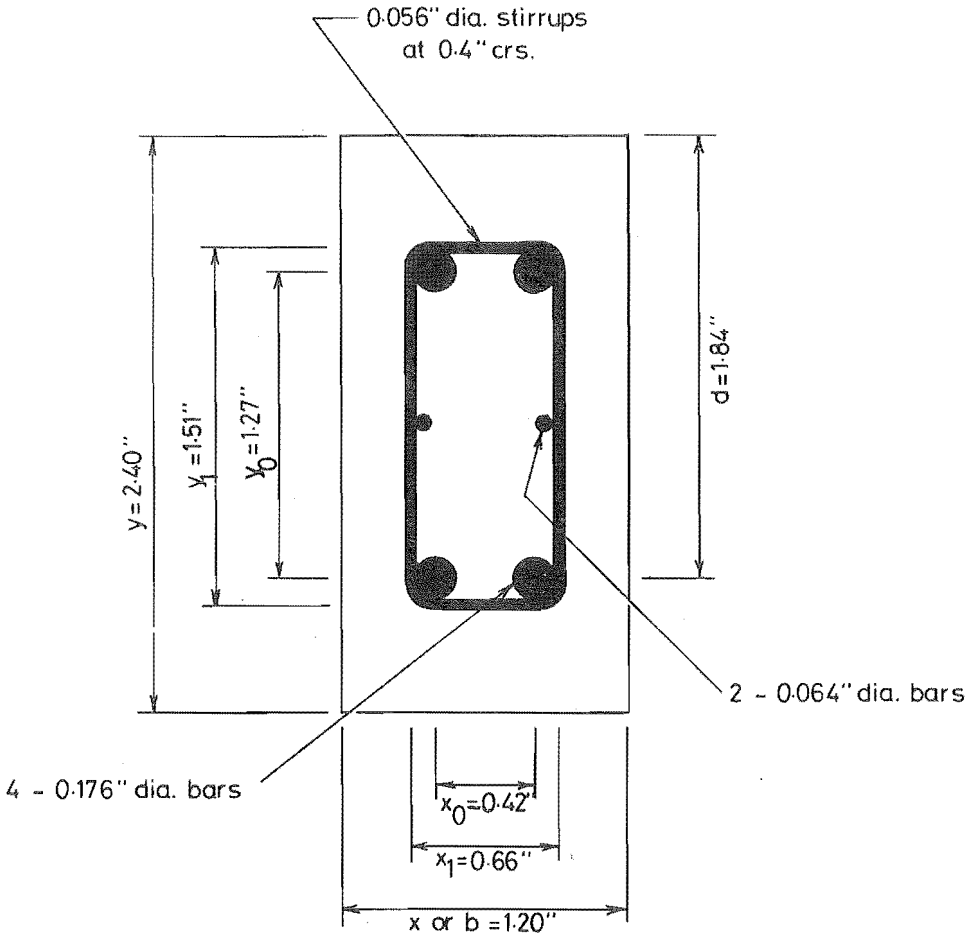


FIGURE 6-11 : CROSS-SECTION OF LATERAL BEAM USED FOR TORSION ANALYSIS

$$v_{tu} = \frac{\psi T_u}{\Sigma x^2 y} \qquad (6\text{-}1)$$

The value to be used for $\psi$ , the stress factor, varies according to whether a membrane analogy (fully elastic) or a sand heap analogy (fully plastic) is used. The stress-strain curve for concrete is not linear but neither is concrete ductile, and so the true value for $\psi$ will lie somewhere between that predicted by elastic and plastic theories. Thus it is common practice to accept a value for $\psi$ of 3, which is a minimum for elastic theory and a maximum for plastic theory.

The value of $v_{tu}$ cannot be directly related to a strength property of the concrete, but on the basis of empirical test results a value of $6\sqrt{f'_c}$ (lb/in$^2$) is commonly accepted. Substituting the values obtained for the model structures into equation 6-1, the ultimate strength of the plain concrete section becomes ...

$$T_u = \frac{(1.2)^2 \times 2.4}{3} \times 6\sqrt{3600}$$

$$= 414 \text{ lbin} \quad (46.8 \text{ KNmm})$$

6.5.2(b) reinforced concrete sections

The ultimate torsional strength of reinforced concrete members has long been predicted by the 45° space truss theory, which forms the basis for ACI Code 318-71 [26]. However, the theory relied heavily on empirical test results and contained a number of anomalies and a recent theory by Lampert [33], also based on a space truss analogy, more accurately represents the mechanism by which a section resists torsion.

The two theories give similar results and both are presented below for comparison.

(i) traditional 45° space truss theory.

This theory takes the form ...

$$T_u = T_c + T_s \qquad (6\text{-}2)$$

where $T_s$ = torsional strength of the reinforcement

$T_c$ = torsional strength attributed to the concrete

From tests conducted it appeared that a portion of the ultimate torque was not resisted by the reinforcement and it was convenient to call this the contribution of the concrete. It was thought that the core, not fully cracked, accounted for the torsional contribution of the concrete.

However, tests by Hsu [34] on hollow sections showed that there is virtually no difference in strength compared with comparable solid sections.

The torsional contribution of the concrete was assumed to take a similar form to that for plain sections except that the concrete stress, $v_{tc}$, was found to be about half of $v_{tu}$, i.e. $3\sqrt{f'_c}$ (lb/in$^2$).

$$T_c = \frac{x^2 y}{3} v_{tc} \qquad (6\text{-}3)$$

$$= 207 \text{ lbin} \quad 23.4 \text{ KNmm})$$

The torsional strength of the reinforcement is expressed as ...

$$T_s = \alpha_t \frac{x_1 y_1 A_t f_y}{s} \qquad (6\text{-}4)$$

where $A_t$ = area of one stirrup leg = 0.00246 in$^2$

$f_y$ = stirrup yield stress = 46,500 lb/in$^2$

$s$ = stirrup spacing = 0.4 in.

$\alpha_t$ = $0.66 + 0.33 \frac{y_1}{x_1} \leqslant 1.5$ (empirical formula incorporated to account for the fact that not all stirrups are yielding)

Substitution of these model values into equation 6-4 gives ...

$T_s$ = 401 lbin (45.3 KNmm)

and thus $T_u$ = 207 + 401 = 608 lbin (68.7 KNmm)

This is the ultimate torque that the section is capable of resisting and is limited by the strength of the stirrups. The lateral beams are partially overreinforced since the longitudinal steel does not yield due to the large amount of steel provided for flexure.

(ii) recent space truss theory.

Lampert [33] suggested that the diagonal tension cracks will initially form at 45° as predicted by the traditional theory, due to the orientation of the principal stresses in the elastic situation, but cracks forming thereafter would be inclined according to the ratio of longitudinal to web reinforcement, in agreement with experimental observations. The theory states ...

$$T_u = 2x_o y_o \sqrt{\frac{A_t f_y}{s} \cdot \frac{A_l f_{ly}}{2(x_o + y_o)}} \qquad (6\text{-}5)$$

where $A_l$ = total area of longitudinal steel = 0.1036 in$^2$

$f_{ly}$ = yield stress of longitudinal steel = 42,500 lb/in$^2$

and all other symbols are as previously defined or indicated on figure 6-11.

Substitution of these model values into equation 6-5 gives ...

$$T_u = 651 \text{ lbin} \quad (73.4 \text{ KNmm})$$

which is slightly more than the 608 lbin predicted by the traditional 45° theory.

Equation 6-5 predicts the total torque and does not imply a contribution from any other source. The exact distribution of longitudinal steel over the section does not matter and nowhere in the evaluation of the torque were the properties of the concrete or the shape of the section considered.

### 6.5.2(c) combined shear and torsion

Numerous equations have been proposed to describe the interaction between shear and torsion and they are all empirically based on test results. The most generally accepted relation is a circular interaction curve; other common interaction curves specify that there should be no reduction in the ultimate torsional strength due to the presence of low shear forces. For the lateral beams the maximum shear force is sufficiently small that any decrease in torsional strength will be negligible.

### 6.5.2(d) combined flexure and torsion

An equation relating flexure and torsion has been developed from the recent space truss theory and is well supported by test results.

$$\left(\frac{T_u}{T_{uo}}\right)^2 = 1 - \frac{M_u}{M_{uo}} \qquad (6\text{-}6)$$

where $T_u$ = external torque
$M_u$ = applied bending moment
$T_{uo}$ = pure torsional capacity of the section
$M_{uo}$ = pure flexural capacity of the section

Substitution of the values obtained for the model structure indicates that flexure will cause about a $2\frac{1}{2}\%$ reduction in the torsional strength.

Thus $T_u = 635$ lbin (71.8 KNmm)

6.5.2(e) torsional stiffness after cracking

The torsional stiffness of reinforced concrete beams decreases drastically after cracking. The recent space truss theory uses an analogy with a thin walled tube and the stiffness of the space truss then largely depends on the torsional steel content.

$$k_{tcr} = \frac{E_s (x_o y_o)^2 A_t}{L(x_o + y_o)s}\sqrt{m_t} \qquad (6\text{-}7)$$

where $m_t$ = $\frac{\text{volume of longitudinal steel}}{\text{volume of transverse steel}}$ = 5.0

$L$ = length of beam

$E_s$ = modulus of elasticity of steel = $29.5 \times 10^6$ lb/in$^2$

and all other variables are as previously defined.

Substitution of these model values into equation 6-7 gives ...

$$k_{tcr} = 0.68 \times 10^5/L \text{ lbin}$$

Now $k_t$ (uncracked) = $\beta G b^3 D/L$ (6-8)

where $\beta$ = St. Venant's stiffness factor = 0.23

$G$ = shear modulus for concrete = $1.4 \times 10^6$ lb/in$^2$

Substitution of model values into equation 6-8 gives ...

$$k_t = 13.3 \times 10^5/L \text{ lbin}$$

and thus $\frac{k_{tcr}}{k_t} = \frac{0.68}{13.3} = 0.05$

This means that the torsional stiffness of the lateral beams after cracking is only 5% of that before cracking. It must be emphasised that this stiffness is only approximate since some effects cannot be adequately accounted for such as :

(i) anchorage slip of main reinforcing bars and stirrups

(ii) shear force effects

(iii) influence of the slab

6.5.3 Structural analysis of the slab - lateral beam system

Torsion is induced into the lateral beams in two distinct ways:

(i) as a secondary load resisting mechanism due to the action of gravity loads on the slab, and

(ii) due to compatibility of deformations when the beam-column joints rotate under lateral loading.

Each of these torsions will be examined in turn to determine its effect on the structure.

6.5.3(a) derivation of the general equation

The analyses presented in this section follow a method developed by Gouda [36] and are based upon the two assumptions mentioned previously, namely:

(i) the slab can be considered as a series of beams of unit width. This effectively underestimates the stiffness of the slab since it neglects any torsional restraint across the slab.

(ii) none of the slab is considered to contribute to the torsional stiffness of the beams. This underestimates the torsional stiffness of the beams.

These two assumptions will have opposing effects since the distribution of edge moments in the slab, which induces torsion in the beams, is dependent on the ratio of the slab stiffness to beam stiffness.

Consider the elemental strip of beam and slab shown in figure 6-12.

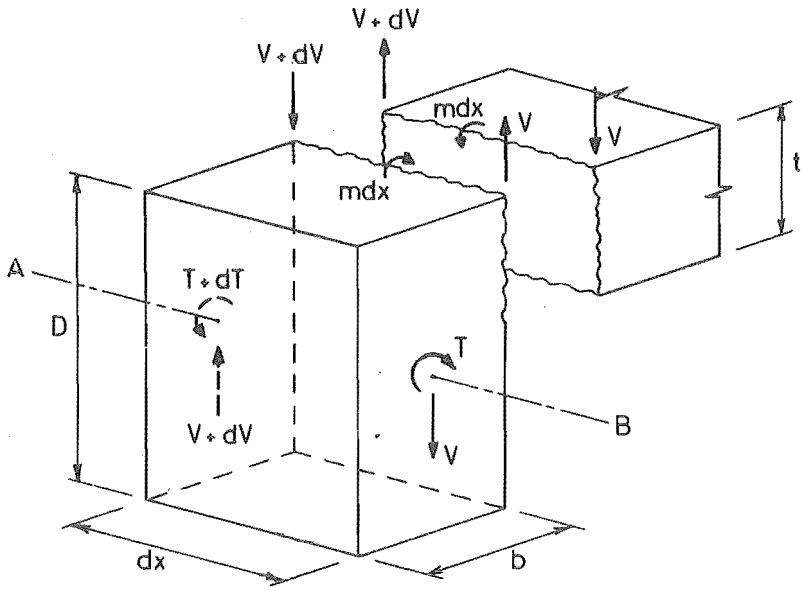


FIGURE 6-12 : ELEMENTAL STRIP OF LATERAL BEAM AND SLAB

Equilibrium of moments about AB yields ...

$$dT - mdx - \frac{b}{2}\,dV = 0$$

$$\text{therefore} \quad \frac{dT}{dx} = m + \frac{dV}{dx} \cdot \frac{b}{2} \qquad (6\text{-}9)$$

where $T$ = torsion in the edge beam

$V$ = shear in the edge beam

$m$ = moment per unit width at the slab edge

but from torsion theory $T = k_t \frac{d\phi}{dx}$ (6-10)

where $\phi$ = angle of twist

$k_t$ = torsional rigidity of the beam $= \beta G b^3 D$

therefore $k_t \frac{d^2\phi}{dx^2} - m - \frac{dV}{dx} \cdot \frac{b}{2} = 0$ (6-11)

6.5.3(b) gravity loading

Any gravity loading acting on the slab will be transferred to the edge beams by flexure and shear. In order to calculate the torsions induced in the edge beams it is necessary to first determine the distribution of loads which will be transferred to each beam. If the edge moments in the slab are calculated from the assumed load transfer mechanism for the case where the edges of the slab are rigidly clamped and are compared with the edge moments determined from plate theory, then the degree of correlation will give an indication of the validity of the assumed load transfer mechanism.

The edge moments derived from plate theory are in the form of an infinite cosine series. A good approximation to this series (accurate to within 1%) is obtained by considering only the first four terms (see Timoshenko et al [38] ):

$$m^F(x) = -gL^2\left(0.04958\cos\frac{\pi x}{L} + 0.0050\cos\frac{3\pi x}{L} - 0.00234\cos\frac{5\pi x}{L} + 0.00128\cos\frac{7\pi x}{L}\right) \quad (6\text{-}12)$$

where $\mu$ = Poisson's ratio = 0.2

$g$ = load/unit area

$x$ = distance from centreline of slab (see figure 6-13)

The maximum value of this function occurs at $x = 0$ and is ...

$$m^F(0) = -0.0536gL^2$$

Two possible loading distributions are indicated in figure 6-13(a) and (b) together with their corresponding fixed edge moments. The fixed edge moments determined from plate theory are shown in figure 6-13(c).

The first loading distribution assumes the load is transferred to the nearest support whilst the second idealises the slab to a series of

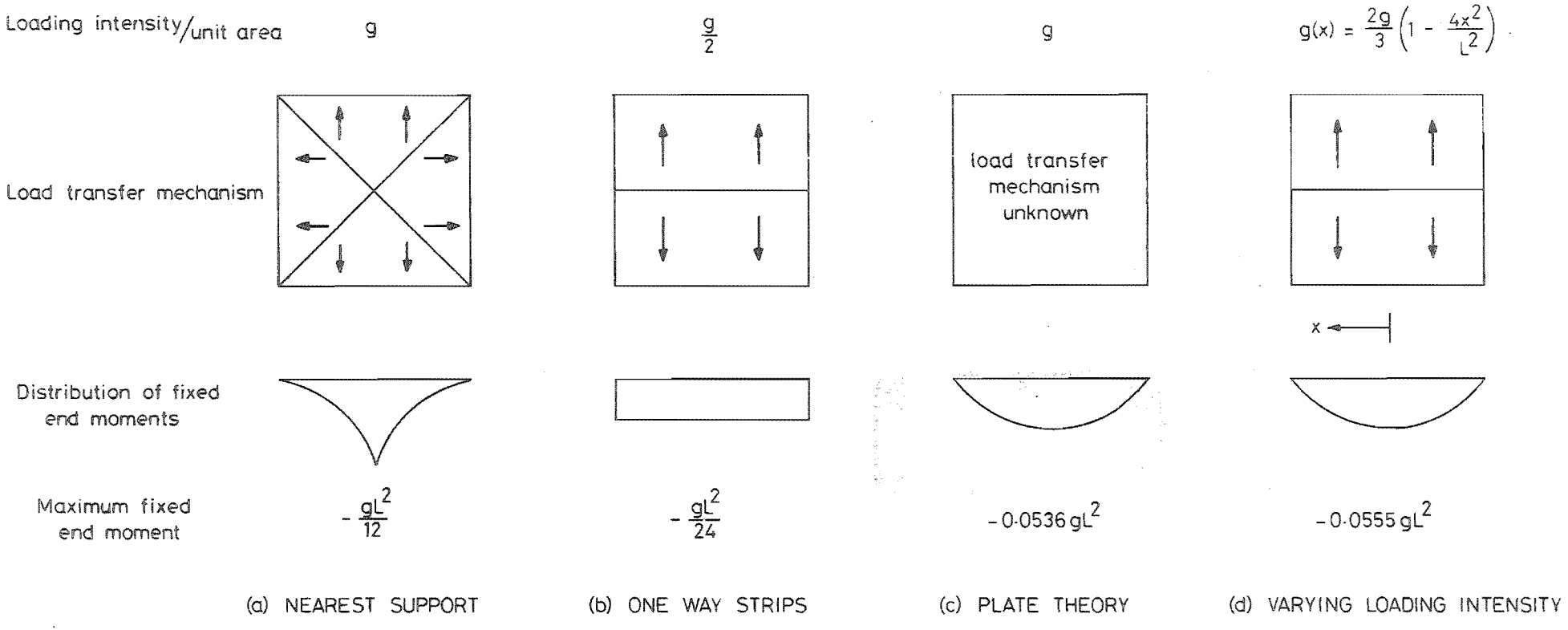


FIGURE 6-13 : SLAB GRAVITY LOADING DISTRIBUTIONS AND CORRESPONDING FIXED END MOMENTS

one way strips spanning in perpendicular directions. It is apparent that the distributions of fixed edge moments corresponding to the two selected loading distributions do not even resemble the distribution of fixed edge moments determined from plate theory. More complex loading distributions were chosen but without success, since the assumed loading distribution must also produce a rational expression for the distribution of shears along the edge of the slab.

A completely different approach to the problem was now formulated. Instead of keeping the loading intensity constant and varying the area distribution it was decided to keep the area constant and vary the intensity of the applied load. The following function was chosen to represent the load ...

$$g(x) = \frac{2g}{3}\left(1 - \frac{4x^2}{L^2}\right) \qquad (6\text{-}13)$$

The equation of the fixed end moments then becomes ...

$$m^F(x) = \frac{gL^2}{18}\left(1 - \frac{4x^2}{L^2}\right) \qquad (6\text{-}14)$$

This distribution is shown in figure 6-13(d). The resemblance to the fixed end moments determined from plate theory is very close. This approach results in a concentration of the applied load near the centre of the slab, rather than being uniformly distributed over the slab. The total load assumed by this method to act upon the slab is slightly less than the actual total applied load:

$$\text{total assumed load} = \frac{8}{9}gL^2$$
$$\text{actual total applied load} = gL^2$$

At this stage no account has been taken as to whether the assumed loading distribution results in a shear distribution along the edge beams which resembles the distribution of edge reactions as determined from plate theory. However it will be later shown in Section 6.5.3(f) that the effect of including the shear term is to reduce the edge moments in the slab by only about 20% and so it is felt this justifies taking a crude approximation for the shear.

$$\frac{dV}{dx} = g(x)\frac{L}{2} = \frac{gL}{3}\left(1 - \frac{4x^2}{L^2}\right) \qquad (6\text{-}15)$$

Consider the end rotation of a strip of slab of unit width, such as that shown in figure 6-14.

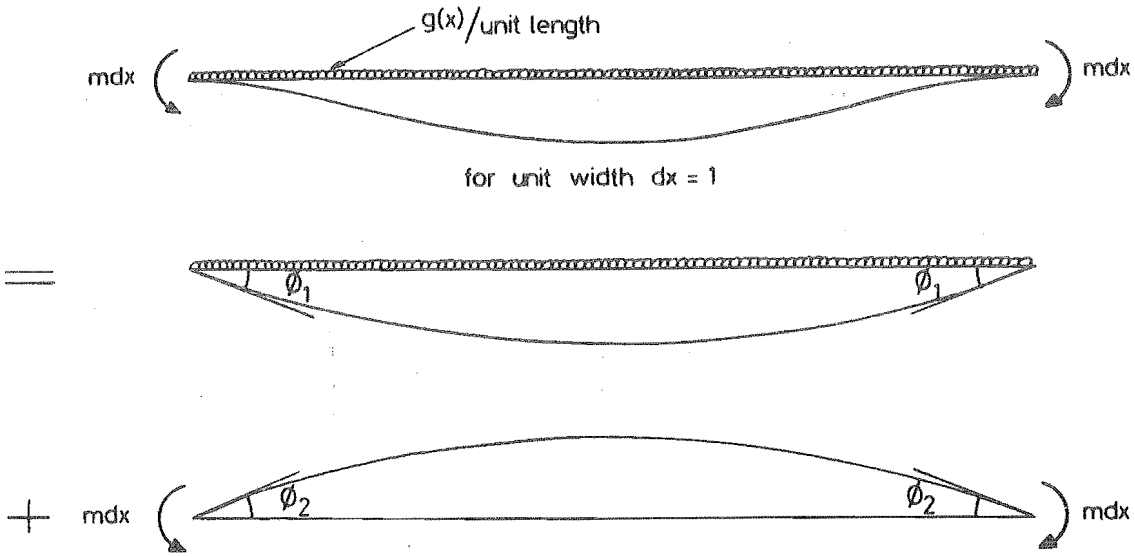


FIGURE 6-14 : END ROTATION OF SLAB UNDER GRAVITY LOADING

slab end rotation due to gravity loading $= \phi_1 = -\frac{g(x)L^3}{24EI}$ (6-16)

slab end rotation due to end moments $= \phi_2 = \frac{mL}{2EI}$ (6-17)

thus net rotation $= \phi = \phi_1 + \phi_2$

$$= \frac{mL}{2EI} - \frac{g(x)L^3}{24EI}$$

$$= \frac{6mL}{Et^3} - \frac{gL^3}{3Et^3}\left(1 - \frac{4x^2}{L^2}\right) \quad (6\text{-}18)$$

where $I = \frac{t^3}{12}$ for a unit width of slab

therefore $\frac{d\phi}{dx} = \frac{6L}{Et^3} \cdot \frac{dm}{dx} + \frac{8gLx}{3Et^3}$

and $\frac{d^2\phi}{dx^2} = \frac{6L}{Et^3} \cdot \frac{d^2m}{dx^2} + \frac{8gL}{3Et^3}$ (6-19)

Upon substitution of equations 6-15 and 6-19 into equation 6-11, the general equation of equilibrium becomes ...

$$k_t\left(\frac{6L}{ET^3} \cdot \frac{d^2m}{dx^2} + \frac{8gL}{3Et^3}\right) - m - \frac{gL}{3}\left(1 - \frac{4x^2}{L^2}\right)\frac{b}{2} = 0$$

which reduces to ...

$$\frac{d^2m}{dx^2} - \frac{Et^3}{6k_tL}m + \left(\frac{4g}{L} - \frac{gbEt^3}{36k_t}\right) + \frac{gbEt^3}{9k_tL^2}x^2 = 0 \qquad (6\text{-}20)$$

which is an equation of the form ...

$$\frac{d^2m}{dx^2} - pm + q + rx^2 = 0$$

the solution of which is ...

$$m(x) = Ae^{cx} + Be^{-cx} + \frac{1}{p}(rx^2 + \frac{r}{p} + q) \qquad (6\text{-}21)$$

where $p = \frac{Et^3}{k_tL}$ $\qquad q = \frac{4g}{9} - \frac{gbEt^3}{36k_t}$

$r = \frac{gbEt^3}{9k_tL^2}$ $\qquad c = p^{\frac{1}{2}}$

thus $\frac{dm}{dx} = Ace^{cx} - Bce^{-cx} + \frac{2r}{p}x$

boundary conditions (i) $\frac{dm}{dx} = 0$ at $x = 0$ yields $A = B$

(ii) $m = o$ at $x = L_1$ yields $A = -\left[\frac{rL_1^2 + \frac{r}{p} + q}{2p\cosh cL_1}\right]$

where $L_1$ = distance from centre of beam to face of column

Substitution of values for A and B into equation 6-21 yields ...

$$m(x) = -\left[\frac{rL_1^2 + \frac{r}{p} + q}{p\cosh cL_1}\right]\cosh cx + \frac{1}{p}(rx^2 + \frac{r}{p} + q) \qquad (6\text{-}22)$$

$$T(x) = \int_0^x m(x)\,dx$$

$$= -\left[\frac{rL_1^2 + \frac{r}{p} + q}{pc\cosh cL_1}\right]\sinh cx + \frac{x}{p}(\frac{rx^2}{3} + \frac{r}{p} + q) \qquad (6\text{-}23)$$

Equations 6-22 and 6-23 above describe the edge moments in the slab and the torsion induced in the edge beams for beams which are fully fixed against rotation at both ends. Rotation of the ends of the beams can be

accounted for by amending these equations and this is carried out in Section 6.5.3(d).

6.5.3(c) lateral loading

Torsion is induced into the lateral edge beams when the beam-column joints rotate as the structure deflects under lateral loading. The magnitude of torsion in the lateral beams is directly proportional to the joint rotation.

Consider the end rotation of a strip of slab of unit width, such as that shown in figure 6-15 :

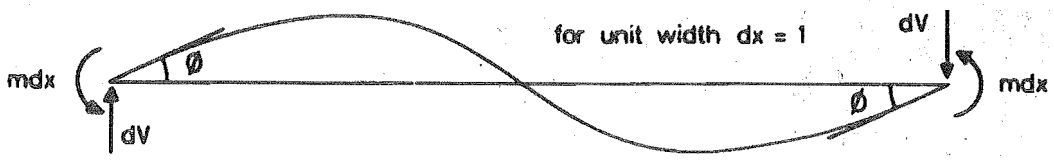


FIGURE 6-15 : END ROTATION OF SLAB UNDER LATERAL LOADING

$$\text{slab end rotation due to end moments} = \phi = \frac{mL}{6EI} \qquad (6\text{-}24)$$

$$= \frac{2mL}{Et^3} \qquad (6\text{-}25)$$

$$\text{therefore} \quad \frac{d^2\phi}{dx^2} = \frac{2L}{Et^3} \cdot \frac{d^2m}{dx^2} \qquad (6\text{-}26)$$

$$\text{and} \quad \frac{dV}{dx} = \frac{2m}{L} \qquad (6\text{-}27)$$

Upon substitution of equations 6-26 and 6-27 into equation 6-11, the general equation of equilibrium becomes ...

$$k_t \frac{2L}{Et^3} \cdot \frac{d^2m}{dx^2} - m - \frac{2m}{L} \cdot \frac{b}{2} = 0$$

$$\text{i.e.} \quad \frac{d^2m}{dx^2} - \frac{Et^3}{2k_tL}\left(1 + \frac{b}{L}\right)m = 0 \qquad (6\text{-}28)$$

which is an equation of the form ...

$$\frac{d^2m}{dx^2} - a^2m = 0$$

the solution of which is ...

$$m = D\cosh ax + E\sinh ax \qquad (6\text{-}29)$$

where $$a = \left[\frac{Et^3}{2k_t L}\left(1 + \frac{b}{L}\right)\right]^{\frac{1}{2}}$$

thus $$\frac{dm}{dx} = aD\sinh ax + aE\cosh ax$$

boundary conditions (i) $\frac{dm}{dx} = 0$ at $x = 0$ yields $E = 0$

(ii) $m = m_j$ at $x = L_1$ yields $D = \frac{m_j}{\cosh aL_1}$

where $m_j$ = edge moment at $x = L_1$ i.e. at beam end

$$= \frac{Et^3}{2L}\theta_j \quad \text{from equation 6-25}$$

where $\theta_j$ = rotation of the beam-column joints

Substitution of values for $D$ and $E$ into equation 6-29 yields ...

$$m(x) = \frac{m_j}{\cosh aL_1}\cosh ax \qquad (6\text{-}30)$$

$$T(x) = \frac{m_j}{a\cosh aL_1}\sinh ax \qquad (6\text{-}31)$$

Equations 6-30 and 6-31 above give the edge moments in the slab and the torsion in the lateral edge beams resulting from a rotation of the beam-column joints.

6.5.3(d) effect of beam end rotation on gravity loading

If the column and beams framing into the joint have a finite flexural stiffness, then the joint will rotate under the action of the torque induced in the edge beams by the gravity loading until an equilibrium position is reached. In this position the torsional moment in the beam will have reduced from the value given by equation 6-23 and it will be equal to the sum of the flexural moments in the beams and columns framing into the joint.

Assume that the joint takes up an equilibrium position with rotation $\theta_e$ and a resultant torsion in the edge beam of $T_e$.

$$\text{then } T_e = T_g - T_1 \qquad (6\text{-}32)$$

where $T_g$ = torsion due to gravity loads at $x = L_1$ in fixed ended beam

$$= -\frac{1}{pc}\left(rL_1^2 + \frac{r}{p} + q\right)\tanh cL_1 + \frac{L_1}{p}\left(\frac{rL_1^2}{3} + \frac{r}{p} + q\right)$$

$T_1$ = torsion in lateral beams at $x = L_1$ due to a rotation $\theta_e$ of the joints

$$= \frac{Et^3\theta_e}{2aL}\tanh aL_1$$

therefore $$T_e = -\frac{1}{pc}\left(rL_1^2 + \frac{r}{p} + q\right)\tanh cL_1 + \frac{L_1}{p}\left(\frac{rL_1^2}{3} + \frac{r}{p} + q\right) - \frac{Et^3\theta_e}{2aL}\tanh aL_1 \qquad (6\text{-}33)$$

Consider the equivalent frame shown in figure 6-16 which represents a typical floor of the structure. If both the frame and loading are

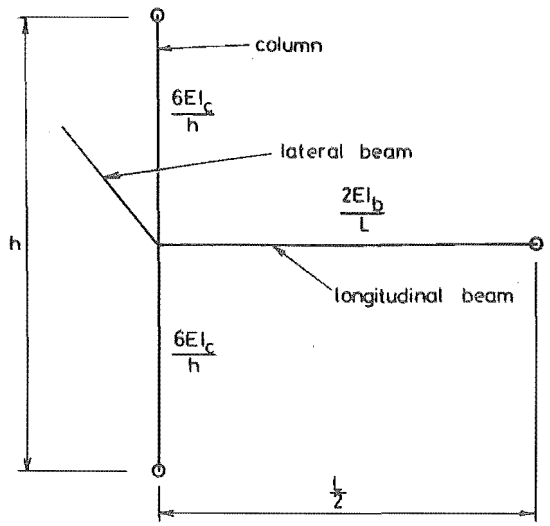


FIGURE 6-16 : EQUIVALENT FRAME FOR CALCULATION OF JOINT STIFFNESS

symmetrical then points of contraflexure will occur at the midpoint of the beam and columns. Equivalent stiffnesses for the members are indicated on the diagram. If the flexural stiffness of the joint is designated S and defined as that moment required to be applied at the joint in order to cause a unit rotation in the longitudinal beam and columns, then ...

$$S = \frac{2EI_b}{L} + \frac{12EI_c}{h} \qquad (6\text{-}34)$$

$$\text{however} \quad T_e = S\theta_e \tag{6-35}$$

and substitution of $T_e$ from equation 6-35 into equation 6-33 yields ...

$$\theta_e = \frac{-\frac{1}{pc}(rL_1^2 + \frac{r}{p} + q)\tanh cL_1 + \frac{L_1}{p}(\frac{rL_1^2}{3} + \frac{r}{p} + q)}{(S + \frac{Et^3}{2aL}\tanh aL_1)} \tag{6-36}$$

$$\text{but} \quad T_e(x) = -\frac{(rL_1^2 + \frac{r}{p} + q)}{pc\cosh cL_1}\sinh cx + \frac{x}{p}(\frac{rx^2}{3} + \frac{r}{p} + q) - \frac{Et^3\theta_e}{2aL\cosh aL_1}\sinh a \tag{6-37}$$

therefore substituting $\theta_e$ from equation 6-36 into equation 6-37 gives ...

$$T_e(x) = -\frac{(rL_1^2 + \frac{r}{p} + q)}{pc\cosh cL_1}\sinh cx + \frac{x}{p}(\frac{rx^2}{3} + \frac{r}{p} + q)$$

$$+ \left[\frac{\frac{1}{pc}(rL_1^2 + \frac{r}{p} + q)\tanh cL_1 - \frac{L_1}{p}(\frac{rL_1^2}{3} + \frac{r}{p} + q)}{\frac{2aL\cosh aL_1}{Et^3}S + \sinh aL_1}\right]\sinh ax \tag{6-38}$$

If the joint is rigidly fixed then $S \to \infty$ and equation 6-38 reduces to equation 6-23.

6.5.3(e) rotation of the beams under lateral loading

Torsion is induced into the lateral beams due to compatibility of deformations when the joints rotate. The torsional strength of the lateral beams may be less important than their capacity to twist without severe distress.

$$\text{Now rotation} \quad \theta(x) = \frac{2L}{Et^3}m(x) \tag{6-25}$$

$$\text{but} \quad m(x) = \frac{Et^3}{2L}\theta_j\frac{\cosh ax}{\cosh aL_1}$$

$$\text{and therefore} \quad \theta(x) = \theta_j(\frac{\cosh ax}{\cosh aL_1}) \tag{6-39}$$

The total beam rotation between the centre of the beam $(x = 0)$ and the end of the beam $(x = L_1)$ becomes ...

$$\theta(L_1) = \theta_j\left(1 - \frac{1}{\cosh aL_1}\right) \qquad (6\text{-}40)$$

i.e. $\theta_a = \theta_j - \theta_b$

where $\theta_a$ = rotation of the midspan of the beam relative to the joint

$\theta_b$ = rotation of the midspan of the beam relative to the initial position of the joint

These rotations are illustrated in figure 6-17. Consider two extremes:

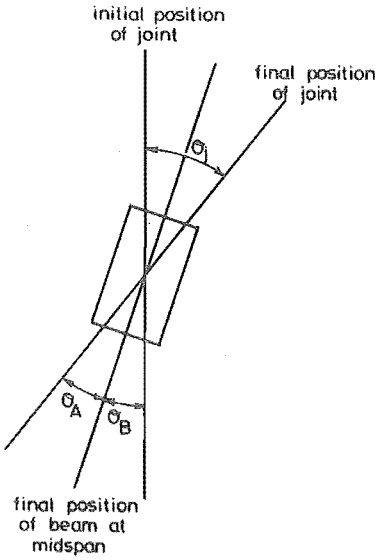


FIGURE 6-17 : RELATIVE ROTATION OF JOINT AND LATERAL BEAM

(i) If $k_t \to 0$ then $a \to \infty$, $\cosh aL_1 \to \infty$ and $\theta_a \to \theta_j$

(ii) if $k_t \to \infty$ then $a \to 0$, $\cosh aL_1 \to 1$ and $\theta_a \to 0$

It is apparent that $\theta_a$ measures the total twist in the lateral beams and that this should be minimised in order to minimise the damage to the beams. This implies that:

$$a = \left[\frac{Et^3}{2k_tL}\left(1 + \frac{b}{L}\right)\right]^{\frac{1}{2}} \to 0$$

This may be possible under two circumstances:

(i) $k_t \to \infty$ which, for most practical purposes, is unobtainable.

(ii) $E_t^3 \to 0$ i.e. the stiffness of the slab is very small.

This latter condition may essentially be obtained if yield occurs along the edges of the slab before the torsion in the lateral beams has increased sufficiently to cause cracking.

6.5.3(f) uncracked lateral beams and slab

Substitution of the dimensions of the model structure will enable determination of the magnitude of the torsion in the edge beams.

$$k_t = \beta G b^3 D = 0.23 \times \frac{3}{7} E \times (1.2)^3 \times 2.4 = 0.408E$$

$$\text{then} \quad \frac{Et^3}{k_t} = \frac{E \times (1.0)^3}{0.408E} = 2.45$$

also $L = 40$ in. $\quad L_1 = 19$ in. $\quad g = 0.27$ lb/in$^2$

(i) lateral loading.

$$\text{Now} \quad m_j = \frac{Et^3}{2L}\phi_j = \frac{4 \times 10^6 \times (1.0)^3}{2 \times 40}\phi_j = 5 \times 10^4 \phi_j$$

$$a = \left[\frac{Et^3}{2k_t L}\left(1 + \frac{b}{L}\right)\right]^{\frac{1}{2}} = \left[\frac{2.45}{2 \times 40}\left(1 + \frac{1.2}{40}\right)\right]^{\frac{1}{2}} = 0.178$$

$$aL_1 = 3.38 \quad \cosh aL_1 = 14.7 \quad \sinh aL_1 = 14.7$$

$$\text{therefore} \quad T(x) = \frac{m_j}{a \cosh aL_1} \sinh ax$$

$$= 1.91 \times 10^4 \phi_j \sinh 0.178x \qquad (6\text{-}41)$$

at the beam ends $x = 19$ and $T(19) = 2.80 \times 10^5 \phi_j$

If the flexural stiffness of the slab - lateral beam system is defined as "that torsional moment which when applied at the ends of the lateral beam, causes unit rotation there", which is the definition used by Paulay [37], then the flexural stiffness of the uncracked slab - lateral beam system = $2.80 \times 10^5$ lbin/radian.

If the shear term had not been considered, then ...

$$a = \left[\frac{Et^3}{2k_t L}\right]^{\frac{1}{2}} = 0.175$$

and $T(19) = 2.84 \times 10^5 \phi_j$

Thus the effect of including the shear term is to decrease the flexural stiffness of the slab - lateral beam system by $1\frac{1}{2}$%.

(ii) gravity loading with beam ends rigidly clamped.

$$p = \frac{Et^3}{6k_t L} = \frac{2.45}{6 \times 40} = 0.0102 \qquad c = p^{\frac{1}{2}} = 0.101$$

$$cL_1 = 1.92 \qquad \cosh cL_1 = 3.48 \qquad \sinh cL_1 = 3.33$$

$$q = \frac{4}{9}g - \frac{gbEt^3}{36k_t} = \frac{4 \times 0.27}{9} - \frac{0.27 \times 1.2 \times 2.45}{36} = 0.098$$

$$r = \frac{gbEt^3}{9k_t L^2} = \frac{0.27 \times 1.2 \times 2.45}{9 \times 40 \times 40} = 0.0000551$$

$$T(x) = -\frac{(rL_1^2 + \frac{r}{p} + q)}{pc \cosh cL_1} \sinh cx + \frac{x}{p}(\frac{rx^2}{3} + \frac{r}{p} + q)$$

$$= -34.4 \sinh 0.101x + 0.0018x^3 + 10.1x$$

and $T(19) = 90$ lbin

If the shear term had not been included then $r = 0$ and $q = \frac{4}{9}g$, all other terms retaining their same values.

$$\text{therefore} \quad T(x) = -\frac{q}{pc \cosh cL_1} \sinh cx + \frac{q}{p}x$$

$$= -33.5 \sinh 0.101x + 11.8x$$

$$\text{and } T(19) = 112 \text{ lbin}$$

Thus the effect of including the shear term is to increase the maximum torsion at the beam end by 20%.

Consider also the slab edge moments:

$$m(x) = -\frac{(rL_1^2 + \frac{r}{p} + q)}{p \cosh cL_1} \cosh cx + \frac{1}{p}(rx^2 + \frac{r}{p} + q)$$

$$= 6.7 \text{ lbin} \quad \text{at the centre of the beam}$$

but the fixed end moment $m^F = \frac{gL^2}{18} = 24$ lbin

Thus the moment at the centre of the slab has reduced to 28% of its original value due to relaxation of the edge beams.

(iii) gravity loading including beam end rotation.

$$\text{Now} \quad S = \frac{2EI_b}{L} + \frac{12EI_c}{h}$$

where $I_b$ and $I_c$ are based on the gross concrete sections

$$\text{therefore} \quad S = \frac{2 \times 4 \times 10^6 \times 1.96}{40} + \frac{12 \times 4 \times 10^6 \times 1.33}{24}$$

$$= 3.05 \times 10^6 \text{ lbin/radian}$$

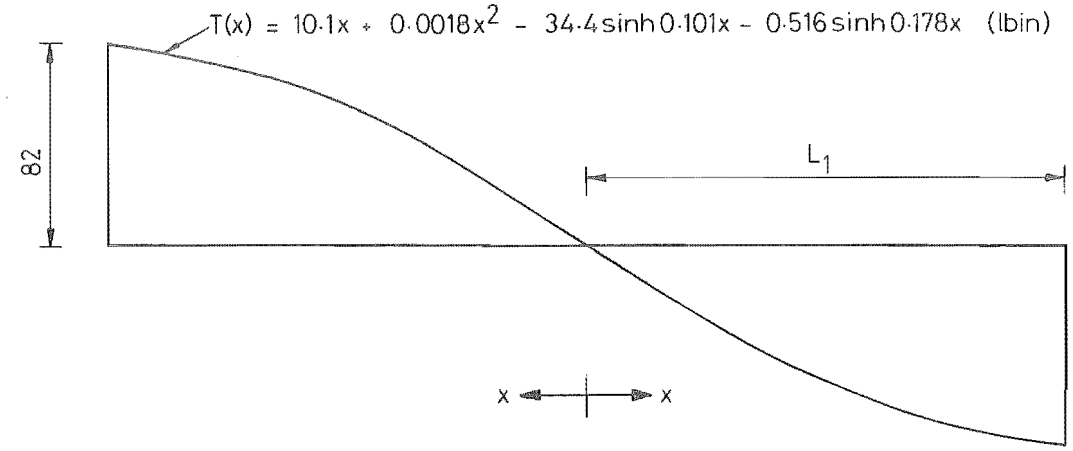


(a) GRAVITY LOADING INCLUDING BEAM END ROTATION

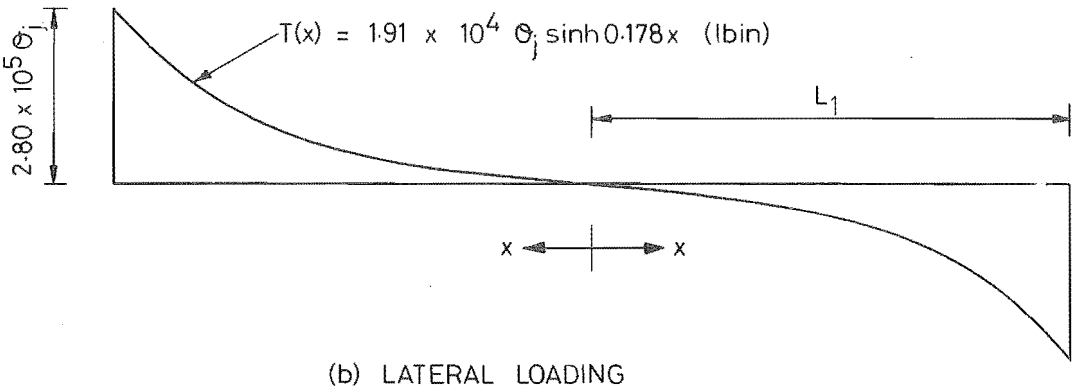


(b) LATERAL LOADING

FIGURE 6-18 : DISTRIBUTION OF TORSION IN LATERAL BEAMS FOR UNCRACKED STRUCTURE

The flexural stiffness of the slab - lateral beam system is (from equation 6-31) :

$$S_t = \frac{Et^3}{2aL}\tanh aL_1 = 2.80 \times 10^5 \quad \text{lbin/radian}$$

At the beam ends equation 6-38 reduces to ...

$$T(L_1) = \left[ -\frac{(rL_1^2 + \frac{r}{p} + q)}{pc}\tanh cL_1 + \frac{L_1}{p}(\frac{rL_1^2}{3} + \frac{r}{p} + q) \right] \times \left[ 1 - \frac{\frac{Et^3}{2aL}\tanh aL_1}{S + \frac{Et^3}{2aL}\tanh aL_1} \right]$$

i.e. $T(19) = 90(1 - \frac{S_t}{S + S_t})$

$= 90(1 - \frac{2.8}{30.5 + 2.8})$

$= 82$ lbin

Thus the effect of accounting for the rotation of the beam ends is to reduce the torsion at the ends of the beam by 9%.

6.5.3(g) cracked lateral beams and slab

Extensive cracking was observed throughout the lateral beams and this cracking extended across the corners of the slabs. Apart from this there was practically no cracking in the slab and so for the purposes of analysis the slab was assumed to remain uncracked. On the other hand, the severe cracking in the lateral beams will cause a drastic reduction in stiffness. From Section 6.5.2(e) ...

$$\frac{k_{tcr}}{k_t} = 0.05 \qquad \text{thus} \quad k_{tcr} = 0.020E$$

(i) lateral loading.

$$a = \left[ \frac{Et^3}{2k_tL}(1 + \frac{b}{L}) \right]^{\frac{1}{2}} = 0.802$$

therefore $T(x) = 0.0150\phi_j \sinh 0.802x$

and $T(19) = 6.23 \times 10^4 \phi_j$

Thus the flexural stiffness of the cracked slab - lateral beam system = $6.23 \times 10^4$ lbin/radian, which is 22% of the uncracked flexural stiffness.

(ii) gravity loading.

As was pointed out in Section 6.5.3(b), under gravity loading the edge moments acting on the beams are of considerably more importance than the shear force in determining the torsion in the edge beams and it was felt that this justified using a loading function which gave a close approximation to the edge moments but only a relatively crude approximation to the shear force distribution. However, when the lateral beams crack their stiffness reduces considerably and the influence of the shear becomes greater than that of the edge moments. Consequently, the assumption made in Section 6.5.3(b) is no longer valid and may give misleading results.

The very low torsional stiffness of the edge beams will result in very small edge moments, and consequently the torsion in the edge beams will be very small, especially in comparison with the torsion induced by the lateral loading. As a result, it was felt that little error would be introduced by neglecting any torsion due to gravity loading altogether.

## 6.5.4 Effect of the slab - lateral beam system

### 6.5.4(a) uncracked lateral beams and slab

The equation relating torsional moment and joint rotation at the lateral beam - column interface is:

$$T = 82 + 2.80 \times 10^5 \theta_j \qquad (6\text{-}42)$$

and the flexural stiffness of the slab - lateral beam system is:

$$S_t = 2.8 \times 10^5 \theta_j \quad \text{lbin/radian}$$

The stiffness of the uncracked longitudinal beams $= \frac{6EI}{L}$

where I is based on the gross concrete section including the steel reinforcing

therefore the longitudinal beam stiffness $= \frac{6 \times 4 \times 10^6 \times 2.54}{40}$

$= 15.2 \times 10^5$ lbin/radian

Thus the total stiffness of the longitudinal beam - lateral beam - slab system is ...

total stiffness $= 18.0 \times 10^5$ lbin/radian

which is an increase of 18%.

The equivalent moment of inertia $= 2.54 \times 1.18 = 3.00$ in$^4$

From Section 6.5.2(a) it was found that the lateral beams will crack at a torque of 414 lbin. Substitution of this value into equation 6-42 gives an indication of the joint rotation required:

$$\theta_j = 0.0012 \text{ radians}$$

6.5.4(b) cracked lateral beams and slab

cracked stiffness of the slab - lateral beam system

$$= 0.62 \times 10^5 \text{ lbin/radian}$$

cracked stiffness of the longitudinal beams $= \frac{6 \times 4 \times 10^6 \times 0.95}{40}$

$$= 5.70 \times 10^5 \text{ lbin/radian}$$

thus the total stiffness $= 6.32 \times 10^5$ lbin/radian

which is an increase of 11%. Thus the stiffening effect of the slab - lateral beam system is diminished relative to the longitudinal beams once cracking has occurred.

equivalent moment of inertia = $0.95 \times 1.11 = 1.05$ in$^4$

6.5.4(c) ultimate strength

As the joint rotation increases, it is likely that yielding will occur at the edge of the slab and thus prevent further transfer of moment from the slab to the lateral beams. This yielding will commence at the ends of the lateral beams and will progress towards the centre of the beams. In the limit case it is possible that the slabs may yield along the entire length of the lateral beam and that the torque thus induced may be insufficient to cause torsional failure of the lateral beams.

The total moment carried by the longitudinal beam and lateral beam - slab system combined is given by one of the two following cases, which are shown in figure 6-19. The critical section for a beam subjected to torsion occurs at d ( 1.5 in. = 38 mm) from the column face.

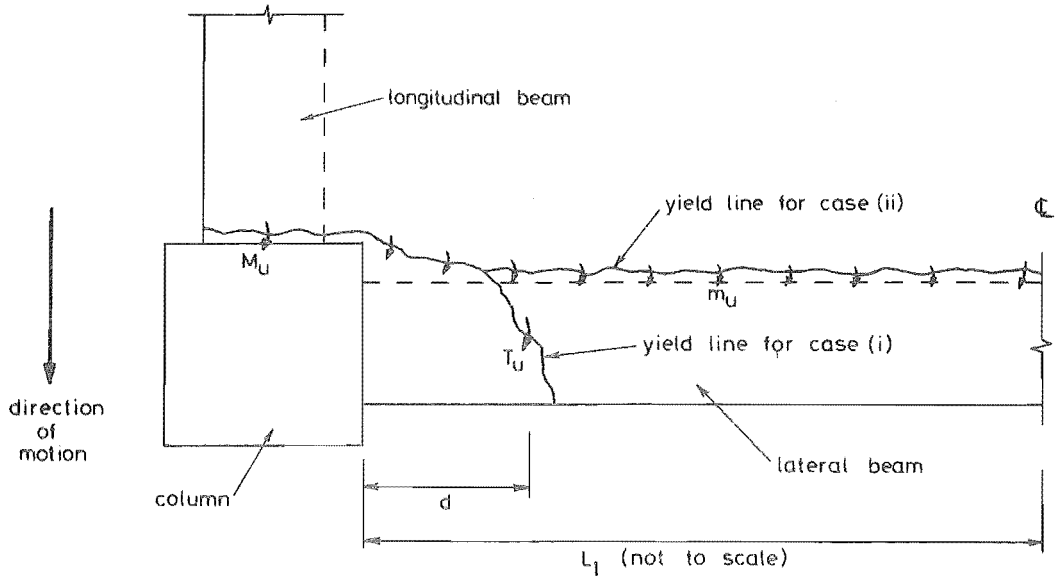


FIGURE 6-19 : YIELD MECHANISMS FOR DETERMINING THE ULTIMATE STRENGTH OF THE LONGITUDINAL BEAM AND LATERAL BEAM - SLAB SYSTEM

(i) the lateral beams yield:

$$\text{total ultimate moment} = M_u + T_u + dm_u \qquad (6\text{-}43)$$

(ii) the lateral beams do not yield:

$$\text{total ultimate moment} = M_u + L_l m_u \qquad (6\text{-}44)$$

Obviously the lesser of the values given by equations 6-43 and 6-44 is the correct ultimate moment. The criterion for yield to occur in the lateral beams is that ...

$$T_u < (L_l - d)m_u \qquad (6\text{-}45)$$

The ultimate negative moment strength of the slab is, from a moment curvature analysis, 42 lbin/in. The ultimate positive moment strength of the slab is 53 lbin/in. but it is doubtful as to whether this full strength could be developed at the edge of the slab since the anchorage length of the positive slab reinforcing in the beam is considerably less than that provided for the negative reinforcing. Accordingly, the negative moment strength of 42 lbin/in. was chosen as most accurately representing the ultimate strength of the slab.

Then, from equation 6-45, for yield to occur in the lateral beams ...

$$T_u < (19 - 1.5)42$$

$$< 735 \text{ lbin}$$

In fact $T_u = 635$ lbin and so yield will occur in the lateral beams. The total ultimate strength of the longitudinal beam and lateral beam-slab system is thus given by equation 6-43 ...

$$\text{total ultimate moment} = M_u + 635 + 1.5 \times 42$$

$$= M_u + 700 \text{ lbin}$$

which is an increase of almost 16% over the average longitudinal beam strength.

### 6.5.5 Equivalent frame method: a comparison with ACI Code 318-71

It was decided to compare the gravity load induced torsion determined from this analysis with that obtained from the equivalent frame method introduced by ACI Code 318-71 [26]. The equivalent frame method involves the representation of the three dimensional slab system by a series of two dimensional frames. The method acknowledges the torsional rotations which are possible in the three dimensional system and attempts to represent these in two dimensions by redefining the flexural

stiffnesses of the various members. The stiffnesses of all members are based on the uncracked section.

The bulk of the calculation is routine and is presented in Appendix D for reference. The torsion in the edge beams as calculated by the two methods is shown in figure 6-20 for comparison.

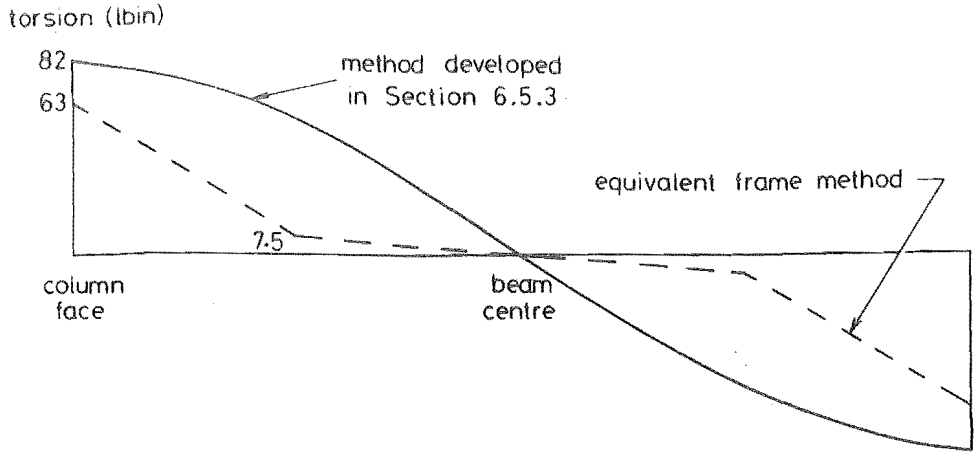


FIGURE 6-20 : COMPARISON OF THE TORSION INDUCED INTO THE EDGE BEAMS BY GRAVITY LOADING BETWEEN THE METHOD OF ANALYSIS DEVELOPED IN SECTION 6.5.3 AND THE EQUIVALENT FRAME METHOD OF THE ACI CODE

It is apparent that the equivalent frame method gives a value for the torsion at the beam-column interface which is about three quarters of that determined in Section 6.5.3 and that the shapes of the two curves are very different. The reason is that the equivalent frame method is a design method and it does not purport to accurately predict the torsion in the edge beams but rather it deliberately sets out with the intention of reducing the edge moments, particularly near the centre of the slab.

## 6.6 STRENGTH OF THE STRUCTURE

### 6.6.1 Experimental load-deflection curves

The load-deflection curves for each floor of Model 1 are shown in figures 6-21 to 6-26. After the first yield cycle the load-deflection curves rapidly degenerate into spring-hardening loops in which the stiffness of the structure increases with increasing deflection until the yield plateau is attained once again, contrary to the common

assumption that the stiffness of the structure decreases with increasing deflection. The hysteresis curves for all six floors are similar in shape and all are of this spring-hardening type.

This softening of the structure near the centre portion of each loop is due to the effect of concrete cracks opening and closing, particularly a large crack which occurs just above the base of each column. These large cracks largely govern the behaviour of the structure and as each load cycle induces progressively greater permanent tensile strains in the reinforcement crossing this crack, so the rotation required to close the crack increases, resulting in a further softening of the structure. After four cycles into the yield range, the stiffness of the structure reduced to 20% of the stiffness on the initial elastic cycle.

A large part of this stiffness degradation would undoubtedly be due to a deterioration of anchorage bond and a consequent slip of the reinforcing steel in the joint, although Bertero and McClure [39] still found a marked reduction in stiffness of some model frames they tested, even though the reinforcing steel was securely anchored by welding it to plates provided at each joint. Their load-deflection hysteresis curves also rapidly degenerated into the hardening spring type.

The ultimate strength of the structure appears to reduce to about 84% of the original ultimate strength after four inelastic load cycles. It is possible the structure could have attained its original ultimate strength on subsequent inelastic load cycles as the peaks of the load-deflection curves had not yet flattened out completely, but this would have involved very large deflections. Any loss in ultimate strength was probably due to a deterioration in the steel anchorage, since the frames tested by Bertero and McClure suffered no loss in ultimate strength.

The area of the load-deflection curves are a measure of the energy dissipation characteristics of the structure. The area of each of the half-loops is approximately the same; in fact, the area of half-loop 5B is 10% greater than the area of half-loop 2B, indicating that the degree of energy dissipation of the structure is unaffected by the decrease in stiffness. Some hysteresis is apparent on the initial elastic cycle and even here the influence of the cracks opening and closing is clear.

### 6.6.2 Theoretical strength of the structure

The step-by-step static structural analysis program developed by Sharpe [19] (see Section 5.4.3) was used to determine the ultimate strength of Model 1. The assumed moment-curvature loop was elasto-plastic and

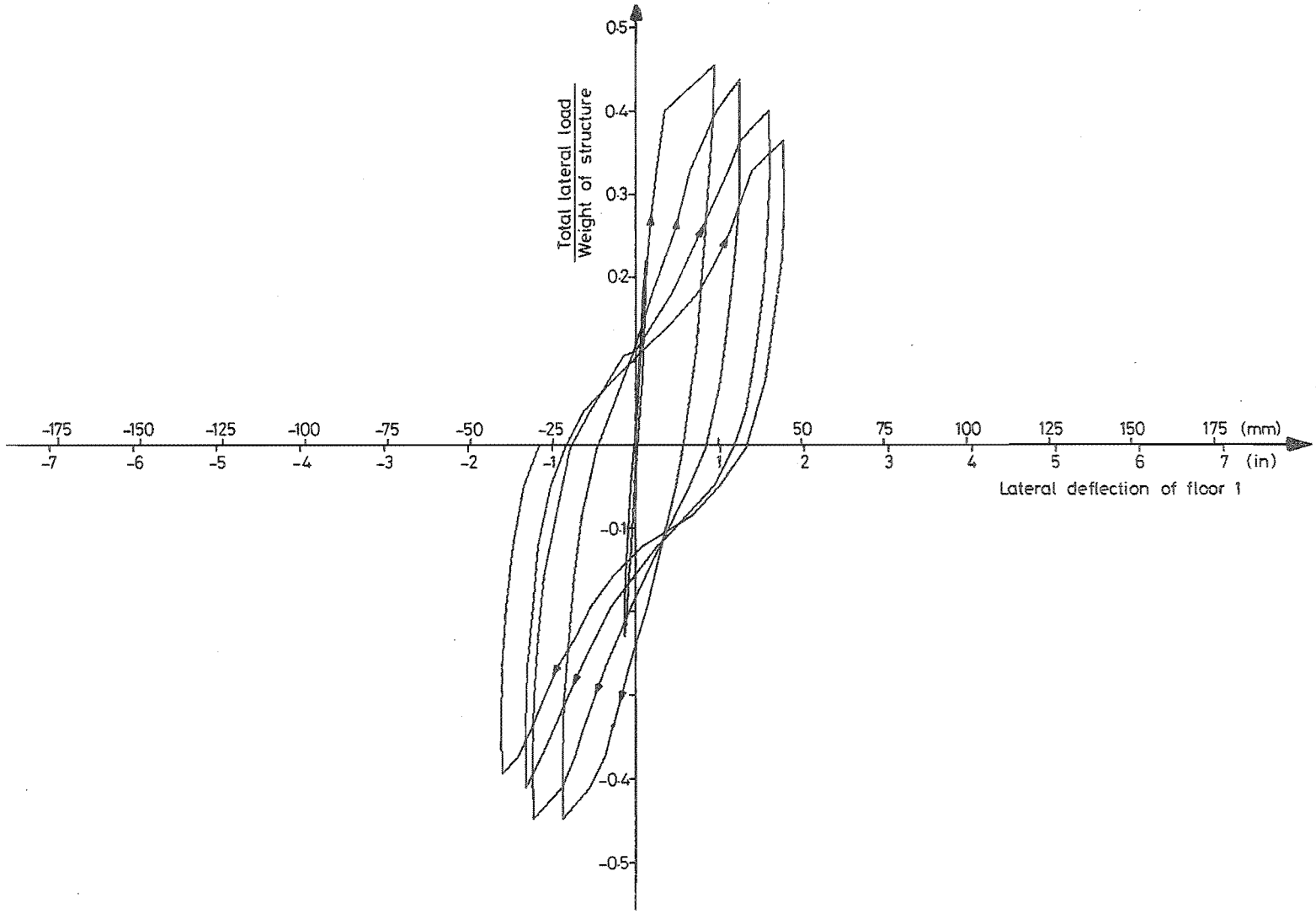


FIGURE 6-21 : EXPERIMENTAL STATIC LOAD-DEFLECTION CURVES FOR FLOOR 1 OF MODEL 1

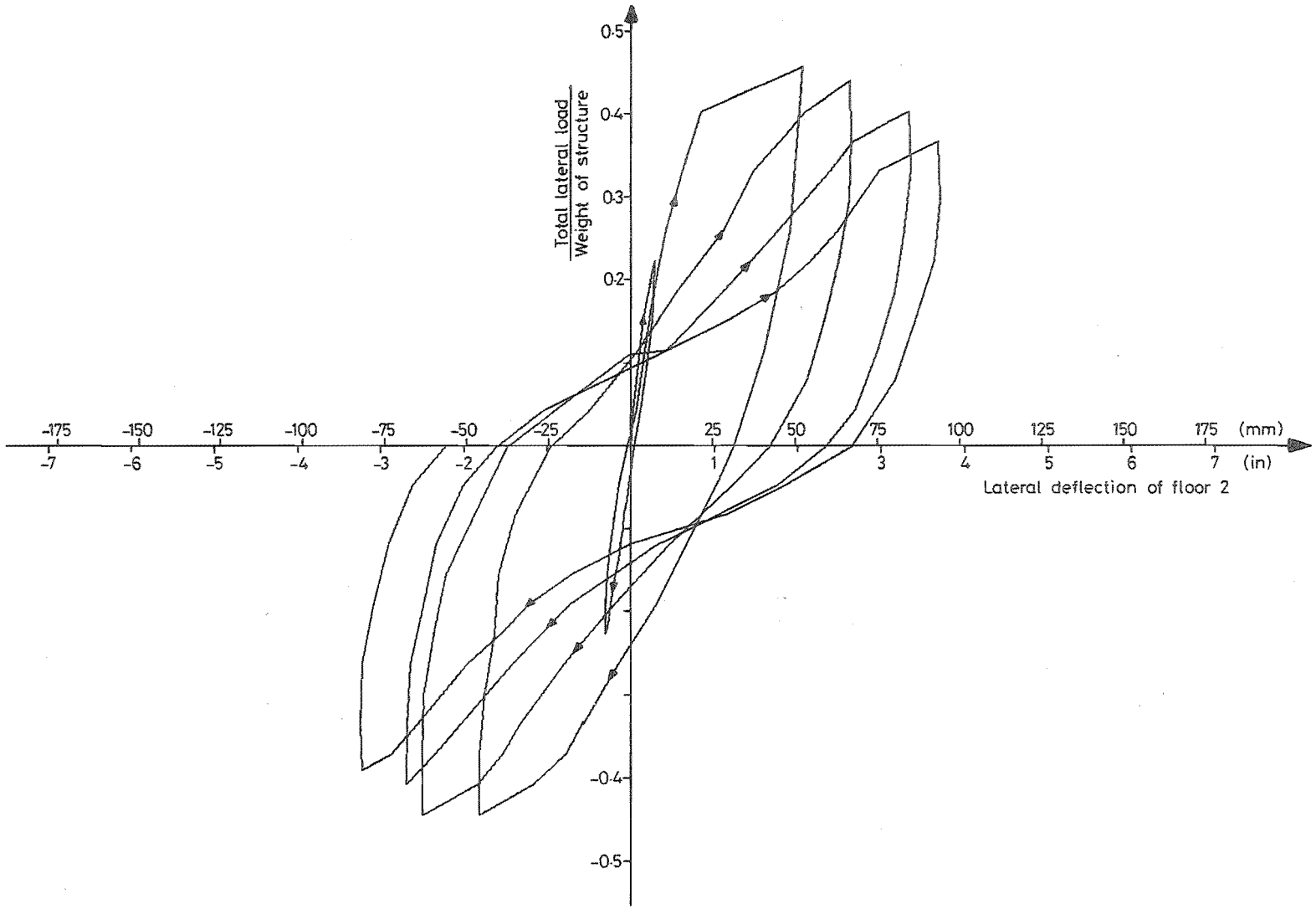


FIGURE 6-22 : EXPERIMENTAL STATIC LOAD-DEFLECTION CURVES FOR FLOOR 2 OF MODEL 1

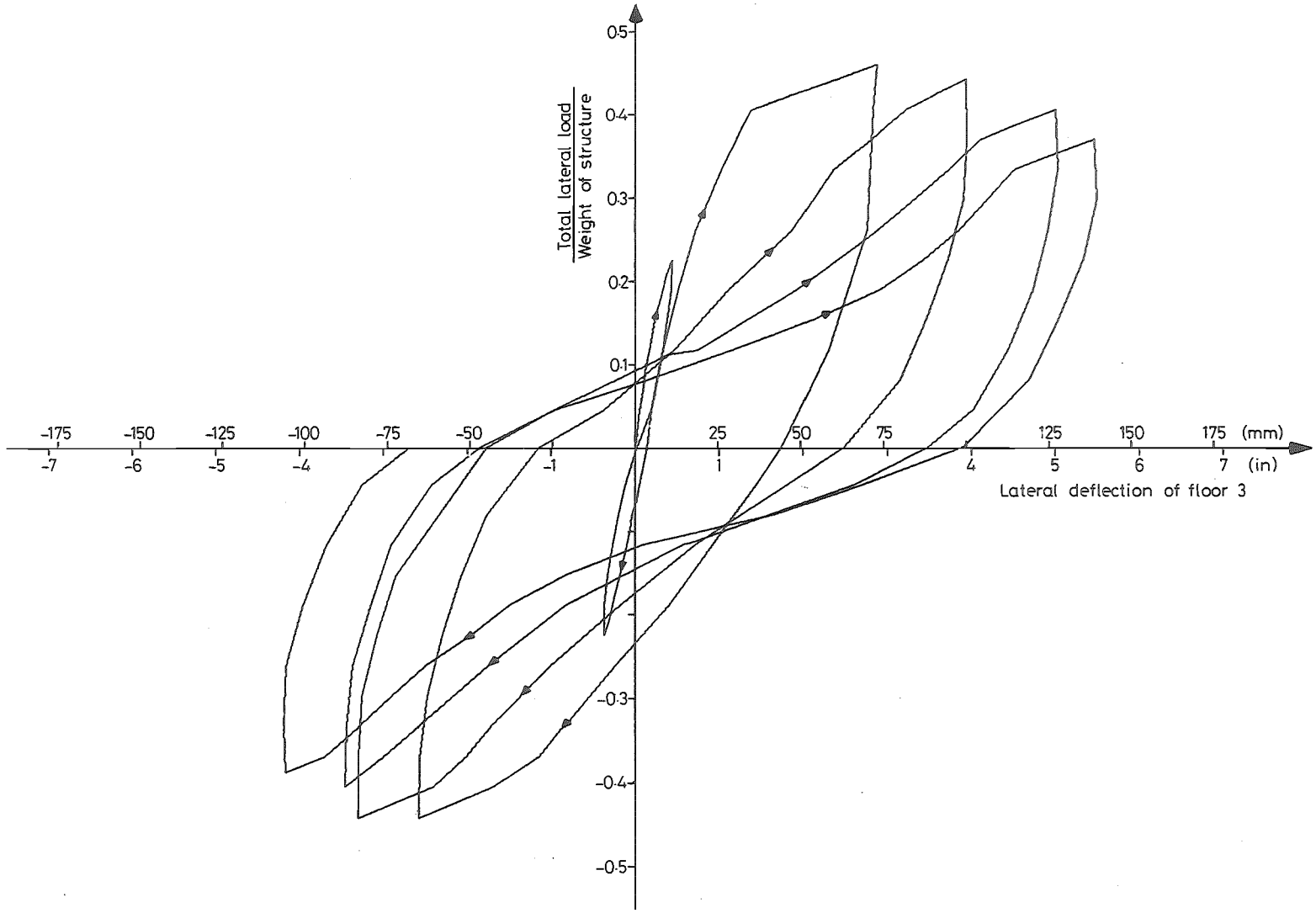


FIGURE 6-23 : EXPERIMENTAL STATIC LOAD-DEFLECTION CURVES FOR FLOOR 3 OF MODEL 1

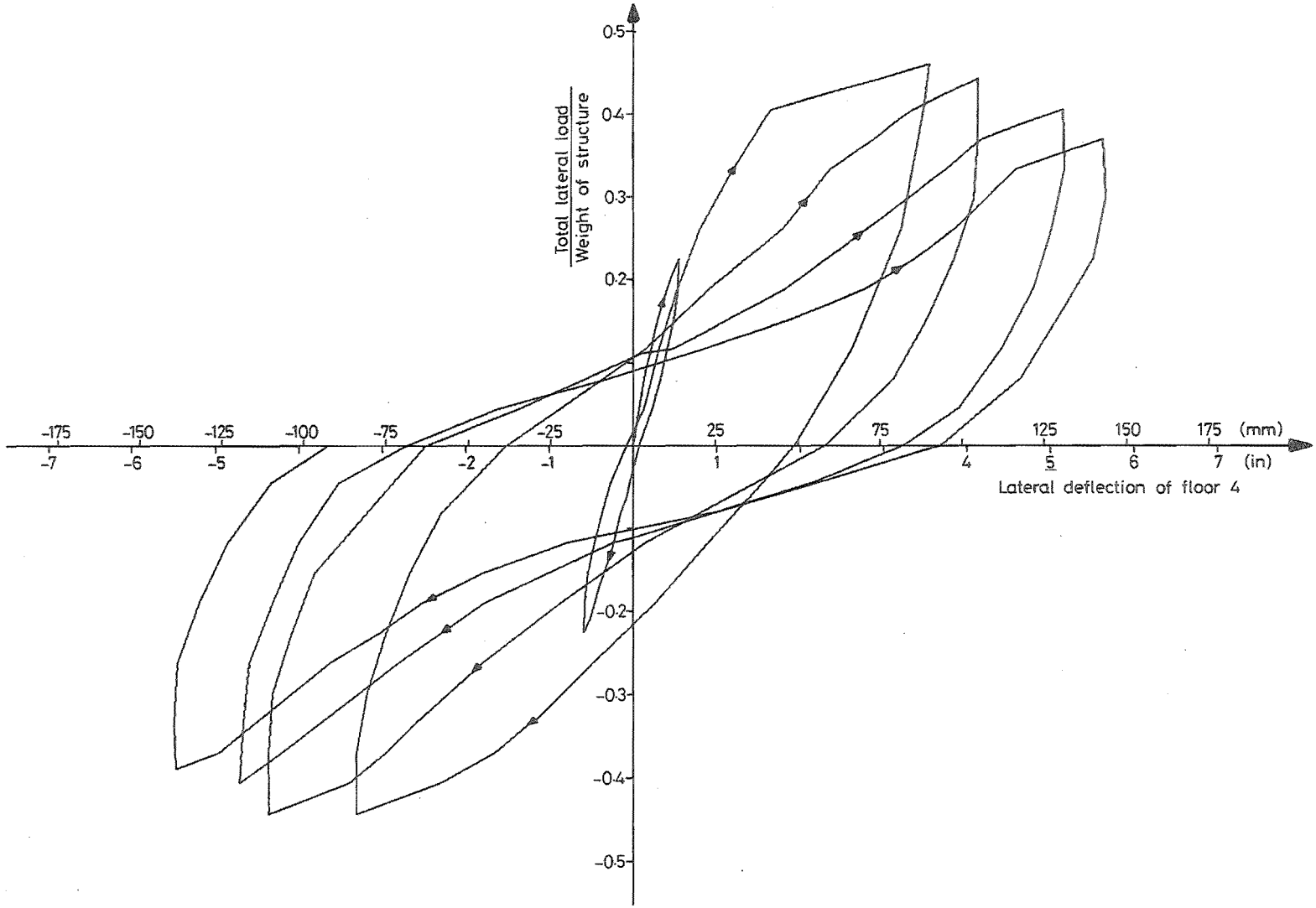


FIGURE 6-24 : EXPERIMENTAL STATIC LOAD-DEFLECTION CURVES FOR FLOOR 4 OF MODEL 1

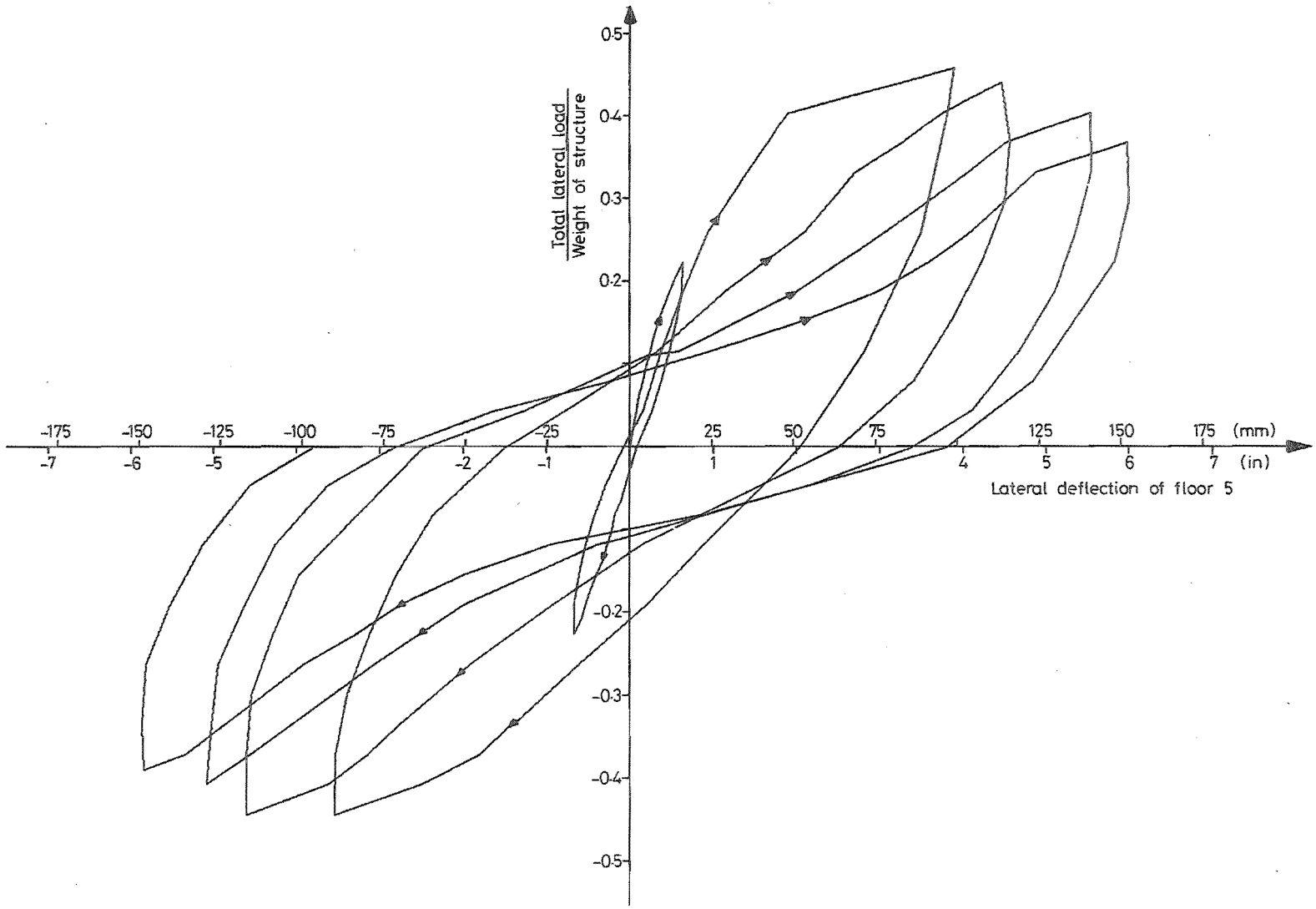


FIGURE 6-25 : EXPERIMENTAL STATIC LOAD-DEFLECTION CURVES FOR FLOOR 5 OF MODEL 1

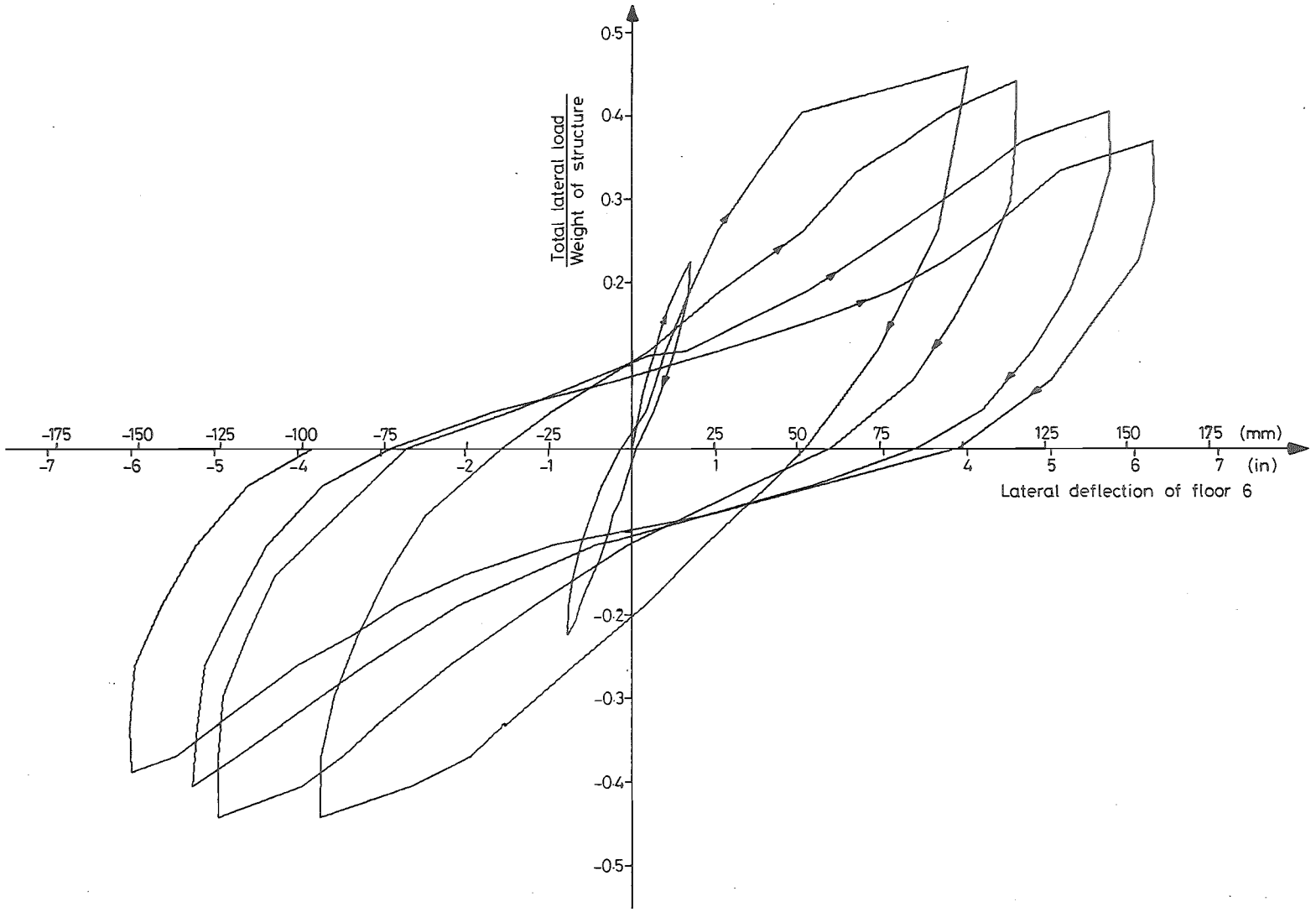


FIGURE 6-26 : EXPERIMENTAL STATIC LOAD-DEFLECTION CURVES FOR FLOOR 6 OF MODEL 1

the member strengths and stiffnesses in Sections 4.6.3 and 4.6.4 were used in the analysis. Use was made of the subroutine modelling the column axial load - moment interaction diagram.

The predicted lateral failure load was 1010 lb (4490 N) which is only 77% of the actual failure load of 1312 lb (5840 N). The failure mechanism was a column sidesway type with plastic hinges forming at the base of the columns and at the tops of the second floor columns. Hinging also occurred at both ends of the beams up to and including those at the fourth floor.

The discrepancy between predicted and actual failure loads is large and the structure was examined for likely reasons which could cause such a discrepancy. The effect of the torsion occurring in the lateral beams and strain hardening of the reinforcing steel were considered two likely reasons.

### 6.6.3 Additional strength due to torsion

The torsion occurring in the lateral beams effectively increases both the strength and stiffness of the longitudinal beams, but does not affect the columns. Although the lateral beams will not reach their ultimate strength until after yield has occurred in the longitudinal beams, at ultimate the net effect is the same and the effective longitudinal beam strength is the sum of the two member strengths. Once again the assumed moment-curvature loop was elasto-plastic and the column axial load - moment interaction subroutine was used.

The adjusted stiffnesses and strengths of the beam became:

| | | |
|---|---|---|
| uncracked stiffness | = | 3.00 $in^4$ (125 x $10^4 mm^4$) |
| cracked stiffness | = | 1.05 $in^4$ (43.7 x $10^4 mm^4$) |
| positive yield moment | = | 5320 lbin |
| negative yield moment | = | 5140 lbin |

The predicted lateral failure load was 1100 lb (4890 N) which is 84% of the actual failure load of 1312 lb (5840 N). Again, collapse was due to a column sidesway mechanism with plastic hinges forming at the base of the columns and at the tops of the second floor columns. Hinges formed at the ends of beams up to and including the third floor.

Thus the inclusion of the torsion effect increased the predicted ultimate strength of the structure from 77% to 84% of the actual failure load.

6.6.4 Additional strength due to strain hardening

Preliminary analyses indicated that the ultimate strength of the structure is greatly influenced by strain hardening of the reinforcing steel and so the moment-curvature analyses of the beams and columns were extended to include this effect. It was found that strain hardening will account for a 23% increase in the strength of the beams but for the columns the increase varies according to the magnitude of the axial load present, the increase in strength decreasing with increasing axial compressive load. At collapse, the axial compression in one column of the model structure frame is about 2000 lb (8900 N) while the other column has an axial tension of 600 lb (2670 N) and the average increase in strength due to strain hardening was found to be 14% for these two axial load levels.

An elasto-plastic moment-curvature curve was obviously unrealistic in describing the behaviour of the members up to ultimate and so a bi-linear curve was used instead. The yield point is defined as before (including the effects of torsion) and the ultimate strength includes the effect of strain hardening. Unfortunately the column axial load - moment interaction subroutine developed by Sharpe [19] could only be used in conjunction with elasto-plastic moment-curvature curves; for bi-linear curves the column had to have a unique yield moment and a unique ultimate moment. These were taken as the average of those values calculated for the column with axial loads of 2000 lb compression and 600 lb tension.

Accurate determination of the yield slopes of the members is difficult since the steel stress-strain curve is not defined accurately throughout the strain hardening range. It was found that the yield slopes could vary widely with negligible effect on the predicted ultimate strength of the structure but with a vast influence on the maximum deflection, as long as the ratio of beam to column yield slopes remained constant. The slopes of the initial strain hardening portions of the members moment-curvature curves were used as the basis for determining the yield slopes but three other constraints were considered as well. These were:

(i) ultimate column moment = 4120 lbin (465 KNmm)

(ii) ultimate beam moment = 6600 lbin (745 KNmm)

(iii) maximum top storey deflection = 4.01 in. (102 mm)

The yield slope for the column was determined as 0.4% of the cracked stiffness and the beam yield slope as 1% of the cracked stiffness. The difficulty with the bi-linear moment-curvature curve is that, unlike the elasto-plastic curve, it is open ended, i.e. the apparent strength of the member will increase indefinitely with increasing curvature. Whereas

for the elasto-plastic curve the structure will collapse once a collapse mechanism forms, for the bi-linear curve collapse does not occur upon formation of a collapse mechanism and the structure may be able to withstand considerable additional loads. A useful moment-curvature idealisation would be a tri-linear curve, which would be the same as the bi-linear curve excepting that the hinge stiffness reduces to zero and full plasticity develops when the member has attained its full ultimate strength.

Without a definite predicted failure load resulting from the bi-linear analysis, the accuracy of the analysis is dependent on how closely the maximum beam and column moments and top storey deflection correlate with the limiting values previously mentioned. At the experimental failure load of 1312 lb (5840 N), these are:

(i) maximum column moment = 4110 lbin (464 KNmm)

(ii) maximum beam moment = 6780 lbin (765 KNmm)

(iii) top storey deflection = 4.18 in. (106 mm)

The correlation between these two sets of values is excellent. The top storey deflection is very sensitive to the yield slopes and can be altered substantially with negligible effect on the maximum beam and column moments. A collapse mechanism actually formed at a lateral load of 1200 lb (5340 N) which is 92% of the experimental ultimate load. The mechanism was a column sidesway one with hinges forming at the base of the columns and at the tops of the second floor columns. The plastic hinge locations corresponding to the actual ultimate load are shown in figure 6-28(a).

The theoretical load-deflection curve is shown in figure 6-27 together with the first yield cycle of the experimental tests. It is apparent that the structure is slightly less stiff than predicted from the cracked member stiffnesses due probably to the anchorage slip of the longitudinal beam reinforcing in the joint regions and also to deformations of the joints. The yield plateaus of both curves have the same slope.

It was not possible to reproduce theoretical cyclic load-deflection curves resembling the experimental ones using simple moment-curvature hysteresis curves such as elasto-plastic, bi-linear or even Ramberg-Osgood curves. The reason is that the deterioration of stiffness of the structure due to anchorage slip, joint deformations and the opening and closing of large cracks are not accounted for. Some attempts have been made to introduce new models to account for these factors [16,42] and with some success but the analysis methods have been too complicated

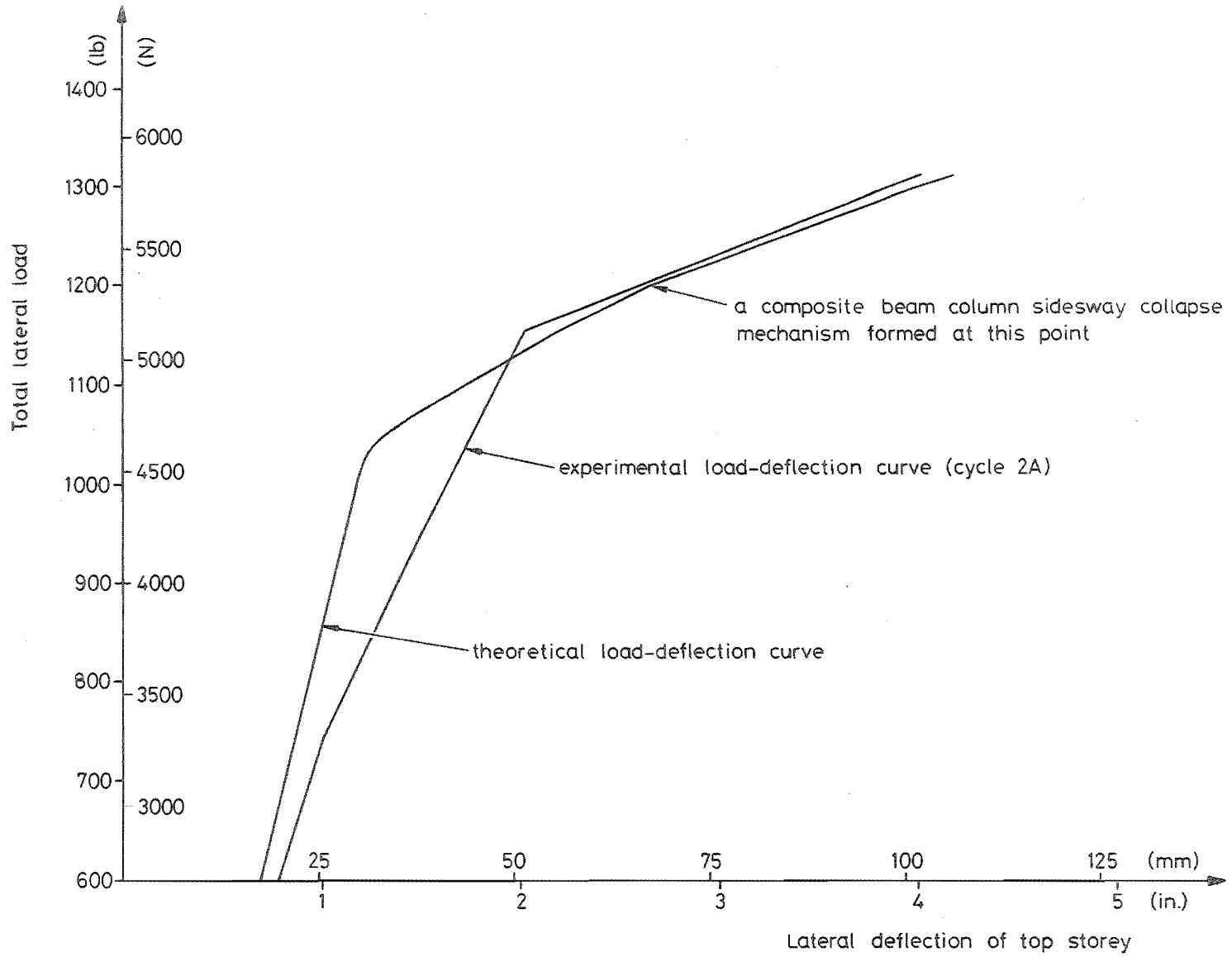


FIGURE 6-27 : COMPARISON OF EXPERIMENTAL AND THEORETICAL LOAD-DEFLECTION CURVES FOR MODEL 1

and inefficient for general use. Accurate prediction of the dynamic cyclic response is the more important objective at this stage since this is how structures actually respond to earthquakes.

### 6.6.5 Ductility of the structure

A measure of the ability of a structure to absorb energy by post-elastic deformation is the ductility factor, which is defined as the ratio of the lateral deflection at ultimate to the lateral deflection at first yield. It has been pointed out [43] that a ductility factor of about 4 is required if reinforced concrete structures are to survive severe earthquakes.

It was not possible to directly measure the deflection at which the structure yielded; nor was it readily apparent from the experimental deflection curve of the structure, since first yield results in only a minimal decrease in the overall stiffness of the structure. The theoretical analysis indicated that first yield would occur at a top storey deflection of 1.17 in. and this value was used in the ductility calculations. On this basis the maximum ductility attained on the first yield cycle was 3.5. Of course the maximum ductility attained on the last cycle would be higher than this on account of its greater deflection but this is not really valid, both because the ultimate strength of the structure had decreased and because the reduced stiffness of the structure would have required a deflection greater than 1.17 in. in order to attain first yield.

The interstorey deflections were small in the upper floors of the structure since most of the deflection occurred in the lower floors, particularly the ground floor. If the overall ductility of the structure is measured at the first floor level then a ductility ratio of 5.5 was attained on the first yield cycle. The computer output gives the plastic rotation $\theta_p$ occurring at each hinge and this is related to the curvature of the section and the length of the plastic hinge by ...

$$\theta_p = (\phi_u - \phi_y)L_p \qquad (6\text{-}46)$$

where $\phi_u$ = curvature corresponding to ultimate

$\phi_y$ = curvature corresponding to yielding of the tension reinforcement

$L_p$ = equivalent plastic hinge length

If the section ductility is defined as $\frac{\phi_u}{\phi_y}$, then rearranging equation 6-46 gives ...

$$\frac{\phi_u}{\phi_y} = 1 + \frac{\theta_p}{L_p \phi_y} \qquad (6\text{-}47)$$

Assuming a plastic hinge length equal to the effective depth of the members, the theoretical analysis indicates that the maximum section ductilities required are 44 for the columns and 31 for the beams.

Thus the section ductilities required in order to provide an overall structure ductility of about 4 are extremely large and may be difficult to achieve in some structures. However, the fact that Model 1 did manage to achieve an overall structure ductility of close to 4 does indicate that it is possible to achieve section ductilities of this magnitude in a well designed and detailed structure. The column bases, where the ductility requirements were greatest, rapidly degenerated to a steel couple and the inherent ductility of the reinforcing steel would enable this section to achieve extremely large ductilities.

## 6.7 COLLAPSE MECHANISMS

It is assumed that failure of a structure will occur once a collapse mechanism has formed. The two classical collapse mechanisms are the beam sidesway mechanism and the column sidesway mechanism and these are shown in figure 6-28. Park [43] has shown that the column sidesway mechanism should be particularly guarded against, especially if it forms in only one floor, because of the large ductilities required and the difficulties of providing them and because of the catastrophic consequences of this type of failure. This point is generally recognised in design by ensuring that the columns are slightly overstrong with respect to the beams.

It is the author's contention that under present design procedures, failure will seldom occur due to a beam sidesway mechanism and the collapse mechanism will almost always be either of the column sidesway type or of a composite beam column sidesway type.

Park's analysis was based on the assumption that the frame reached yield at all the plastic hinge sections simultaneously and at sufficient sections to form a mechanism and he indicated that if moment redistribution was necessary before all the plastic hinges developed,

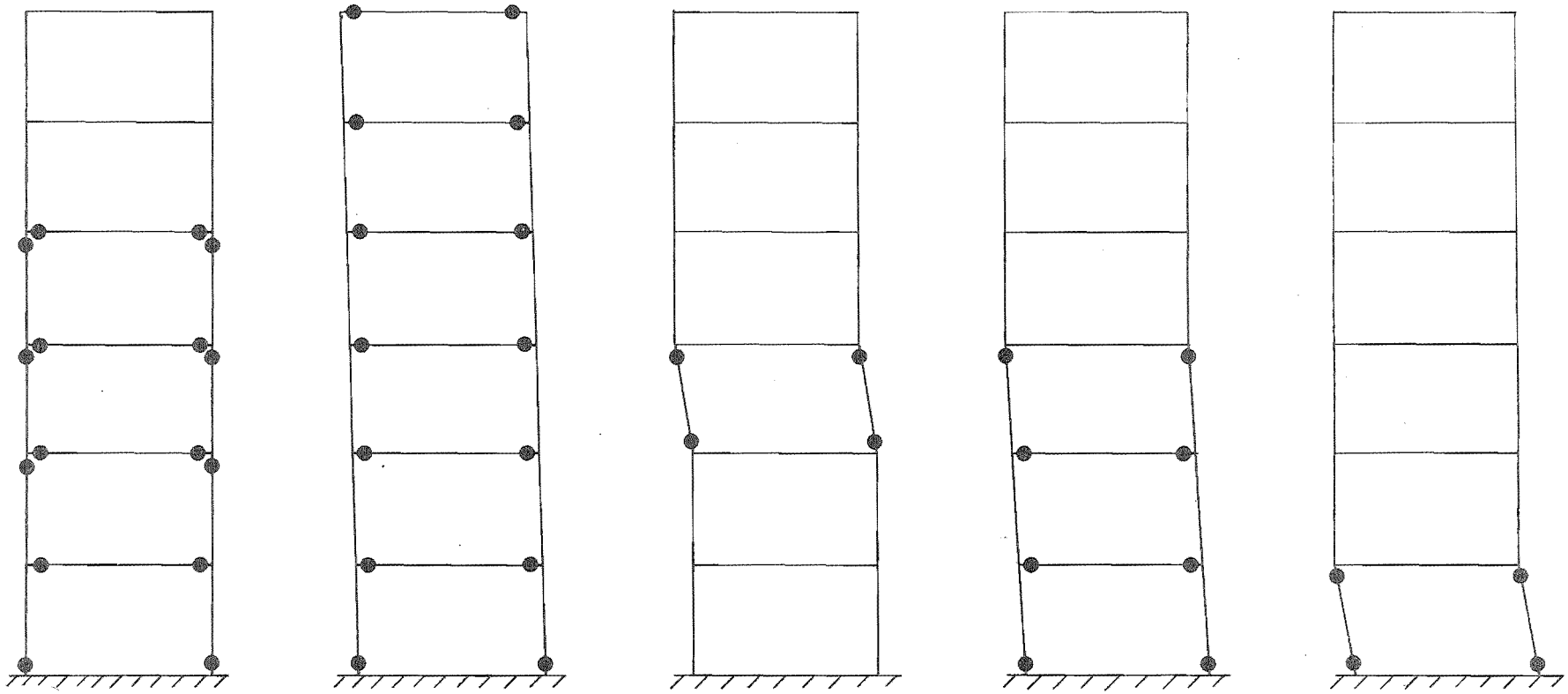

(a) PLASTIC HINGE LOCATIONS AT ULTIMATE LOAD OF MODEL 1

(b) CLASSICAL BEAM SIDESWAY COLLAPSE MECHANISM

(c) CLASSICAL COLUMN SIDESWAY COLLAPSE MECHANISM (SECOND FLOOR)

(d) THEORETICAL COLLAPSE MECHANISM (COMPOSITE BEAM COLUMN SIDE-SWAY)

(e) ACTUAL COLLAPSE MECHANISM (GROUND FLOOR COLUMN SIDE-SWAY)

FIGURE 6-28 : COLLAPSE MECHANISMS

then the ductility required at the first hinges to form may need to be larger.

The chance of yield occurring simultaneously at all plastic hinge sections is exceedingly remote, for a variety of reasons. Members are not generally designed to resist their own specific load but are often designed in groups up the height of the structure, wherein several floors are designed to the same loads. Architectural considerations may mean that all beams and columns have constant dimensions up the height of the structure and minimum steel requirements could result in overstrength members in the upper floors. The distribution of the equivalent lateral design load is based on the assumption that the structure will respond in its fundamental mode but this may not always be the case, especially for tall slender structures whose response is often dominated by the higher modes of vibration. Finally, design is only an approximate procedure and the assumed distribution of moments may differ somewhat from that occurring in the completed structure.

First yield will generally occur at the first or second floor beams or at the base of the columns. As the lateral load increases, moment redistribution will take place and yielding will move progressively up the structure, being generally confined to the beams and the base of the ground floor columns however. Close examination of this moment redistribution reveals that the point of contraflexure is dropping in all of the columns and that the moments at the ends of the beams and at the tops of the columns are increasing. Depending on the relative strengths of the columns and the beams either a beam sidesway mechanism or a column sidesway mechanism could form, but under existing design procedures it will almost always be the column sidesway mechanism which forms. This column sidesway mechanism is not generally confined to only one floor but may be spread over several floors as shown in figure 6-28(d), in which case it may be more correctly described as a composite beam column sidesway mechanism.

Proof that the points of contraflexure will drop in the columns can be obtained from consideration of the ground floor column shown in figure 6-29. Assume that yield has occurred at the end of the first floor beam and at the base of the ground floor column. If the total lateral load increases, then the shear V required to be carried by the column will also increase. But ...

$$M_{cl} + M_{uc} = VL \qquad (6\text{-}48)$$

and since $M_{uc}$ cannot increase then $M_{c1}$ must increase, thus lowering the point of contraflexure in the ground floor column. However ...

$$M_{c1} + M_{c2} = M_{ub} \tag{6-49}$$

and since $M_{ub}$ cannot increase, then if $M_{c1}$ increases $M_{c2}$ must decrease, thus lowering the point of contraflexure in the first floor column. This process will tend to repeat itself up the height of the structure. Expressed algebraically ...

$$M_{c2} = M_{ub} + M_{uc} - VL \tag{6-50}$$

The implication of this drop in the points of contraflexure are apparent upon consideration of a typical middle storey floor joint, say floor three, shown in figure 6-30. As the lateral load increases, the drop in the points of contraflexure will cause an increase in $M_{c3}$ and a decrease in $M_{c4}$. In the limit, the point of contraflexure in the fourth floor column may drop to the beam level and thus $M_{c4} = 0$. The column moment $M_{c3}$ will then be equal to the beam moment $M_b$ and it is apparent that the condition to be met so that yield does not occur in the column is ...

$$M_{uc} > M_{ub} \tag{6-51}$$

This is much more severe on the columns than the accepted condition of ...

$$2M_{uc} > M_{ub} \tag{6-52}$$

For an interior joint the condition to ensure a column sidesway collapse mechanism does not form would be ...

$$M_{uc} > 2M_{ub} \tag{6-53}$$

The preceding discussion applies to a structure subjected to an equivalent static loading; if the loading is dynamic then the moment distribution may vary as the response of the structure is affected by the higher modes of vibration. The drop of the point of contraflexure has been confirmed by Kelly [44] who found that the disproportionate moment distribution between two column members framing into a joint increased as the height of the structure increased. During the dynamic analysis of a twelve storey two bay frame Kelly found that the point of contraflexure in some columns dropped so far that the columns were actually in single curvature and the maximum column moment at a joint

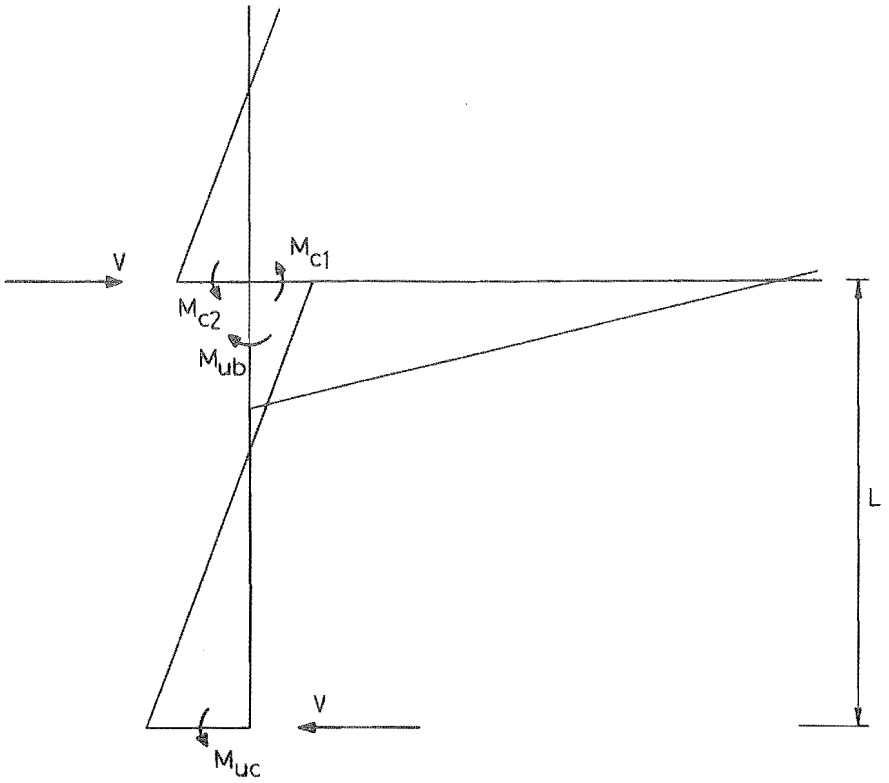


FIGURE 6-29 : MOMENTS INDUCED IN GROUND FLOOR COLUMN BY LATERAL LOADING

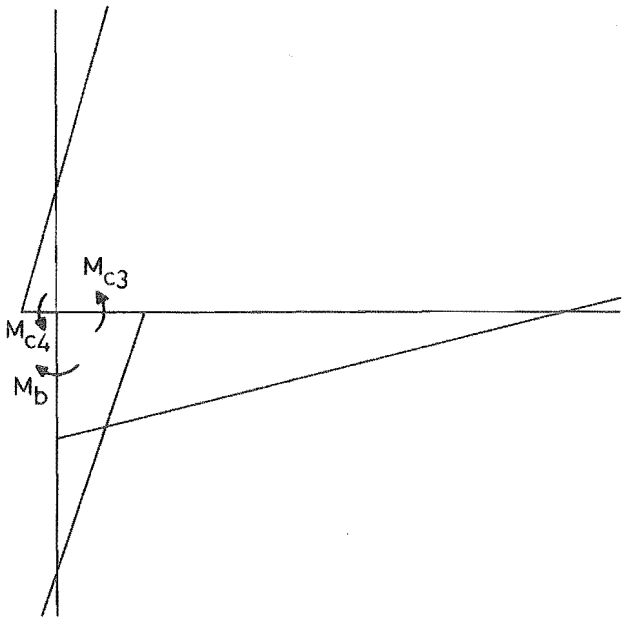


FIGURE 6-30 : MOMENTS IN MEMBERS FRAMING INTO A TYPICAL EXTERIOR JOINT (THIRD FLOOR) DUE TO LATERAL LOADING

was equal to 134% of the total beam moments.

This effect of the points of contraflexure dropping in the columns was observed during the testing of Model 1, where the structure was more severely damaged near the tops of the columns than at the bottoms, the ground floor excepted of course. The theoretical collapse mechanism is shown in figure 6-28(d) and is of the composite beam column sidesway type, since being spread over three storeys it is dependent on hinges forming in the lower two beams as well. The actual collapse mechanism was the ground floor column sidesway mechanism and is shown in figure 6-28(e). Even though the theoretical analysis predicted a composite beam column sidesway mechanism, the moments at the tops of the ground floor columns were very large and were not much below yield. The theoretical analysis assumed constant member properties up the height of the structure, whereas the decreased stiffness of the lower floors meant that they attracted larger moments than expected.

It is concluded that present design procedures will not ensure the formation of a beam sidesway collapse mechanism and in view of this, these design procedures should be re-examined with a view to increasing the flexural strengths of the columns with respect to the flexural strengths of the beams. This point is discussed further in Chapter Eight.

# CHAPTER SEVEN

# TESTING OF MODEL TWO

## 7.1 INTRODUCTION

The response of structures to seismic excitations has long been approximated by their behaviour under equivalent static lateral loads. The static tests impose a deflection upon the structure similar to that which might be expected if the building was vibrated at its fundamental frequency. However, although the first mode dominates the response of a structure to a typical seismic excitation, the higher modes may also play a prominent part, especially in tall slender structures. With the advent of sophisticated closed loop electrohydraulic testing systems the problem of accurately simulating random vibrations over a wide range of frequencies and displacements appears to have been overcome.

The primary objective of the dynamic tests was to check the accuracy with which inelastic frame analysis computer programs predict the displacement response of the structure to a typical severe earthquake. The introduction of large digital computers and rapid advances in numerical analysis techniques have resulted in widespread usage of dynamic frame analysis programs, the results of which are accepted unquestioned, even though the accuracy and applicability of these programs has never been satisfactorily established.

The response of any structure to a seismic excitation is largely dependent on the values for the damping ratio and the fundamental frequency which are assumed or calculated for the structure. The energy input to the structure is determined by the proximity of the fundamental frequency to the earthquake response spectra and so accurate estimation of the stiffness of the structure is essential. In a reinforced concrete structure this stiffness is dependent on such factors as cracking of the concrete, inelastic strains, anchorage slip of the beam reinforcing steel, and the influence of steel couples across large cracks. It was hoped to obtain an estimate of the magnitude of these effects. The damping ratio is a measure of the ability of the structure to absorb energy and it has a large influence on the displacement of the structure. Typical damping ratios have generally been determined from small amplitude free vibration tests and may differ from values obtained from large amplitude forced vibration tests.

It was hoped to establish some typical load-deflection curves since these provide an insight into understanding the dynamic response of the structure.

The primary concern of any designer is whether his building will survive severe earthquake shaking without collapse and, if so, what sort of damage it will suffer. It was hoped to assist in answering those questions since the model structure represents a typical building which has been designed and detailed in accordance with current building code requirements and design philosophies.

## 7.2 EARTHQUAKE RECORDS

### 7.2.1 Selection of the earthquake

Ideally the dynamic testing of a structure should involve the use of as many earthquake records as possible since each recorded earthquake signal is a unique phenomenon strongly influenced by local geological conditions. However, if the structure yields whilst responding to the first earthquake, then it is apparent that the properties of the structure will be altered for the application of the second and all subsequent earthquakes. In the circumstances, meaningful information can only be obtained from the use of one particular earthquake record, which may then be increased in magnitude for subsequent test runs if necessary.

Unfortunately the number of strong motion earthquake records available is very limited. As a result, artificial earthquake records were introduced by Jennings et al [45] in an attempt to fill the gaps in the existing collection of recordings of strong motion earthquakes. Jennings generated four types of earthquake records, of which type B most closely models the maximum shaking a structure is likely to receive. Type B earthquakes model the shaking in the epicentral areas of earthquakes of magnitude 7 on the Richter Scale and are of comparable magnitude to recorded earthquakes such as El Centro 1940 and Taft 1952.

However it must be emphasised that these artificial earthquakes were intended only to supplement actual existing records. Considerable discussion has taken place as to the merits of their use. For this project it was considered that if only one earthquake is to be selected in the testing of the model structure then it may as well be an actual recorded earthquake rather than an artificial earthquake. The North-South component of El Centro, May 18, 1940 is the earthquake which has been most often used by researchers over the years and so this earthquake

was the one used for the dynamic testing of Model 2.

### 7.2.2 The laws of similarity relating the earthquake to the model structure

The laws of similarity indicate the following relationships between model parameters and prototype parameters:

(i) acceleration $a_p = a_m$

(ii) displacement $L_p = LL_m$

(iii) time $t_p = L^{\frac{1}{2}} t_m$

(iv) velocity $v_p = L^{\frac{1}{2}} v_m$

where L = ratio of prototype to model length scale (> 1) and all the symbols used above are defined in Section 3.2.

These relationships indicate that the earthquake record should be speeded up by a factor of $L^{\frac{1}{2}}$ when used in conjunction with the model building. This means that the frequency components of the earthquakes are increased by $L^{\frac{1}{2}}$ which for L = 5 as in this series of tests is 2.24. The fundamental frequency of a perfect model would be increased by $L^{\frac{1}{2}}$ also but since the structure is not a perfect model, the actual increase will be less than that. Thus the fundamental frequency of the structure has reduced in relation to the frequency components of the earthquake.

The response of the MTS 903.79 testing system is limited by certain constraints which are listed below:

(i) acceleration - 3.5 g approximately

(ii) velocity - 15.7 in/sec (399 mm/sec)

(iii) displacement - 4 in. (102 mm)

For the dynamic tests envisaged, the acceleration restraint will not prove critical and therefore the base motion is limited by a maximum displacement of 4 in. and a maximum velocity of 15.7 in/sec. The maximum velocity and displacement of the El Centro earthquake record lies within these values when the earthquake record is speeded up by a factor of $L^{\frac{1}{2}}$ as mentioned above. This speeded up version of the El Centro record became the standard earthquake for these tests and any further variations in speed or magnitude introduced are referenced to this waveform.

No suitable index exists for measuring the damaging potential of earthquakes: the comparison of maximum accelerations is not a good index since no account is taken of the duration of the acceleration. Spectrum intensities based on the area under a velocity response spectrum curve

between certain periods are often used but these give a general indication only and are not directly related to the characteristics of the structure.

It will be generally agreed however that increasing the accelerations will increase the damage potential of the earthquake. This may be achieved by either increasing the displacements or, up to a certain point, by speeding up the earthquake record.

### 7.2.3 Form of the earthquake record

The MTS 903.79 testing system has the capability to accurately follow random wave functions and provision was made for these to be input to the system from the CEC Datatape VR-3300. The command function can be in the form of either displacement, velocity or acceleration, since integration circuits in the MTS model 428.02 command mode selector derive an equivalent displacement waveform which becomes the dynamic command for the system.

The earthquake records were supplied on cards by Berg and Housner [46] in the form of time and acceleration. This record was transferred to paper tape and then fed into a Hybrid Computer belonging to the Electrical Engineering Department. This was comprised of an EAI 580 Analog/Hybrid Computing System and an EAI 640 Digital Computing System. This produced an analog signal representing the acceleration waveform onto the Datatape whilst an EAI 1130 Variplotter simultaneously monitored the signal.

Comparison of the equivalent displacement waveform derived from this acceleration record with that reproduced in many texts indicated that the two were completely dissimilar. A digital integration of the original time, acceleration cards was carried out on the Burroughs B6718 computer and this resulted in a waveform which was different again to the two previous waveforms.

The reason for the discrepancy between the displacement waveform obtained by direct digital integration and that reproduced in texts was that certain correction techniques that minimise instrumental errors had been applied to the latter but not to the former. A discussion of these techniques is given by Brady [47]. The correction techniques represent an attempt to correlate the actual ground displacement with that determined after double integration of the measured acceleration waveform and also to reduce errors in the digitization of the original accelerogram and in the location of the true base line of zero acceleration. The correction is applied to the acceleration waveform in the form of a quadratic equation and thus the correction applied to the displacement waveform is

a quartic equation. The correction makes little difference to the acceleration values and would have a negligible effect on the behaviour of the structure.

The equivalent displacement waveform was dissimilar because the integration circuits of the command mode selector contained an amplifier frequency cut-off which prevented the integration of any components with a frequency less than 3 c.p.s. The cut-off was installed to prevent low frequency components, or d-c drift, or offset in the acceleration record, from attempting to drive the ram into its end-stops. An input coupling switch installed for the purpose of disconnecting the amplifier frequency cut-off had little effect. Hence it appeared that the command signal would have to be in the form of displacement.

Initially it was attempted to doubly integrate the acceleration waveform on the EAI 580 Analog/Hybrid Computing System but d-c offsets below the maximum resolution of the system caused unacceptably large drifts in the resultant displacement waveform. Consequently the double integration was carried out on the Burroughs B6718 digital computer and the resultant digital displacement record was converted to an analog displacement record by the Hybrid Computer. The correction techniques described by Brady [47] were not applied to this waveform.

### 7.2.4 Conversion techniques

A major obstacle in the production of the earthquake analog records was the transfer of the digital record from cards to paper tape. Initially there were no facilities available either commercially or at the University Computer Centre which could be used and so the earthquake acceleration record was punched onto paper tape by hand.

By the time it was subsequently decided to use the earthquake displacement record rather than the acceleration record as input to the Hybrid Computer, some conversion facilities had been established at the University Computer Centre. The displacement output from the digital integration program was automatically punched onto cards at 0.01 second intervals. No direct correlation between the paper tape language ASCII, where the characters were written in 8-bit octal, and the card language FORTRAN, where the characters had a hexadecimal bit representation, was available and so the program EQPTC was written for this purpose.

EQPTC read the hexadecimal displacements from the cards, converted the characters to octal and punched them onto paper tape with a comma

after every number and a carriage return line feed after every eighth number to facilitate editing. A listing of EQPTC is reproduced in Appendix C and an octal-hexadecimal conversion chart is given in table 7-1.

The earthquake displacements were recorded on the Datatape numerous times and the time scale was varied for each recording. When Model 2 was being tested, a whole range of speeds was then available at which the earthquake could be run, which meant that a much more flexible testing program could be planned than if only the coarse speed steps corresponding to the Datatape speed controls had been available. A ramp function, shown in figure 7-1, was generated between each earthquake recording in order to provide a smooth transition from one recording to the next.

### 7.2.5 The earthquakes

Details of the earthquake waveforms which were used to test Model 2 are given in table 7-2. All are based on El Centro, May 18, 1940 (North-South component). The magnitude of the earthquake was increased initially by increasing the displacements, and, when that was no longer possible, by speeding up the earthquake record.

Run 2 was identical with run 3 and so is not listed; similarly run 5 was a repeat of run 1. Further test runs were attempted after run 8 but the displacements had been reduced and the earthquake record speeded up to such an extent that they had practically no effect on the structure and so will not be given any further consideration.

The earthquake waveforms were recorded on the Datatape at as great an amplitude as possible and were attenuated to the desired amplitude in the MTS model 428.02 command mode selector by adjusting a potentiometer, designated span. This span control effectively controls the magnitude of the earthquake, although it does not have any engineering meaning by itself, and does not work as a reference if the input earthquake signal is changed.

Otani and Sozen [16] found that the maximum accelerations increased with span settings, but they were not linearly proportional to the span settings and suggested that it may be because the base acceleration contains high frequency components and the maximum value is very sensitive to the existence of high frequency noise. However, they found that the spectrum intensities of base acceleration signals measured on their earthquake simulator platform were linearly proportional to the span setting and so concluded that the span setting was a good index of the intensity of the base motion.

TABLE 7-1 : OCTAL-HEXADECIMAL CONVERSION

| ASCII character | Octal | Binary representation | Hexadecimal | FORTRAN character |
|---|---|---|---|---|
| 0 | 260 | 1 0 1 1 0 0 0 0 | B0 | 0 |
| 1 | 261 | 1 0 1 1 0 0 0 1 | B1 | 1 |
| 2 | 262 | 1 0 1 1 0 0 1 0 | B2 | 2 |
| 3 | 263 | 1 0 1 1 0 0 1 1 | B3 | 3 |
| 4 | 264 | 1 0 1 1 0 1 0 0 | B4 | 4 |
| 5 | 265 | 1 0 1 1 0 1 0 1 | B5 | 5 |
| 6 | 266 | 1 0 1 1 0 1 1 0 | B6 | 6 |
| 7 | 267 | 1 0 1 1 0 1 1 1 | B7 | 7 |
| 8 | 270 | 1 0 1 1 1 0 0 0 | B8 | 8 |
| 9 | 271 | 1 0 1 1 1 0 0 1 | B9 | 9 |
| minus | 255 | 1 0 1 0 1 1 0 1 | AD | minus |
| space | 240 | 1 0 1 0 0 0 0 0 | A0 | space |
| decimal point | 256 | 1 0 1 0 1 1 1 0 | AE | decimal point |
| comma | 254 | 1 0 1 0 1 1 0 0 | AC | comma |
| carriage return | 215 | 1 0 0 0 1 1 0 1 | 8D | |
| line feed | 212 | 1 0 0 0 1 0 1 0 | 8A | |

TABLE 7-2 : SIMULATED EARTHQUAKE TEST RUNS FOR MODEL 2

| Earthquake test run no. | Maximum displacement in. (mm) | Length of earthquake seconds | Percentage increase in earthquake accelerations over standard El Centro |
|---|---|---|---|
| 1 | 2.48 (63.0) | 13.16 | 0 |
| 3 | 3.23 (81.9) | 13.16 | 30 |
| 4 | 3.97 (100.8) | 13.16 | 60 |
| 6 | 2.48 (63.0) | 9.34 | 100 |
| 7 | 2.48 (63.0) | 7.63 | 200 |
| 8 | 2.48 (63.0) | 6.58 | 300 |

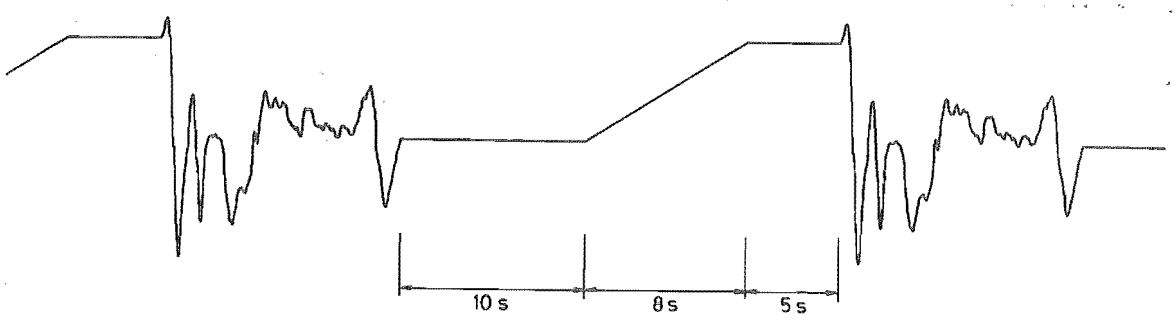


FIGURE 7-1 : RAMP FUNCTION CONNECTING SUBSEQUENT EARTHQUAKE RECORDINGS

## 7.3 DESCRIPTION OF THE TESTS

These tests are generally mentioned in the chronological order in which they were conducted and it is important that this is borne in mind since the properties of the structure changed considerably in the course of the tests. The order of testing was as follows:

(i) The test program commenced with a free vibration test of the untested structure. These free vibration tests were conducted regularly after all of the earthquake test runs and other severe excitations. The displacements at all floors were measured by Hewlett Packard Model 24DCDT-3000 LVDTs and recorded by a Rapet RMS-11CPT chart recorder in order to establish the mode shape. In addition, the displacement at the top floor was recorded on the Hewlett Packard Model 7402A chart recorder so that the natural frequency and damping ratio could be accurately determined.

(ii) Next a series of sinusoidal forced vibration tests were undertaken to establish the displacement response curve of the structure in the elastic range. The amplitude of base motion was kept small to ensure that the maximum deflection of the structure never exceeded 0.4 in. (10.2 mm), which was well within the elastic range. A series of differential amplifiers were used to subtract the measured base displacement from the displacements measured at each floor level and thus each floor displacement was recorded relative to the base. The displacements of all floors were recorded on a Rapet RMS-11CPT chart recorder, after first being attenuated by 10K pots. In addition, the displacements of the base and floor 6 were recorded on the Brush Mark 280 chart recorder and the displacements of floors 2 and 4 were recorded on the Hewlett Packard Model 7402A chart recorder.

(iii) Then several load-deflection tests were conducted by subjecting the base of the structure to a sinusoidal excitation. The displacement and acceleration at the top floor were recorded on the Brush Mark 280 chart recorder. The acceleration was measured by the Kistler Model 305A servo accelerometer.

(iv) Next the structure was subjected to simulated earthquake shaking. During this part of the testing a 8 mm and a 16 mm movie camera filmed the response of the structure. Again the displacements at all floors were recorded on a Rapet RMS-11CPT chart recorder, after first being attenuated by 10K pots. The second Rapet chart recorder monitored the displacements at floors 1 and 3 and also the accelerations at floors 1 and 3 as measured by Kyowa AS-10B accelerometers. The acceleration

(measured by a Kyowa AS-10B accelerometer) and the displacement at floor 6 were recorded on the Hewlett Packard chart recorder whilst the Brush chart recorder monitored the base displacement as measured by the LVDT mounted inside the actuator and the base acceleration as measured by the Kistler accelerometer. The Datatape was used to supply the command displacement waveform.

(v) Finally the earthquake test runs were followed by a series of sinusoidal shaking tests in which information was obtained on damping, mode shapes, natural frequencies and load-deflection hysteresis curves. These ultimately led to attempts to collapse the structure by sinusoidal excitation at its resonant frequencies.

## 7.4 VARIATION IN DAMPING AND NATURAL FREQUENCIES

Both the fundamental frequency and damping of the structure, as measured by free vibration tests, underwent considerable variation as the structure was progressively damaged. Since both the damping and the natural frequency are dependent on the amplitude of the displacement, the structure was given an impulse with an initial displacement of about 0.5 in. (12.7 mm) for all free vibration tests and the values measured from the first cycle were used for comparison.

It was found that the fundamental resonant frequency decreased drastically as the tests proceeded, ultimately reducing to 23% of the original (before test) resonant frequency. This represents a decrease in stiffness to 5.3% of the original (before test) stiffness - the term "before test" is used in preference to the term "uncracked" since the presence of minute shrinkage cracks meant that at no stage was the structure uncracked. The original before test resonant frequency was 2.64 c.p.s., a value which is in good agreement with the 2.67 c.p.s. obtained for Model 1.

The effect of the stiffness degradation is shown in figure 7-2 which indicates the increase in the percentage of critical damping when plotted against the fundamental resonant frequency at various stages during the testing. The damping of the structure before testing was just under 2% of critical damping, increasing to almost 19% of critical damping as the structure was progressively damaged. The curve of the graph seems to indicate that the damping of the structure would never increase beyond about 20% of critical damping and it was attempted to obtain several more points in order to establish this fact by decreasing the natural frequency of the structure to between 10% and 20% of the original

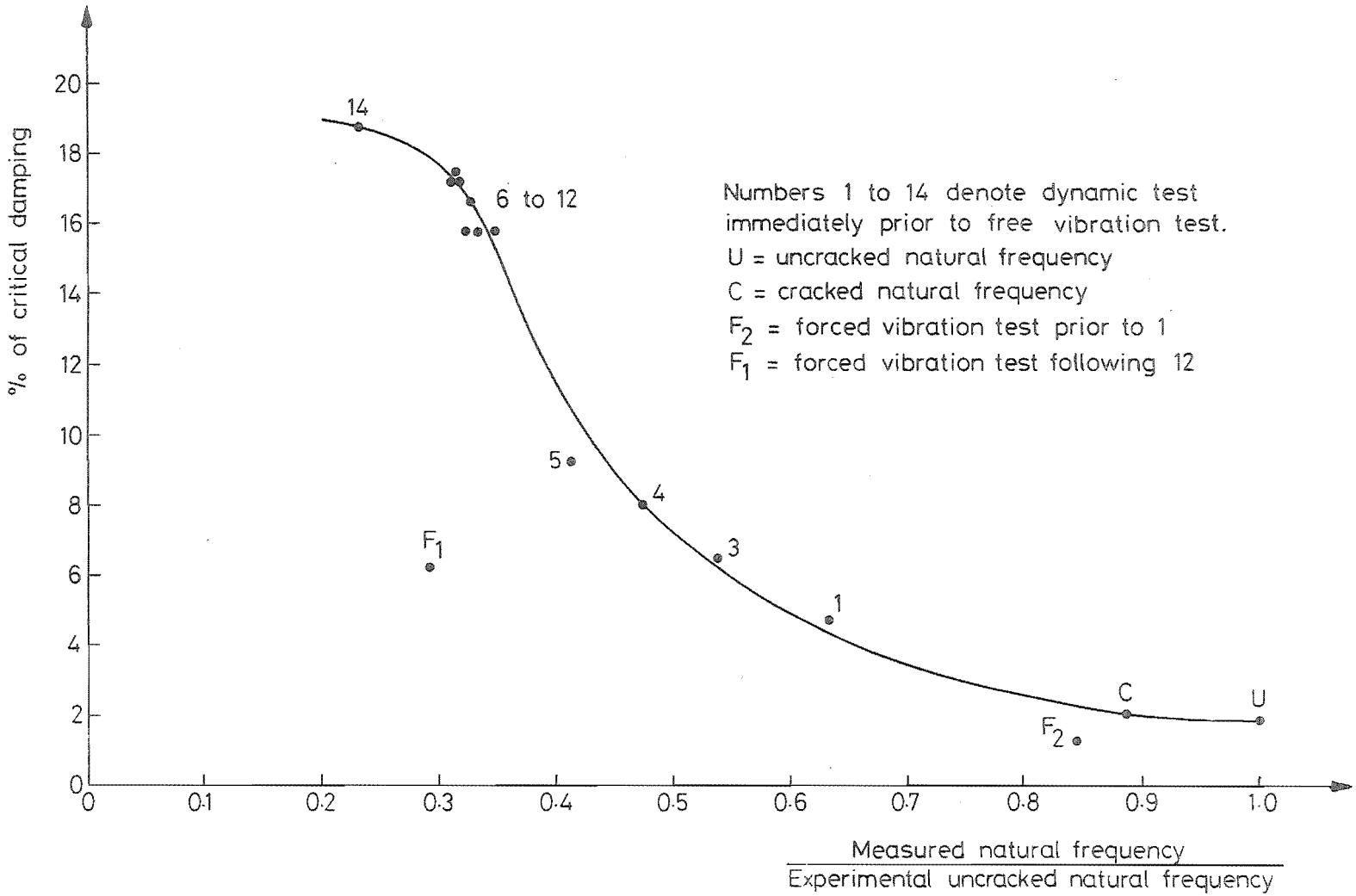


FIGURE 7-2 : VARIATION OF DAMPING WITH NATURAL FREQUENCY AS DETERMINED FROM FREE VIBRATION TESTS OF MODEL 2

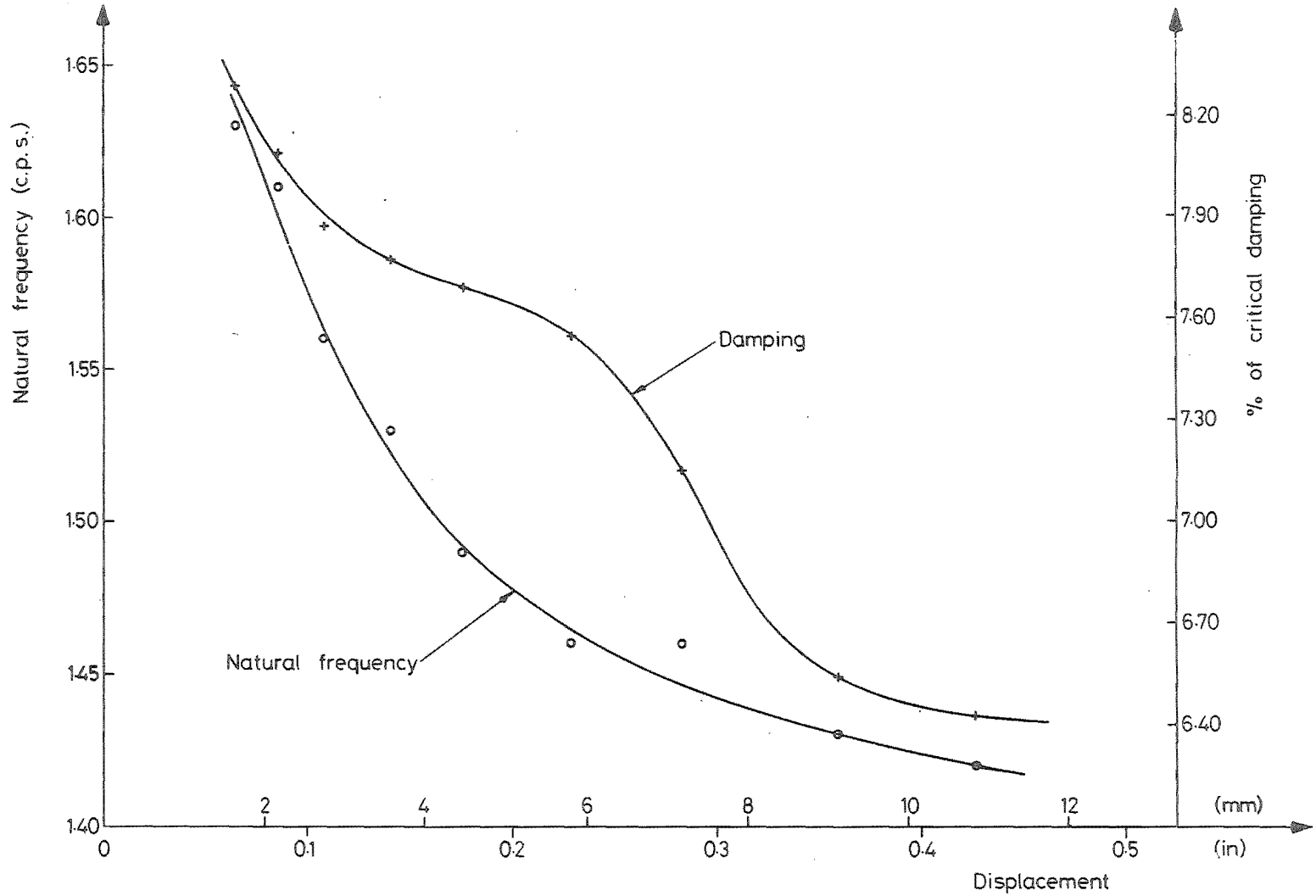


FIGURE 7-3 : VARIATION OF 1st MODE DAMPING AND NATURAL FREQUENCY WITH DISPLACEMENT AS DETERMINED FROM A FREE VIBRATION TEST OF MODEL 2 FOLLOWING RUN 3

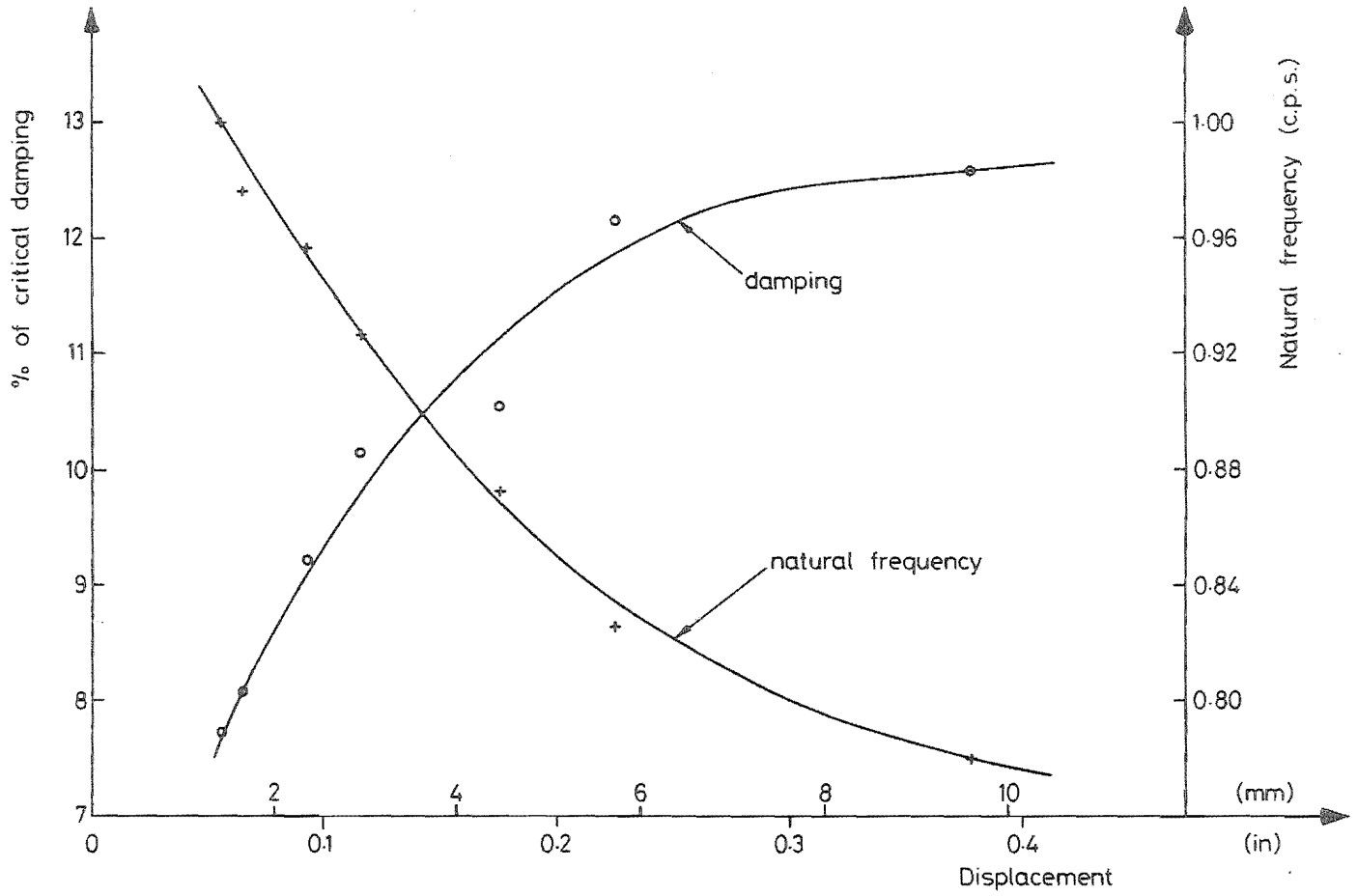


FIGURE 7-4 : VARIATION OF 1st MODE DAMPING AND NATURAL FREQUENCY WITH DISPLACEMENT AS DETERMINED FROM A FREE VIBRATION TEST OF MODEL 2 AFTER THE COMPLETION OF ALL OTHER TESTS

experimental untested natural frequency. The structure was then badly damaged by severe sinusoidal excitation at its resonant frequencies and further free vibration tests were carried out to measure its damping and fundamental resonant frequency. However, it was found that not only did the damping of the structure actually decrease, but that the fundamental resonant frequency increased. Tentatively, it appears that the damping of this structure will not increase beyond about 20% of critical damping and that the line drawn connecting the experimental points in figure 7-2 represents a bound below which all other combinations of fundamental resonant frequency and damping for this structure will lie.

Both the fundamental natural frequency and the damping of the structure varied according to the deflection, apart from the stage when the structure was only very slightly cracked. Up to the stage when the structure was moderately damaged, both the fundamental natural frequency and the damping increased with decreasing displacement as shown by figure 7-3, which is based on the results of a free vibration test conducted after run 3. As the structure was further damaged, the fundamental natural frequency continued to increase with decreasing deflection but the damping went through a transition. As the first cycle damping began to stabilize about a maximum value of between 16% and 19% of critical damping, the damping tended to remain constant with decreasing deflection and after the structure was further damaged the damping actually appeared to decrease with decreasing displacement, as shown in figure 7-4 which is based on the results of a free vibration test conducted after the completion of all the forced vibration tests.

The damping ratios obtained from the free vibration tests appear to considerably overestimate the damping ratios determined from forced vibration tests. Figure 7-2 shows two damping ratios determined from forced vibration tests which lie well within the curve connecting the free vibration damping values. One point was obtained immediately prior to the earthquake test runs and the other point immediately following them.

## 7.5 DISPLACEMENT RESPONSE CURVES

An observer watching a structure undergoing forced sinusoidal excitation will often notice that one or more of the floors of the structure appear to be motionless - however this is not a node point and neither is the structure vibrating in a resonant frequency, since although the floor is motionless with respect to the observer it is moving with respect to

the base of the structure. It was found that none of the floors were motionless at the resonant frequencies determined and that the resonant frequencies cannot be identified by observation of the motion of the structure, except in a general sense.

The displacement response ratio is the ratio of the displacement of the structure measured relative to the base to the displacement of the base. The displacement response ratio varies according to the forcing frequency, reaching a maximum whenever the forcing frequency coincides with one of the resonant frequencies. This maximum displacement response ratio ($B_d$ max.) is a measure of the amount of damping present in the structure since ...

$$B_d \text{ max.} = \frac{1}{2\lambda}$$

where $\lambda$ = percentage of critical damping.

This relationship holds even in a multidegree of freedom system since the structure is linear and orthogonality of the modes is preserved.

The displacements were measured at floors 2, 4 and 6 and a cracked elastic displacement response curve for the structure was established, shown here in figure 7-5. The peaks corresponding to the lowest three resonant frequencies are clearly defined. These peaks have a smaller magnitude at higher modes because the required energy input is greater at higher modes. Only the three lowest resonant frequencies could be established in this manner for fear that the severe shaking required to satisfactorily obtain the higher modes would have badly damaged the structure.

Practical difficulties in measuring the displacements and limitations on the available recorder meant that only the displacement ratios for floors 2, 4 and 6 could be determined. Obviously floor 6 has the maximum displacement of any floor in mode 1, and it was also established that floor 2 had the maximum displacement of any floor in modes 2 and 3. If however, any part of the structure did have a displacement greater than those measured (this would be a portion of one of the columns), then the displacement response ratio measured underestimates the actual displacement response. Also, if the frequency of excitation does not exactly coincide with the resonant frequency then the maximum displacement response ratio measured underestimates the actual displacement response. Since a lesser displacement response ratio indicates a greater damping ratio, the damping ratios determined from displacement response tests represent an upper bound to the actual damping ratios.

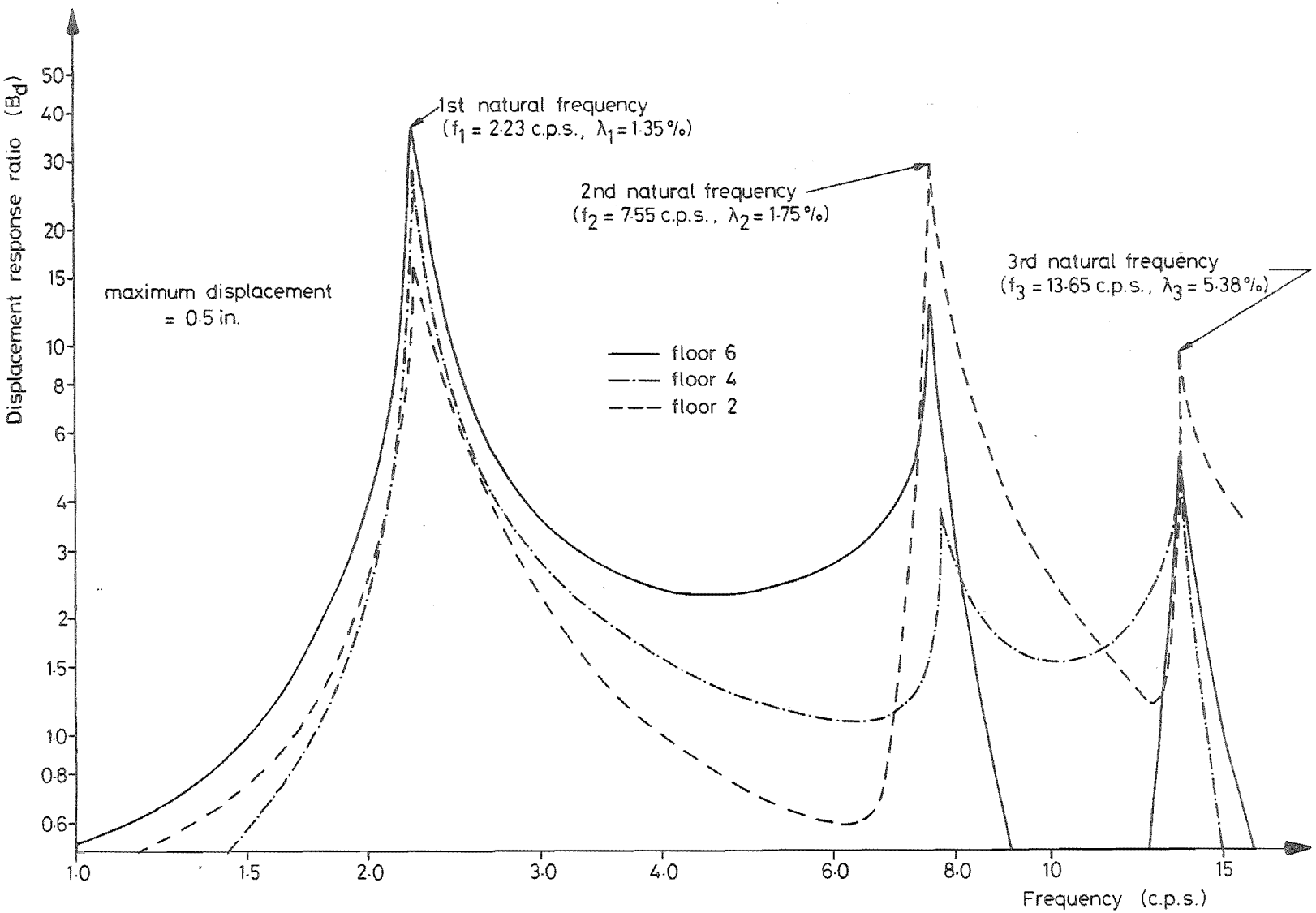


FIGURE 7-5 : CRACKED ELASTIC DISPLACEMENT RESPONSE CURVES FOR MODEL 2

TABLE 7-3 : DAMPING DETERMINED FROM DISPLACEMENT RESPONSE TESTS BEFORE SIMULATED EARTHQUAKE TESTS

| Mode | 1 | 2 | 3 |
|---|---|---|---|
| $B_d$ max. measured at floor | 6 | 2 | 2 |
| Percentage of critical damping | 1.35 | 1.75 | 5.4 |

TABLE 7-4 : DAMPING DETERMINED FROM DISPLACEMENT RESPONSE TESTS AFTER SIMULATED EARTHQUAKE TESTS

| Mode | 1 | 2 | 3 | 4 |
|---|---|---|---|---|
| $B_d$ max. measured at floor | 6 | 2 | 4 | 3 |
| Percentage of critical damping | 6.2 | 8.8 | 11.8 | 14.3 |

The damping ratios determined from the displacement response tests are indicated in table 7-3. The second mode damping ratio is only slightly greater than the first and it is apparent that the damping ratio increases with higher modes. The first mode damping determined from free vibration tests was 2.1% of critical damping which is over 50% greater than the value obtained from the displacement response tests. The latter value is more relevant to the response of the structure since a seismic excitation is a forced vibration of the structure and thus it is apparent that the damping ratios obtained from free vibration tests overestimate the actual damping ratios of the structure.

When a structure is set into free vibration, all modes of the structure are excited as well as the fundamental mode and the greater decay observed could be partially or wholly due to the rapid decay of the higher modes. After all of the main dynamic earthquake test runs had been completed, a further series of displacement response tests were carried out, the results of which are tabulated in table 7-4. Similar results to those found previously were obtained and in fact the first mode damping ratio determined from the displacement response tests had reduced to only about one third of the value determined from free vibration tests.

An interesting phenomenon was observed when the structure was excited close to or at its resonant frequencies. Even though a steady state condition had been achieved, the displacement of the structure would often vary considerably in amplitude over a period of several minutes, although it would ultimately stabilize at a constant value. The reason for this is that the structure is damping controlled in this frequency region and its equilibrium is delicately balanced. Because the damping of the structure varies slightly with varying displacement, the amplitude of vibration of the structure will oscillate for some time before stabilizing and this was typically found to take between 20 and 200 cycles.

## 7.6 LOAD-DEFLECTION CURVES

Steady state dynamic load-deflection curves were obtained by applying a sinusoidal excitation to the base of the structure and simultaneously sampling the acceleration (force) and displacement at a particular location. At any floor, the net force is equal to the algebraic sum of the forces acting on it and the floors above it. However, a lack of suitable data reduction facilities prevented the obtaining of load-deflection curves for any floor other than the top floor.

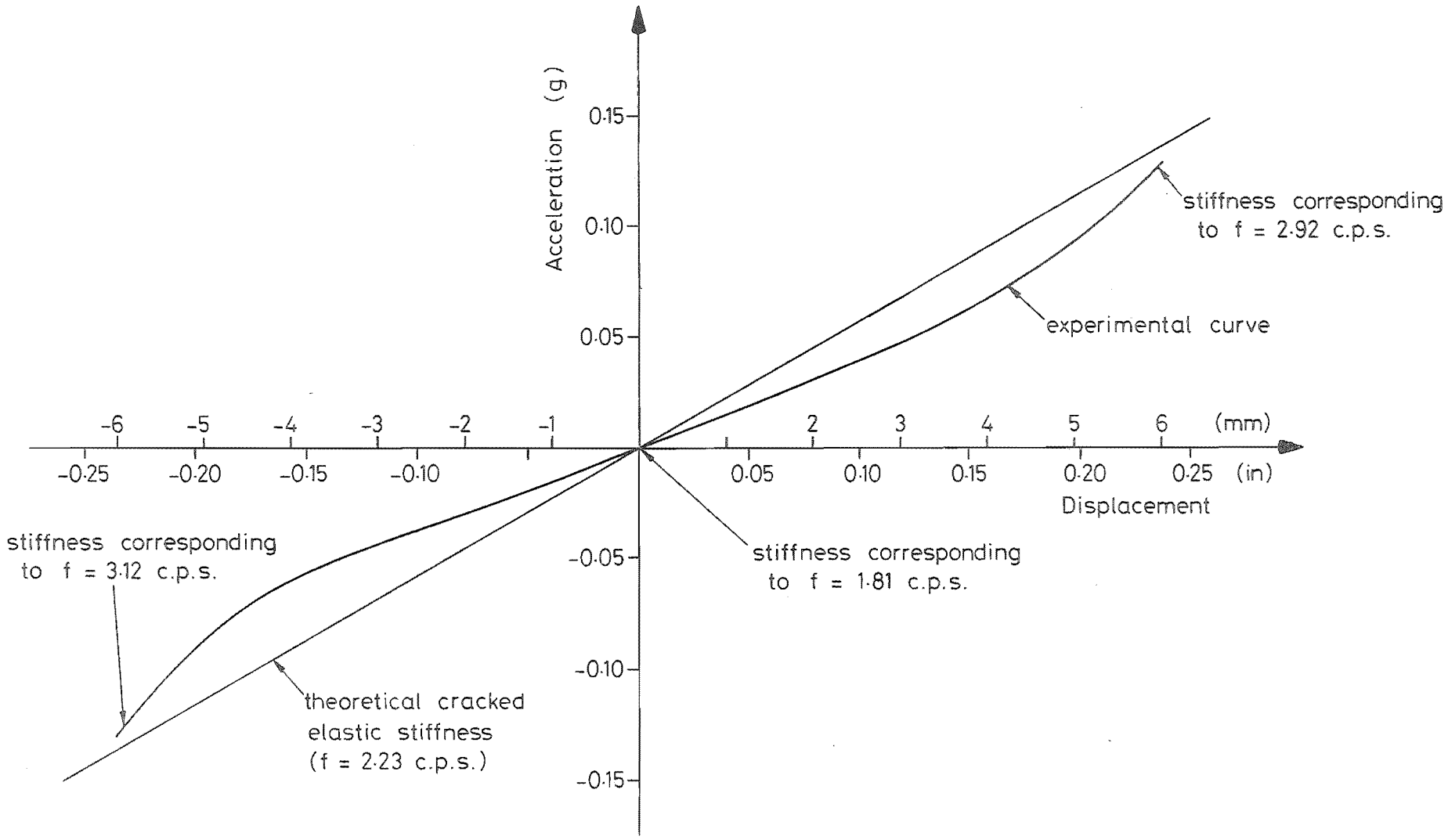


FIGURE 7-6 : CRACKED ELASTIC LOAD-DEFLECTION CURVE FOR FLOOR 6 OF MODEL 2

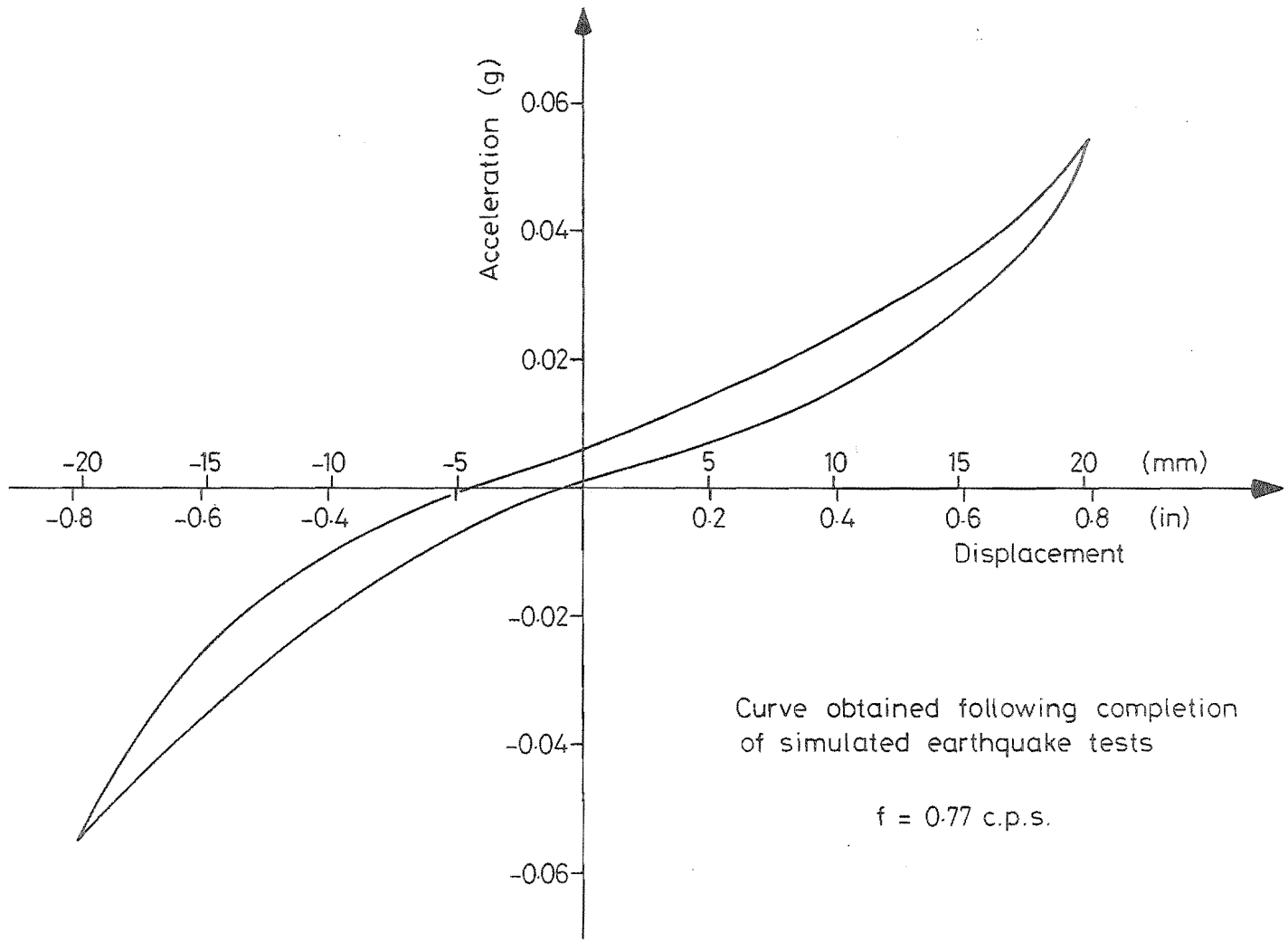


FIGURE 7-7 : LOAD-DEFLECTION CURVE FOR FLOOR 6 OF MODEL 2 DETERMINED AT FIRST NATURAL FREQUENCY

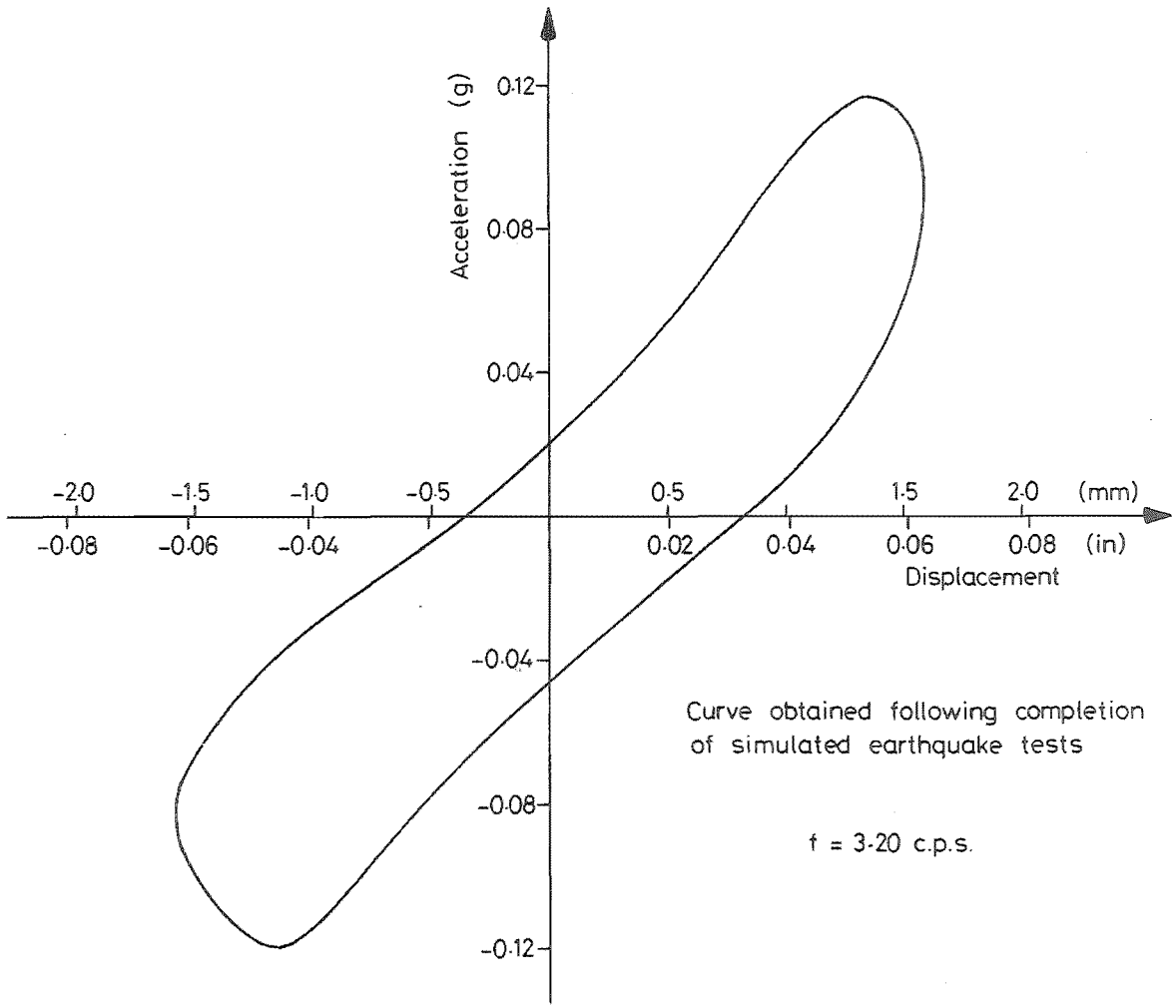


FIGURE 7-8 : LOAD-DEFLECTION CURVE FOR FLOOR 6 OF MODEL 2 DETERMINED AT SECOND NATURAL FREQUENCY

The load-deflection curve obtained for the cracked elastic structure is shown in figure 7-6. The curve is of the spring hardening type and the low degree of damping exhibited by the structure is reflected in the width of the hysteresis loop, which apart from local variations is zero as near as can be determined. An equivalent hysteretic damping value based on the area of the loop would be zero although of course there was some damping present. The stiffness of the structure varies considerably with deflection and at virtually any position on the curve the "instantaneous" natural frequency differs from the average value of 2.23 c.p.s. The maximum natural frequency attained of 3.12 c.p.s. reflects the partial closure of the shrinkage cracks; any increase in the modulus of elasticity of the concrete due to dynamic effects is negligible.

After the completion of all of the earthquake test runs, further load-deflection tests were carried out at both first and second resonant frequencies and these are shown in figures 7-7 and 7-8. The loop determined at the first resonant frequency was of the familiar spring hardening type and by this stage it had a significant width. The loop determined at the second resonant frequency did bear some resemblance to the spring hardening type although it was very much wider, reflecting a very much greater dissipation of energy.

## 7.7 DAMAGE TO THE STRUCTURE

Shrinkage cracks appeared in the structure after casting and the small amplitude forced vibration tests initially conducted had the effect of opening up these shrinkage cracks as well as initiating some fresh cracks in the lower two storeys.

The earthquake test runs up until run 6 resulted in further cracking throughout the structure but the cracking was still slight. No yielding appeared to have occurred, as would have been indicated by permanent cracks opening at the ends of the beams. The effect of test runs 6, 7 and 8 was much more severe however and the appearance of permanent cracks at the ends of the lower three longitudinal floor beams as well as some crushing of the concrete indicated that yielding of reinforcing steel may have occurred. However the permanent cracks were probably due to anchorage slip of the longitudinal beam steel, rather than yielding of the steel. It appeared that the structure was still in the elastic range at this stage, especially since the longitudinal beams were only slightly cracked. Nevertheless, large torsional cracks had appeared in the lateral beams,

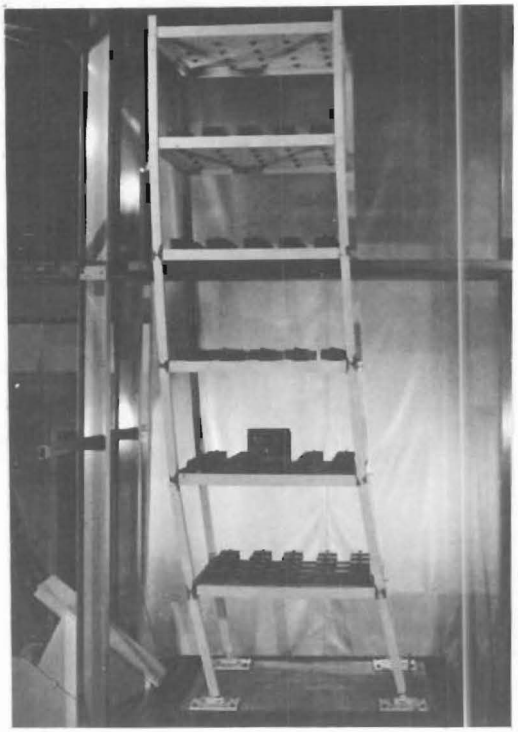

FIGURE 7-9 : MODEL 2

NOTE: All photographs on this page were taken after the completion of all tests of Model 2.

FIGURE 7-10 : NODE 2

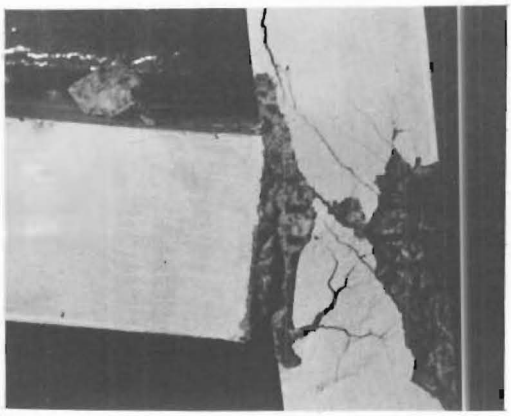

FIGURE 7-11 : LONGITUDINAL VIEW OF NODE 4

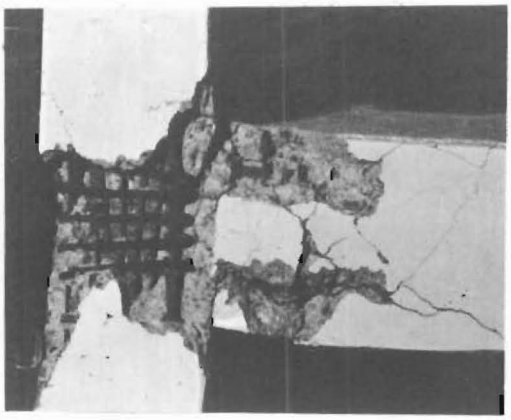

FIGURE 7-12 : LATERAL VIEW OF NODE 4

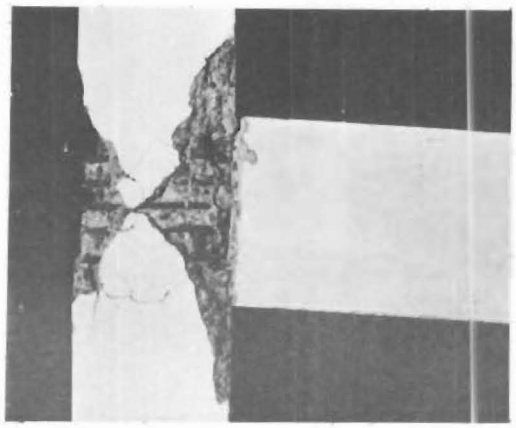

FIGURE 7-13 : LONGITUDINAL VIEW OF NODE 9

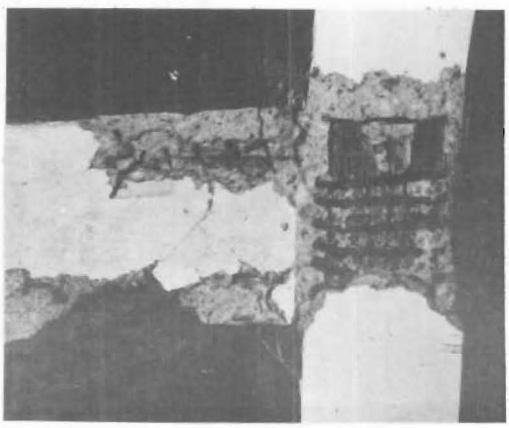

FIGURE 7-14 : LATERAL VIEW OF NODE 9

and the corners of the slabs and the joints were badly cracked, particularly at the second floor. The severest cracking occurred in the columns, and the large cracks which had formed just above the base of each column were beginning to fragment.

The large amplitude sinusoidal forced vibration tests following the earthquake test runs resulted in severe damage to all parts of the structure with the exception of the longitudinal beams which, in comparison with the remainder of the structure, were relatively unscathed. However the lower four longitudinal beams all appeared to yield, in spite of anchorage slip of the reinforcing, and spalling from the joints and from the lateral beams was apparent. The joints appeared to function well and any deterioration appeared to result from the large number of load reversals rather than the severity of loading.

Some torsional vibration of the structure was noted but only when it was excited at its fundamental resonant frequency when close to collapse. Because of its flexibility, it proved to be quite difficult to collapse the structure and it had to be severely shaken at its resonant frequencies for a considerable length of time before collapse was achieved. The collapse mechanism was a column sidesway mechanism due to the large deformations which occurred in the lower three storeys of the structure, particularly the ground floor. Some photographs of the damaged structure after it had collapsed onto several supporting planks are shown in figures 7-9 to 7-14.

## 7.8 CORRELATION OF MEASURED AND PREDICTED EARTHQUAKE DISPLACEMENTS

The accelerations of the structure were measured at the base and at floors 2, 4 and 6, but unfortunately the recorded acceleration waveforms were unsatisfactory, for two reasons:

(i) a high frequency noise was present in the recordings which tended to obliterate the accelerations it was desired to measure. This noise was partly derived from hum on the magnetic tape, partly from the fact that the displacement waveform as it existed on the magnetic tape consisted of a series of steps which only approximated the true waveform, and partly from electrical noise emanating from elsewhere in the testing system. Although this noise had a very high acceleration amplitude, its displacement amplitude was very small and it was considered to have a negligible effect on the structure.

(ii) the response of the pen recorders was insufficiently fast to record the high frequency acceleration signals and although the response of the

Rapet series RMS-11CPT light-beam galvanometer chart recorders was sufficiently fast, the available channel width was inadequate.

In the event, it was not possible to obtain a satisfactory record of the accelerations of the structure but displacement records at the base and at each floor level were obtained and these appeared to be satisfactory. The displacement records were digitised by hand from the chart paper on which they were recorded and this digitised data was then plotted using the Burroughs B6718 computer and the two plots were compared. If any discrepancies occurred between the two waveforms then the digitised data was altered accordingly.

The measured and predicted displacements of the structure are presented for four earthquake test runs; namely, runs 1, 4, 6 and 8, since the inclusion of runs 3 and 7 would be repetitous. Similarly, the displacements are compared only for floors 2, 4 and 6 and these graphs are presented in figures 7-15 to 7-26. The predicted displacements were computed using a two-dimensional dynamic inelastic frame analysis program developed by Sharpe [19], which is discussed in Section 5.4.3.

Generally it was found that the response of the structure could be predicted reasonably accurately provided the actual stiffness and amount of damping of the structure were closely estimated, since these were found to have an immense effect on the predicted response. Initially, the predicted displacements of the structure were obtained assuming that the stiffness of the beams and columns were accurately represented by their cracked stiffnesses and that the damping was about 5% of critical damping. Under these conditions the analyses predicted yielding of the structure at a number of locations but examination of the predicted displacement waveforms revealed that they did not resemble the measured ones at all.

Subsequently the stiffness of the structure was measured from the predominant frequency component of the measured displacement waveforms and a trial and error process was used to determine the corresponding amount of damping. The resulting stiffness values used were very much less than the cracked stiffnesses and the values of damping used were substantially less than those values determined from free vibration tests immediately following each earthquake test run. Table 7-5 gives the damping and stiffness values found to fit each test run the best. These damping and stiffness values are average values only and are dependent on the accuracy with which the stiffness and mass distribution of the structure are modelled. They are also affected by inherent inaccuracies in the dynamic analysis, such as the choice of a suitable piece-wise scheme for the

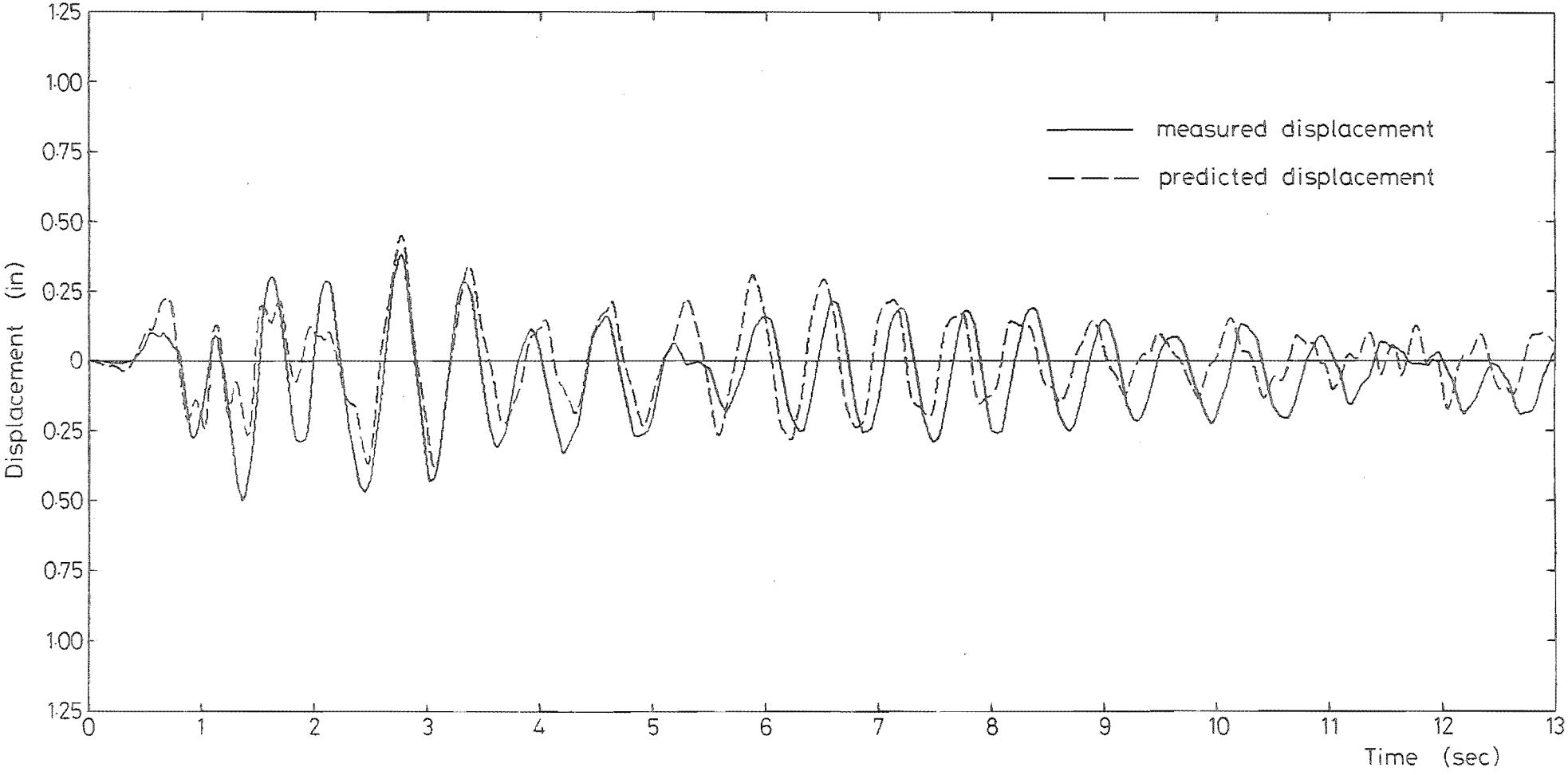


FIGURE 7-15 : MEASURED AND PREDICTED DISPLACEMENTS FOR FLOOR 2 DURING RUN 1

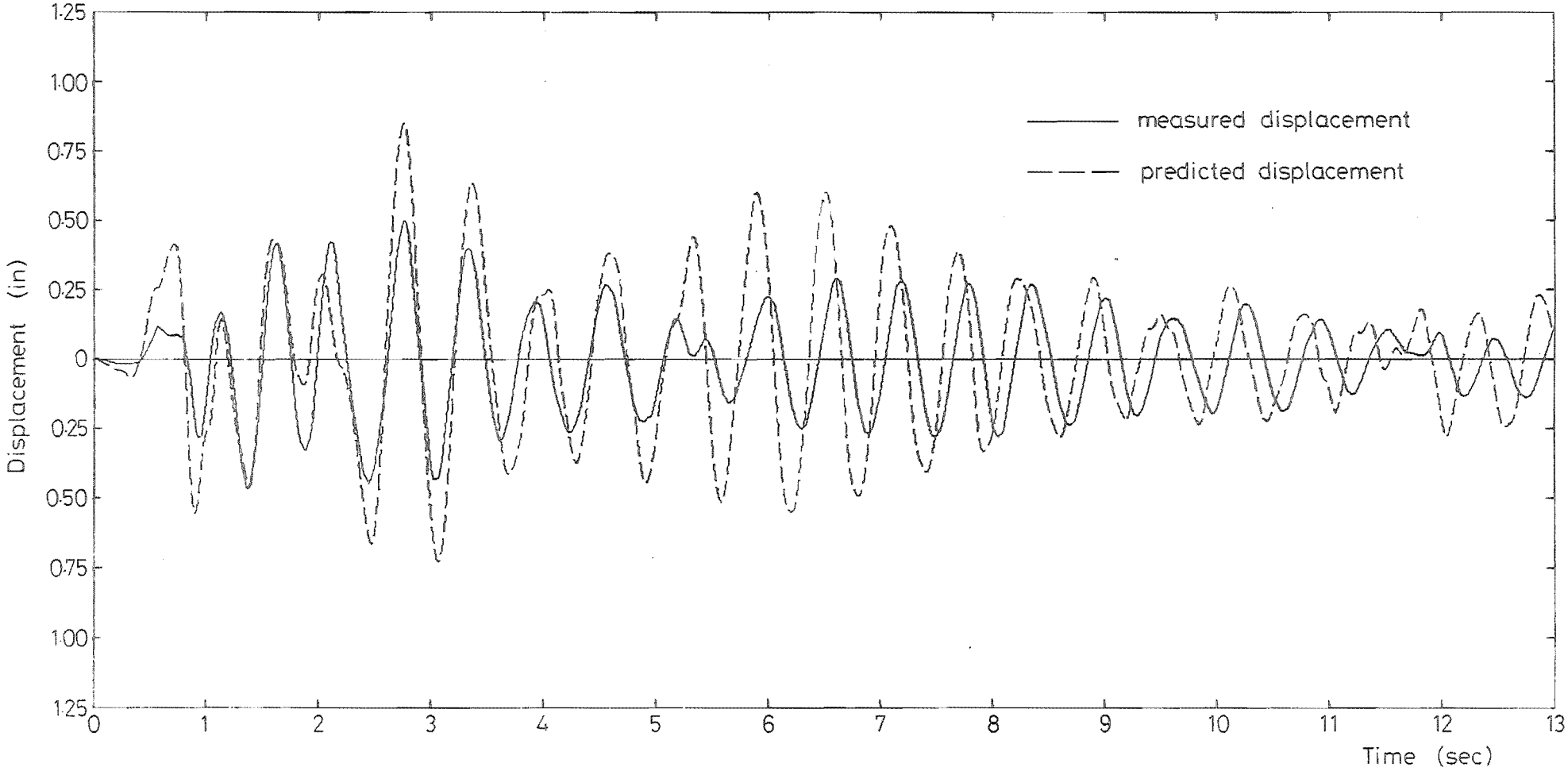


FIGURE 7-16 : MEASURED AND PREDICTED DISPLACEMENTS FOR FLOOR 4 DURING RUN 1

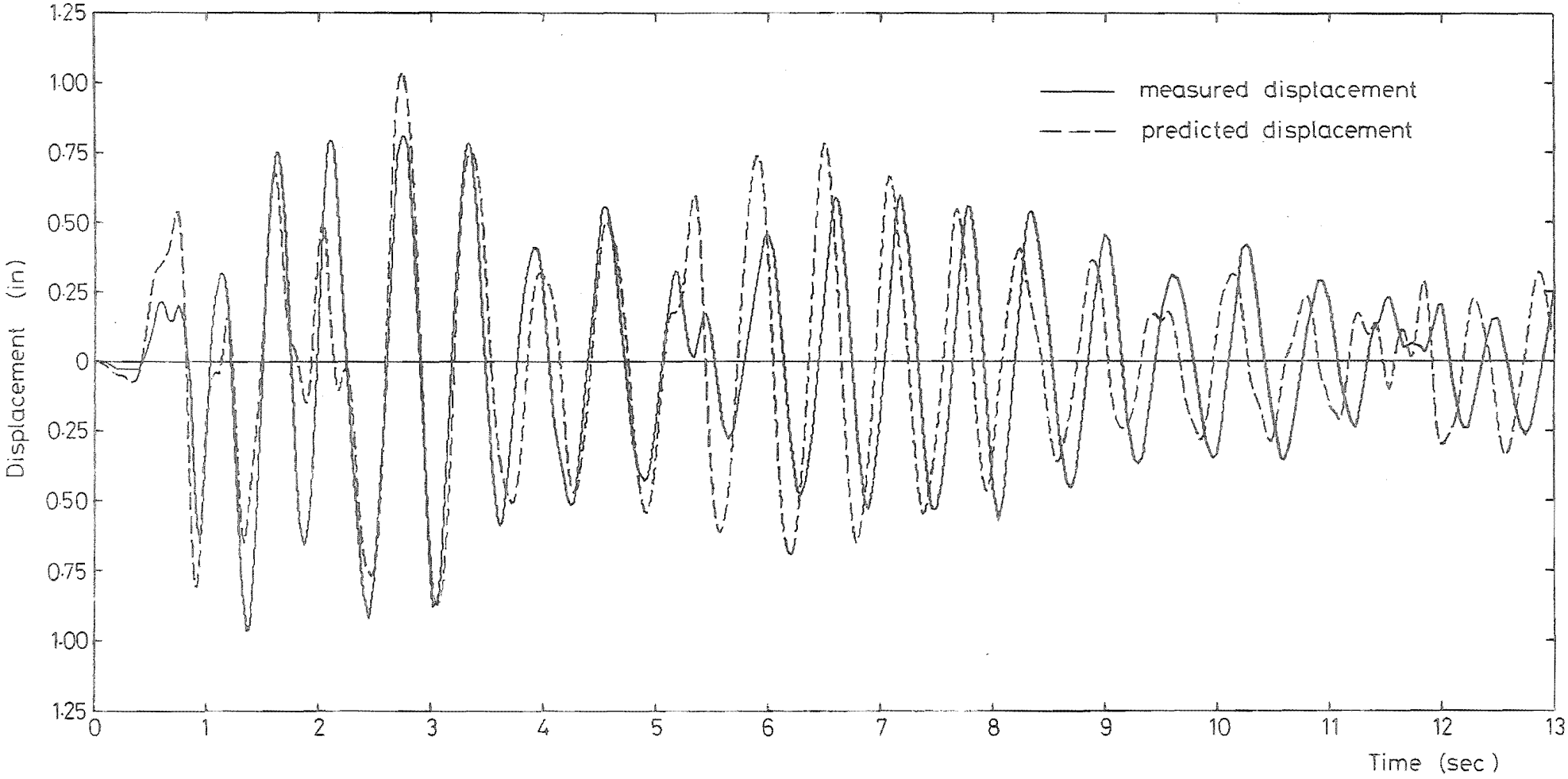


FIGURE 7-17 : MEASURED AND PREDICTED DISPLACEMENTS FOR FLOOR 6 DURING RUN 1

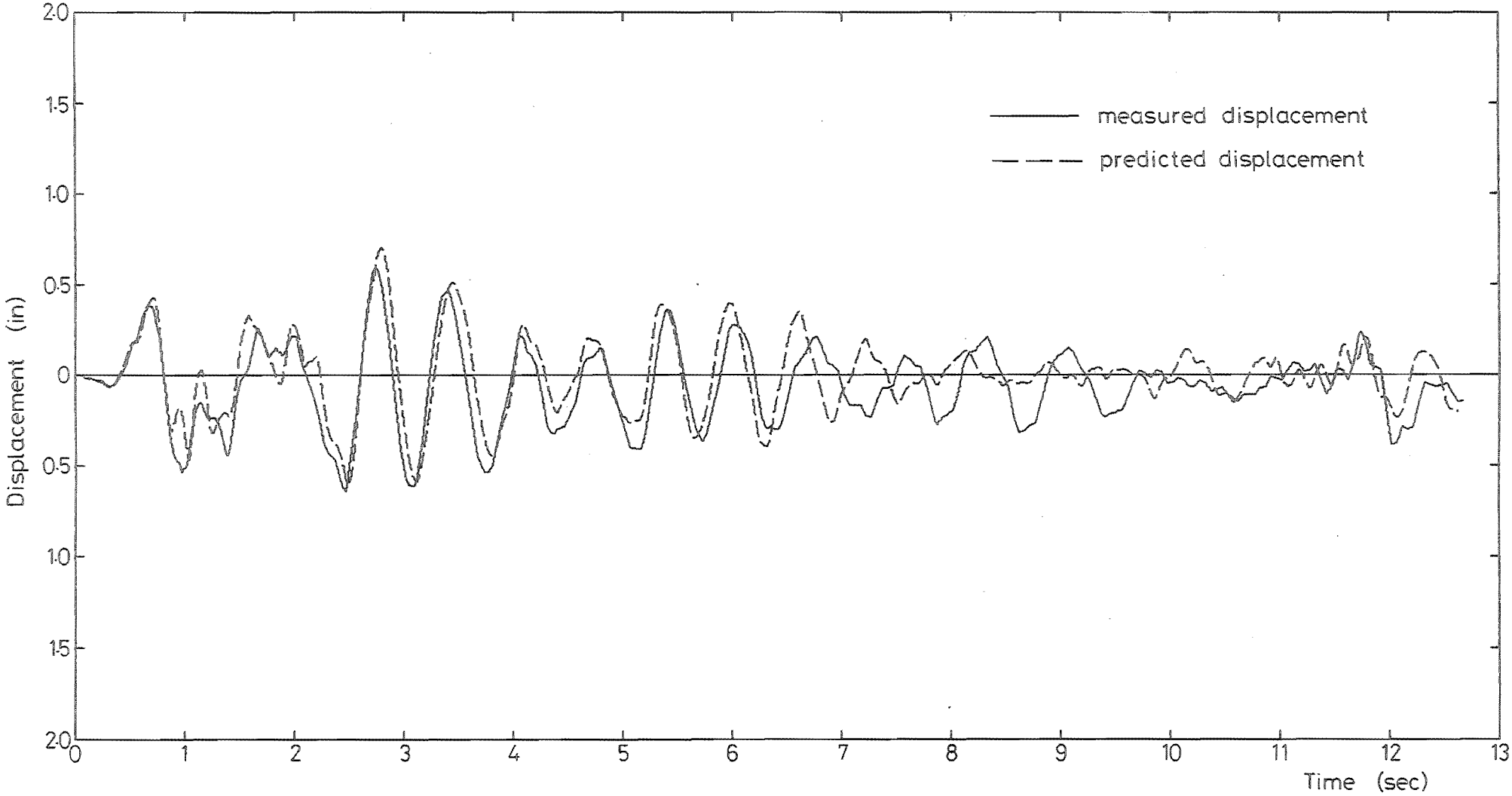


FIGURE 7-18 : MEASURED AND PREDICTED DISPLACEMENTS FOR FLOOR 2 DURING RUN 4

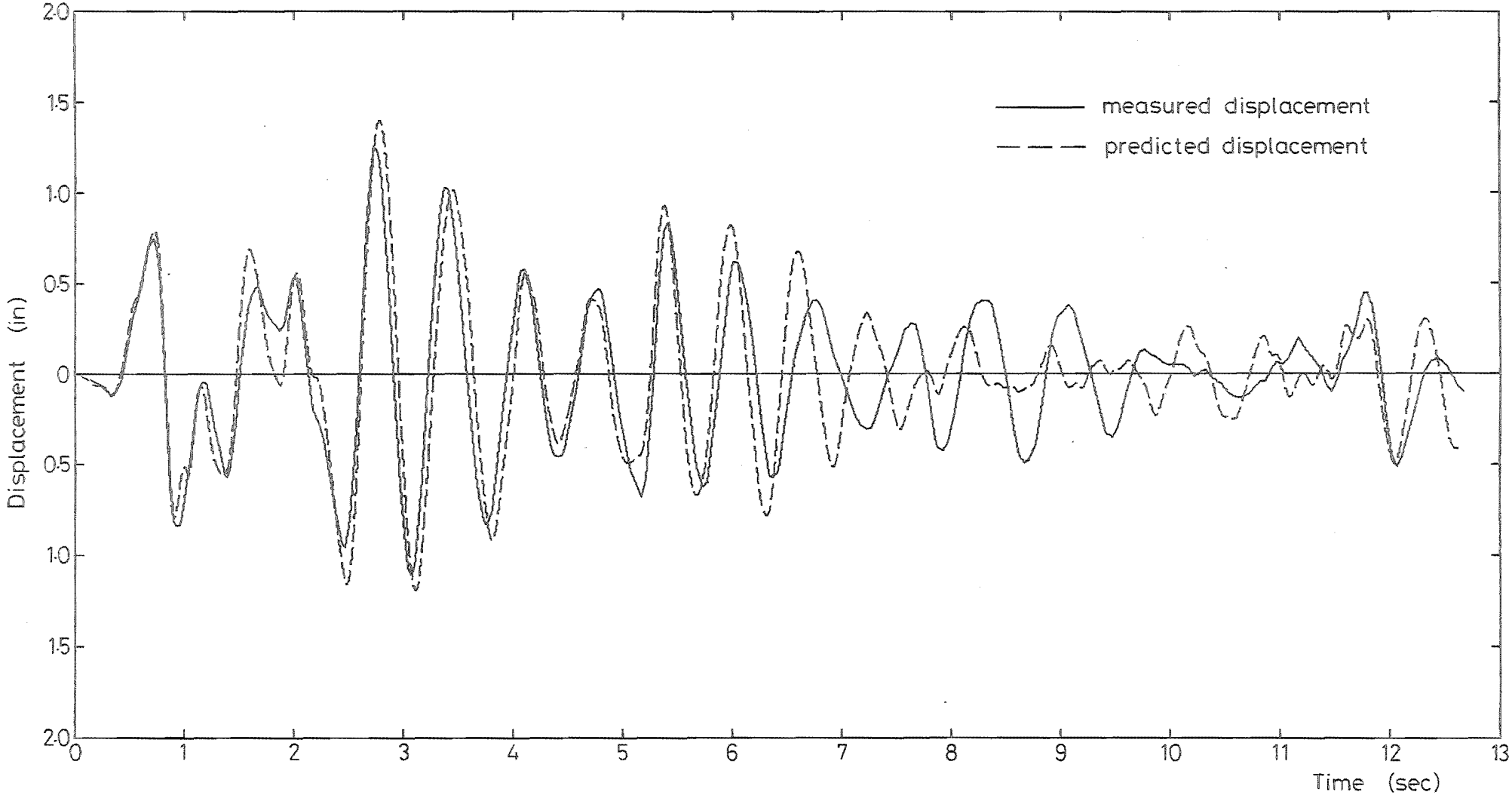


FIGURE 7-19 : MEASURED AND PREDICTED DISPLACEMENTS FOR FLOOR 4 DURING RUN 4

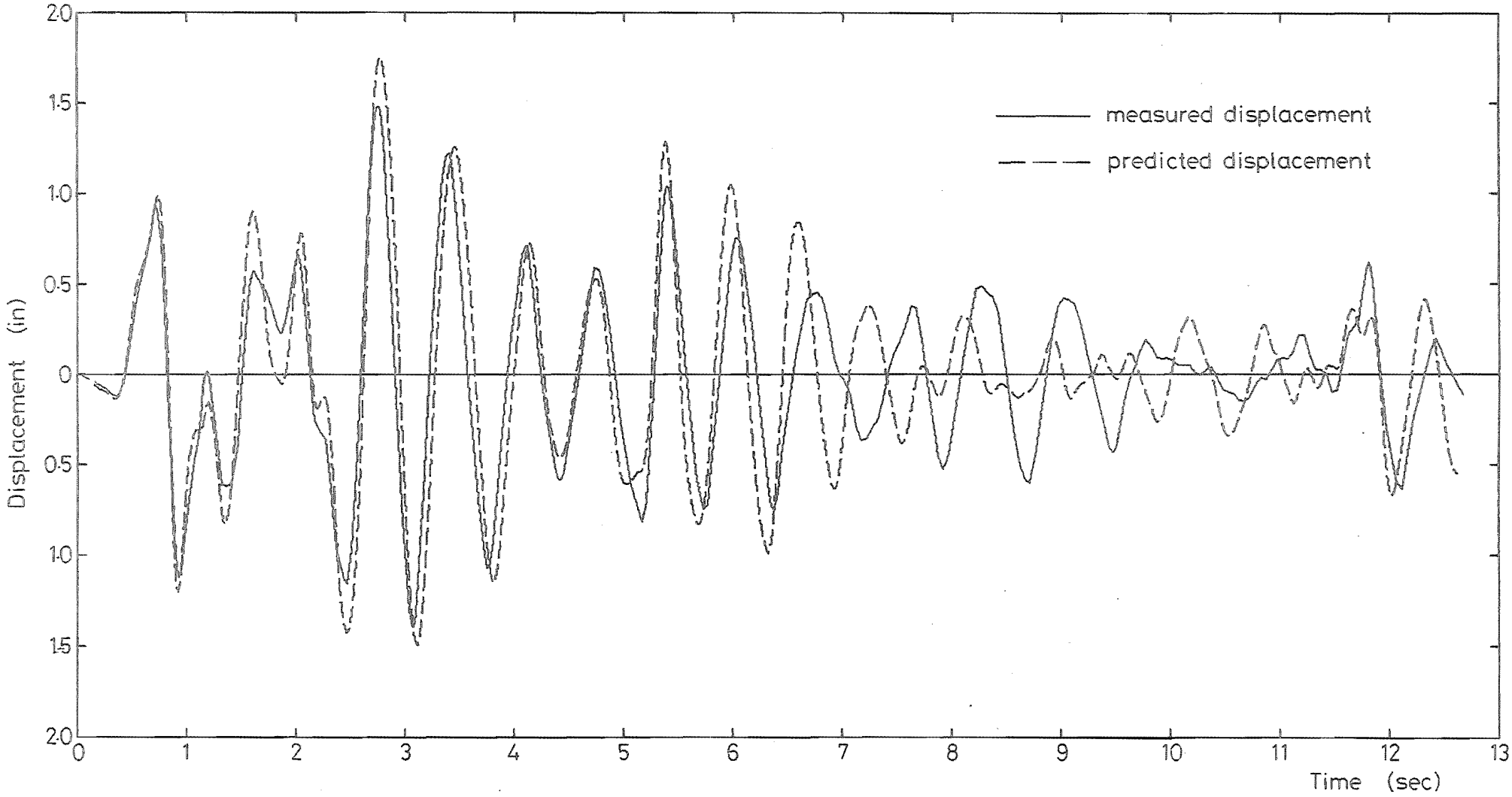


FIGURE 7-20 : MEASURED AND PREDICTED DISPLACEMENTS FOR FLOOR 6 DURING RUN 4

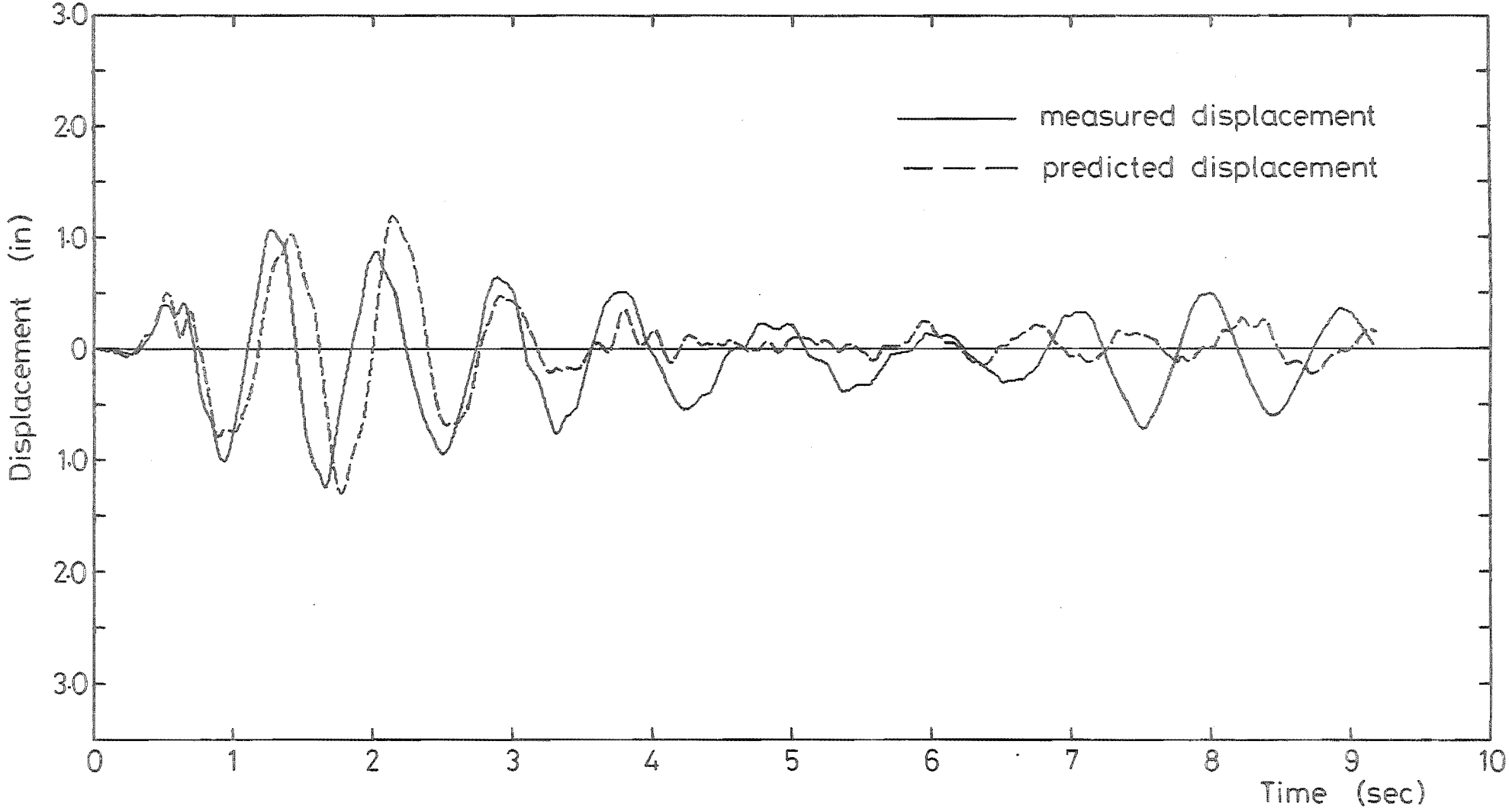


FIGURE 7-21 : MEASURED AND PREDICTED DISPLACEMENTS FOR FLOOR 2 DURING RUN 6

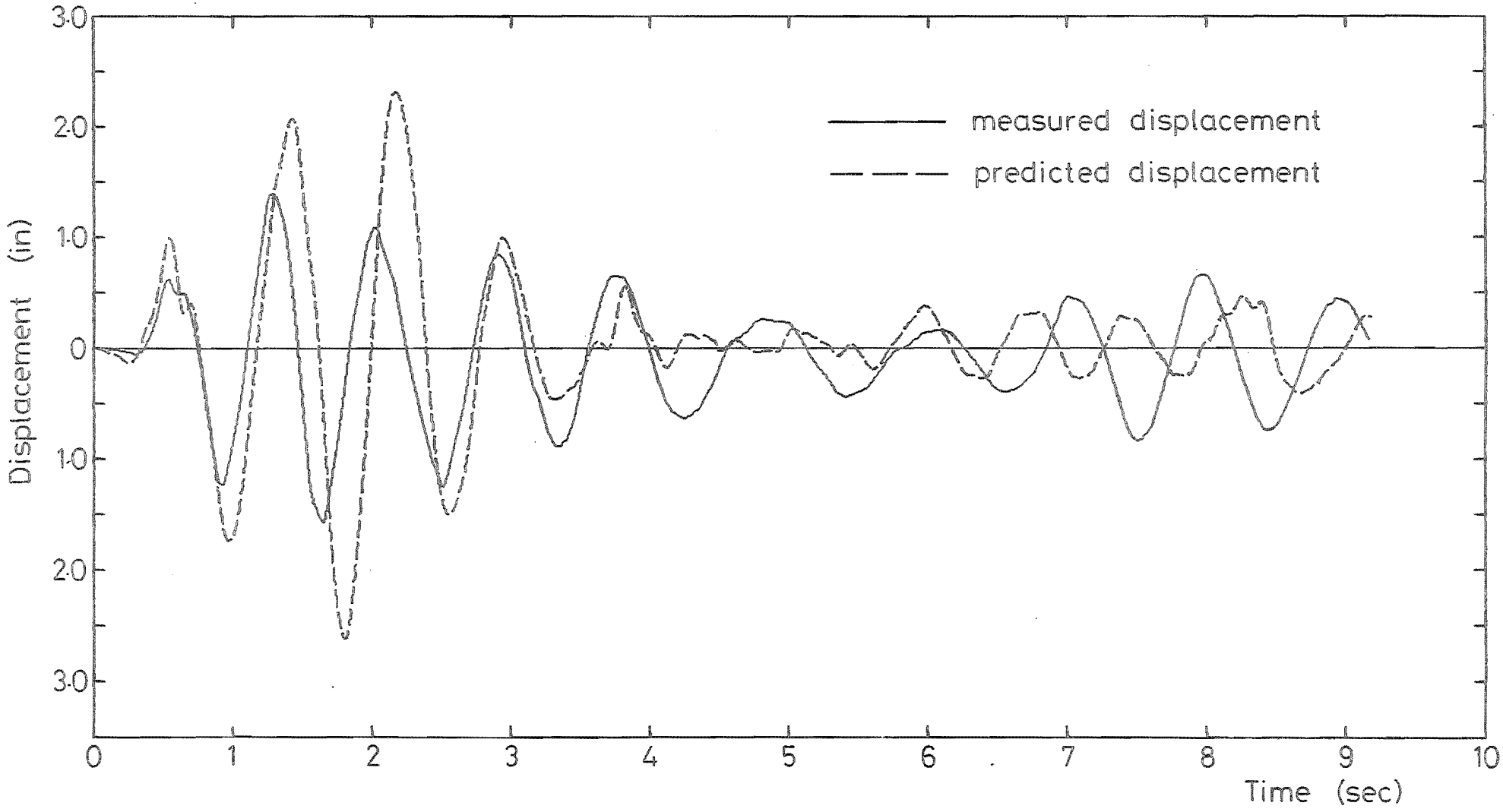


FIGURE 7-22 : MEASURED AND PREDICTED DISPLACEMENTS FOR FLOOR 4 DURING RUN 6

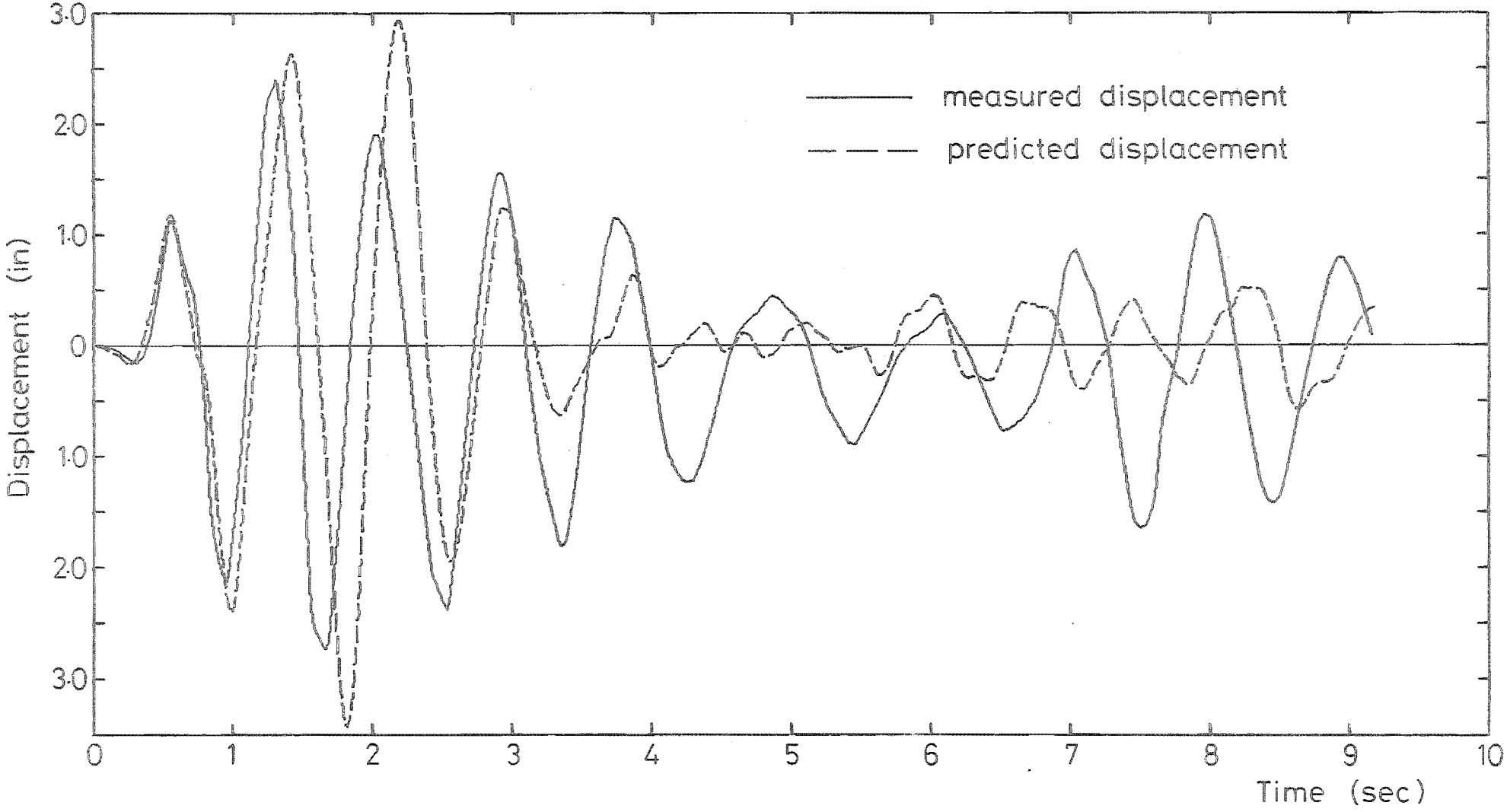


FIGURE 7-23 : MEASURED AND PREDICTED DISPLACEMENTS FOR FLOOR 6 DURING RUN 6

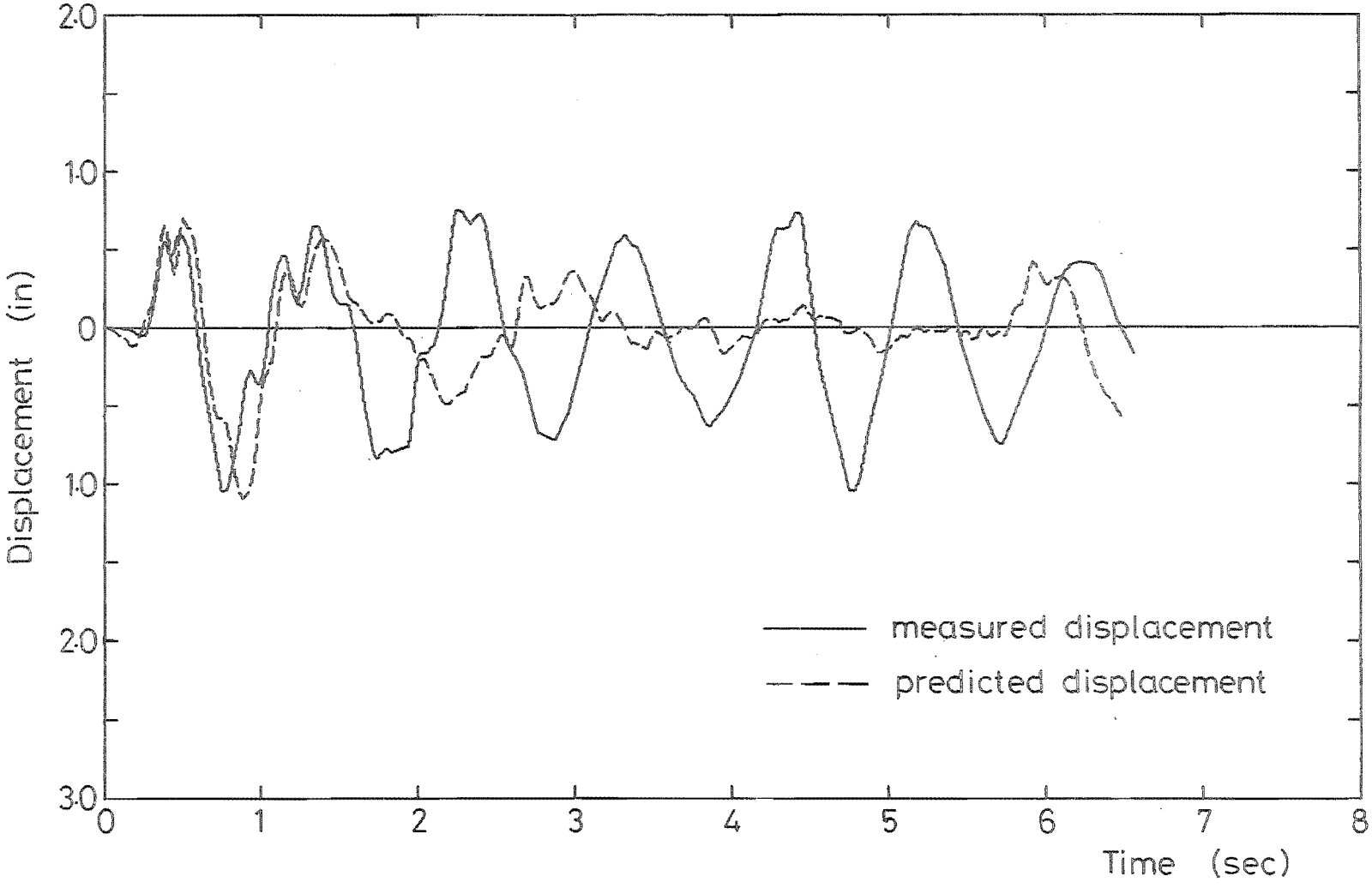


FIGURE 7-24 : MEASURED AND PREDICTED DISPLACEMENTS FOR FLOOR 2 DURING RUN 8

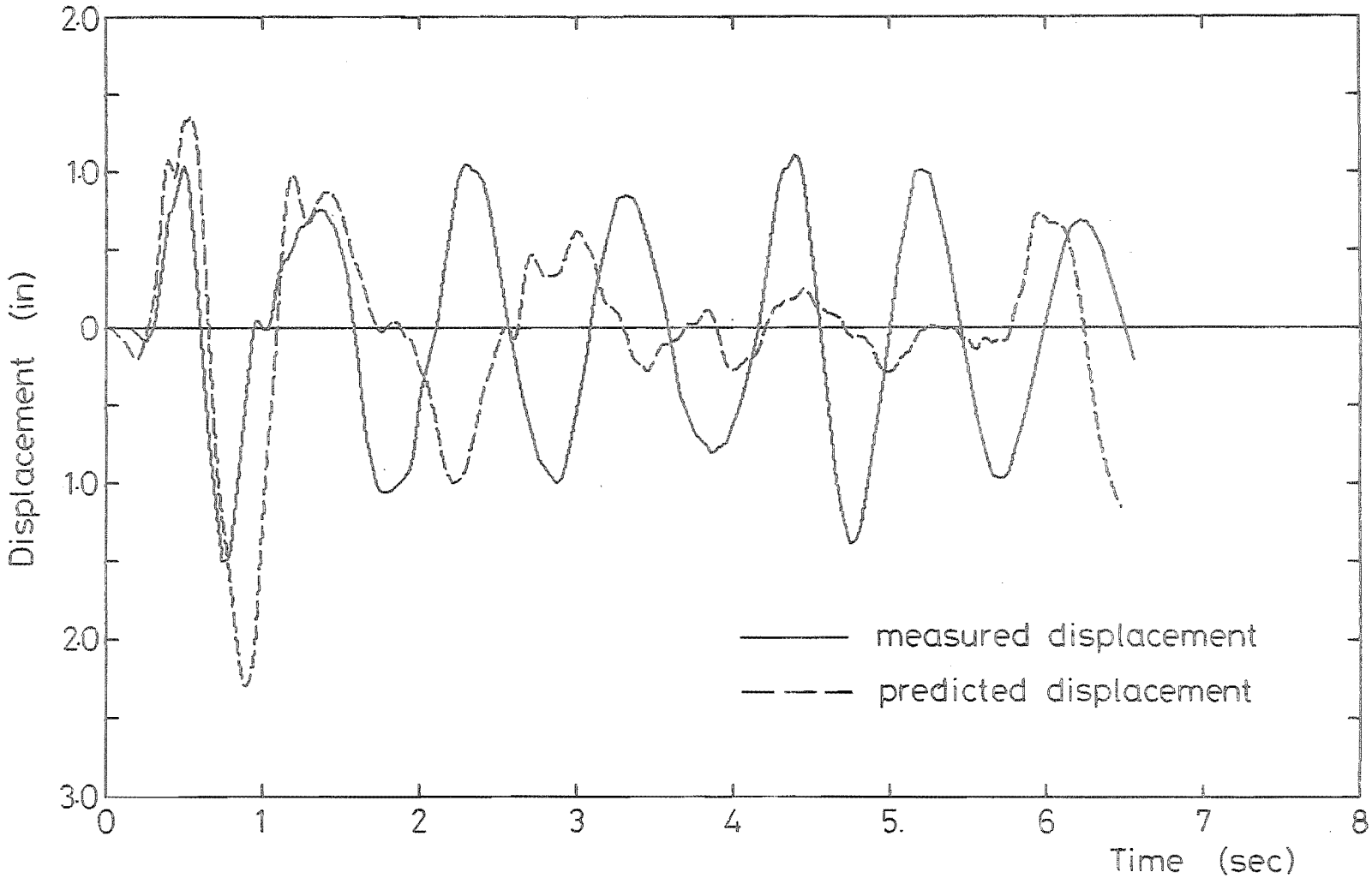


FIGURE 7-25 : MEASURED AND PREDICTED DISPLACEMENTS FOR FLOOR 4 DURING RUN 8

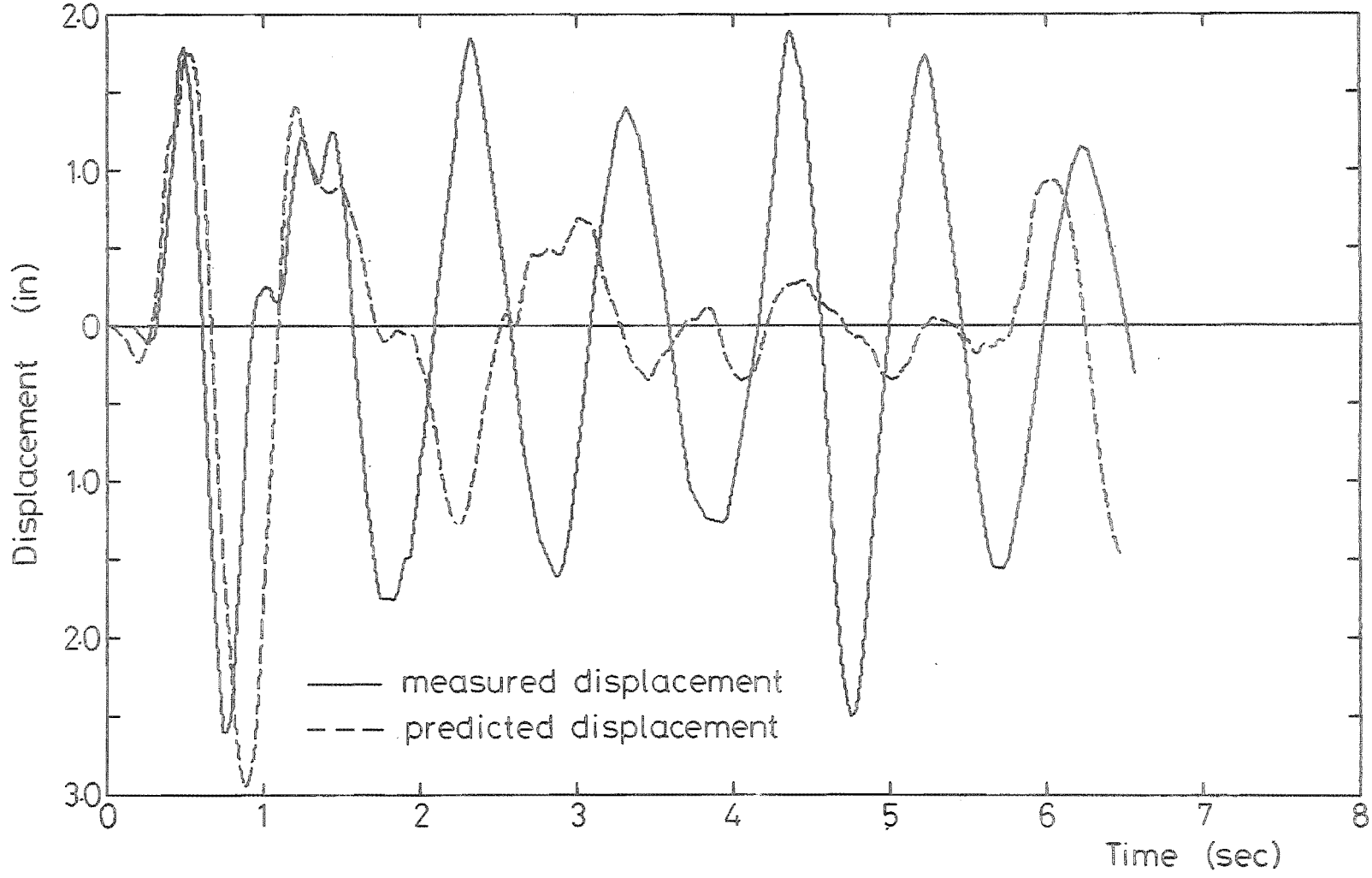


FIGURE 7-26 : MEASURED AND PREDICTED DISPLACEMENTS FOR FLOOR 6 DURING RUN 8

numerical integration of the kinematic equations: the satisfactory tracking of the assumed moment-curvature relationship should present no difficulties since yielding only occurred during test run 6.

The extremely large reduction in stiffness of the structure, due primarily to anchorage slip of the main beam reinforcing bars and to the presence of steel couples at the large full depth cracks just above the base of the columns, in combination with the speeding up of the earthquake record, had the unfortunate effect of reducing the fundamental resonant frequency of the structure as compared with those frequencies which contained most of the energy of the earthquake. Consequently the earthquake energy input to the structure was low and the structure was relatively unaffected by the earthquake test runs, to the extent that yielding of the structure as indicated by the theoretical analyses occurred only during test run 6 and even then the plastic hinges were confined to the base of the columns. That this situation was occurring was apparent during the course of the dynamic tests, since no displacement drift of the structure was observed on the recorded displacement waveform.

A problem encountered in the course of the theoretical analyses was that unique values of stiffness and damping had to be assigned to the structure for each test run and these had to remain constant during the course of that run. The complexity of the problem may be demonstrated when it is realised that the stiffness of the structure increases with displacement due to closing of the cracks, decreases during the course of the test as damage occurs, and varies over the structure depending on the member under consideration. The stiffness of the structure was varied in the theoretical analyses by keeping the moments of inertia of both the beams and columns constant at their cracked values while varying the modulus of elasticity of the concrete. An example of the increase in natural frequency with increasing deflection due to the closing of the cracks is the measured displacement waveform for floor 6 during test run 6. During the main earthquake impetus, which occurs during the first 4 seconds, the fundamental frequency of the structure is 1.23 c.p.s.; this drops to 0.86 c.p.s. for the next three seconds during a period of reduced displacements and then increases to about 1.03 c.p.s. for the remainder of the test run.

The damping and stiffness values used for the test runs were based on the initial strong motion portion of the earthquake record and as such the accurate prediction of this part of the displacement waveform was assured. However, the accurate prediction of the remainder of the

earthquake record depended on the extent to which these values represented the state of the structure beyond the initial region. While the structure was barely damaged, such as during test run 1, the predicted and measured displacement waveforms were in excellent agreement. However as the beam reinforcing anchorages began to fail and non-linearity set in, the predicted waveform became accurate for an ever-decreasing length of the earthquake record, finally culminating in test run 8 where only the first few cycles are predicted accurately. Generally the predicted displacement waveforms (beyond the region of accurate prediction) were of a much lesser magnitude than the recorded waveforms, which still appeared to be completely dominated by the fundamental resonant frequency. The value assigned to the second resonant mode damping in the theoretical analyses was found to have a negligible effect on the predicted displacement waveform, even for extremely large variations in damping. An indication of the extent to which the deterioration in the beam steel anchorages and the presence of steel couples at the large full depth cracks which formed just above the base of the columns had on the stiffness of the structure is given in table 7-5.

TABLE 7-5 : DAMPING AND STIFFNESS OF MODEL 2 DURING EACH SIMULATED EARTHQUAKE TEST RUN

| Simulated earthquake test run no. | Percentage of critical damping | | Stiffness (percentage cracked section value) |
|---|---|---|---|
| | from simulated earthquake tests | from free vibration tests | |
| 1 | 5 | 4.7 | 55 |
| 4 | 6 | 8.0 | 48 |
| 6 | 7 | 15.7 | 34 |
| 8 | 7 | 16.6 | 16 |

An attempt was made to try and ascertain the relative magnitudes of the reduction in stiffness due to the deterioration of the beam steel anchorages and the effect of the concrete cracks opening and closing.

It can be shown that the influence of the cracks opening and closing is greater in a small scale structure than it is in a larger one. Consider two columns cantilevering from the ground which are identical in every respect except that one is $L$ times bigger than the

other. If lateral loads are applied at the top of each column of sufficient magnitude to just cause each column to yield, then the lateral deflection of the larger column will be L times that of the smaller column. If, due to a series of load reversals, a large crack is present just above the base of each column, then the width of the crack will be approximately the same for each column, since the steel strain will be the same. That being the case, then the rotation required at the base of the columns in order to close the crack will be L times greater for the smaller column than it will be for the larger one, and consequently the lateral deflections at the top of each column due to the closing of the crack will be the same. In a typical load-deflection cycle for these columns, part of the lateral deflection occurs when closing the cracks and part when yielding the structure after the cracks have closed. Consequently, the effect of the opening and closing of the concrete cracks is relatively more pronounced in smaller structures than it is in larger ones.

A bound to the reduction in stiffness of the structural members due to cracking is the stiffness of the reinforcing steel only, since this ignores any contribution from the concrete. For the columns this stiffness was found to be 0.27 $in^4$ and for the beams it was 0.48 $in^4$, which is 45% and 51% of the cracked section values respectively. Thus, on the average, the maximum possible influence of the cracking is to reduce the member stiffness to about 48% of the cracked section values. This is in general agreement with the results of Bertero and McClure [39], who investigated the cyclic behaviour of small scale reinforced concrete portal frames. They minimised any reduction in stiffness due to anchorage slip by welding the reinforcing wires to steel plates provided at each joint and they also minimised any reduction in stiffness due to joint deformation by the use of haunched joints. Although precise figures are difficult to determine from their data, it does seem that the overall stiffness of the frames reduced to less than 50% of the cracked section value.

The overall stiffness of Model 2 reduced to only 16% of the cracked section value by test run 8 and so if the maximum effect of cracking is to reduce the stiffness of the structure to 48% of the cracked section value then the remaining reduction in stiffness, equivalent to 32% of the cracked section value, must be primarily due to anchorage slip of the beam reinforcing steel. There is an obvious need for further study to provide typical values of the magnitudes of these two effects.

The recorded base displacement during the test runs appeared to

be an accurate reproduction of the actual earthquake displacement record but it was not possible to make such a comparison for the base acceleration. Nevertheless, the fact that the displacements of the structure whilst it was linear were accurately predicted by a mathematical model subjected to the command earthquake acceleration implies that the earthquake displacement record must have been accurately reproduced on the magnetic tape and also that the MTS 903.79 testing system is capable of accurately reproducing a seismic disturbance.

# CHAPTER EIGHT

# SUMMARY AND SUGGESTIONS FOR FURTHER RESEARCH

## 8.1 MODELLING AND DYNAMIC TESTING

The modelling problem is an area of difficulty when destructive dynamic tests of a model reinforced concrete structure are contemplated.

It has been shown that the perfect modelling of a prototype structure requires the use of an extremely dense modelling material and that this requirement is generally not able to be complied with. It is possible to introduce distorted models if the effects of only one or two parameters are important but this is not generally the case and although two distorted modelling criteria were examined, neither were satisfactory. A variety of artificial methods can be used to circumvent this problem; the most common of these is to suspend weights from the structure. However, these weights may alter the mass distribution of the structure and their method of attachment may cause undesirable side effects to be introduced into the structure.

The approach to the problem that was adopted was to not model a prototype structure at all but to design and construct a miniature building, the response of which is analysed strictly in terms of its own behaviour. It has been shown, however, that when a structure is reproduced at a smaller scale the forces in the structure decrease more rapidly than the strength of the structure and so this approach results in very slender structural members. In addition, the low weight of the structure reduces the gravity loading effects in relation to the earthquake loading effects.

The low stiffness of the structure was responsible for many of the problems encountered during the course of this work, ranging from obtaining LVDTs with a sufficiently large displacement range to the fact that the fundamental natural frequency of the structure decreased to a value that was below those frequencies containing most of the energy of an earthquake. Compounding this latter problem was the fact that the modelling process had to be applied to the earthquake waveform as well, both to maintain geometric similarity and to keep within the maximum displacement and velocity capabilities of the shaking table, and this scaling process involved a speeding up of the earthquake record.

More research is required into the development of techniques for artificially increasing the weight of a model structure, for it is apparent that it is this approach to the modelling problem which will ultimately

prove most successful. The model test results could then be compared directly with the results of theoretical analyses and extrapolated directly to the prototype structure. The increase in weight of the model structure resulting from this approach would enable the height of the structure to be decreased, with a consequent increase in its fundamental natural frequency and resulting in a simplified structure to analyse.

The development of torsion in the lateral beams of the structure that was highlighted by the models tested in this work points to the importance of testing complete structures, rather than parts of structures such as frames. Accurate construction of three dimensional structures is possible using the construction techniques reported in this study.

That accurate results can be obtained using small scale models was shown by the flexural tests conducted on the beam and column structural members. The experimental moment-curvature curves were closely predicted by the theory with the exception of some of the cyclic loading tests, where the experimental flexural moments were sometimes greater than predicted, possibly due to strain hardening of the reinforcing steel. However, in general the tests on both the single and the six storey model structures indicated no increase in strength due to their small size.

A major problem encountered when working with small scale reinforced concrete models is that of obtaining suitable reinforcing steel in the small diameters required. The drastic deterioration of the main reinforcing steel anchorages indicates that while smooth wire may be suitable for ties and stirrups, it is unsuitable for the main reinforcing, no matter how pitted due to surface rusting. It is essential that properly deformed bars are used for the main reinforcing steel. Since the smallest deformed bar commercially available in New Zealand is 0.25 in. (6.35 mm) dia., then this effectively limits the minimum possible model size.

It would have been possible to improve the anchorage of the longitudinal beam reinforcing if the anchorage length had been increased. However, the beam steel was already bent to protrude several inches into the columns above and below the beam-column connections and this would have tended to increase the flexural strength of the columns in those regions. The beam reinforcing could have been securely anchored by providing a beam stub or by welding to anchorage plates as did Bertero and McClure [39], but the applicability of the tests would have been lost, since in a real structure the steel is not anchored in this way and anchorage slip does occur as the concrete deteriorates in the joint.

The bases of the columns are an area for concern since plastic hinges will form there and a large amount of ductility must be provided. The constant yielding of reinforcing bars in opposite faces of the columns means that the permanent deformation of the steel will continually increase, causing large cracks to form in the columns at the plastic hinge locations, in the absence of substantial column axial loading. Thus for much of the time the behaviour at the base of the columns will be governed by a steel couple only and this will cause a large reduction in the stiffness of the structure.

The joint ties provided appeared to be sufficient to adequately confine the joint concrete although the effect of the beam steel slipping through the joint caused a deterioration of the concrete there.

The small scale concrete mix used in the structures was found to have a satisfactory strength and workability. However, the relatively low aggregate/cement ratio and high water/cement ratio found necessary to maintain workability caused an increase in the inherent shrinkage of the concrete, which, together with the fact that the concrete dried quickly due to the large surface area to volume ratio of the small specimens, increased the shrinkage to such an extent that unavoidable minute shrinkage cracks formed all over the structure.

Dynamic testing is an order of magnitude more difficult than static testing and for this reason only the measurement of the following two quantities is usually attempted:

(i) displacements (at each floor level and at the base)

(ii) accelerations (at each floor level and at the base).

There are numerous acceleration transducers available which are suitable for measuring the accelerations, as long as adequate amplifier circuits can be provided for them. The response of these transducers is generally so good that they pick up a great deal of high frequency "noise" from the excitation source and this must be reduced or filtered out in some way. The displacement transducers used in this study were satisfactory although their limited range put constraints on their use and so it is advisable to keep the model structure reasonably stiff in order to keep within this range.

Given the satisfactory performance of the measuring instruments, the adequacy of the test results depends upon the quality (and quantity) of the recording instruments and it is this aspect that makes dynamic instrumentation difficult and expensive. The problem is that the signals determined by the measuring instruments are in an analog form of voltage

versus time and these have to be converted to a digital form to be suitable for analysis purposes. This analog-digital conversion can be performed either as the signal is measured, or after it has been recorded as an analog signal on magnetic tape. Recording the analog signals directly onto chart recorders is generally unsatisfactory, since the recordings then have to be digitised before they can be used in analysis. In any case the response of pen recorders is generally inadequate to accurately record the high frequency acceleration signals. If the signals are recorded directly on magnetic tape, they can be played back at slower speeds to facilitate digital sampling.

It has been shown that it is not feasible to use an acceleration command signal with the MTS 903.79 structural testing system to drive the shaking table and that a displacement waveform should be used instead. The techniques used to record the digital displacement waveform onto analog magnetic tape were generally satisfactory but further development work is required to eliminate the high frequency components due to noise on the magnetic tape and to the minimum signal step, since these badly distort the acceleration measurements, even though they have a negligible effect on the structure.

## 8.2 EFFECT OF THE TORSION INDUCED IN THE LATERAL BEAMS

It has been shown that torsion is induced into the lateral beams in two distinct ways: as a secondary load resisting mechanism due to the action of gravity loads on the slab, and due to compatibility of deformations when the beam-column joints rotate under lateral loading.

A brief review has been given of some of the theories which have been advanced to assess the ultimate torsional strength and stiffness of reinforced concrete sections. A comprehensive analysis has been presented to determine the torsion in the lateral beams for the case of a single slab bounded by four edge beams. There is a need to develop this analysis further to determine the effects of adjoining slabs and of different boundary conditions. Additional research is required to determine the width of slab which is effective in resisting torsion.

The interaction of the slab and the lateral beams was found to cause a significant increase in the effective stiffness and flexural strength of the longitudinal beams. The effective flexural strength of the longitudinal beams is equal to the flexural strength of the longitudinal beams plus the torsional strength of the lateral beams, unless the strength of the slab is insufficient to cause torsional

yielding of the lateral beams. If this exception is the case, the torsional strength of the lateral beams should be replaced by the sum of the flexural strengths of those areas of slab causing the torsion. For the model structure described in this study, the increase in stiffness due to the lateral beams was 11% and the increase in flexural strength was 16%. This may cause the beams to become overstrong in relation to the columns.

The greatest effect of the torsion induced in the lateral beams was to cause severe torsional cracking to those beams and a consequent decrease in stiffness. These cracks did not close on the reversed loading cycle and this caused large pieces of concrete to spall off with each load reversal, leaving only a core of concrete confined within the stirrups of the reinforcing cage. The consequence of this was a large decrease in the flexural and torsional stiffness and flexural strength (but not torsional strength) of the lateral beams, although this was not critical since the lateral loading was perpendicular to those beams.

Skew loading of the structure, however, will cause severe torsional cracking in all beams, which will reduce their flexural strength and stiffness at the same time as they are required to withstand large flexural loads. This will result in premature flexural yielding of the beams and a consequent reduction in the overall strength of the structure. This spalling of the concrete may only be prevented by either extremely rigid lateral beams or by reducing the flexural strength of the slab at the edges so that insufficient torsion is induced into the beams to crack them. Both the positive and negative moment slab reinforcement should be sufficiently well anchored in the edge beams that they can develop their full strength at the edge of the slab.

## 8.3 COLLAPSE MECHANISMS AND THE STRENGTH OF THE STRUCTURE

A valid sidesway collapse mechanism for a structure may be composed entirely of column hinges or it may be composed partly of column hinges and partly of beam hinges. If the collapse mechanism forms in a single storey and is thus comprised entirely of column hinges, then the collapse mechanism may be designated a column sidesway collapse mechanism. If, however, the collapse mechanism forms over several storeys, then some beam hinging will be necessary in those storeys and the collapse mechanism may be more correctly described as a composite beam column sidesway collapse mechanism. If the collapse mechanism forms over the full height of the structure, then hinges will be necessary at the base of the columns and at the ends of all the beams: this is the beam sidesway

collapse mechanism. Thus it is apparent that the column sidesway mechanism and the beam sidesway mechanism are special cases forming the two bounds of the composite beam column sidesway mechanism.

The importance of preventing a column sidesway collapse mechanism (or a composite beam column sidesway collapse mechanism) from forming has generally been recognised in seismic design by ensuring that the sum of the column strengths at a joint are slightly greater than the sum of the beam strengths at the joint. It has been demonstrated in this study that such a design procedure will not ensure that the collapse mechanism is of the beam sidesway type and that it will almost always result in either a column sidesway or a composite beam column sidesway collapse mechanism.

The reason for this is that moment redistribution will cause the points of contraflexure in the columns to drop, thereby increasing the moment at the top of each column and decreasing the moment at the bottom of each column. If the point of contraflexure in the column above a joint falls to the level of that joint, then the column framing into the joint from below will be required to resist the total moment input by all of the beams framing into that joint. From consideration of a structure subjected to an incremental static loading, it is submitted that the formation of the beam sidesway collapse mechanism can only be assured if the strength of each column framing into a joint is greater than the sum of the strengths of all of the beams framing into that joint, including the torsional strengths of the lateral beams.

It is also acknowledged that under dynamic conditions the column above the joint may be in single curvature and thus the column below the joint may be required to resist the sum of the beam moments plus the moment from the column above the joint, which is an even more severe condition. However, the columns cannot be strengthened indefinitely and hence it is suggested that the above recommendation (strength of each column > sum of strengths of the beams) be adhered to until the results of further research, which is necessary on a wide range of structures, prove that it is unsatisfactory.

Both the six storey structures, and the single storey structure, tested during the course of this study failed in a column sidesway collapse mechanism, even though they had been designed in accordance with the current design philosophy. It is recommended that this design philosophy should be examined with a view to strengthening the columns with respect to the beams. In accordance with this finding, a reassessment of the adequacy of some existing structures may be necessary.

It is recognised that the presence of a collapse mechanism does not necessarily mean that the structure will collapse. This follows because of the transient nature of the response of the structure and also because the structural members still retain some stiffness after yielding. However, in the absence of any other criteria by which the ultimate strength of a structure may be assessed, the formulation of an equivalent static strength is a convenient, if somewhat misleading, parameter.

The equivalent static lateral load used in seismic design generally has a triangular type of distribution up the height of the structure, since this is considered to be an adequate approximation to the fundamental mode shape of the structure, from which the inertia loads will be primarily derived. This concept is justified for squat buildings where the deflected shape of the structure is reasonably represented by the triangular distribution, but for tall slender buildings this may not generally be the case. The response of a flexible structure is greatly affected by the higher modes of vibration and Sharpe [19] has shown that it is characterised by bands of inelastic behaviour migrating upward through the frame. Further study is required to determine whether some modification to the distribution of the equivalent static lateral design load for flexible structures is justified.

The primary concern of any designer is whether or not his structure is sufficiently strong to withstand the loads which might be applied to it. The six storey model buildings of this study were designed, in accordance with current building standards, to withstand a static lateral load of 0.15 g. The ultimate strength of the models were actually attained under a unidirectional static lateral load of 0.459 g, which is an increase of over 200%. Some of the reasons for this increase are:

(i) capacity reduction factors were used when calculating the steel areas

(ii) steel in excess of that required for flexure was provided in the beams

(iii) column design moment magnification due to low slenderness ratio

(iv) an increase in the strength of the columns due to an attempt to ensure that the plastic hinges formed in the beams

(v) an increase in the effective flexural strength of the longitudinal beams due to the effect of the slab - lateral beam system.

(vi) the actual strengths of both the steel and the concrete were greater than those values assumed in the design

(vii) strain hardening of the steel.

These factors are likely to be present in any building and will add considerable strength to a structure when it is built. It has been shown that by accounting for these factors, the equivalent lateral strength of the various model structures could be closely predicted. The predicted ultimate static lateral load of the single storey structure was 97% of the actual load and the predicted ultimate static lateral load of Model 1, although difficult to quantify exactly, would be almost 99% of the actual load.

During the static cyclic loading tests on Model 1, it was found that the ultimate strength of the structure appeared to reduce to about 84% of the original ultimate strength after four inelastic loading cycles. The decrease in ultimate strength was probably due to a deterioration in the beam reinforcing steel anchorages.

The dynamic accelerations at which the various model structures collapsed were all very much greater than the "static" value of 0.459 g. The single storey structure withstood square waves with base accelerations of greater than 5 g but collapsed under sinusoidal resonance testing at its fundamental frequency at a base acceleration of 1.55 g. Both Model 1 and Model 2 collapsed under sinusoidal resonance testing at their fourth natural frequencies. Model 1, which had been severely damaged during the static tests, when it withstood a static load of 0.459 g, collapsed at a base acceleration of 1.83 g and Model 2 collapsed at a base acceleration of 2.59 g.

If a relative intensity index is defined as the maximum base acceleration during dynamic loading divided by the limiting base shear (equivalent static lateral strength) of the structure, then the relative intensity index is 4.0 for Model 1 and 5.6 for Model 2. Similar results have been reported by Otani and Sozen [16], whose small scale 1 bay, 3 storey frames withstood maximum accelerations ranging from 2.1 g to 3.4 g with a maximum relative intensity index of approximately 6.0. However, the single storey structure of the present series, which failed at a base acceleration of 1.55 g, actually had a limiting base shear of 3.05 g, which meant its relative intensity index was 0.51. The reason that the single storey structure had such a low relative intensity index was because the structure attracted a large amount of energy since it was excited at its fundamental resonant frequency where its displacement response factor is a maximum.

Consequently, it is apparent that the equivalent static lateral strength does not give an adequate indication of the dynamic strength of the structure. Because the equivalent static lateral strength can be expressed in terms of the weight of the structure, the concept of a "static"

acceleration has arisen. Although this is a good indication of the static strength of the structure, it bears no relation to the maximum base acceleration that the structure can withstand, since it takes no account of the actual inertia loads applied to the structure or the duration of the loading. The maximum base acceleration that a structure can withstand varies with the frequency of excitation. It is probable that both Model 1 and Model 2 would have failed at considerably lower accelerations than they actually did if the maximum table displacement had not restricted the acceleration which could be applied to them at their fundamental resonant frequency.

## 8.4 ACCURACY OF DYNAMIC ANALYSES

The response of a structure to a seismic disturbance can be predicted accurately if the mathematical model used in such an analysis realistically describes that structure. The mathematical model must take into account many different factors and two of the most important of these were found to be the stiffness and the damping of the structure.

It has been found that the damping ratio determined from successive cycles of a free vibration test is not sufficiently accurately described by the approximate relationship commonly used (see equation 5-9) unless the damping is less than about 2% of critical damping. The damping of the untested structure was less than 2% of critical damping, although the structure was covered with minute shrinkage cracks. Care should be taken when determining the damping ratio over many cycles of a free vibration test in order to obtain greater accuracy, since it was found that the damping ratio did not stay constant but varied for successive cycles. The damping ratio increased with decreasing deflection when the structure was only lightly damaged but increased with increasing deflection as the damage became more extensive. The damping ratio as determined from free vibration tests conducted between loading runs at various stages during testing appeared to attain a maximum of 20% of critical damping.

It was found that in all cases the damping ratios determined from the forced vibration tests (including the simulated earthquake tests) were significantly less than the damping ratios determined from the free vibration tests. The maximum first mode damping ratio determined from the sinusoidal displacement response tests was 6.2% of critical damping regardless of the damaged state of the structure and the damping ratios determined from the displacement response of the structure to the strong motion portion of the simulated El Centro 1940 N-S component earthquake

test runs varied between 5% and 7% of critical damping. This is in accordance with the results of Otani and Sozen [16], who found that the first mode damping ranged between 4% and 7% of critical damping, even when the structure was severely damaged. The second mode damping determined from displacement response tests was 8.8% of critical damping but the theoretical analyses showed that the magnitude of this damping ratio had a negligible effect on the displacement response of the structure, even when varied over wide limits. The discrepancy between those damping ratios determined from forced vibration tests and those determined from free vibration tests is probably partially due to the fact that when a structure is set into free vibration, all the modes of the structure are excited as well as the fundamental mode and the greater decay observed could be due to the rapid decay of the higher modes.

The equivalent viscous damping factor determined from the area of the dynamic load-deflection hysteresis loop was almost identical to the damping ratio determined from forced vibration tests of the single storey structure. The equivalent viscous damping factor based on the static loops was 15% greater than that based on the dynamic loops. The energy dissipation based on the areas of the loops of the static load-deflection tests for Model 1 was found to remain constant or increase slightly for all four static ultimate load cycles, indicating that the energy dissipation characteristics were unaffected by the decreasing stiffness. This was true for the load-deflection loops of all of the floors.

The modes of lateral vibration of the structure could be readily identified from displacement response tests, the number of modes depending on how severely the structure was permitted to be shaken. The values of damping determined in this manner were found to agree closely with the damping ratios determined by other methods, the free vibration tests excepted. The bandwidth for the displacement response curve was narrower than predicted by theory. A problem associated with the displacement response tests was the fact that the amplitude of the displacement of the structure oscillated for some time before stabilizing when it was excited at its resonant frequencies. The structure is damping controlled in this region and its equilibrium is delicately balanced and this effect was thought to be due to the non-linearity of damping and stiffness with displacement.

All of the load-deflection curves established for the structures in the elastic range were of the spring hardening type in which the stiffness of the structure increased with increasing deflection until the yield plateau was reached. The softening of the structure near the centre

portion of each loop was due to the opening of the concrete cracks, particularly a large crack which occurred immediately above the base of each column. The static hysteresis curves for all six floors of Model 1 were found to be similar in shape and the dynamic hysteresis curves increased in width as the damping increased. Both the dynamic and the static hysteresis curves had a similar shape and a cubic curve proposed by Shiga et al [17] was found to give a good approximation to these curves.

It was found that the stiffness of the structures decreased drastically during testing due primarily to anchorage slip of the beam reinforcing steel and the opening of large cracks at the base of the columns. The magnitude of the decrease in stiffness was such that by simulated earthquake run 8, the stiffness of Model 2 had reduced to only 16% of the cracked section stiffness. This had the unfortunate effect of reducing the fundamental resonant frequency of the structure to less than that band of frequencies containing most of the energy of the earthquake. As a consequence, the structure was relatively unaffected by the simulated earthquakes, to the extent that yielding of reinforcing steel occurred only in test run 6.

An assessment of the relative magnitudes of the reduction in stiffness due to the deterioration of the beam steel anchorages and the effects of the concrete cracks opening and closing was made. It has been shown that the effect of the concrete cracks opening and closing is greater in a smaller structure than in a larger one because the cracks remain open for a relatively greater portion of the loading cycle. By ignoring any contribution of the concrete to the stiffness of the structure, the maximum possible effect of cracking was found to be to reduce the stiffness of the structure to 48% of the cracked section value. The remaining reduction in stiffness of the structure, equivalent to 32% of the cracked section value, must be primarily due to anchorage slip of the beam reinforcing steel. There is a need for further study to provide typical values of the magnitudes of these two effects.

An accurate estimation of the stiffness of the structure is essential to the accurate prediction of its response to an earthquake. The inherent inaccuracies of any dynamic analysis may be fully appreciated by the engineer when attempting to realistically estimate the stiffness of a structure which (1) decreases due to anchorage slip and to opening of cracks, (2) increases with displacement as the cracks close, (3) decreases during the course of the earthquake as the structure becomes damaged, and

(4) varies over the structure depending on the member under consideration. Estimation of the stiffness of the structure is further complicated by the difficulty of calculating the width of the slab which effectively acts with the beams. Guidelines for estimating this width of the slab, such as given in ACI 318-71 [26], are based on attempts to correctly estimate the strength of the beams, not their stiffness.

Using those stiffness and damping values which gave the best fit between the predicted and measured responses of the structure to the strong motion portion of the simulated El Centro 1940 N-S earthquake component, it was generally found that the displacement response of the structure could be predicted reasonably accurately for the duration of the earthquake, at least for the less severe simulated earthquakes (those up to and including run 4). However, as the beam steel anchorages began to fail and non-linearity set in, the predicted response became accurate for an ever-decreasing portion of the earthquake record. The displacement response was completely dominated by the first mode.

The reduction in stiffness was greater during the dynamic tests on Model 2 than during the static tests on Model 1, even though visually the damage suffered by Model 2 was small in comparison with that suffered by Model 1. This was because the beam steel anchorages appeared to deteriorate more under dynamic loading, mainly because of the greater number of load cycles.

Other things being equal, tall slender structures are likely to be less severely damaged in earthquakes than squat ones, because their fundamental resonant frequency is less than that band of frequencies which typically contains most of the energy of an earthquake. The New Zealand loadings code [18] recognises this factor by decreasing the equivalent lateral design load for buildings with a long natural period. Anchorage slip of the reinforcing steel at beam-column connections typically occurs in many structures and although it will cause the strength of the structure to be decreased, at least the structure will tend to attract less energy from the earthquake. However, the very large deflections resulting from the decrease in stiffness are likely to cause significant secondary damage.

As a consequence of the difficulty in realistically estimating the stiffness of the structure it is recommended that when the dynamic response of the structure is to be determined, several analyses should be conducted for each selected earthquake. In one of the analyses the stiffness used should be equal to the cracked section stiffness of the

structure; the stiffnesses used in the other analyses should be less than this value. The maximum values of the response of the structure should then be selected from the most critical of these analyses. This may be particularly important for those structures in which the lateral drift is critical.

Because during the tests Model 2 yielded during only one simulated earthquake run (and even then only momentarily), it was not possible to examine the various moment-curvature relationships available to the computer program to determine which best predicted the response of the structure. However, given that the response is extraordinarily dependent upon the accurate prediction of the stiffness and damping, then it is possible that the extra computational time required by any moment-curvature function more complex than a multi-linear one is not justified. A tri-linear curve is proposed as being worthy of investigation; this would be similar to the bi-linear curve but it would include a third line which would be horizontal. This would represent the ultimate strength of the member including the effects of strain hardening of the reinforcing steel and at this point the hinge stiffness would reduce to zero and full plasticity would develop.

These tests have provided the basis from which further investigation of the response of concrete structures to seismic motions can be made. The development of construction and testing techniques will need to be continued in future studies. Further investigations are required of problems such as modelling and steel anchorage slip, including the effect of scale on cracking and the moment-curvature relationship. With the undoubted heavy reliance on the results of dynamic analyses in the future, there is a continuing need for simulated earthquake tests on model structures to provide physical verification of the accuracy of those analyses and to provide data on the magnitude of some of the factors critical to the modelling procedure.

REFERENCES


1. Gyengo, T., "Effect of Type of Test Specimen and Gradation of Aggregate on Compressive Strength of Concrete", Journal of the American Concrete Institute, Proceedings Vol. 34, No. 3, January-February, 1938, pp. 269-284.

2. Price, W.H., "Factors Influencing Concrete Strength", Journal of the American Concrete Institute, Proceedings Vol. 47, No. 6, February, 1951, pp. 417-432.

3. Neville, A.M., "The Influence of Size of Concrete Test Cubes on Mean Strength and Standard Deviation", Magazine of Concrete Research, Vol. 8, No. 23, August, 1956, pp. 101-110.

4. Litle, W.A., and Paparoni, M., "Size Effect In Small-Scale Models of Reinforced Concrete Beams", Journal of the American Concrete Institute, Vol. 63, No. 9, November, 1966, pp. 1191-1204.

5. White, R.N., and Chowdhury, A.H., "Behaviour of Multi-Storey Reinforced Concrete Frames subjected to Severe Reversing Loads", Preliminary Report, Symposium, Resistance and Ultimate Deformability of Structures Acted on by Well Defined Repeated Loads, International Association for Bridge and Structural Engineering, Lisbon, Portugal, 1973.

6. Hanson, T.C., and Mattock, A.H., "Influence of Size and Shape of Member on the Shrinkage and Creep of Concrete", Journal of the American Concrete Institute, Proceedings Vol. 63, No. 2, February, 1966, pp. 267-290.

7. ACI Committee 439, "Effect of Steel Strength and of Reinforcement Ratio on the Mode of Failure and Strain Energy Capacity of Reinforced Concrete Beams", Journal of the American Concrete Institute, Proceedings Vol. 66, No. 3, March, 1969, pp. 165-173.

8. Mirza, M.S., White, R.N., and Roll, R., "Materials for Structural Models", Symposium on Models of Concrete Structures, Preprints sponsored by ACI Committee 444, Annual Convention, Dallas, Texas, March, 1972, pp. 19-57.

9. Alami, Z.Y., and Fergusson, P.M., "Accuracy of Models used in Research on Reinforced Concrete", Journal of the American Concrete Institute, Proceedings Vol. 60, No. 11, November, 1963, pp. 1643-1662.

10. Sabnis, G.M., and White, R.N., "Behaviour of Reinforced Concrete Frames Under Cyclic Loads Using Small Scale Models", Journal of the American Concrete Institute, Proceedings Vol. 66, No. 9, September, 1969, pp. 703-714.

11. Reay, A.M., "Dynamic Characteristics of Civil Engineering Structures", Ph.D. Thesis, University of Canterbury, Christchurch, New Zealand, 1970.

12. Kawasumi, K., and Kanai, K., "Small Amplitude Vibrations of Actual Buildings", Proceedings, World Conference on Earthquake Engineering, Berkeley, California, June, 1956, pp. $7_1$ 1-13.

13. Dawson, R.V., "Design and Development of a Shake Table for Use in Structural Research", Msc. Thesis, University of Calgary, Alberta, 1968.

14. Johnson, R.P., "Strength tests of scaled-down concrete suitable for models, with a note on mix design", Magazine of Concrete Research, Vol. 14, No. 40, March, 1962, pp. 47-53.

15. Magura, D.D., "Structural Model Testing - Reinforced And Prestressed Mortar Beams", Journal of the Portland Cement Association Research and Development Laboratories, Vol. 9, No. 1, January, 1967, pp. 2-24.

16. Otani, S., and Sozen, M.A., "Behaviour of Multistorey Reinforced Concrete Frames During Earthquakes", Civil Engineering Studies, Structural Research Series No. 392, University of Illinois, Urbana, Illinois, November, 1972.

17. Shiga, T., Ogawa, J., Shibata, A., and Shibuya, J., "The Dynamic Properties of Reinforced Concrete Frames", Proceedings, U.S.-Japan Seminar on Earthquake Engineering with Emphasis on the Safety of School Buildings, Sendai, September, 1970, pp. 346-363.

18. "Basic Design Loads", New Zealand Standard Model Building Bylaw, NZSS 1900, Draft Revision of Chapter 8, 1973.

19. Sharpe, R.D., "The Seismic Response of Inelastic Structures", Ph.D. Thesis, University of Canterbury, Christchurch, New Zealand, 1974.

20. Higashi, Y., and Ohkubo, M., "Static and Dynamic Loading Tests of Reinforced Concrete Frames with Thin Spandrel or Wing Walls", Proceedings, U.S.-Japan Seminar on Earthquake Engineering with Emphasis on the Safety of School Buildings, Sendai, September, 1970, pp. 225-239.

21. "Actuator Performance Bulletin, MTS Systems Corporation, No. 200.03-2.

22. Preece, B.W., and Davies, J.D., "Models For Structural Concrete", C.R. Books Ltd., London, 1964, pp. 252.

23. Oberti, G., and Lauletta, E., "Dynamic Tests on Models of Structures", Proceedings, Second World Conference on Earthquake Engineering, Tokyo, Japan, July, 1960, Vol. 2, pp. 947-960.

24. Pereira, J., and Priestley, M.J.N., "Materials and Testing Techniques for Seismic Model Studies", Laboratório Nacional de Engenharia Civil, Lisbon, Portugal, April, 1969.

25. Muto, K., "Seismic Analysis of Reinforced Concrete Buildings", Shokoku-sha Publishing Company, Tokyo, Japan, 1965, pp. 116.

26. "Building Code Requirements for Reinforced Concrete", ACI Standard 318-71, American Concrete Institute, 1971.

27. Aldridge, W.A., Gamble, W.L., and Sabnis, G.M., "Structural Models : Fabrication, Instrumentation and Test Techniques", Symposium on Models of Concrete Structures, Preprints sponsored by ACI Committee 444, Annual Convention, Dallas, Texas, March, 1972, pp. 113-125.

28. Hognestad, E., Hanson, N.W., and McHenry, D., "Concrete Stress Distribution In Ultimate Strength Design", Journal of the American Concrete Institute, Proceedings Vol. 52, No. 28, December, 1955, pp. 455-480.

29. Kent, D.C., and Park, R., "Flexural Members With Confined Concrete", Journal of the Structural Division, ASCE, Vol. 97, No. ST7, July, 1971, pp. 1969-1990.

30. Newmark, N.M., and Rosenblueth, E., "Fundamentals of Earthquake Engineering", Prentice-Hall Inc., Englewood Cliffs, New Jersey, 1971, pp. 640.

31. Blake, R.E., "Basic Vibration Theory", Shock and Vibration Handbook, Harris, C.M., and Crede, C.E., editors, McGraw-Hill Book Co. Inc., Vol. 1, Ch. 2, New York, 1961, pp. 27.

32. Timoshenko, S.P., and Young, D.H., "Theory of Structures", Kōgakusha Co. Ltd., 2nd edition, 1965, pp. 629.

33. Lampert, P., "Torsion and bending in reinforced and prestressed concrete members", The Institute of Civil Engineers, Proceedings, Vol. 50, December, 1971, pp. 487-505.

34. Hsu, T.T.C., "Torsion of Structural Concrete - Behaviour of Reinforced Concrete Rectangular Members", Torsion of Structural Concrete, SP-18, ACI, Detroit, 1968, pp. 261-306.

35. Park, R., and Paulay, T., "Reinforced Concrete Structures", John Wiley and Sons, New York, (in the press).

36. Gouda, M.A., "Distribution of Torsion and Bending Moments in Connected Beams and Slabs", Journal of the American Concrete Institute, Proceedings Vol. 56, No. 43, February, 1960, pp. 757-774.

37. Paulay, T., Discussion on reference 36, Journal of the American Concrete Institute, Proceedings Vol. 56, No. 43, Part 2, September, 1960, pp. 1432-1442.

38. Timoshenko, S., and Woinowski-Krieger, S., "Theory of Plates and Shells", 2nd edition, McGraw-Hill, New York, 1959, pp. 580.

39. Bertero, V.V., and McClure, G., "Behaviour of Reinforced Concrete Frames Subjected to Repeated Reversible Loads", Journal of the American Concrete Institute, Proceedings Vol. 61, No. 10, October, 1964, pp. 1305-1330.

40. Bertero, V.V., and Bresler, B., "Seismic Behaviour of Reinforced Concrete Framed Structures", Proceedings, Fourth World Conference on Earthquake Engineering, Santiago, Chile, January, 1969, pp. B-2 109-124.

41. Park, R., "Theorization of Structural Behaviour With a View to Defining Resistance and Ultimate Deformability", Introductory Report for Theme I, Symposium, Resistance and Ultimate Deformability of Structures Acted on by Well Defined Repeated Loads, International Association for Bridge and Structural Engineering, Lisbon, Portugal, 1973.

42. Takeda, T., Sozen, M.A., and Nielsen, N.N., "Reinforced Concrete Response to Simulated Earthquakes", Journal of the Structural Division, ASCE, Vol. 96, No. ST12, December, 1970, pp. 2557-2573.

43. Park, R., "Ductility of Reinforced Concrete Frames Under Seismic Loading", New Zealand Engineering, NZIE, Vol. 23, No. 11, November, 1968, pp. 427-435.

44. Kelly, T.E., "Some Seismic Design Aspects of Multistorey Concrete Frames", M.E. Report, Civil Engineering Department, University of Canterbury, 1974.

45. Jennings, P.C., Housner, G.W., and Tsai, N.C., "Simulated Earthquake Motions for Design Purposes", Proceedings, Fourth World Conference on Earthquake Engineering, Santiago, Chile, January, 1969, Vol. 1, pp. A1 145-160.

46. Berg, G.V., and Housner, G.W., "Integrated Velocity and Displacement of Strong Earthquake Ground Motion", Bulletin of the Seismological Society of America, Vol. 51, No. 2, April, 1961, pp. 175-189.

47. Brady, A.G., "Studies of Responses to Earthquake Ground Motion", Earthquake Engineering Research Laboratory Report, California Institute of Technology, Pasadena, California, 1966.

# APPENDIX A

## PLANS OF THE SHAKING TABLE AND FOUNDATIONS

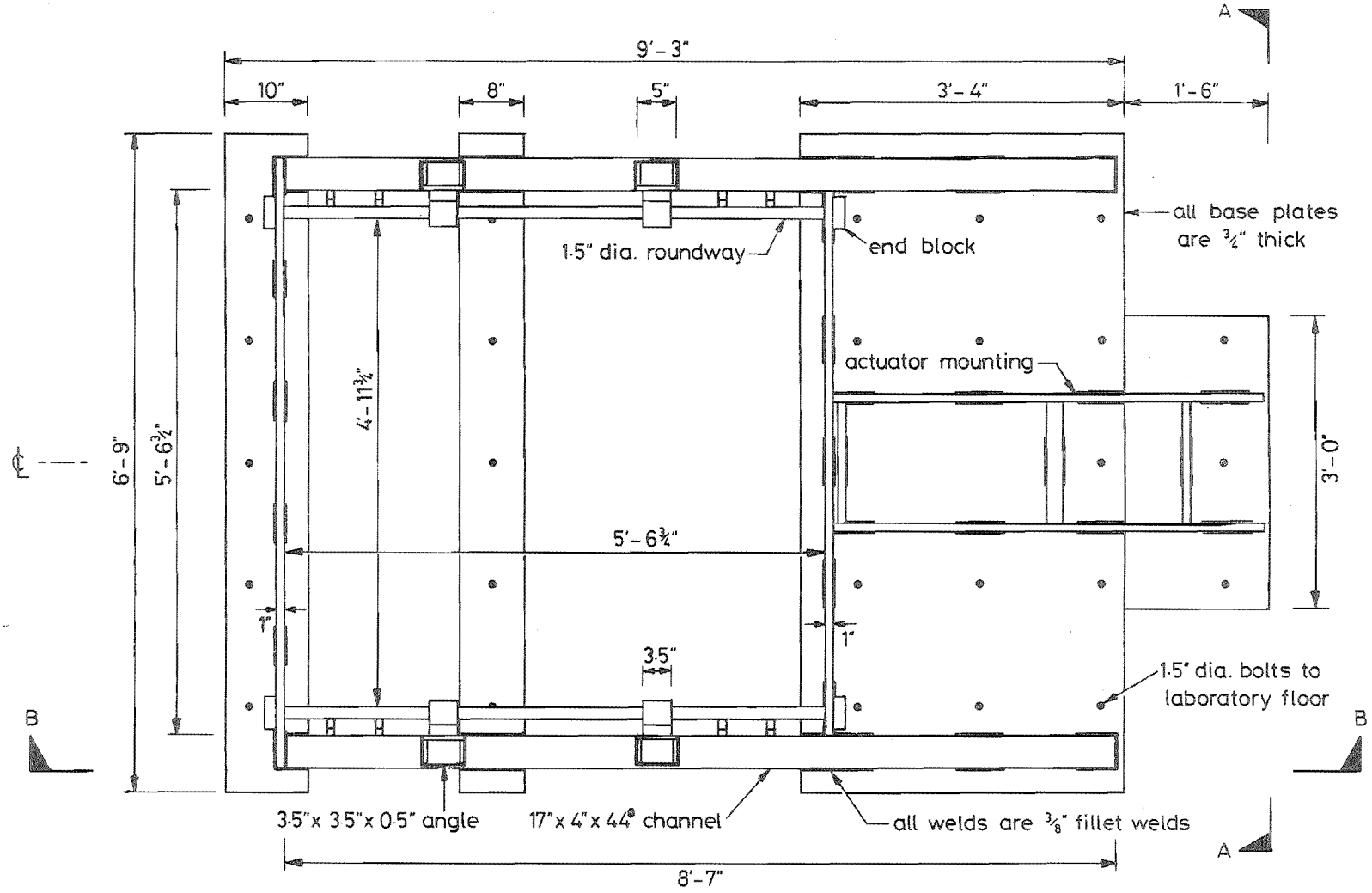


FIGURE A-1 : PLAN OF SHAKING TABLE FOUNDATIONS

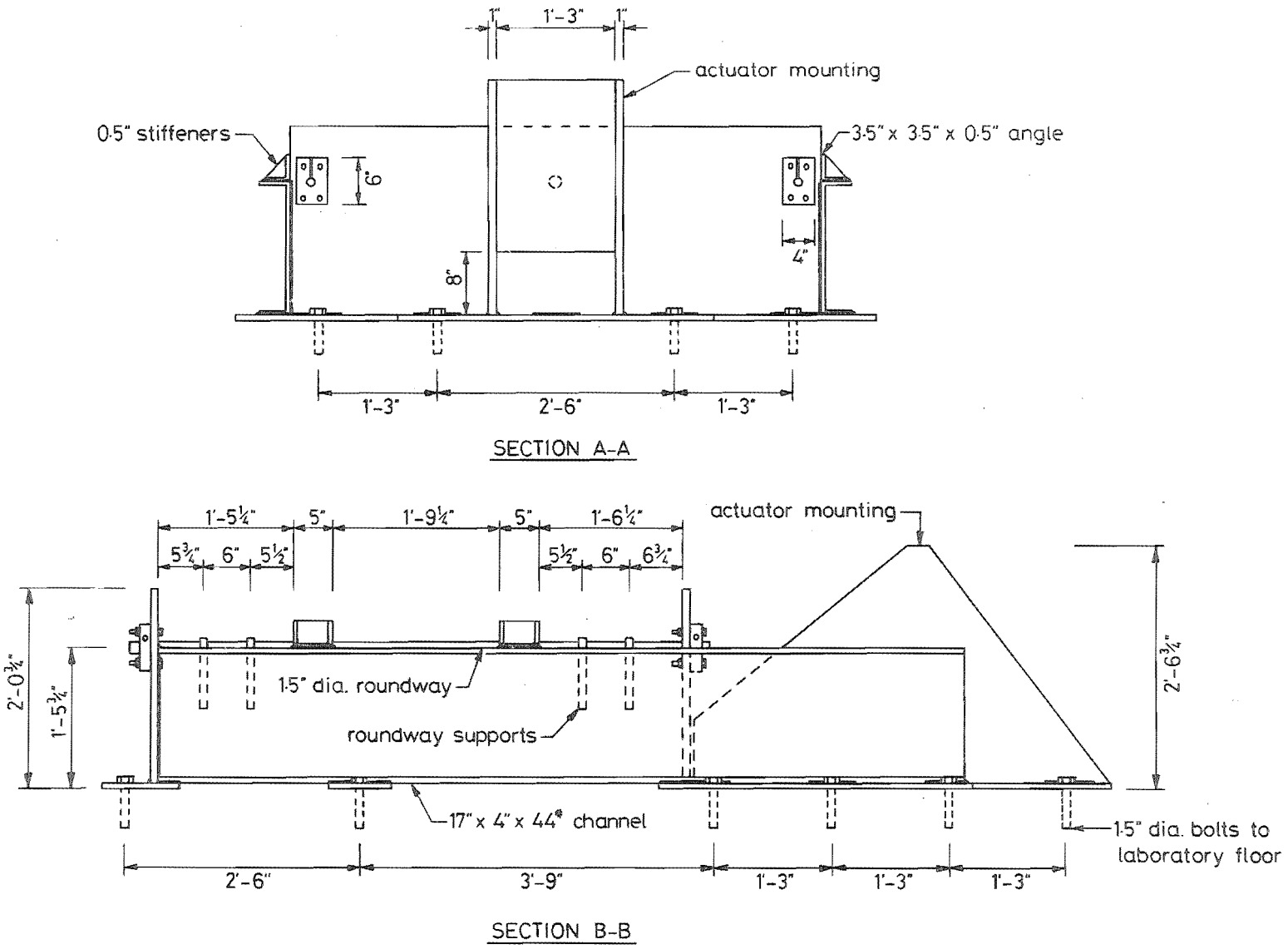


FIGURE A-2 : ELEVATIONS OF SHAKING TABLE FOUNDATIONS

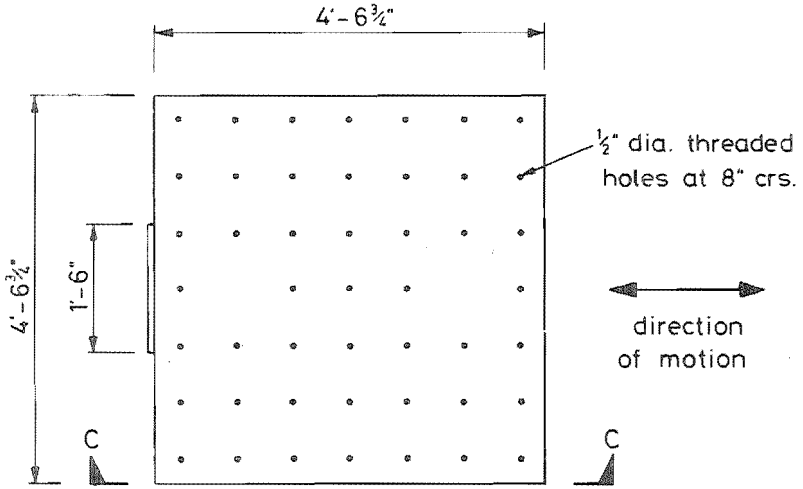


PLAN OF SHAKING TABLE

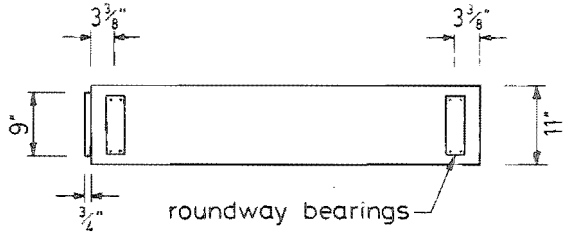


SECTION C-C

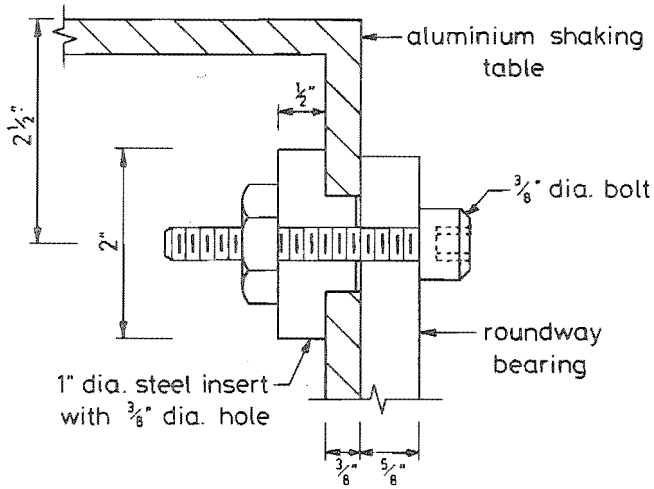


BEARING-TABLE CONNECTION

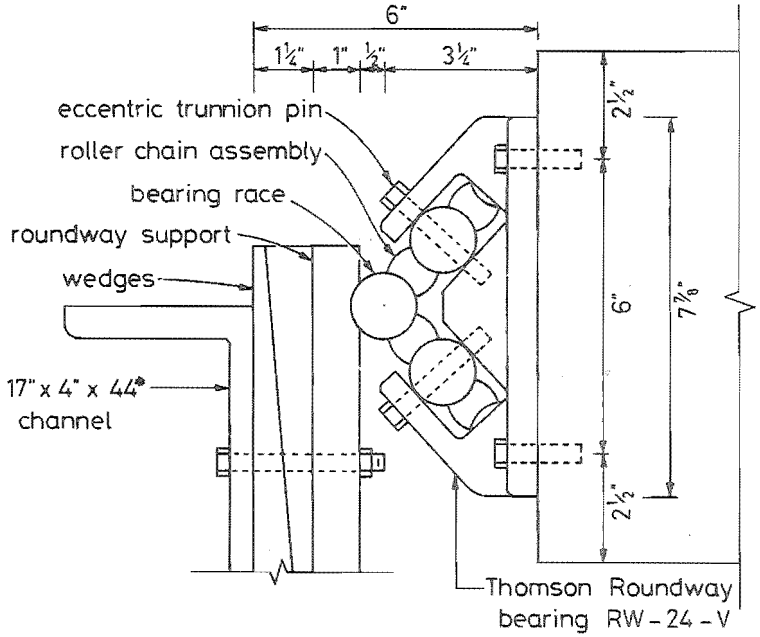


ROUNDWAY BEARING DETAIL

FIGURE A-3 : SHAKING TABLE AND ROUNDWAY BEARINGS

# APPENDIX B

## PLANS OF THE STRUCTURE

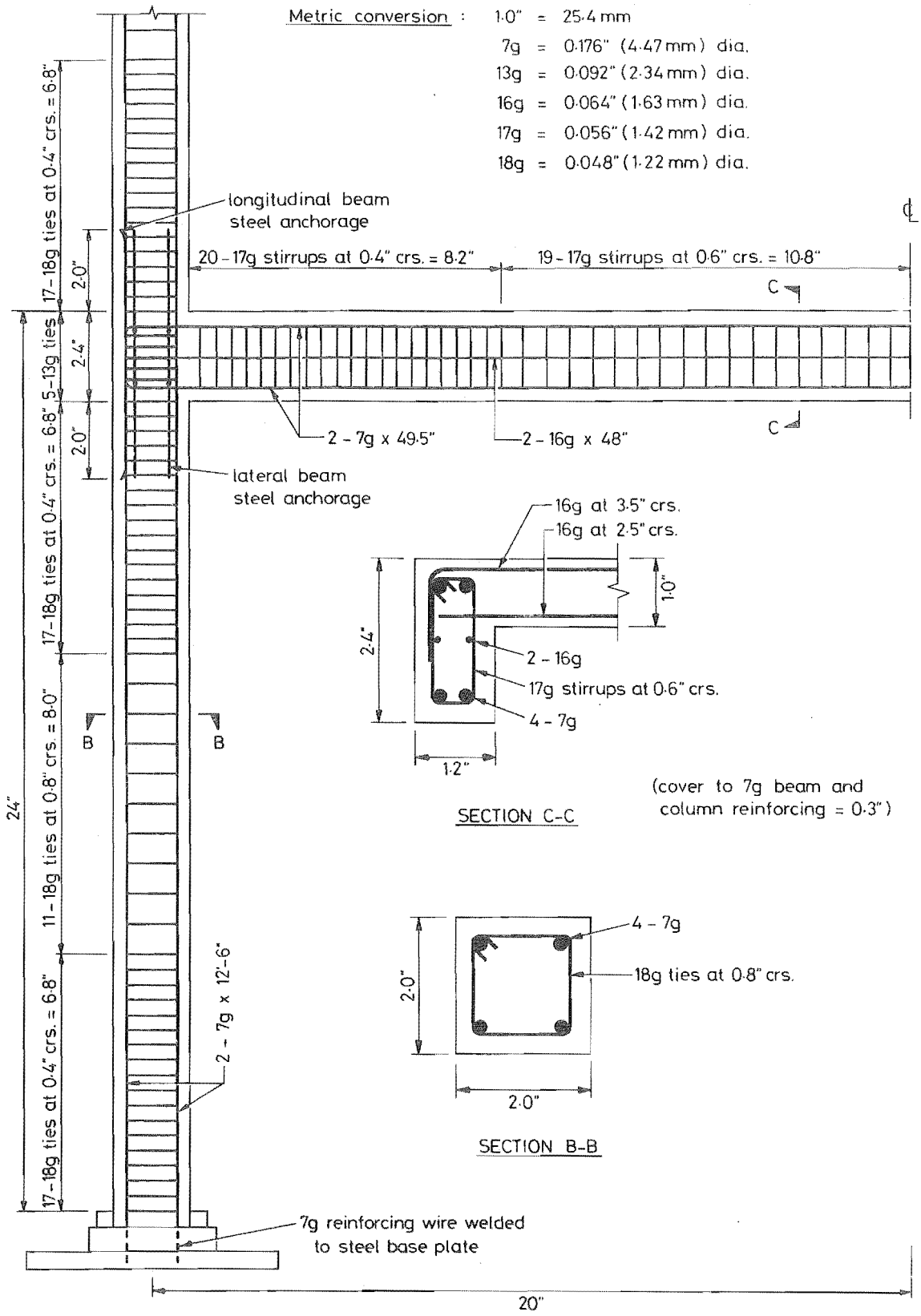


FIGURE B-1 : LONGITUDINAL FRAME REINFORCING DETAILS

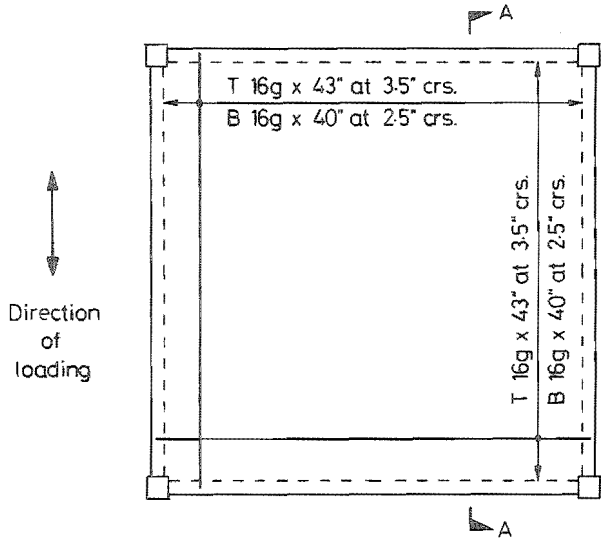


PLAN

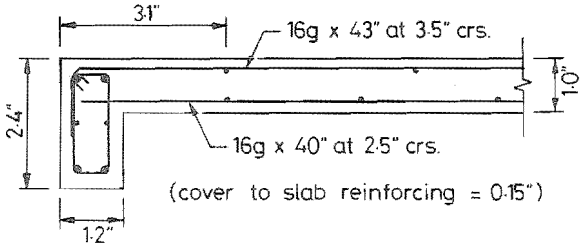


SECTION A-A

FIGURE B-2 : SLAB REINFORCING DETAILS

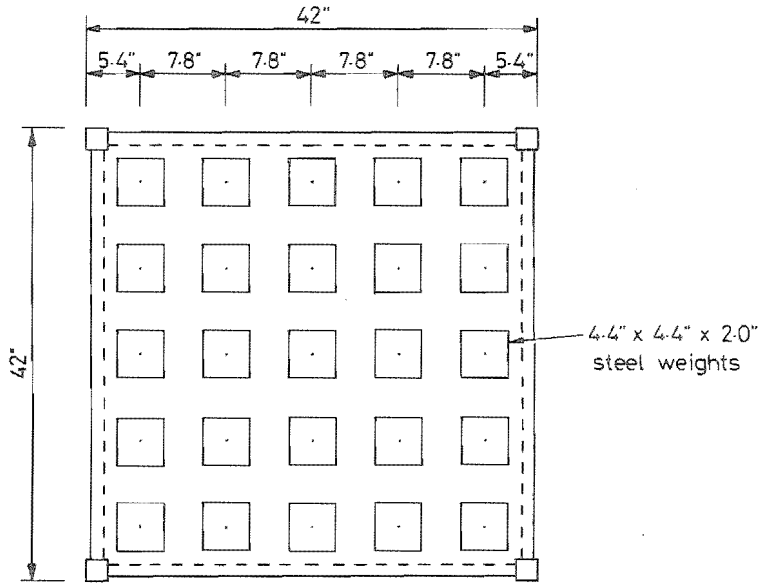


PLAN

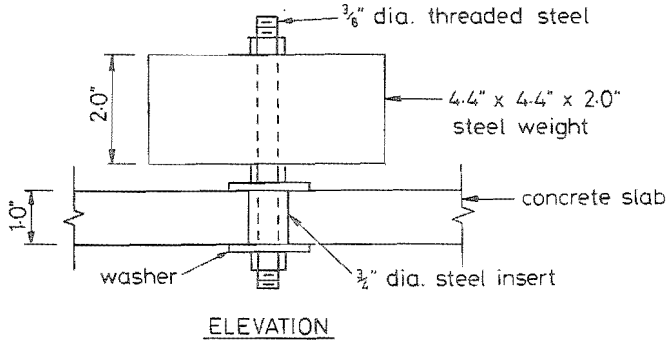


ELEVATION

FIGURE B-3 : ATTACHMENT OF STEEL WEIGHTS

# APPENDIX C

## LISTING OF COMPUTER PROGRAMS

### C.1 MOCU

A program to determine the theoretical monotonic moment-curvature relationship for a beam or column structural member.

Input data :

1. Header card - identification of the section
2. Data card - A, FC, CK, B, T, SD(1), SD(2), SD(3), AST(1), AST(2), AST(3)
   Format (2F10.2, 6F5.2, 3F10.6)

A = axial load on column (compression positive)
FC = cylinder strength of the concrete
CK = ratio of maximum concrete flexural stress to concrete cylinder strength
B = width of the compression area of the section
T = depth to the centre of the section
SD(1) = depth to top steel
SD(2) = depth to steel at mid-depth of section
SD(3) = depth to bottom steel
AST(1) = area of top steel
AST(2) = area of steel at mid-depth of section
AST(3) = area of bottom steel

Output data :

1. Input data echo check - header card, data card
2. Printed output - maximum concrete strain, depth to neutral axis, moment, curvature
3. Auxiliary output - moment, curvature

```
C     ***********************************************
C     THEORETICAL MOMENT  CURVATURE CALCULATIONS
C     ***********************************************
C
      DIMENSION SD(3),SS(3),SP(3),ST(3),P(3),AS(3),RD(3),AST(3)
      WRITE(6,52)
   52 FORMAT(1H8/1H1////)
      LOGICAL*1 LABEL(75)
      READ(5,100) LABEL
  100 FORMAT(75A1)
      WRITE(6,100) LABEL
      READ(5,1)  A,FC,CK,B,T,(SD(I),I=1,3),(AST(I),I=1,3)
    1 FORMAT(2F10.2,6F5.2,3F10.6)
      WRITE(6,2) A,FC,CK,B,T,(SD(I),I=1,3),(AST(I),I=1,3)
    2 FORMAT(/////14X,37HAXIAL LOAD (A)                              =,F6.0//
     1               14X,37HCYLINDER STRENGTH OF CONCRETE (FC)       =,F6.0//
     2               14X,37HMAX CONC STRESS/CONC CYL STR (CK)        =,F6.2//
     3               14X,37HWIDTH OF SECTION (B)                     =,F6.2//
     4               14X,37HDEPTH TO CENTRE OF SECTION (T)           =,F6.2//
     5               14X,37HDEPTH TO STEEL (SD(1))                   =,F6.2//
     6               14X,37HDEPTH TO STEEL (SD(2))                   =,F6.2//
     7               14X,37HDEPTH TO STEEL (SD(3))                   =,F6.2//
     8               14X,37HAREA OF STEEL (AST(1))                   =,F6.5//
     9               14X,37HAREA OF STEEL (AST(2))                   =,F6.5//
     1               14X,37HAREA OF STEEL (AST(3))                   =,F6.5///)
      WRITE(6,90)
   90 FORMAT(///10X,15HMAX CONC STRAIN,5X,21HDEPTH TO NEUTRAL AXIS,10X,
     1      6HMOMENT,10X,9HCURVATURE////)
      C=0.8*T
C
C     CALCULATE STRAIN DUE TO AXIAL LOAD
C
      AX=0.001*A
      FK=0.001*CK*FC
      AE=SQRT(2.236*4.*FK*FK*(5.982-1.0256*AX)*FK)
      AXS=0.001*(1.495*2.*FK-AE)/FK
      R=500.*AXS*0.05
   46 EC=0.002*R
      J=1
  106 K=1
   39 N=1
    6 CONTINUE
C
C     CALCULATE STRESS BLOCK PARAMETERS CORRESPONDING TO CONC STRAIN EC
C
C     IF N=1 STRESS BLOCK PARAMETERS CORRESPOND TO MAIN CONC COMPV AREA
C     IF N=2 NEUTRAL AXIS LIES BELOW SECTION AND STRESS BLOCK PARAMETERS
C            CORRESPOND TO AREA BELOW SECTION
C
      IF(R.GT.6.0) GO TO 40
      IF(R.GT.1.0) GO TO 7
C
C     RD(N) = RATIO OF DEPTH TO RESULTANT FORCE TO DEPTH TO NEUTRAL AXIS
C     AS(N) = AVERAGE STRESS OVER DEPTH C
C
      AS(N)=CK*FC*R*(1.-R/3.)
      RD(N)=(1.-R/4.)/(3.-R)
      GO TO 9
    7 AS(N)=CK*FC*(1.16-0.4133/R-0.08*R)
      RD(N)=(0.08*R*R-1.74*R+1.24-0.33/R)/(0.24*R*R-3.48*R+1.24)
      GO TO 9
   40 AS(N)=CK*FC*(0.2+2.467/R)
      RD(N)=(6.*R*R+148.*R-379.)/(148.*R+12.*R*R)
    9 CONTINUE
      IF(N.EQ.2) GO TO 10
C
C     C1=MAIN CONCRETE COMPRESSIVE FORCE
C
      C1=AS(1)*C*B
      IF(C.GT.2.*T) GO TO 8
      C2=0.
C
C     C2=CONCRETE COMPRESSIVE FORCE CORRESPONDING TO AREA BELOW SECTION
C
      GO TO 11
    8 W=R
      R=R*2.*T/C
      N=2
      GO TO 6
   10 C2=AS(2)*(C-2.*T)*B
C
C     C3=CONCRETE TENSILE FORCE (OCCURS WHEN C.LT.2*T)
C
      C3=0.
      R=W
      GO TO 15
   11 CONTINUE
```

```
      ET=(2.*T-C)*EC/C
      IF(ET.LT.0.0001475) GO TO 14
      CT=0.0001475*C/EC
      C3=295. *B*CT
      GO TO 15
   14 C3=ET*B*(2.*T-C)*2000000.
      CT=2.*T-C
   15 CONTINUE
C
C     CALCULATE STEEL STRAINS, STRESSES AND FORCES
C
   42 DO 30 I=1,3
      SS(I)=EC*(SD(I)-C)/C
      SS(I)=ABS(SS(I))
      IF(SS(I).GT.0.00077) GO TO 31
      ST(I)=30000000.*SS(I)
      GO TO 30
   31 IF(SS(I).GT.0.0068) GO TO 32
      ST(I)=47000.-18.4/SS(I)
      GO TO 30
   32 IF(SS(I).GT.0.0189) GO TO 33
      ST(I)=182000.*SS(I)+43060.
      GO TO 30
   33 IF(SS(I).GT.0.07102)  GO TO 36
      ST(I)=403000.*SS(I)+30880.
      GO TO 30
   36 ST(I)=67500.
   30 SF(I)=ST(I)*AST(I)
C
C     SF(1) = FORCE IN TOP 7G STEEL
C     SF(2) = FORCE IN CENTRAL 16G STEEL
C     SF(3) = FORCE IN BOTTOM 7G STEEL
C
      IF(C.GT.SD(1)) SF(1)=-SF(1)
      IF(C.GT.SD(2)) SF(2)=-SF(2)
      IF(C.GT.SD(3)) SF(3)=-SF(3)
C
C     SFF = TOTAL STEEL FORCE (TENSION POSITIVE)
C     CFF = TOTAL CONCRETE FORCE (COMPRESSION POSITIVE)
C
      SFF=SF(1)+SF(2)+SF(3)
      CFF=C1-C2-C3
C
C     CHECK EQUILIBRIUM OF FORCES
C
      X=ABS(CFF-SFF-A)
      IF(X.LE.10) GO TO 43
      P(K)=C
C
C     CORRECT C
C
      C=C*(1.-0.5*(CFF-SFF-A)/C1)
      IF(K.EQ.3) GO TO 105
      K=K+1
      GO TO 39
  105 C=0.5*(P(2)+P(3))
      J=J+1
      IF(J.LT.10) GO TO 94
      WRITE(6,93) X
   93 FORMAT(///10X,37HINTERNAL FORCES NOT IN EQUILIBRIUM BY,F6.1///)
   94 CONTINUE
      IF(J.EQ.10) GO TO 43
      GO TO 106
C
C     TAKE MOMENTS ABOUT CENTRE OF SECTION
C
   43 Y1=C1*(T-RD(1)*C)
      Y2=C2*(C-T-RD(2)*(C-2.*T))
      Y3=C3*2.*CT/3.
      Y4=-SF(1)*(T-SD(1))
      Y5=SF(3)*(SD(3)-T)
C
      AM=Y1+Y2+Y3+Y4+Y5
      CU=EC/C
C
C     WRITE MAX CONC STRAIN, NEUTRAL AXIS DEPTH, MOMENT AND CURVATURE
C
      WRITE(6,45)EC,C,AM,CU
   45 FORMAT(//11X,F10.5,12X,F10.3,14X,F10.0,9X,F10.6)
      WRITE(7,48) AM,CU
   48 FORMAT(F10.0,F10.5)
      R=R+0.05
      IF(R.GT.3.0) GO TO 47
      GO TO 46
C
   47 CONTINUE
      WRITE(6,52)
      STOP
      END
```

## C.2 EQPTC

A program to convert an earthquake displacement record from FORTRAN on cards to ASCII on paper tape.

Input data :

1. NC = number of cards (I5)
2. Earthquake displacements (11F7.4)

Output data :

1. Input data echo check - earthquake displacements
2. Paper tape - earthquake displacements

```
C     ********************************************************************
C     PROGRAM TO CONVERT EARTHQUAKE DISPLACEMENT RECORD FROM CARDS UNTO
C                    DISK IN HEXADECIMAL BIT REPRESENTATION
C     ********************************************************************
C
      DIMENSION DISPL(80) ,BRRAY(13),ARRAY(16),BIT(12000),BITS(12000)
      DATA BRRAY /'-','.','0','1','2','3','4','5','6','7','8','9'/
      DATA ARRAY/ZA0000000000,ZA0000000000,ZAE000000000,ZB0000000000
     1          ,ZB1000000000,ZB2000000000,ZB3000000000,ZB4000000000
     2          ,ZB5000000000,ZB6000000000,ZB7000000000,ZB8000000000
     3          ,ZB9000000000,ZAC000000000,ZBD000000000,ZBA000000000
     4          /
C
C     ARRAY = MINUS(1),SPACE(2),DECIMAL POINT(3),INTEGERS 0 TO 9 (4-13)
C             COMMA(14),CARRIAGE RETURN(15),LINE FEED(16)
C
      READ(5,19) NC
   19 FORMAT(I5)
C
C     NC=NUMBER OF CARDS
C
C     DISPLACEMENT RECORD FORMAT = F7.4
C
      M=1
      MM=1
      GO TO 1
    3 MM=MM+1
      IF(MM.GT.NC)GO TO 17
C
C     READ DISPLACEMENT RECORD
C
    1 READ(5,2) (DISPL(I),I=1,77)
    2 FORMAT(77A1)
      WRITE(6,27) (DISPL(I),I=1,77)
   27 FORMAT(1X,77A1/)
      DO 18 I=1,77
      DO 18 K=1,13
      IF(.NOT.(DISPL(I).IS.BRRAY(K))) GO TO 18
      BIT(M)=ARRAY(K)
      M=M+1
   18 CONTINUE
      GO TO 3
   17 CONTINUE
C
C     INSERT COMMAS AFTER EVERY NUMBER AND A CARRIAGE RETURN LINE FEED
C                         AFTER EVERY EIGHTH NUMBER
C
      MN=1
      N=1
      NN=1
   12 CONTINUE
      IF(MN.EQ.8*N+2*NN-2) GO TO 11
      BITS(MN)=BIT(MN-N-2*NN+3)
      GO TO 13
   11 BITS(MN)=ARRAY(14)
      N=N+1
      IF(N-1.EQ.8*NN)GO TO 15
      GO TO 13
   15 MN=MN+1
      BITS(MN)=ARRAY(15)
      MN=MN+1
      BITS(MN)=ARRAY(16)
      NN=NN+1
   13 MN=MN+1
      IF(MN.EQ.M+N+2*NN-3) GO TO 14
      GO TO 12
C
C     WRITE HEXADECIMAL BIT REPRESENTATION ONTO FILE 1 AND LOCK
C
   14 WRITE(1,8) (BITS(I),I=1,MN)
    8 FORMAT(80A1)
      LOCK 1
      STOP
      END
```

# APPENDIX D

## CALCULATIONS FOR THE EQUIVALENT FRAME METHOD

### D.1 INTRODUCTION

The routine calculations are presented for the prediction of the torsion induced in the edge beams of the slab under gravity loading by the equivalent frame method of ACI Code 318-71 [26]. The stiffnesses of all members are based on the uncracked sections.

### D.2 LONGITUDINAL BEAM STIFFNESS

The equivalent frame for calculating the moment of inertia of the longitudinal beams outside of the columns is ...

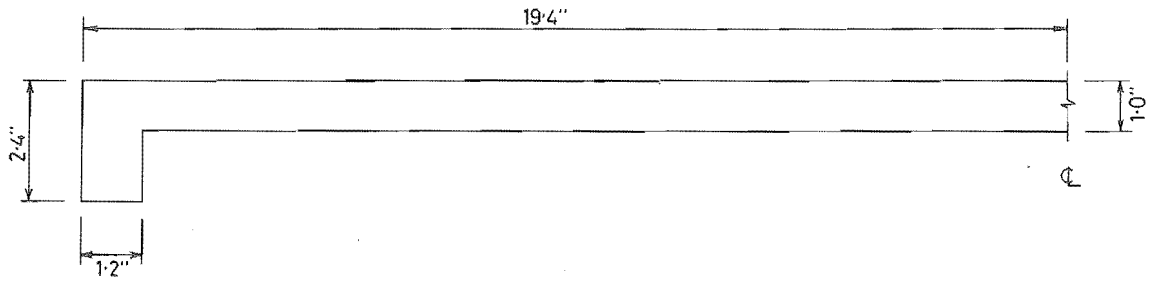


the moment of inertia $I_{sb} = 4.23 \text{ in}^4$

### D.3 TRANSVERSE BEAM STIFFNESS

The assumed cross-section of the transverse beams is ...

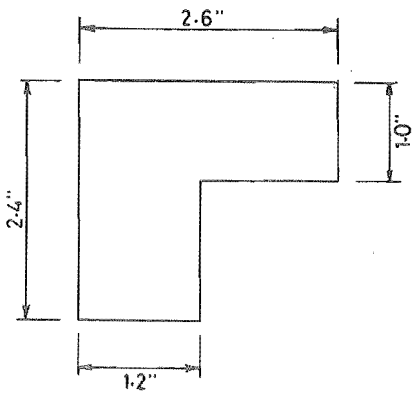


the moment of inertia $I_b = 1.96 \text{ in}^4$

$$\text{Thus} \quad C = \left(1 - 0.63 \times \frac{1.2}{2.4}\right) \frac{2.4 \times 1.2^3}{3} + \left(1 - 0.63 \times \frac{1.0}{1.4}\right) \frac{1.4 \times 1.0^3}{3}$$

$$= 1.20 \text{ in}^4$$

$$\text{and} \quad K_t = \frac{9 \times 4 \times 10^6 \times 1.20}{40\left(1 - \frac{2}{40}\right)^3}$$

$$= 1.26 \times 10^6 \text{ lbin/rad}$$

However $K_t$ will have to be modified since beams frame into the column in the direction the moments are being determined. The moment of inertia of the slab is ...

$$I_s = \frac{20.6 \times 1.0^3}{12} = 1.72 \text{ in}^4$$

$K_t$ is increased by $\frac{I_{sb}}{I_s}$ and thus $K_t = 3.11 \times 10^6$ lbin/rad

## D.4 COLUMN STIFFNESS

The column stiffness may be modified by the moment-area method to take into account the depth of beam or slab attached to either end. The moment of inertia of the columns at sections with the beam or slab attached may be assumed to be infinity.

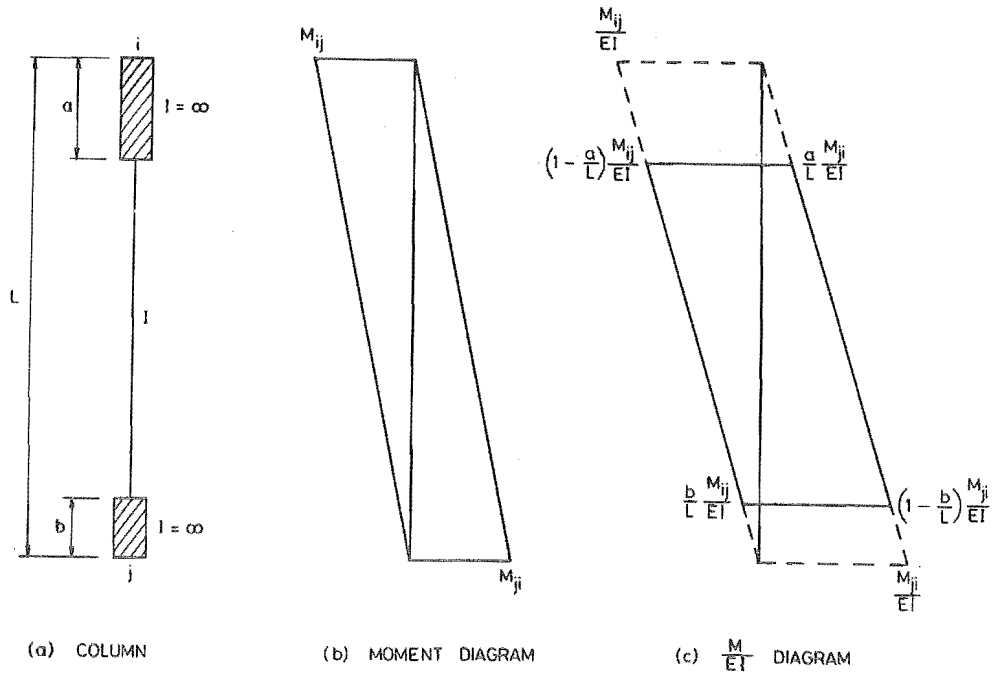


(a) COLUMN (b) MOMENT DIAGRAM (c) $\frac{M}{EI}$ DIAGRAM

FIGURE D-1 : DETERMINATION OF COLUMN STIFFNESS USING MOMENT-AREA METHOD

Consider a unit rotation at i , no rotation at j :

$$(1 - \frac{a}{L}) \frac{M_{ij}}{EI} \frac{1}{2}(L - a) - \frac{b}{L} \frac{M_{ij}}{EI} \frac{b}{2} - (1 - \frac{b}{L}) \frac{M_{ji}}{EI} \frac{1}{2}(L - b) + \frac{a}{L} \frac{M_{ji}}{EI} \frac{a}{2} = 1$$

$$M_{ij} \left[(L - a)^2 - b^2\right] - M_{ji} \left[(L - b)^2 - a^2\right] = 2LEI \qquad \text{(D-1)}$$

Consider the deflection of i relative to j , which is zero :

$$\frac{(L - a)^2}{2L} \frac{M_{ij}}{EI} \left[L - \frac{2}{3}(L - a)\right] - \frac{b^2}{2L} \frac{M_{ij}}{EI} (L - \frac{2}{3}b)$$

$$- \frac{(L - b)^2}{2L} \frac{M_{ji}}{EI} \frac{2}{3}(L - b) + \frac{a^2}{2L} \frac{M_{ji}}{EI} \frac{2}{3}a = 0$$

$$M_{ij} \left[(L - a)^2 (L + 2a) - b^2(3L - 2b)\right] = 2M_{ji} \left[(L - b)^3 - a^3\right] \qquad \text{(D-2)}$$

$$C_{ij} = \frac{(L - a)^2 (L + 2a) - b^2 (3L - 2b)}{2 (L - b)^3 - a^3} = \frac{M_{ji}}{M_{ij}} \qquad \text{(D-3)}$$

Equation D-1 then becomes ...

$$M_{ij} \left[[(L - a)^2 - b^2] - [(L - b)^2 - a^2] \frac{[(L - a)^2 (L + 2a) - b^2 (3L - 2b)]}{2[(L - b)^3 - a^3]}\right]$$

$$= 2LEI \qquad \text{(D-4)}$$

and if $x = \frac{a}{L}$ and $y = \frac{b}{L}$ equation D-4 becomes ...

$$M_{ij} \left[2[(1 - x)^2 - y^2] - [(1 - y)^2 - x^2] \frac{[(1 - x^2) (1 + 2x) - y^2 (3 - 2y)]}{[(1 - y)^3 - x^3]}\right]$$

$$= \frac{4EI}{L} \qquad \text{(D-5)}$$

$$S_{ij} = \frac{\frac{4EI}{L}}{2[(1 - x)^2 - y^2] - \frac{(1 + x - y) [(1 - x)^2 (1 + 2x) - y^2 (3 - 2y)]}{[(1 - y)^2 + x(1 - y) + x^2]}} \qquad \text{(D-6)}$$

For the column above the slab ...

$$x = 0.079 \qquad y = 0.021 \qquad \text{and} \qquad S_{ij} = 4.76\frac{EI}{L}$$

For the column below the slab ...

$$x = 0.021 \qquad y = 0.079 \qquad \text{and} \qquad S_{ij} = 5.72\frac{EI}{L}$$

and therefore the total column stiffness $K_c = 10.48 \frac{EI_c}{L}$

$$I_c = \frac{2 \times 2^3}{12} = 1.33 \text{ in}^4$$

thus $K_c = 10.48 \times \frac{4 \times 10^6 \times 1.33}{24} = 2.33 \times 10^6$ lbin/rad

The stiffness of the column is reduced to account for the torsional stiffness of the transverse beams ...

$$\frac{1}{K_{ec}} = \frac{1}{\Sigma K_c} + \frac{1}{K_t} = \frac{1}{2.33 \times 10^6} + \frac{1}{3.11 \times 10^6}$$

thus $K_{ec} = 1.33 \times 10^6$ lbin/rad

## D.5 DISTRIBUTION OF GRAVITY MOMENTS

Total static design moment $M_o = \frac{0.27 \times 20 \times (38.8)^2}{8} = 1016$ lbin

$$\alpha_{ec} = \frac{K_{ec}}{\Sigma(K_s + K_b)} = \frac{1.33 \times 10^6}{\frac{4 \times 4 \times 10^6}{40}(1.72 + 1.96)} = 0.906$$

Exterior negative design moment $= M_o\left(\frac{0.65}{1 + \frac{1}{2\alpha_{ec}}}\right) = 426$ lbin

$$\alpha_c = \frac{\Sigma K_c}{\Sigma(K_s + K_b)} = \frac{2.33 \times 10^6}{1.47 \times 10^6} = 1.58$$

and thus $\alpha_c \frac{l_2}{l_1} = 1.58$

$$\beta_t = \frac{C}{2I_s} = \frac{1.20}{2 \times 1.72} = 0.35$$

Therefore the column strip resists 96.5% of the exterior negative design moment and 15% of this is resisted by the slab

$= 426 \times 0.965 \times 0.15 = 62$ lbin

The middle strip resists 3.5% of the exterior negative design moment and all of this is resisted by the slab

$= 426 \times 0.035 = 15$ lbin

Each column strip has a width of 10 in. and the middle strip is 20 in. wide.